Ioannis Maniatis
Mozartstrasse 25
D-67655 Kaiserslautern
Geburtsort: Athen / Griechenland

Joint channel estimation in service area based OFDM air interfaces for beyond 3G mobile radio systems

deutscher Titel:

Gemeinsame Kanalschätzung in OFDM- Luftschnittstellen für Mobilfunksysteme jenseits der 3. Generation auf der Basis von Service-Gebieten

Vom Fachbereich Elektrotechnik und Informationstechnik
der Technischen Universität Kaiserslautern
zur Verleihung des akademischen Grades
Doktor der Ingenieurwissenschaften (Dr.–Ing.)
genehmigte Dissertation

von
Dipl.-Ing. Ioannis Maniatis

D 386

Tag der Einreichung: 25.10.2004
Tag der mündlichen Prüfung: 04.02.2005

Dekan des Fachbereichs
Elektrotechnik: Prof. Dr.-Ing. G. Huth

Vorsitzender der
Prüfungskommission: Prof. Dr.-Ing. habil. L. Litz

1. Berichterstatter: Prof. Dr.-Ing. habil. Dr.-Ing. E. h. P.W. Baier

2. Berichterstatter: Prof. Dr. H. Haas

Foreword

The present thesis accrued in the time period from April 2001 until October 2004 during my occupation as a scientific researcher at the Research Group for RF Communications of Prof. Dr.-Ing. habil. Dr.-Ing. E.h. P.W. Baier at the Technical University of Kaiserslautern. I would like to thank all those who supported me during this period.

A special thanks goes to Prof. Dr.-Ing. habil. Dr.-Ing. E.h. P.W. Baier for the incitation, the furtherance and the supervision of this work. Through his permanent cooperativeness and willingness for discussions he contributed a major part to the success of this work. I also would like to thank Prof. Dr. H. Haas of the International University of Bremen for undergoing the process of issuing the necessary certificate of conformity for my thesis and for the fruitful exchange of ideas during our involvement in joint research projects. Furthermore, I would like to thank the chairman of the examination committee, Prof. Dr.-Ing. habil. L. Litz.

Another special thanks goes to Dr.-Ing. habil. T. Weber for the outmost efficient teamwork during my research activities. His advises and hints contributed considerably to the quality of this thesis.

The results presented in the thesis were generated in the scope of research projects supported by the SIEMENS AG. I would like to thank Dr.Ing. E. Schulz, Dr.-Ing. E. Costa and Dr.-Ing. M. Weckerle from SIEMENS for the support and the exchange of ideas. During the course of said projects a valuable co-operation with the research groups of Prof. Dr. H. Rohling, Technical University Hamburg-Harburg, of Prof. You, Southeastern University – Nanjing, China, of Prof. Zhou, University of Science and Telecommunications – Hefei, China, and of Prof. Zhang Ping, Beijing University of Post and Telecommunication – Beijing, China was established.

The present and past colleagues at the Research Group of RF Communications I thank for the inspiring and pleasant working environment. An additional thanks goes to all the students who contributed to my work in the scope of their junior and master theses.

My present girlfriend and future wife Patricia I thank with all my heart for her support in the last ten months. She gave me peace of mind and strength and always held on to me. Last but not least, my biggest thanks I give to my parents Katerina and Anastasios, who supported me morally as well as financially during my entire life and never gave up on me. This I will always remember, cherish and strive to imitate. I dedicate this work to the three of them.

Kaiserslautern, February 7^{th} 2005 Ioannis Maniatis

Contents

Chapter 1

Introduction

1.1 Service area based architecture versus cellular architecture

Even though 3G mobile radio networks up to now have not yet come widely into operation, already today research activities directed towards the definition and design of Beyond 3G (B3G) systems are being started in many parts of the world [WM02, Nat03, EKLG+03]. According to the observations made in connection with the emergence of 2G and 3G systems, the time, which elapses from the first system considerations until eventually system operation commences, easily reaches one decade. Therefore, today's activities towards B3G systems are far from being premature. Among the various demands put by operators and potential users on B3G systems, the flexible support of data rates significantly above those typical of 2G and 3G systems is of paramount importance [TNA+01]. Because also in the future the available and allotted frequency bands will be a scarce resource, the support of high data rates requires system designs which make optimum use of the assigned frequency spectrum and, thus, guarantee a high spectrum efficiency. Spectrum efficiency can be enhanced by measures on different layers of the IS0/0SI reference model [EF86]. Basically, we can discern between measures on the physical layer, which beneficially exploit the phenomena of wave propagation, and measures on higher layers, which aim at making optimum use of the resources offered by the physical layer by assigning them advantageously to the different communication links. In a balanced system design, measures on all layers would interplay in such a way that spectrum efficiency is maximized. As a basis for such a maximization, the physical layer deserves special attention. This thesis deals with a novel architecture of the physical layer suitable for B3G systems.

As a rule, in conventional 2G [RW95, EV97, Wal98] cellular architectures the mobile terminals (MTs) of each cell are radio linked exclusively to the base station (BS) of their individual cell. This is also true for 3G [ETS97, Wal98] cellular architectures with the exception of the few MTs being in soft handoff [Wal98]. The straightforward assignment of MTs to BSs is advantageous with respect to the signalling requirements, but it has the following drawbacks:

- In the uplink (UL), the signals radiated by the MTs not only impinge at their own BS as desired signals, but also at the BSs of other cells as undesired signals.
- In the downlink (DL), the signals radiated by the BS not only impinge at their own MTs as desired signals, but also at MTs of other cells as undesired signals.

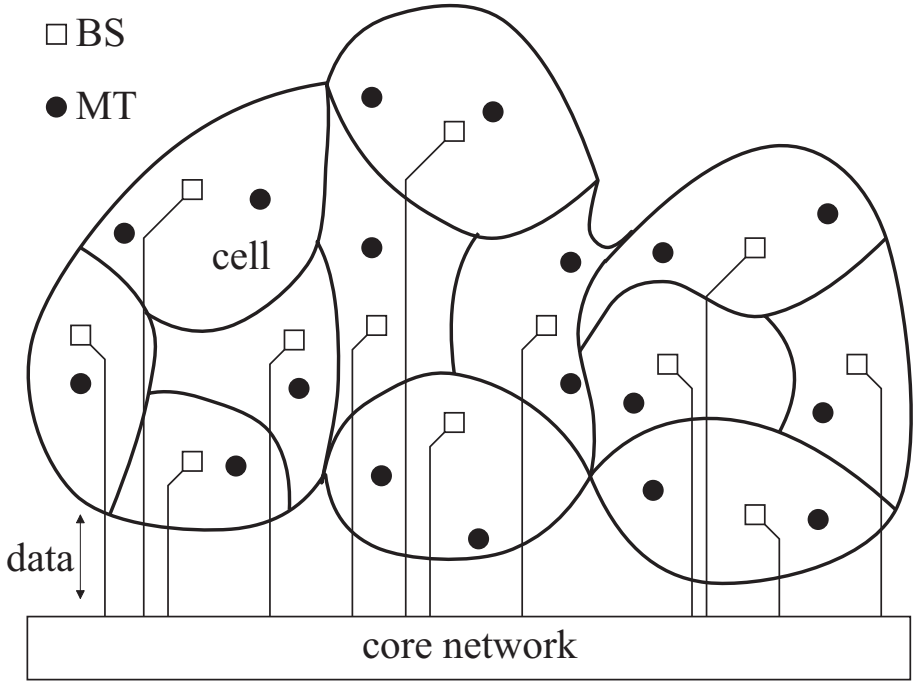

Fig. 1.1. Conventional cellular architecture, example with 12 cells

The mentioned undesired signals act as interference instead of being constructively utilized. This detrimental effect is particularly pronounced if rather high transmit powers are required in order to compensate the high propagation losses when supporting MTs being far away from their BS or suffering from heavy shadowing.

In the novel architecture proposed in this thesis, instead of individual BSs access points (APs) are introduced with groups of such APs being linked to a central unit (CU). Each such group defines a service area (SA), and the MTs of each SA can communicate with the SA-specific CU via all APs of the SA. By means of Figs. 1.1 and 1.2 the conventional cellular architecture [MD79, Gib99, DB96, Wes02] and the novel SA-based architecture [WMSL02] are compared with each other. Fig. 1.1 shows a generic conventional cellular architecture. Each cell contains a BS, and the MTs of each cell communicate solely with this BS. In the structure shown in Fig. 1.1 all BSs are connected to a central entity termed core network, which, in the case of GSM, consists of the base station controllers and the mobile switching centers [RW95, EV97, Wal98]. The core network can be considered the data source and data sink in the communication with the MTs. Fig. 1.2 shows the novel SA-based architecture. Instead of a number of cells – each with a BS – of conventional cellular architectures we now have a SA with a number of APs, which are connected to a CU. The CUs in their turn are connected to the core network. In the conventional cellular architecture, see Fig. 1.1, each cell constitutes a multipoint–to–point structure in the UL and a point–to–multipoint structure

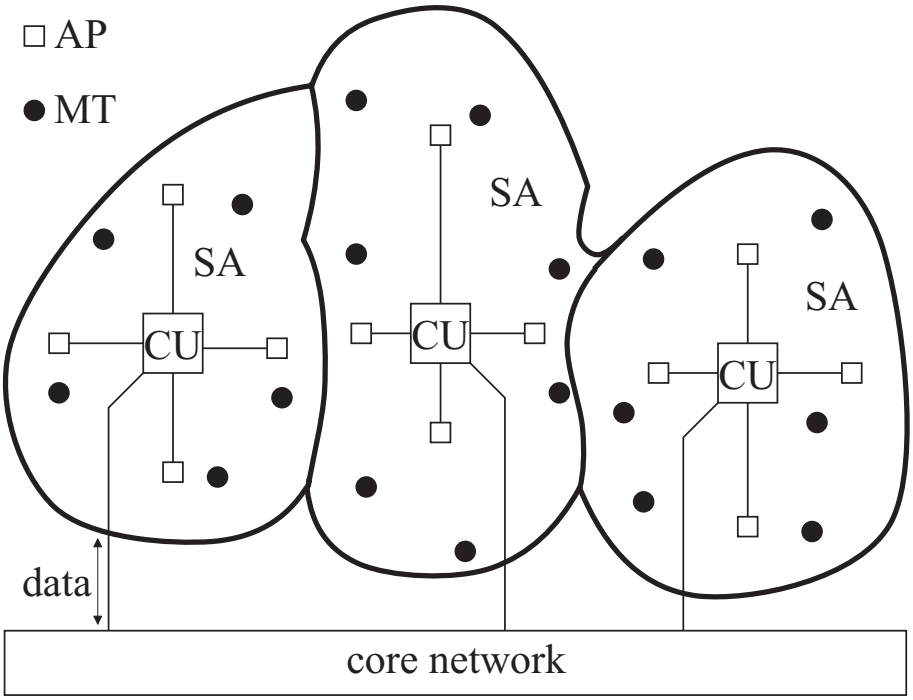

Fig. 1.2. Novel SA based architecture, example with three SAs

in the DL. In contrast to this, see Fig. 1.2, each SA of the SA-based architecture constitutes a multipoint–to–multipoint structure both in the UL and in the DL.

The basic way of operation of the SA-based architecture as shown in Fig. 1.2 is the following:

- In the UL the transmit signals of the MTs of a SA are received by all APs of the SA and fed to the CU, where they are jointly processed. The aim of this joint processing consists in exploiting the energies of all signals received by the APs of the SA in such a way that the required total transmit energy in the SA is minimized and that the complexity of the MTs can be kept low. An UL transmission scheme which allows to reach these goals is joint detection (JD) published in [Kle96, Skl04].
- In the DL each MT of a SA is supported by all APs of the SA, which radiate corresponding signals. These signals are jointly generated in the CU based on the data for each MT of the SA in such a way that the required total transmit energy in the SA is minimized, and that the complexity of the MTs can be kept low. A DL transmission scheme which allows to reach these goals is joint transmission (JT) published in [MBW$^+$00, TWMB01, Skl04].

Because JD and JT are important features of the proposed architecture, the designation ”Joint Transmission and Detection Integrated Network” (JOINT) has been coined for this architecture. The rationale of JOINT can be applied both in conglomerates of SAs as shown in Fig. 1.2 and in single, that is isolated SAs.

In the case of the conventional cellular architecture the MTs of each cell form a group of MTs which can be supported without causing mutual interference [Ver98, Kle96, Pap00], that is intracell interference may be eliminated. In the case of the SA based architecture the MTs of each SA form such a group of MTs which can be supported without causing mutual interference [WMSL02, Skl04], that is intra-SA interference can be eliminated. A look at Figs. 1.1 and 1.2 shows that in the case of the SA-based architecture the groups of MTs which can be supported without mutual interference are larger than in the case of the conventional cellular architecture. Therefore, in the SA-based architecture the interference problems are relaxed as compared to those in the case of the conventional cellular architecture. This relaxation is expected to entail a capacity increase.

1.2 Basic features of JOINT as considered in the thesis

In the framework of the basic architecture of JOINT described in Section 1.1 and illustrated in Fig. 1.2, many degrees of freedom exist for the system designer as for instance with respect to the design criteria

- multiple access (MA) scheme (FDMA, TDMA, CDMA, SDMA),
- transmission mode (single carrier, multi–carrier),
- duplexing scheme (TDD, FDD), and
- antenna arrangements at the APs and the MTs (single-element antennas, multi-element antennas).

Considering these freedoms, the following choices are made in this thesis:

- MA scheme: SDMA,
- transmission mode: multi–carrier, specifically OFDM,
- duplexing scheme: TDD, and
- antenna arrangements: single-element or multi–element antennas at the APs, single-element antennas at the MTs.

In what follows these choices are briefly motivated. The MA scheme SDMA is an obvious separation scheme for spatially dislocated MTs which communicate with a number of spatially dislocated APs, as it is the case in JOINT. Of course, SDMA could be combined with other MA schemes, which, however, is beyond the scope of this thesis. The choice of OFDM is made with respect to the advantages claimed for this transmission mode as for instance suitability for high data rates, flexibility, low transmitter, and receiver complexity [WE71, Bin90, Pra98, vNP00, KS01, RGG01] etc. As opposed to the duplexing scheme

FDD, the selected scheme TDD facilitates the flexible support of highly different data rates in UL and DL, and allows to exploit the reciprocity of the UL and DL channels in the context of channel estimation. At the MTs, single-element antennas are chosen with a view to keep the MT complexity low. This argument does not count so much for the APs, where, in addition to single-element antennas, also multi-element antennas are considered with a view to performance enhancements.

In addition to the above mentioned design criteria also criteria like

- splitting up of the signal processing effort between the APs and the CU of a SA,
- implementation of the links between the APs and the CU of a SA (base band, RF band, coaxial cable, optical fibre, radio relay etc.),
- geometrical definition of SAs and placement of APs, and
- algorithms to perform JD and JT

could be considered. However, these criteria shall not play a major role in the context of this thesis.

1.3 Channel estimation in JOINT, the topic of the thesis

As mentioned in Section 1.2, each SA of the SA-based architecture constitutes a multipoint–to–multipoint system, in which JD is performed in the UL and JT is performed in the DL. In order to perform JD and JT, channel knowledge is required at the CU. This knowledge has to be gained by channel estimation, which is the topic of this thesis. This thesis belongs to a triplet of theses on JOINT, in which the other two theses deal with the problems of data estimation [Skl04] and overall system modelling and simulations [Liu05], respectively.

Because, as mentioned in Section 1.2, the selected duplexing scheme is TDD, due to the reciprocity theorem the channel properties in UL and DL are the same. This fact shall be exploited in the following way: In JOINT channel estimation is only performed in the UL, and for DL transmission the channel knowledge gained in the UL transmission is again used. In this way one can dispose with channel estimation in the DL. This approach is advantageous with respect to saving DL transmission resources – anyhow, the DL is capacity-wise more critical than the UL –, and is applicable as long as the time which elapses between UL and DL transmissions is sufficiently short. To be more precise, the MTs should not move by more than a small fraction of the carrier wavelength λ between UL and DL transmissions. As a consequence, the validity of the considerations performed in this thesis are restricted to scenarios with low to medium scale MT velocities.

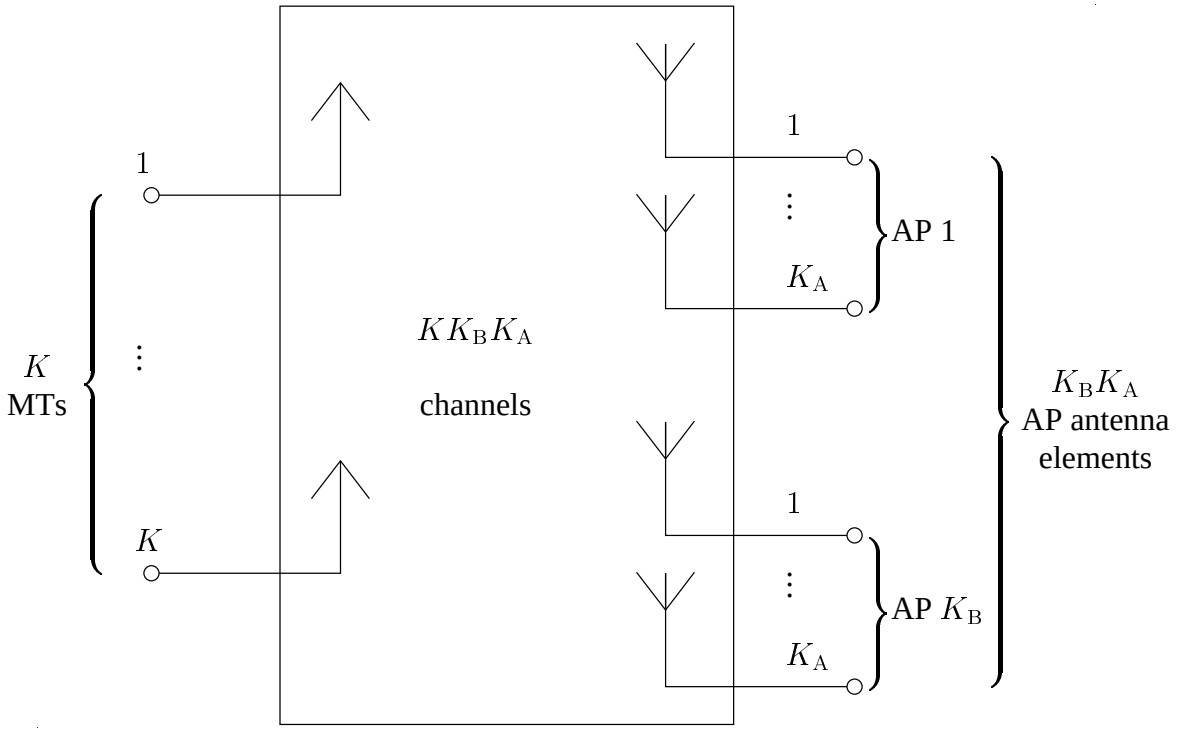

Fig. 1.3. MIMO antenna configuration valid for the entire UL of a SA

Due to the fact that each SA has to be considered as a multipoint–to–multipoint structure, a multitude of channels have to be estimated in the UL. This estimation could be performed serially, that is channel by channel, which, however, would consume considerable transmission resources. In order to avoid this disadvantage, in this thesis the channels are estimated simultaneously, which leads to the concept of joint channel estimation (JCE) [Ste95, SMWB01].

Let us assume that we have K_{B} APs and K MTs in a SA, and that each AP has a multi–element antenna with K_{A} elements and each MT has single–element antenna. In the case of the UL being of interest here, this situation can be illustrated by a multiple–input–multiple–output (MIMO) antenna configuration as shown in Fig. 1.3 with K inputs and $K_{\mathrm{B}}K_{\mathrm{A}}$ outputs. Consequently, the total number of channels to be estimated equals $KK_{\mathrm{B}}K_{\mathrm{A}}$. In order to perform JCE, the K channels from the K MTs $k = 1 \ \ldots \ K$ to each of the $K_{\mathrm{B}}K_{\mathrm{A}}$ AP antenna elements can be treated separately. This means that JCE as considered in this thesis can be based on the multiple–input–single–output (MISO) antenna configuration shown in Fig. 1.4.

As shown in Fig. 1.5, in OFDM transmission featured in this thesis

- the time domain is subdivided into OFDM symbol slots, and

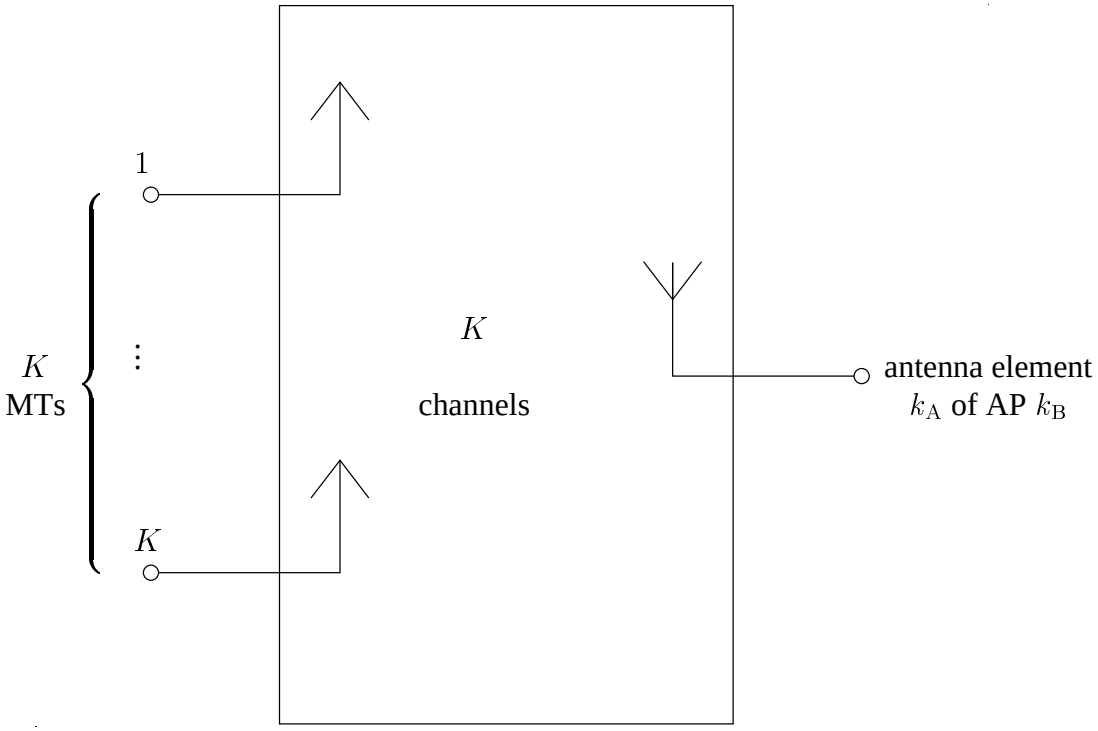

Fig. 1.4. MISO antenna configuration valid for the channels of all K MTs and antenna element k_{A} of AP k_{B}

- the available system bandwidth B is shared by N_{F} subcarriers with each subcarrier using exclusively a partial bandwidth

$$\Delta f = B/N_{\mathrm{F}}. \tag{1.1}$$

A number of N_{B} OFDM symbol slots constitute an OFDM frame. In this thesis, as mentioned in Section 1.2, we apply the MA scheme SDMA, which means that the K MTs of the SA are separated by resorting to the spatial domain. This also means that each of the K MTs has access to all N_{F} subcarriers.

In this thesis we consider non-blind channel estimation. Quite generally, non-blind channel estimation in OFDM systems is enabled by radiating training or pilot symbols on certain subcarriers and in certain OFDM symbol slots [vdBES+95, ESvdB+96, Li99]. In the novel JCE scheme to be developed and studied in this thesis

- certain OFDM symbol slots are reserved for solely channel estimation, and
- in each of these OFDM symbol slots all K MTs of the SA are allowed to radiate pilot symbols simultaneously.

Within this general framework different options exist how to use the different subcarriers by the individual MTs. For example,

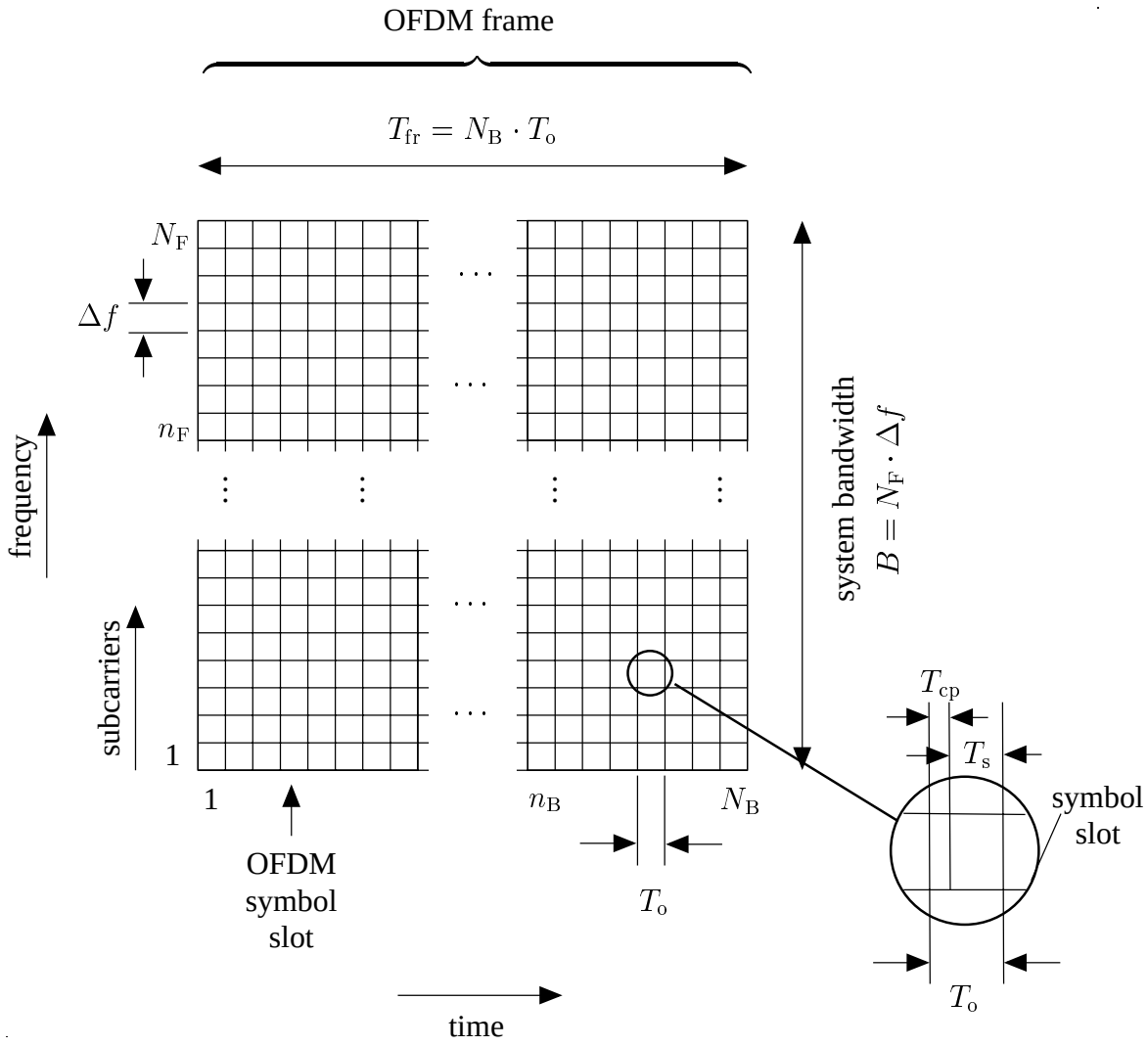

Fig. 1.5. Time-frequency representation of OFDM

- each of the K MTs may use all N_{F} subcarriers for pilot symbol transmission, or
- certain subcarriers are exclusively allotted to certain MTs.

The suitable choice between such options is an open question, which will be addressed in this thesis.

1.4 State of the art and open questions

Especially for the case of point–to–point OFDM transmission systems with single-element antennas at both the transmitter and the receiver, i. e., single–input–single–output (SISO)

channels are considered, the problem of channel estimation has been already intensively studied [ESvdB+96, LCS98]. In addition, in [Li99], a single–output–multiple–input (SIMO) channel is considered, and channel estimation is performed based on the minimum mean square error (MMSE) estimation principle [Wha71]. In [LSA99, Li02] and [LWS02], channel estimation in MIMO-OFDM systems applying transmit antenna diversity techniques is considered. JCE in multiuser OFDM systems has also been investigated e. g. in [SMWB01, KJ02, PK02, BXX+03]. In the case of JOINT, open questions in this respect concern

- the concise and correct mathematical formulation of an advantageous pilot based JCE algorithm,
- the introduction of suitable performance criteria for the pilot symbols, and
- the optimum choice of the pilot symbols.

The performance criteria to be elaborated in the thesis are quantities termed SNR degradation [Kle96, Pap00, SMWB01, Wec02, MWSL02] and variation coefficient [Hal67, Fis76, Sch90, Sch92, MWSL02]. As compared to channel estimation in point–to–point OFDM transmission systems, the price for separating different MTs in the process of JCE goes along with a decrease of the effective SNR. This decrease can be quantified by the SNR degradation, which characterizes the performance of the applied JCE in a SA of JOINT in the presence of noise. In addition, the interference stemming from adjacent SAs limits the performance of JCE in JOINT. The variation coefficient describes the impact of this inter-SA interference on the JCE performance.

1.5 Structure of the thesis

The thesis is structured according to the goals given in Section 1.4. Starting from the general case of a linear transmission system, Chapter 2 gives a brief overview of the conventional point–to–point OFDM transmission. The conventional OFDM transmission is characterized by its robustness against the delay spread of the mobile radio channel and by the simple signal processing due to the application of the FFT. Also, basic parametrization aspects concerning the dimensioning of the OFDM symbol slots with respect to the channel characteristics and to the maximum Doppler frequency are addressed.

Chapter 3 takes a closer look at the UL of JOINT. The problems of pilot-aided channel estimation and data estimation in the UL of JOINT are briefly described based on the multipoint–to–multipoint scenario in a SA. The problem of time synchronization in JOINT is discussed

and a proposal for the duration of the cyclic prefix is made. At the end of Chapter 3 a parameter set for JOINT is presented.

In Chapter 4 the main topic of the thesis, i. e., JCE, is presented. The multiuser scenario in the UL of a SA of JOINT is considered for the case of single-element receive antennas. Under the assumption of perfect time and frequency synchronization, the signal received at the APs and forwarded to the CU is a superposition of partial received signals containing the radiated complex amplitudes of the pilot symbols weighted with the respective channel coefficients plus the noise present at the APs. After reducing the number of unknown values to be estimated in the CU, maximum likelihood joint channel estimation is applied in order to gain estimates of the channel impulse responses and/or of the channel transfer functions characterizing the radio channels in the SA. At the end of Chapter 4, the two quality criteria mentioned in Section 1.4 are presented in order to characterize the performance of JCE in JOINT. The SNR degradation characterizes the performance of JCE in each SA of JOINT by comparing the SNR of the estimates gained by JCE in the case of multiuser pilot transmission to the SNR of the estimates of a reference system, the performance of which is considered as optimum. Since the real world application of JOINT will consist of multiple SAs, the variation coefficient is defined as the respective performance criterion giving a qualitative impression about the impact of inter-SA interference on the performance of JCE.

Chapter 5 addresses the topic of pilot vector design for JOINT. The aim of pilot vector design for JOINT is to generate such pilot vectors which maximize the achieved SNR and, thus, minimize the SNR degradation. A selection of four different methods of pilot vector design is presented. Randomly generated pilot vectors do not meet the requirement of minimum SNR degradation. On the contrary, the pilot vectors based on the approach of disjoint subcarriers, the pilot vectors based on Walsh codes and the pilot vectors based on CAZAC codes achieve said minimization of the SNR degradation. The performance of the pilot vectors generated by these four pilot design methods is also studied in terms of the variation coefficient. Two adjacent SAs are considered along with the worst case, where both SAs are in pilot transmission mode and use the same frequency band. In order to keep the impact of the inter-SA interference low, adjacent SAs must apply different sets of pilot vectors. Only the pilot vectors generated based on the approach of disjoint subcarriers fail at fulfilling this requirement, since the resulting set of pilot vectors minimizing the SNR degradation is the only one possible for any fixed parameter triplet consisting of the number of available subcarriers, the number of active MTs and the dimension of the channel impulse response.

In Chapter 6 the enhancement of the JCE performance based on the application of multi-element receive antennas at the APs of JOINT is discussed. Applying array antennas at the APs of JOINT makes the inclusion of additional information in the estimation process feasible. This information may concern directional properties of the mobile radio channel and

also directional information about the undesired signals impinging at the AP array. In order to exploit said directional properties of the mobile radio channel, the directions of arrival of the desired signals impinging at the AP array antenna are included in the estimation process. To demonstrate this, the assumption of single direction of arrival per impinging signal is made along with the assumption of perfect knowledge of all directions of arrival at the CU. Further, the application of array antennas allows the exploitation of directional information about the undesired signals impinging at the AP array antenna. Two different directional scenarios are considered for the undesired signals, based on which, the performance of maximum likelihood JCE is investigated with respect to the SNR degradation. As an alternative to maximum likelihood, the application of the minimum mean square error estimation principle for JCE is also considered for the multi-element receive antenna case. In addition to the directional information, a-priori information concerning the radio channel can be included in the estimation process in the form of the power delay profile of the considered channel model. By the application of array antennas the SNR degradation is reduced by both maximum likelihood JCE and minimum mean square error JCE with the latter one outperforming due to the additional knowledge of the power delay profile of the radio channel. As stated above, for the considerations about the application of array antennas at the APs of JOINT, the assumption of perfect knowledge of the directions of arrival of the desired impinging signals is made. In reality, these directions of arrivals must be estimated by respective estimation techniques, which do not deliver perfect estimates. Therefore, at the end of Chapter 6 the impact of non-perfect knowledge of the directions of arrival on the performance of JCE is discussed. Again, the assumption of a single direction of arrival per impinging signal is made and maximum likelihood JCE is considered. Said impact is demonstrated by simulation results. It is also shown that the channel estimation error of a certain MT depends on the direction of arrival estimation error of only the same MT and it is not affected by the direction of arrival estimation errors of the remaining MTs.

Apart of the utilization of multi-element receive antennas at the APs of JOINT, the performance of JCE can be enhanced by the application of two dimensional channel estimation as discussed in Chapter 7. The algorithms presented this far both for single-element and multi-element receive antennas consider JCE over the subcarriers, i. e., one dimensionally in frequency direction. Two dimensional channel estimation also considers the possibility of channel estimation in time direction, that is over the OFDM symbol slots. Since the optimum two dimensional channel estimator is prohibitively complex, two consecutive one dimensional channel estimators are considered instead. Therefore, in an additional step to one dimensional JCE over the subcarriers, the one dimensional channel estimation over the OFDM symbol slots is performed based on interpolation techniques.

Chapter 8 tackles the impact of non-perfect channel knowledge on the performance of data estimation in the UL and in the DL of JOINT. The respective techniques applied in JOINT

- JD in the UL and JT in the DL - rely on the channel knowledge gained by JCE in order to deliver the data estimates. The impact of the time variance of the radio channel is not considered since the radio channel is assumed as time invariant for the time period elapsing between the application of JCE and JD and for the time period elapsing between the application JCE and JT, respectively. Therefore, only the noise present at the APs affects the quality of the channel estimates and results to a channel estimation error. In the case of JD, this channel estimation error provokes a data estimation error at the CU additiv to the one already caused by the presence of noise at the APs. The bit error probability is consulted for the performance of JD, which is degraded as compared to the case of perfect channel knowledge. Similar is the impact of non-perfect channel knowledge on the performance of JT in the DL of JOINT. In addition to the degradation of the bit error probability performance, the transmit energy of JT is also increased as compared to the case of perfect channel knowledge.

Finally, Chapter 9 summarizes the thesis.

Chapter 2

Brief review of conventional point–to–point OFDM transmission

2.1 Motivation

In order to generate a solid basis for the considerations in the following chapters, which concern the problem of JCE in multipoint–to–multipoint OFDM transmission systems, in the present Chapter 2 a brief review of conventional point–to–point OFDM transmission is given, which relies on the abound literature available in this field [Doe57, WE71, PR80, Bin90, Pra98, KS01, FK03].

2.2 Channel and data estimation

Let us first consider a general linear transmission system as shown in Fig. 2.1a in the undisturbed case [Kle96]. At the input to this system we have a complex vector

$$\underline{\mathbf{x}} = (\underline{x}_1 \ \ldots \ \underline{x}_N)^{\mathrm{T}}, \tag{2.1}$$

and this input vector leads to the vector

$$\underline{\mathbf{y}} = \left(\underline{y}_1 \ \ldots \ \underline{y}_N\right)^{\mathrm{T}} \tag{2.2}$$

at the system output. With the system matrix

$$\underline{\mathbf{A}} \in \mathbb{C}^{N \times N} \tag{2.3}$$

the relation between $\underline{\mathbf{x}}$ and $\underline{\mathbf{y}}$ reads

$$\underline{\mathbf{y}} = \underline{\mathbf{A}} \ \underline{\mathbf{x}}. \tag{2.4}$$

Usually, it would be desirable that $\underline{\mathbf{A}}$ is a diagonal matrix, because then a unique relation between each component $\underline{x}_n$ of $\underline{\mathbf{x}}$ of (2.1) and the corresponding component $\underline{y}_n$ of $\underline{\mathbf{y}}$ of (2.2) exists. In the case of transmission situations suffering from ISI and MAI, $\underline{\mathbf{A}}$ would not a priori fulfill this desire, and various methods to achieve a diagonalization of $\underline{\mathbf{A}}$ are known [Kle96, Ver98, Pap00].

a)

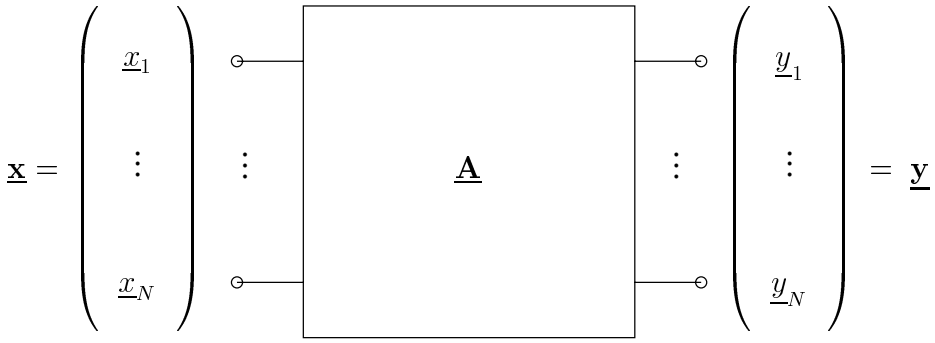

b)

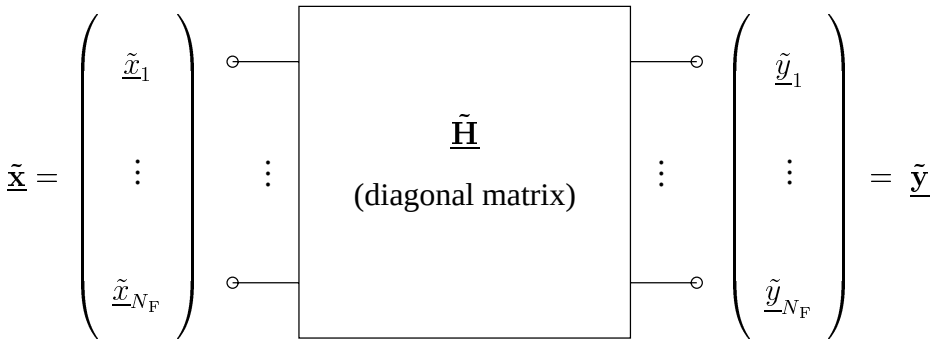

Fig. 2.1. Linear transmission system
a) general case,
b) OFDM point-to-point transmission

In the case of OFDM transmission systems, see Fig. 2.1b, the components $\underline{x}_n$ of $\underline{\mathbf{x}}$ of (2.1) and the components $\underline{y}_n$ of $\underline{\mathbf{y}}$ of (2.2) represent complex amplitudes of the different subcarriers n_{F}, $n_{\mathrm{F}} = 1 \ldots N_{\mathrm{F}}$. If we designate complex amplitudes by a tilde, we may write instead of $\underline{\mathbf{x}}$ of (2.1)

$$\underline{\tilde{\mathbf{x}}} = \left(\underline{\tilde{x}}_1 \ \ldots \ \underline{\tilde{x}}_{N_{\mathrm{F}}}\right)^{\mathrm{T}} \tag{2.5}$$

and instead of $\underline{\mathbf{y}}$ of (2.2)

$$\underline{\tilde{\mathbf{y}}} = \left(\underline{\tilde{y}}_1 \ \ldots \ \underline{\tilde{y}}_{N_{\mathrm{F}}}\right)^{\mathrm{T}}. \tag{2.6}$$

Conventional OFDM transmission is characterized by

- providing a cyclic prefix in the radiated signals in order to cope with the delay spread of the radio channel [PR80, Bin90], and

- utilizing plain FFT for processing the received signals [WE71, Bin90].

Thanks to these two characteristics, we obtain a diagonal system matrix in the case of OFDM transmission. We term this matrix $\underline{\tilde{\mathbf{H}}}$, and its diagonal elements $\underline{\tilde{h}}_{n_\mathrm{F}}$, $n_\mathrm{F} = 1 \ldots N_\mathrm{F}$, are the values of the channel transfer function (CTF) for the N_F different subcarrier frequencies [SMWB01, SWBC02]. To conclude, we can write

$$\underline{\tilde{\mathbf{y}}} = \left(\underline{\tilde{y}}_1 \ \ldots \ \underline{\tilde{y}}_{N_\mathrm{F}}\right)^\mathrm{T} = \begin{pmatrix} \underline{\tilde{h}}_1 & \cdots & 0 \\ \vdots & \ddots & \vdots \\ 0 & \cdots & \underline{\tilde{h}}_{N_\mathrm{F}} \end{pmatrix} \left(\underline{\tilde{x}}_1 \ \ldots \ \underline{\tilde{x}}_{N_\mathrm{F}}\right)^\mathrm{T} = \underline{\tilde{\mathbf{H}}} \ \underline{\tilde{\mathbf{x}}} \tag{2.7}$$

in the case of conventional point–to–point OFDM transmission, if no noise is present.

In the case of channel estimation, a vector $\underline{\tilde{\mathbf{x}}}$ to be also known in the receiver is radiated, and the diagonal elements $\underline{\tilde{h}}_{n_\mathrm{F}}$ of $\underline{\tilde{\mathbf{H}}}$ of (2.7) have to be estimated based on this knowledge and the received signal $\underline{\tilde{\mathbf{y}}}$. In the case of data estimation, $\underline{\tilde{\mathbf{H}}}$ is assumed to be known in the receiver, and based on this knowledge and the received signal $\underline{\tilde{\mathbf{y}}}$ now $\underline{\tilde{\mathbf{x}}}$ has to be estimated. In the above mentioned case of absent noise, said estimations would lead to the true $\underline{\tilde{\mathbf{H}}}$ or $\underline{\tilde{\mathbf{x}}}$, respectively. Under the impact of noise, estimation errors would occur.

2.3 Parametrization aspects

We return for the moment to Fig. 1.5. Each OFDM symbol slot consists of two parts [Pra98, vNP00, FK03]:

- The OFDM symbol of duration T_s, which contains the data or the pilots to be transmitted by being mapped on the subcarriers, and
- the above mentioned cyclic prefix of duration T_cp, which contains a cyclic extension of the OFDM symbol [PR80, vNP00].

Consequently,

$$T_\mathrm{o} = T_\mathrm{cp} + T_\mathrm{s} \tag{2.8}$$

holds for the duration of the OFDM symbol slot.

Fig. 2.2 shows schematically the magnitude $|\underline{h}(\tau)|$ of a radio channel impulse response (CIR) versus τ. Such a CIR can be characterized by

- its minimum delay τ_min,
- its maximum delay τ_max, and

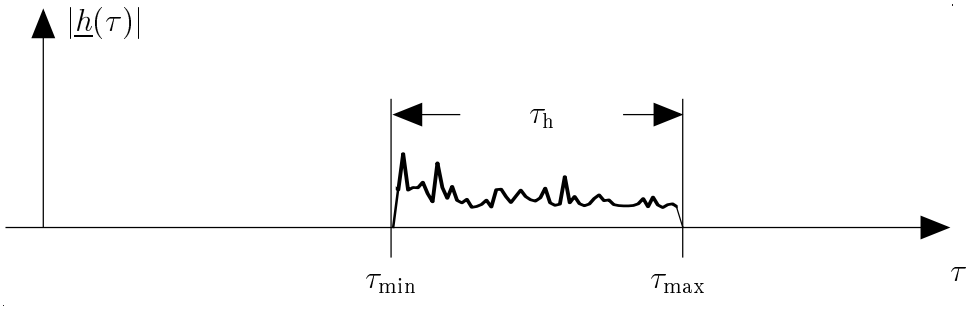

Fig. 2.2. Schematic run of the magnitude $|\underline{h}(\tau)|$ of a CIR $\underline{h}(\tau)$

- its duration

$$\tau_{\mathrm{h}} = \tau_{\mathrm{max}} - \tau_{\mathrm{min}} \ . \tag{2.9}$$

Now, following the well known rationale of conventional OFDM [WE71, Bin90, vNP00, FK03], certain relations have to be fulfilled between the quantities Δf, T_{s}, τ_{h} and T_{cp} introduced above. In order to achieve the orthogonality between adjacent subcarriers typical for OFDM and expressed by the fact that $\underline{\tilde{\mathbf{H}}}$ in Fig. 2.1b is a diagonal matrix,

$$T_{\mathrm{s}} \cdot \Delta f = 1 \tag{2.10}$$

has to be valid [Bin90, vNP00, FK03]. In order to obtain in the receiver on each subcarrier receive signals with a constant-envelope section of duration T_{s},

$$T_{\mathrm{cp}} \geq \tau_{\mathrm{h}} \tag{2.11}$$

has to be guaranteed [Bin90, vNP00, FK03], that is T_{cp} must not be smaller than τ_{h}. Providing a cyclic prefix of the required non-zero duration T_{cp} reduces transmission capacity and is the price to be paid for enabling low cost signal processing at the receiver by FFT also in the case of radio channels exhibiting a non-zero CIR duration τ_{h} [PR80, Bin90, Pra98, vNP00, FK03]. This price can be quantified by a quantity $T_{\mathrm{cp}}/T_{\mathrm{s}}$ termed overhead. Usually, OFDM systems are designed in such a way that

$$T_{\mathrm{cp}}/T_{\mathrm{s}} = 0.1 \ \ldots \ 0.25 \tag{2.12}$$

holds for the overhead [PR80, Bin90, Pra98, vNP00, FK03].

One of the drawbacks of the OFDM transmission technique is its sensitivity to Doppler shifts [vNP00, KS01, FK03]. A measure for the Doppler shift is the maximum Doppler frequency $f_{\mathrm{D,\,max}}$. With the carrier frequency f_{c}, the maximum relative velocity v_{max} between transmitter and receiver and the speed c_0 of light

$$f_{\mathrm{D,\,max}} = f_{\mathrm{c}} \frac{v_{\mathrm{max}}}{c_0} \tag{2.13}$$

holds [Kam96, Hay01]. The sensitivity of OFDM to Doppler shifts is assumed to be negligible if

$$\Delta f \gg f_{\mathrm{D,\,max}} \tag{2.14}$$

holds [vNP00, KS01, FK03], a requirement to be observed in OFDM system design.

Chapter 3

A closer look in the UL of JOINT

3.1 Motivation

As opposed to the well known point–to–point OFDM transmission system briefly described in Chapter 2, JOINT is a multipoint–to–multipoint OFDM transmission system, see Section 1.2. In the present Chapter 3 some details of the UL of JOINT will be considered. In these considerations we first introduce quantities and matrices to describe the relevant radio channels, see Section 3.2. Then, we deal with the problems of channel and data estimation in Sections 3.3 and 3.4, respectively. In Section 3.5 we briefly consider the problem of time synchronization in JOINT. Finally, in Section 3.6 parameter values to be applied in the numerical simulations of JCE for JOINT are given. In Chapter 3 we assume that each AP has only one antenna element, that is K_{A} is equal to one.

3.2 Radio channels

As explained in Section 1.3, we have to deal with KK_{B} radio channels in each SA of JOINT. The radio channel between MT k and AP k_{B} can be characterized by its channel impulse response (CIR) vector [SMWB01]

$$\underline{\mathbf{h}}^{(k,\,k_{\mathrm{B}})} = \left(\underline{h}_1^{(k,\,k_{\mathrm{B}})} \;\ldots\; \underline{h}_W^{(k,\,k_{\mathrm{B}})}\right)^{\mathrm{T}} \tag{3.1}$$

of dimension W. The channel can also be described in the frequency domain. Let us designate the CTF value of the channel between MT k and AP k_{B} on subcarrier n_{F} by $\underline{\tilde{h}}_{n_{\mathrm{F}}}^{(k,\,k_{\mathrm{B}})}$. Then, the channel between MT k and AP k_{B} can be characterized by the CTF vector

$$\underline{\tilde{\mathbf{h}}}^{(k,\,k_{\mathrm{B}})} = \left(\underline{\tilde{h}}_1^{(k,\,k_{\mathrm{B}})} \;\ldots\; \underline{\tilde{h}}_{N_{\mathrm{F}}}^{(k,\,k_{\mathrm{B}})}\right)^{\mathrm{T}} \tag{3.2}$$

of dimension N_{F}. For the sake of brevity we designate the vectors $\underline{\mathbf{h}}^{(k,\,k_{\mathrm{B}})}$ of (3.1) and $\underline{\tilde{\mathbf{h}}}^{(k,\,k_{\mathrm{B}})}$ of (3.2) as CIR or CTF, respectively, in what follows.

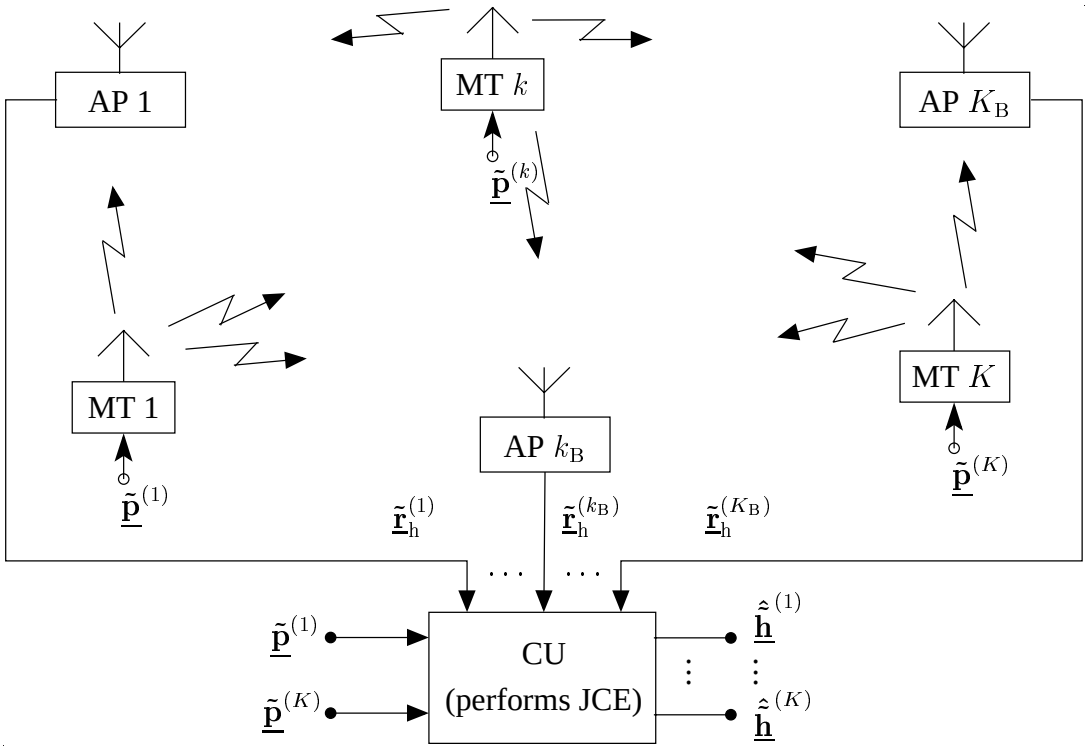

Fig. 3.1. JCE in a SA of JOINT

3.3 Channel estimation

Fig. 3.1 shows a more detailed display of a SA of JOINT for the case of JCE. For the purpose of JCE, MT k radiates subcarrier n_F with the complex amplitude $\underline{\tilde{p}}_{n_\mathrm{F}}^{(k)}$. The complex amplitudes $\underline{\tilde{p}}_{n_\mathrm{F}}^{(k)}$, $n_\mathrm{F} = 1 \ldots N_\mathrm{F}$, are termed pilots of MT k. The N_F pilots pertaining to MT k are stacked in the vector

$$\underline{\tilde{\mathbf{p}}}^{(k)} = \left(\underline{\tilde{p}}_1^{(k)} \ \ldots \ \underline{\tilde{p}}_{N_\mathrm{F}}^{(k)} \right)^\mathrm{T}. \tag{3.3}$$

This vector is termed the MT-specific pilot vector. $\underline{\tilde{\mathbf{p}}}^{(k)}$ of (3.3) has the energy

$$E_\mathrm{p}^{(k)} = \frac{1}{2} \, \underline{\tilde{\mathbf{p}}}^{(k)\mathsf{H}} \, \underline{\tilde{\mathbf{p}}}^{(k)}. \tag{3.4}$$

The subcarrier radiated by MT k at subcarrier frequency number n_F with the complex amplitude $\underline{\tilde{p}}_{n_\mathrm{F}}^{(k)}$ of (3.3) leads at AP k_B to a subcarrier with the same frequency and the complex amplitude $\underline{\tilde{e}}_{\mathrm{h},n_\mathrm{F}}^{(k,\,k_\mathrm{B})}$. The total signal originating in MT k and received at AP k_B can be written as

$$\underline{\tilde{\mathbf{e}}}_\mathrm{h}^{(k,\,k_\mathrm{B})} = \left(\underline{\tilde{e}}_{\mathrm{h},1}^{(k,\,k_\mathrm{B})} \ \ldots \ \underline{\tilde{e}}_{\mathrm{h},N_\mathrm{F}}^{(k,\,k_\mathrm{B})} \right)^\mathrm{T}. \tag{3.5}$$

The K signals $\underline{\tilde{\mathbf{e}}}_{\mathrm{h}}^{(k,\,k_{\mathrm{B}})}$ of (3.5) are now superimposed to form the total receive vector

$$\underline{\tilde{\mathbf{e}}}_{\mathrm{h}}^{(k_{\mathrm{B}})} = \sum_{k=1}^{K} \underline{\tilde{\mathbf{e}}}_{\mathrm{h}}^{(k,\,k_{\mathrm{B}})} = \left(\underline{\tilde{e}}_{\mathrm{h},1}^{(k_{\mathrm{B}})} \;\ldots\; \underline{\tilde{e}}_{\mathrm{h},N_{\mathrm{F}}}^{(k_{\mathrm{B}})}\right)^{\mathrm{T}} \tag{3.6}$$

at the AP k_{B}. This vector has the dimension N_{F} and is termed AP-specific receive vector for the case of UL channel estimation. It is communicated from the AP k_{B} to the CU. If noise

$$\underline{\tilde{\mathbf{n}}}_{\mathrm{h}}^{(k_{\mathrm{B}})} = \left(\underline{\tilde{n}}_{\mathrm{h},1}^{(k_{\mathrm{B}})} \;\ldots\; \underline{\tilde{n}}_{\mathrm{h},N_{\mathrm{F}}}^{(k_{\mathrm{B}})}\right)^{\mathrm{T}} \tag{3.7}$$

is superimposed on $\underline{\tilde{\mathbf{e}}}_{\mathrm{h}}^{(k_{\mathrm{B}})}$ of (3.6), then the CU obtains from AP k_{B} instead of $\underline{\tilde{\mathbf{e}}}^{(k_{\mathrm{B}})}$ of (3.6) the noise corrupted AP-specific receive vector

$$\underline{\tilde{\mathbf{r}}}_{\mathrm{h}}^{(k_{\mathrm{B}})} = \underline{\tilde{\mathbf{e}}}_{\mathrm{h}}^{(k_{\mathrm{B}})} + \underline{\tilde{\mathbf{n}}}_{\mathrm{h}}^{(k_{\mathrm{B}})}. \tag{3.8}$$

Now, with respect to JCE, the CU has the task to determine the estimates

$$\underline{\hat{\tilde{\mathbf{h}}}}^{(k,\,k_{\mathrm{B}})} = \left(\underline{\hat{\tilde{h}}}_{1}^{(k,\,k_{\mathrm{B}})} \;\ldots\; \underline{\hat{\tilde{h}}}_{N_{\mathrm{F}}}^{(k,\,k_{\mathrm{B}})}\right)^{\mathrm{T}} \tag{3.9}$$

of the KK_{B} CTFs of (3.2) on the basis of the known MT-specific pilot vectors $\underline{\tilde{\mathbf{p}}}^{(k)}$ of (3.3) and the AP-specific receive vectors $\underline{\tilde{\mathbf{r}}}_{\mathrm{h}}^{(k_{\mathrm{B}})}$ of (3.8).

3.4 Data estimation

Fig. 3.2 shows a more detailed display of a SA of JOINT for the case of UL data estimation. Each MT k radiates subcarrier n_{F} with a complex amplitude $\underline{\tilde{d}}_{n_{\mathrm{F}}}^{(k)}$ which represents a certain data symbol [Skl04, Liu05]. The N_{F} complex amplitudes pertaining to MT k are stacked in the vector

$$\underline{\tilde{\mathbf{d}}}^{(k)} = \left(\underline{\tilde{d}}_{1}^{(k)} \;\ldots\; \underline{\tilde{d}}_{N_{\mathrm{F}}}^{(k)}\right)^{\mathrm{T}} \tag{3.10}$$

of dimension N_{F}, which is termed the MT-specific data vector. The subcarrier radiated by MT k at subcarrier frequency n_{F} with the complex amplitude $\underline{\tilde{d}}_{n_{\mathrm{F}}}^{(k)}$ of (3.10) leads at AP k_{B} to a subcarrier with the same frequency and the complex amplitude $\underline{\tilde{e}}_{\mathrm{d},n_{\mathrm{F}}}^{(k,\,k_{\mathrm{B}})}$. The total signal originating in MT k and received at AP k_{B} can be written as

$$\underline{\tilde{\mathbf{e}}}_{\mathrm{d}}^{(k,\,k_{\mathrm{B}})} = \left(\underline{\tilde{e}}_{\mathrm{d},1}^{(k,\,k_{\mathrm{B}})} \;\ldots\; \underline{\tilde{e}}_{\mathrm{d},N_{\mathrm{F}}}^{(k,\,k_{\mathrm{B}})}\right)^{\mathrm{T}}. \tag{3.11}$$

The K signals $\underline{\tilde{\mathbf{e}}}_{\mathrm{d}}^{(k,\,k_{\mathrm{B}})}$ of (3.11) are now superimposed to form the total receive vector

$$\underline{\tilde{\mathbf{e}}}_{\mathrm{d}}^{(k_{\mathrm{B}})} = \sum_{k=1}^{K} \underline{\tilde{\mathbf{e}}}_{\mathrm{d}}^{(k,\,k_{\mathrm{B}})} = \left(\underline{\tilde{e}}_{\mathrm{d},1}^{(k_{\mathrm{B}})} \;\ldots\; \underline{\tilde{e}}_{\mathrm{d},N_{\mathrm{F}}}^{(k_{\mathrm{B}},\,N_{\mathrm{F}})}\right)^{\mathrm{T}} \tag{3.12}$$

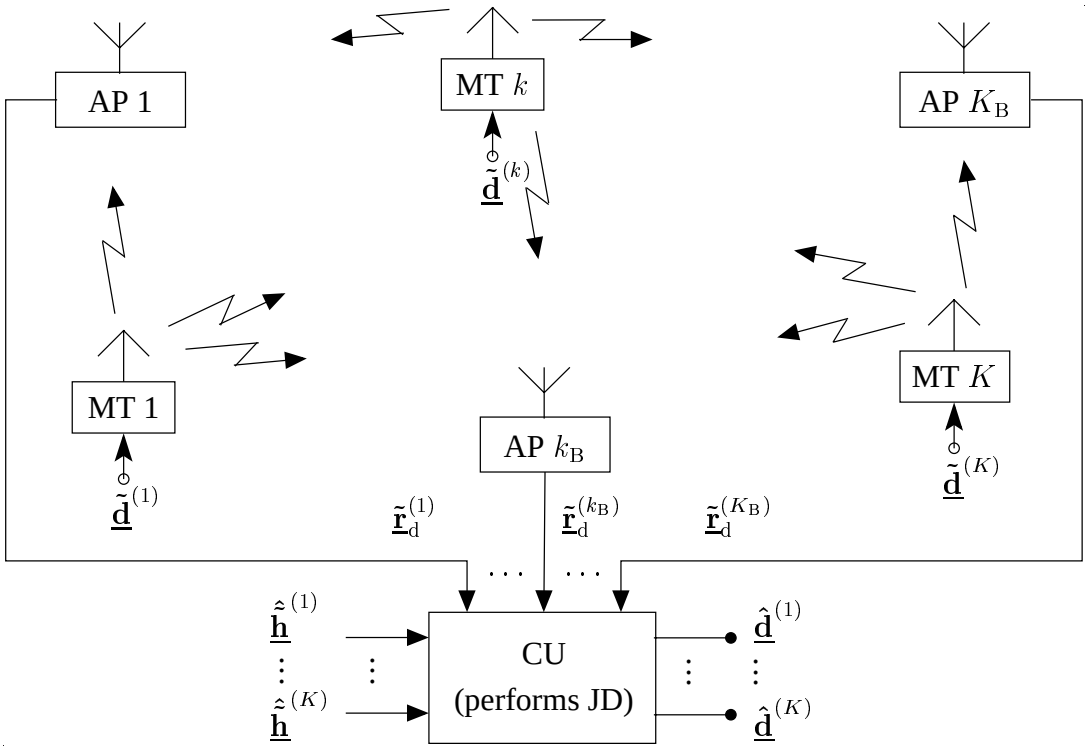

Fig. 3.2. UL data estimation in a SA of JOINT

at the AP k_{B}. This vector has the dimension N_{F} and is termed AP-specific receive vector for the case of UL data estimation. It is communicated from the AP k_{B} to the CU. If noise

$$\underline{\tilde{\mathbf{n}}}_{\mathrm{d}}^{(k_{\mathrm{B}})} = \left(\underline{\tilde{n}}_{\mathrm{d},1}^{(k_{\mathrm{B}})} \ \ldots \ \underline{\tilde{n}}_{\mathrm{d},N_{\mathrm{F}}}^{(k_{\mathrm{B}})}\right)^{\mathrm{T}} \tag{3.13}$$

is superimposed on $\underline{\tilde{\mathbf{e}}}_{\mathrm{d}}^{(k_{\mathrm{B}})}$ of (3.12), then the CU receives from AP k_{B} instead of $\underline{\tilde{\mathbf{e}}}_{\mathrm{d}}^{(k_{\mathrm{B}})}$ of (3.12) the noise corrupted AP-specific receive vector

$$\underline{\tilde{\mathbf{r}}}_{\mathrm{d}}^{(k_{\mathrm{B}})} = \underline{\tilde{\mathbf{e}}}_{\mathrm{d}}^{(k_{\mathrm{B}})} + \underline{\tilde{\mathbf{n}}}_{\mathrm{d}}^{(k_{\mathrm{B}})}. \tag{3.14}$$

Now, the CU has the task to determine estimates

$$\underline{\hat{\tilde{\mathbf{d}}}}^{(k)} = \left(\underline{\hat{\tilde{d}}}_{1}^{(k)} \ \ldots \ \underline{\hat{\tilde{d}}}_{N_{\mathrm{F}}}^{(k)}\right)^{\mathrm{T}} \tag{3.15}$$

of the K MT-specific data vectors $\underline{\tilde{\mathbf{d}}}^{(k)}$ of (3.10) on the basis of the estimates $\underline{\hat{\tilde{\mathbf{h}}}}^{(k,\,k_{\mathrm{B}})}$ of (3.9) of the KK_{B} CTFs $\underline{\tilde{\mathbf{h}}}^{(k,\,k_{\mathrm{B}})}$ of (3.2) and the received vectors $\underline{\tilde{\mathbf{r}}}_{\mathrm{d}}^{(k_{\mathrm{B}})}$ of (3.14).

3.5 Time synchronization

A crucial task in OFDM systems are time and frequency synchronization [KMH98, vNP00, FK03]. In this section we consider the problem of time synchronization. In the case of point–to–point OFDM transmission systems time synchronization is a well studied problem, which can be solved by controlling the timing reference of e. g. the transmitter [vNP00, FK03]. If we extend such a point–to–point system to a multipoint–to–point system as shown in

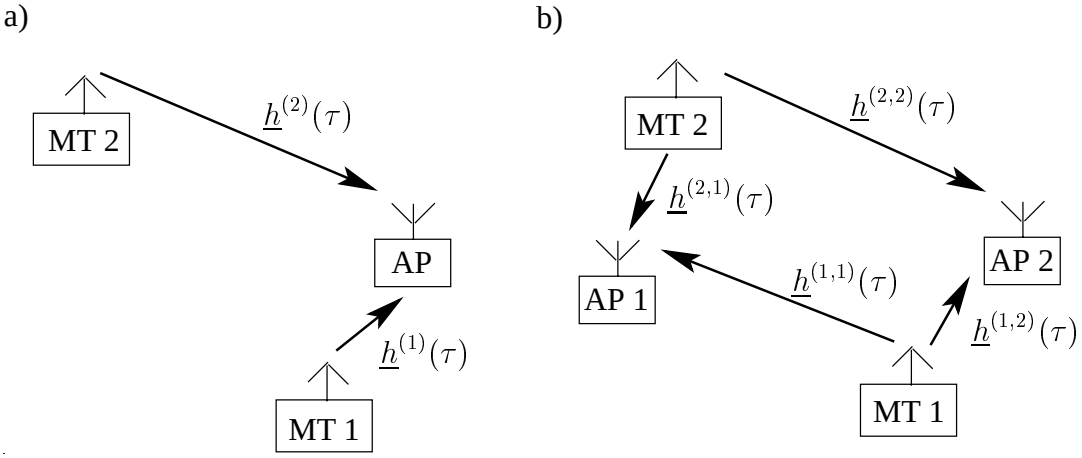

Fig. 3.3. Time synchronization issues in the UL
a) multipoint-to-point transmission
b) multipoint-to-multipoint transmission as in JOINT

Fig. 3.3a with different time delays between the MTs and the AP, also in this case well known solutions to the time synchronization problem exist [KMH98, vdBBB+99]. Totally different is the situation in the case of JOINT, see Fig. 3.3b, where we have a multipoint–to–multipoint system. In such a system - in the example of Fig. 3.3b we consider the case K and K_{B} equal to two - it is generally impossible to achieve that the signals of MT 1 and MT 2 arrive synchronously both at AP 1 and AP 2. An exception would be the unlikely situation that all distances between APs and MTs would be equal. In what follows we will briefly show how time synchronization of JOINT can be achieved in situations as the one shown in Fig.3.3b. Fig. 3.4 shows schematically the magnitudes of the four CIRs $\underline{h}^{(k,\ k_{\mathrm{B}})}(\tau)$, $k,\ k_{\mathrm{B}} \in \{1,\ 2\}$ introduced in Fig. 3.3b, which have the minimum and maximum delays $\tau_{\mathrm{min}}^{(k,\ k_{\mathrm{B}})}$ and $\tau_{\mathrm{max}}^{(k,\ k_{\mathrm{B}})}$, respectively. The smallest allowed value of T_{cp} would be given by the maximum difference

$$\tau_{\mathrm{sup}} = \max_{k,k_{\mathrm{B}}} \left(\tau^{(k,\ k_{\mathrm{B}})}\right) \tag{3.16}$$

of the maximum and minimum delays over all K CIRs. In the example of Fig. 3.3 we would obtain

$$T_{\mathrm{cp}} \geq T_{\mathrm{cp,min}} = \tau_{\mathrm{max}}^{(1,1)} - \tau_{\mathrm{min}}^{(1,2)}. \tag{3.17}$$

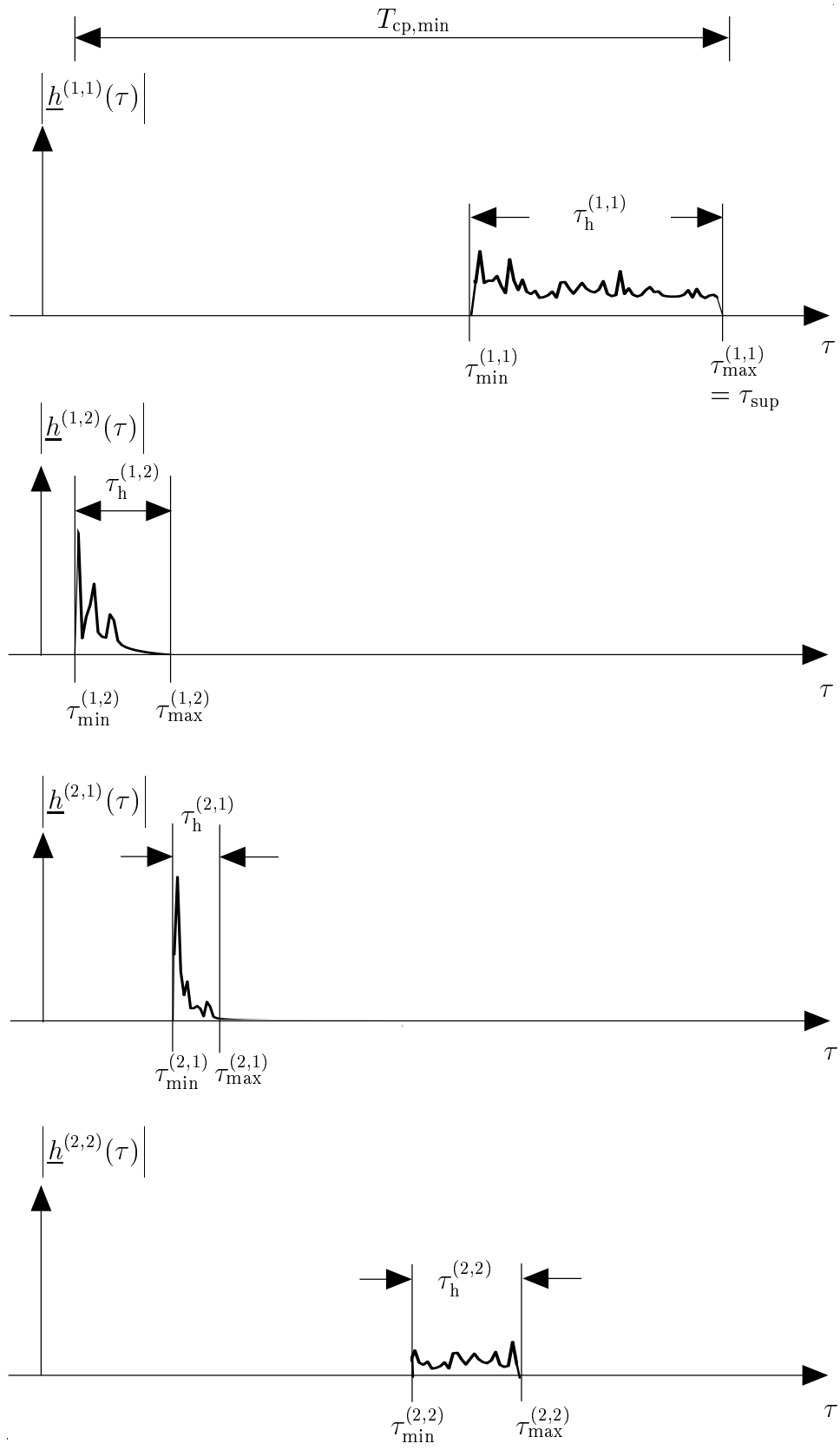

Fig. 3.4. Choice of the duration T_{cp} of the cyclic prefix in JOINT

3.6 Parametrization

In order to illustrate the theoretical considerations of this thesis by quantitative examples, a certain parameter set of JOINT should be chosen. In this section such a parameter set will be introduced, which later serves as a basis for the simulations of the JCE algorithms. Table 3.1 shows the basic system setting chosen in our quantitative investigations of JOINT. Table 3.2 shows specific parameter choices which take into consideration the parametrization aspects discussed in Section 2.3.

Table 3.1. Basic system setting

quantity	**value**
system bandwidth	B=20 MHz
carrier frequency	f_{c}=5.5 GHz
maximum velocity	$v_{\max}$=200 km/h
maximum Doppler frequency	$f_{\mathrm{D,\ max}}$=1.018 kHz

Table 3.2. Specific parameter choices

parameter	**value**
OFDM symbol duration	$T_{\mathrm{s}} = 25.6\ \mu$s
cyclic prefix duration	$T_{\mathrm{cp}} = 6.4\ \mu$s
OFDM symbol slot duration	$T_{\mathrm{o}} = 32\ \mu$s
number of subcarriers (FFT length)	N_{F}=512
subcarrier spacing	Δf=39.063 kHz
modulation	QAM

Chapter 4

Joint channel estimation in JOINT

4.1 Preliminary remarks

As explained in Section 1.3, see Fig. 1.4, the problem of estimating the properties of $KK_{\mathrm{B}}K_{\mathrm{A}}$ channels by JCE in JOINT can be reduced to the simpler problem of estimating only the properties of the K channels from all K MTs to a single AP antenna element. Then, in order to obtain the required estimates of the properties of all $KK_{\mathrm{B}}K_{\mathrm{A}}$ channels, see Fig. 1.3, said procedure for the case of a single-element AP antenna has to be simultaneously performed in total $K_{\mathrm{B}}K_{\mathrm{A}}$ times. In what follows we focus on the case of a single-element AP antenna. Then, we can drop the superscript k_{B} in (3.1), (3.2), (3.6), (3.7), (3.8) and (3.9). Because we now, as opposed to the considerations in Chapter 3, do not have to discern between channel estimation and data estimation marked by the subscripts h or d, respectively, we can also omit the subscript h in (3.6) to (3.8). Then, we obtain instead of (3.1), (3.2), (3.6), (3.7), (3.8) and (3.9)

$$\underline{\mathbf{h}}^{(k)} = \left(\underline{h}_1^{(k)} \ \ldots \ \underline{h}_W^{(k)}\right)^{\mathrm{T}}, \tag{4.1}$$

$$\underline{\tilde{\mathbf{h}}}^{(k)} = \left(\underline{\tilde{h}}_1^{(k)} \ \ldots \ \underline{\tilde{h}}_{N_{\mathrm{F}}}^{(k)}\right)^{\mathrm{T}}, \tag{4.2}$$

$$\underline{\tilde{\mathbf{e}}} = \left(\underline{\tilde{e}}_1 \ \ldots \ \underline{\tilde{e}}_{N_{\mathrm{F}}}\right)^{\mathrm{T}}, \tag{4.3}$$

$$\underline{\tilde{\mathbf{n}}} = \left(\underline{\tilde{n}}_1 \ \ldots \ \underline{\tilde{n}}_{N_{\mathrm{F}}}\right)^{\mathrm{T}}, \tag{4.4}$$

$$\underline{\tilde{\mathbf{r}}} = \underline{\tilde{\mathbf{e}}} + \ \underline{\tilde{\mathbf{n}}}, \tag{4.5}$$

and

$$\underline{\hat{\tilde{\mathbf{h}}}}^{(k)} = \left(\underline{\hat{\tilde{h}}}_1^{(k)} \ \ldots \ \underline{\hat{\tilde{h}}}_{N_{\mathrm{F}}}^{(k)}\right)^{\mathrm{T}}, \tag{4.6}$$

respectively.

4.2 Signal available at the CU

With the MT-specific pilot vector $\underline{\tilde{\mathbf{p}}}^{(k)}$ of (3.3) we form the MT-specific pilot matrix

$$\underline{\tilde{\mathbf{P}}}^{(k)} = \begin{pmatrix} \underline{\tilde{p}}_1^{(k)} & \cdots & 0 \\ \vdots & \ddots & \vdots \\ 0 & \cdots & \underline{\tilde{p}}_{N_\mathrm{F}}^{(k)} \end{pmatrix} = \mathrm{diag}\left(\underline{\tilde{\mathbf{p}}}^{(k)} \right) \tag{4.7}$$

of dimension $N_\mathrm{F} \times N_\mathrm{F}$. Then, with $\underline{\tilde{\mathbf{h}}}^{(k)}$ of (4.2) and in the case of absent noise, we obtain the output signal

$$\underline{\tilde{\mathbf{e}}}^{(k)} = \underline{\tilde{\mathbf{P}}}^{(k)} \underline{\tilde{\mathbf{h}}}^{(k)} \tag{4.8}$$

of dimension N_F of the radio channel between MT k and the considered AP antenna element. The K MT-specific CTFs $\underline{\tilde{\mathbf{h}}}^{(k)}$ of (4.2) and the K MT-specific pilot matrices $\underline{\tilde{\mathbf{P}}}^{(k)}$ of (4.7) can be stacked to form the total CTF

$$\begin{aligned} \underline{\tilde{\mathbf{h}}} &= \left(\underline{\tilde{\mathbf{h}}}^{(1)^\mathrm{T}} \ \ldots \ \underline{\tilde{\mathbf{h}}}^{(K)^\mathrm{T}} \right)^\mathrm{T} \\ &= \left(\underline{\tilde{h}}_1^{(1)} \ \ldots \ \underline{\tilde{h}}_{N_\mathrm{F}}^{(1)} \ \ldots \ \underline{\tilde{h}}_1^{(K)} \ \ldots \ \underline{\tilde{h}}_{N_\mathrm{F}}^{(K)} \right)^\mathrm{T} = \left(\underline{\tilde{h}}_1 \ \ldots \ \underline{\tilde{h}}_{KN_\mathrm{F}} \right)^\mathrm{T} \end{aligned} \tag{4.9}$$

of dimension KN_F and the total pilot matrix

$$\underline{\tilde{\mathbf{P}}} = \left(\underline{\tilde{\mathbf{P}}}^{(1)} \ \ldots \ \underline{\tilde{\mathbf{P}}}^{(K)} \right) \tag{4.10}$$

of dimension $N_\mathrm{F} \times (KN_\mathrm{F})$, respectively. With the received noise $\underline{\tilde{\mathbf{n}}}$ of (4.4) the total signal at the CU takes the form

$$\underline{\tilde{\mathbf{r}}} = \sum_{k=1}^{K} \underline{\tilde{\mathbf{e}}}^{(k)} + \underline{\tilde{\mathbf{n}}} = \underline{\tilde{\mathbf{P}}}\, \underline{\tilde{\mathbf{h}}} + \underline{\tilde{\mathbf{n}}} \,. \tag{4.11}$$

Based on the signal $\underline{\tilde{\mathbf{r}}}$ of (4.11) the total CTF $\underline{\tilde{\mathbf{h}}}$ of (4.9) has to be estimated. (4.11) can be considered as a system of N_F equations, in which the matrix $\underline{\tilde{\mathbf{P}}}$ and the receive signal $\underline{\tilde{\mathbf{r}}}$ are known and the vectors $\underline{\tilde{\mathbf{h}}}$ and $\underline{\tilde{\mathbf{n}}}$ are unknown, and from which the KN_F unknown components $\underline{\tilde{h}}_{n_\mathrm{F}}^{(k)}$ of $\underline{\tilde{\mathbf{h}}}$ of (4.9) should be determined. Obviously, this system of equations is underdetermined, because $\underline{\tilde{\mathbf{P}}}$ of (4.10) is a wide matrix. Therefore, a unique solution cannot be obtained, unless the number of unknowns is reduced. As an important issue of this thesis, it will be shown that such a reduction is possible, if the dimension W of the CIRs $\underline{\mathbf{h}}^{(k)}$ is below a certain limit. Said reduction is the topic of Section 4.3.

For the sake of illustration, we consider the exemplary case characterized by the parameter triplet

$$\{N_\mathrm{F},\ K,\ W\} = \{4,\ 2,\ 2\} \tag{4.12}$$

and display (4.11) component-wise as follows:

$$\underline{\tilde{\mathbf{r}}} = \begin{pmatrix} \underline{\tilde{r}}_1 \\ \underline{\tilde{r}}_2 \\ \underline{\tilde{r}}_3 \\ \underline{\tilde{r}}_4 \end{pmatrix} = \begin{pmatrix} \underline{\tilde{p}}_1^{(1)} & 0 & 0 & 0 & \underline{\tilde{p}}_1^{(2)} & 0 & 0 & 0 \\ 0 & \underline{\tilde{p}}_2^{(1)} & 0 & 0 & 0 & \underline{\tilde{p}}_2^{(2)} & 0 & 0 \\ 0 & 0 & \underline{\tilde{p}}_3^{(1)} & 0 & 0 & 0 & \underline{\tilde{p}}_3^{(2)} & 0 \\ 0 & 0 & 0 & \underline{\tilde{p}}_4^{(1)} & 0 & 0 & 0 & \underline{\tilde{p}}_4^{(2)} \end{pmatrix} \cdot \begin{pmatrix} \underline{\tilde{h}}_1^{(1)} \\ \underline{\tilde{h}}_2^{(1)} \\ \underline{\tilde{h}}_3^{(1)} \\ \underline{\tilde{h}}_4^{(1)} \\ \underline{\tilde{h}}_1^{(2)} \\ \underline{\tilde{h}}_2^{(2)} \\ \underline{\tilde{h}}_3^{(2)} \\ \underline{\tilde{h}}_4^{(2)} \end{pmatrix} + \begin{pmatrix} \underline{\tilde{n}}_1 \\ \underline{\tilde{n}}_2 \\ \underline{\tilde{n}}_3 \\ \underline{\tilde{n}}_4 \end{pmatrix}$$

$$= \begin{pmatrix} \sum_{k=1}^{2} \underline{\tilde{p}}_1^{(k)} \underline{\tilde{h}}_1^{(k)} \\ \sum_{k=1}^{2} \underline{\tilde{p}}_2^{(k)} \underline{\tilde{h}}_2^{(k)} \\ \sum_{k=1}^{2} \underline{\tilde{p}}_3^{(k)} \underline{\tilde{h}}_3^{(k)} \\ \sum_{k=1}^{2} \underline{\tilde{p}}_4^{(k)} \underline{\tilde{h}}_4^{(k)} \end{pmatrix} + \begin{pmatrix} \underline{\tilde{n}}_1 \\ \underline{\tilde{n}}_2 \\ \underline{\tilde{n}}_3 \\ \underline{\tilde{n}}_4 \end{pmatrix}. \tag{4.13}$$

4.3 Reduction of the number of unknowns

Instead of characterizing the K radio channels between the MTs and the considered AP antenna element by their K CTFs $\underline{\tilde{\mathbf{h}}}^{(k)}$ of (4.2), that is in the frequency domain, these channels can be equivalently described in the time domain by their K CIRs $\underline{\mathbf{h}}^{(k)}$ of (4.1). The relation between $\underline{\tilde{\mathbf{h}}}^{(k)}$ and $\underline{\mathbf{h}}^{(k)}$ is determined by the calculus of the Fourier transformation [Rup93], and the crux of the proposed method for reducing the number of unknowns consists in estimating the components $\underline{h}_w^{(k)}$ of $\underline{\mathbf{h}}^{(k)}$ instead of estimating the components $\underline{\tilde{h}}_{n_\mathrm{F}}^{(k)}$ of $\underline{\tilde{\mathbf{h}}}^{(k)}$.

The dimension of $\underline{\tilde{\mathbf{h}}}^{(k)}$ of (4.2) is given by the number N_F of subcarriers. For determining the dimension W of the CIRs $\underline{\mathbf{h}}^{(k)}$ of (4.1) we set out from the timing situation typical of JOINT and illustrated in Fig. 3.4. Even though the CIRs $\underline{\mathbf{h}}^{(k,\,k_\mathrm{B})}$ – for the moment we again introduce the superscript k_B – are non-identically zero only for $\tau_{\min}^{(k,\,k_\mathrm{B})} \leq \tau \leq \tau_{\max}^{(k,\,k_\mathrm{B})}$, we formally assign to each of the KK_B CIRs the same duration τ_sup of (3.17) and assume that

$\underline{\mathbf{h}}^{(k,\,k_\mathrm{B})}$ is non-identically zero for $0 \leq \tau \leq \tau_\mathrm{sup}$. Then, according to the sampling theorem [Rup82], the relation

$$W = \tau_\mathrm{sup} \cdot B \tag{4.14}$$

between the dimension W of the CIRs $\underline{\mathbf{h}}^{(k)}$, the system bandwidth B and τ_sup exists.

It will be shown that the following considerations towards a reduction of the number of unknowns are based on the requirement that the number N_F of used subcarriers is not smaller than the product of the number K of MTs and the dimension W of the CIRs:

$$N_\mathrm{F} \geq KW. \tag{4.15}$$

This implies the requirement

$$N_\mathrm{F} > W. \tag{4.16}$$

(4.15) and (4.16) are fulfilled if the number W of elements of the CIRs $\underline{\mathbf{h}}^{(k)}$ and the number K of MTs are sufficiently small as compared to the number N_F of subcarriers. A reasonable assumption for practical situations may be that the number N_F of subcarriers and the dimension W of the CIRs $\underline{\mathbf{h}}^{(k)}$ are given by the chosen system setting and parametrization, see Tables 3.1 and 3.2. Then, from (4.15) follows the maximum number K of supportable MTs.

Quite generally, the dimensions of two vectors in the frequency domain or time domain, respectively, related by the Fourier transformation are equal. In our case of the CTF $\underline{\tilde{\mathbf{h}}}^{(k)}$ and the CIR $\underline{\mathbf{h}}^{(k)}$, due to (4.16) these dimensions are different. In order to obtain formally a CIR with a dimension equal to the dimension N_F of $\underline{\tilde{\mathbf{h}}}^{(k)}$, $\underline{\mathbf{h}}^{(k)}$ is padded by $N_\mathrm{F} - W$ zero elements, which leads to the modified CIR

$$\underline{\mathbf{h}}_0^{(k)} = \underbrace{\Big(\overbrace{\underline{h}_1^{(k)} \ \ldots \ \underline{h}_W^{(k)}}^{W} \overbrace{0 \ \ldots \ 0}^{N_\mathrm{F}-W}\Big)^\mathrm{T}}_{N_\mathrm{F}}. \tag{4.17}$$

Now, with the Fourier matrix [Rup93]

$$\underline{\tilde{\boldsymbol{\mathcal{F}}}} = \begin{pmatrix} 1 & 1 & 1 & \cdots & 1 \\ 1 & \mathrm{e}^{-\mathrm{j}\frac{2\pi}{N_\mathrm{F}}} & \mathrm{e}^{-\mathrm{j}\frac{4\pi}{N_\mathrm{F}}} & \cdots & \mathrm{e}^{-\mathrm{j}\frac{2\pi(N_\mathrm{F}-1)}{N_\mathrm{F}}} \\ 1 & \mathrm{e}^{-\mathrm{j}\frac{4\pi}{N_\mathrm{F}}} & \mathrm{e}^{-\mathrm{j}\frac{8\pi}{N_\mathrm{F}}} & \cdots & \mathrm{e}^{-\mathrm{j}\frac{2\pi 2(N_\mathrm{F}-1)}{N_\mathrm{F}}} \\ \vdots & \vdots & \vdots & \cdots & \vdots \\ 1 & \mathrm{e}^{-\mathrm{j}\frac{2\pi(N_\mathrm{F}-1)}{N_\mathrm{F}}} & \mathrm{e}^{-\mathrm{j}\frac{2\pi 2(N_\mathrm{F}-1)}{N_\mathrm{F}}} & \cdots & \mathrm{e}^{-\mathrm{j}\frac{2\pi(N_\mathrm{F}-1)^2}{N_\mathrm{F}}} \end{pmatrix} \tag{4.18}$$

$$= \begin{pmatrix} \underbrace{1}_{\underline{\tilde{\mathbf{f}}}_1} & \underbrace{1}_{\underline{\tilde{\mathbf{f}}}_2} & \underbrace{1}_{\underline{\tilde{\mathbf{f}}}_3} & \cdots & \underbrace{1}_{\underline{\tilde{\mathbf{f}}}_{N_\mathrm{F}}} \\ 1 & \mathrm{e}^{-\mathrm{j}\frac{2\pi}{N_\mathrm{F}}} & \mathrm{e}^{-\mathrm{j}\frac{4\pi}{N_\mathrm{F}}} & \cdots & \mathrm{e}^{-\mathrm{j}\frac{2\pi(N_\mathrm{F}-1)}{N_\mathrm{F}}} \\ 1 & \mathrm{e}^{-\mathrm{j}\frac{4\pi}{N_\mathrm{F}}} & \mathrm{e}^{-\mathrm{j}\frac{8\pi}{N_\mathrm{F}}} & \cdots & \mathrm{e}^{-\mathrm{j}\frac{2\pi 2(N_\mathrm{F}-1)}{N_\mathrm{F}}} \\ \vdots & \vdots & \vdots & \cdots & \vdots \\ 1 & \mathrm{e}^{-\mathrm{j}\frac{2\pi(N_\mathrm{F}-1)}{N_\mathrm{F}}} & \mathrm{e}^{-\mathrm{j}\frac{2\pi 2(N_\mathrm{F}-1)}{N_\mathrm{F}}} & \cdots & \mathrm{e}^{-\mathrm{j}\frac{2\pi(N_\mathrm{F}-1)^2}{N_\mathrm{F}}} \end{pmatrix}$$

$$= \left(\left(\underline{\tilde{f}}_{1,1} \ \dots \ \underline{\tilde{f}}_{1,N_\mathrm{F}} \right)^\mathrm{T} \ \dots \ \left(\underline{\tilde{f}}_{N_\mathrm{F},1} \ \dots \ \underline{\tilde{f}}_{N_\mathrm{F},N_\mathrm{F}} \right)^\mathrm{T} \right) = \left(\underline{\tilde{\mathbf{f}}}_1 \ \dots \underline{\tilde{\mathbf{f}}}_{N_\mathrm{F}} \right)$$

of dimension $N_\mathrm{F} \times N_\mathrm{F}$ the relation

$$\underline{\tilde{\mathbf{h}}}^{(k)} = \underline{\tilde{\boldsymbol{\mathcal{F}}}} \, \underline{\mathbf{h}}_0^{(k)} \tag{4.19}$$

between $\underline{\tilde{\mathbf{h}}}^{(k)}$ of (4.2) and $\underline{\mathbf{h}}_0^{(k)}$ of (4.17) holds. This relation can be equivalently expressed by the reduced Fourier matrix $\left[\underline{\tilde{\boldsymbol{\mathcal{F}}}}\right]_{N_\mathrm{F},W}^{1,1}$ of dimension $N_\mathrm{F} \times W$, which consists of the first W columns of the Fourier matrix $\underline{\tilde{\boldsymbol{\mathcal{F}}}}$ of (4.18), and the CIR $\underline{\mathbf{h}}^{(k)}$ of (4.1) as

$$\underline{\tilde{\mathbf{h}}}^{(k)} = \left[\underline{\tilde{\boldsymbol{\mathcal{F}}}}\right]_{N_\mathrm{F},W}^{1,1} \underline{\mathbf{h}}^{(k)} = \left(\underline{\tilde{\mathbf{f}}}_1 \ \dots \ \underline{\tilde{\mathbf{f}}}_W \right) \underline{\mathbf{h}}^{(k)}. \tag{4.20}$$

By repeating the reduced Fourier matrices $\left[\underline{\tilde{\boldsymbol{\mathcal{F}}}}\right]_{N_\mathrm{F},W}^{1,1}$ in a blockdiagonal fashion and by stacking the K CIRs $\underline{\mathbf{h}}^{(k)}$ of (4.1) we obtain the full rank blockdiagonal matrix

$$\underline{\tilde{\boldsymbol{\mathcal{F}}}}_\mathrm{W} = \begin{pmatrix} \left[\underline{\tilde{\boldsymbol{\mathcal{F}}}}\right]_{N_\mathrm{F},W}^{1,1} & \cdots & 0 \\ \vdots & \ddots & \vdots \\ 0 & \cdots & \left[\underline{\tilde{\boldsymbol{\mathcal{F}}}}\right]_{N_\mathrm{F},W}^{1,1} \end{pmatrix} \tag{4.21}$$

of dimension $(KN_\mathrm{F}) \times (KW)$ and the total CIR

$$\begin{aligned} \underline{\mathbf{h}} &= \left(\underline{\mathbf{h}}^{(1)^\mathrm{T}} \ \dots \ \underline{\mathbf{h}}^{(K)^\mathrm{T}} \right)^\mathrm{T} = \left(\underline{h}_1^{(1)} \ \dots \ \underline{h}_W^{(1)} \ \dots \ \underline{h}_1^{(K)} \ \dots \ \underline{h}_W^{(K)} \right)^\mathrm{T} \\ &= \left(\underline{h}_1 \ \dots \ \underline{h}_{KW} \right)^\mathrm{T} \end{aligned} \tag{4.22}$$

of dimension KW, respectively. Now, $\underline{\tilde{\mathbf{h}}}$ of (4.9) can be expressed as

$$\underline{\tilde{\mathbf{h}}} = \underline{\tilde{\boldsymbol{\mathcal{F}}}}_\mathrm{W} \underline{\mathbf{h}}. \tag{4.23}$$

Finally, by substituting (4.23) into (4.11) we obtain

$$\underbrace{\tilde{\mathbf{e}}}_{\tilde{\mathbf{h}}} \quad \underbrace{\tilde{\mathbf{P}} \, \underbrace{\tilde{\boldsymbol{\mathcal{F}}}_\mathrm{W} \underline{\mathbf{h}}}_{\tilde{\boldsymbol{\mathcal{G}}}}}_{\tilde{\mathbf{h}}} + \ \tilde{\mathbf{n}} \, . \tag{4.24}$$

The matrix

$$\underline{\tilde{\boldsymbol{\mathcal{G}}}} = \begin{pmatrix} \underline{\tilde{g}}_{1,1} & \cdots & \underline{\tilde{g}}_{1,KW} \\ \vdots & & \vdots \\ \vdots & & \vdots \\ \underline{\tilde{g}}_{N_\mathrm{F},1} & \cdots & \underline{\tilde{g}}_{N_\mathrm{F},KW} \end{pmatrix} \tag{4.25}$$

of (4.24) has the dimension $N_{\mathrm{F}} \times (KW)$ and in analogy to the considerations in [Ste95, Kle96] is termed system matrix. Due to (4.15) it is a non-wide matrix. The situation that for a given value N_{F} the product KW is chosen equal to the maximum possible value N_{F} is designated as full system load. From the definition of $\underline{\tilde{\boldsymbol{\mathcal{G}}}}$ in (4.24) and (4.25) and of $\underline{\tilde{\boldsymbol{\mathcal{F}}}}_{\mathrm{W}}$ in (4.21) follows with the pilot energies $E_{\mathrm{p}}^{(k)}$ of (3.4)

$$\begin{aligned}
\mathrm{diag}\left(\underline{\tilde{\boldsymbol{\mathcal{G}}}}^{\mathsf{H}}\underline{\tilde{\boldsymbol{\mathcal{G}}}}\right) &= \mathrm{diag}\left(\underline{\tilde{\boldsymbol{\mathcal{F}}}}_{\mathrm{W}}^{\mathsf{H}}\,\underline{\tilde{\mathbf{P}}}^{\mathsf{H}}\,\underline{\tilde{\mathbf{P}}}\,\underline{\tilde{\boldsymbol{\mathcal{F}}}}_{\mathrm{W}}\right) \\
&= \begin{pmatrix}
\overbrace{2E_{\mathrm{p}}^{(1)} \;\; \ddots \;\; 2E_{\mathrm{p}}^{(1)}}^{W} & \cdots & 0 \\
\vdots & & \vdots \\
\vdots & & \overbrace{2E_{\mathrm{p}}^{(K)} \;\; \ddots \;\; 2E_{\mathrm{p}}^{(K)}}^{W}
\end{pmatrix} \Bigg\} KW,
\end{aligned} \tag{4.26}$$

that is the W columns of $\underline{\tilde{\boldsymbol{\mathcal{G}}}}$ pertaining to MT k have the norm $2E_{\mathrm{p}}^{(k)}$. For the parameter triplet of (4.12), (4.24) can be component-wise presented as

$$\begin{aligned}
\underline{\tilde{\mathbf{r}}} = \begin{pmatrix} \underline{\tilde{r}}_1 \\ \underline{\tilde{r}}_2 \\ \underline{\tilde{r}}_3 \\ \underline{\tilde{r}}_4 \end{pmatrix} &= \begin{pmatrix}
\underline{\tilde{p}}_1^{(1)} & 0 & 0 & 0 & \underline{\tilde{p}}_1^{(2)} & 0 & 0 & 0 \\
0 & \underline{\tilde{p}}_2^{(1)} & 0 & 0 & 0 & \underline{\tilde{p}}_2^{(2)} & 0 & 0 \\
0 & 0 & \underline{\tilde{p}}_3^{(1)} & 0 & 0 & 0 & \underline{\tilde{p}}_3^{(2)} & 0 \\
0 & 0 & 0 & \underline{\tilde{p}}_4^{(1)} & 0 & 0 & 0 & \underline{\tilde{p}}_4^{(2)}
\end{pmatrix} \cdot \\
&\quad \begin{pmatrix}
\underline{\tilde{f}}_{1,1} & \underline{\tilde{f}}_{1,2} & 0 & 0 \\
\underline{\tilde{f}}_{2,1} & \underline{\tilde{f}}_{2,2} & 0 & 0 \\
\underline{\tilde{f}}_{3,1} & \underline{\tilde{f}}_{3,2} & 0 & 0 \\
\underline{\tilde{f}}_{4,1} & \underline{\tilde{f}}_{4,2} & 0 & 0 \\
0 & 0 & \underline{\tilde{f}}_{1,1} & \underline{\tilde{f}}_{1,2} \\
0 & 0 & \underline{\tilde{f}}_{2,1} & \underline{\tilde{f}}_{2,2} \\
0 & 0 & \underline{\tilde{f}}_{3,1} & \underline{\tilde{f}}_{3,2} \\
0 & 0 & \underline{\tilde{f}}_{4,1} & \underline{\tilde{f}}_{4,2}
\end{pmatrix} \cdot \begin{pmatrix} \underline{h}_1^{(1)} \\ \underline{h}_2^{(1)} \\ \underline{h}_1^{(2)} \\ \underline{h}_2^{(2)} \end{pmatrix} + \begin{pmatrix} \underline{\tilde{n}}_1 \\ \underline{\tilde{n}}_2 \\ \underline{\tilde{n}}_3 \\ \underline{\tilde{n}}_4 \end{pmatrix} \\
&= \begin{pmatrix}
\underline{\tilde{p}}_1^{(1)}\underline{\tilde{f}}_{1,1} & \underline{\tilde{p}}_1^{(1)}\underline{\tilde{f}}_{1,2} & \underline{\tilde{p}}_1^{(2)}\underline{\tilde{f}}_{1,1} & \underline{\tilde{p}}_1^{(2)}\underline{\tilde{f}}_{1,2} \\
\underline{\tilde{p}}_2^{(1)}\underline{\tilde{f}}_{2,1} & \underline{\tilde{p}}_2^{(1)}\underline{\tilde{f}}_{2,2} & \underline{\tilde{p}}_2^{(2)}\underline{\tilde{f}}_{2,1} & \underline{\tilde{p}}_2^{(2)}\underline{\tilde{f}}_{2,2} \\
\underline{\tilde{p}}_3^{(1)}\underline{\tilde{f}}_{3,1} & \underline{\tilde{p}}_3^{(1)}\underline{\tilde{f}}_{3,2} & \underline{\tilde{p}}_3^{(2)}\underline{\tilde{f}}_{3,1} & \underline{\tilde{p}}_3^{(2)}\underline{\tilde{f}}_{3,2} \\
\underline{\tilde{p}}_4^{(1)}\underline{\tilde{f}}_{4,1} & \underline{\tilde{p}}_4^{(1)}\underline{\tilde{f}}_{4,2} & \underline{\tilde{p}}_4^{(2)}\underline{\tilde{f}}_{4,1} & \underline{\tilde{p}}_4^{(2)}\underline{\tilde{f}}_{4,2}
\end{pmatrix} \cdot \begin{pmatrix} \underline{h}_1^{(1)} \\ \underline{h}_2^{(1)} \\ \underline{h}_1^{(2)} \\ \underline{h}_2^{(2)} \end{pmatrix} + \begin{pmatrix} \underline{\tilde{n}}_1 \\ \underline{\tilde{n}}_2 \\ \underline{\tilde{n}}_3 \\ \underline{\tilde{n}}_4 \end{pmatrix}
\end{aligned} \tag{4.27}$$

$$= \begin{pmatrix} \underline{\tilde{g}}_{1,1} & \underline{\tilde{g}}_{1,2} & \underline{\tilde{g}}_{1,3} & \underline{\tilde{g}}_{1,4} \\ \underline{\tilde{g}}_{2,1} & \underline{\tilde{g}}_{2,2} & \underline{\tilde{g}}_{2,3} & \underline{\tilde{g}}_{2,4} \\ \underline{\tilde{g}}_{3,1} & \underline{\tilde{g}}_{3,2} & \underline{\tilde{g}}_{3,3} & \underline{\tilde{g}}_{3,4} \\ \underline{\tilde{g}}_{4,1} & \underline{\tilde{g}}_{4,2} & \underline{\tilde{g}}_{4,3} & \underline{\tilde{g}}_{4,4} \end{pmatrix} \cdot \begin{pmatrix} \underline{h}_1^{(1)} \\ \underline{h}_2^{(1)} \\ \underline{h}_1^{(2)} \\ \underline{h}_2^{(2)} \end{pmatrix} + \begin{pmatrix} \underline{\tilde{n}}_1 \\ \underline{\tilde{n}}_2 \\ \underline{\tilde{n}}_3 \\ \underline{\tilde{n}}_4 \end{pmatrix}.$$

(4.24) is a system of N_{F} equations, from which the KW unknown components $\underline{h}_w^{(k)}$ of the total CIR $\underline{\mathbf{h}}$ of (4.22) should be estimated. This estimation has to rely on the fact that the matrices $\underline{\tilde{\mathbf{P}}}$ and $\underline{\tilde{\boldsymbol{\mathcal{F}}}}_{\mathrm{W}}$ as well as the vector $\underline{\tilde{\mathbf{r}}}$ occurring in (4.24) are known in the receiver, whereas the vectors $\underline{\tilde{\mathbf{e}}}$, $\underline{\mathbf{h}}$, $\underline{\tilde{\mathbf{h}}}$ and $\underline{\tilde{\mathbf{n}}}$ are unknown. Said estimation is feasible, because the matrix $\underline{\tilde{\boldsymbol{\mathcal{G}}}}$ in (4.24) is assumed to be non-wide. This implies that the number KW of unknowns $\underline{h}_w^{(k)}$ in the system of equations (4.24) in the case of full system load just reaches the number N_{F} of equations and otherwise is always below N_{F}. $\underline{\tilde{\boldsymbol{\mathcal{G}}}}$ depends on the chosen pilot vectors $\underline{\tilde{\mathbf{p}}}^{(k)}$ of (3.3).

According to (4.24), each component $\underline{h}_w^{(k)}$ of $\underline{\mathbf{h}}$ of (4.22) entails a certain contribution $\underline{\tilde{\mathbf{r}}}_w^{(k)}$ to the receive signal $\underline{\tilde{\mathbf{r}}}$. If we designate with $[\cdot]_i$ the column i of a matrix in brackets, then

$$\underline{\tilde{\mathbf{r}}}_w^{(k)} = \left[\underline{\tilde{\boldsymbol{\mathcal{G}}}}\right]_{(k-1)W+w} \underline{h}_w^{(k)} \tag{4.28}$$

holds. Intuitively, it is obvious that it would be beneficial for the channel estimation, which is the topic of Section 4.4, if the columns of $\underline{\tilde{\boldsymbol{\mathcal{G}}}}$ and, therefore, the contributions $\underline{\tilde{\mathbf{r}}}_w^{(k)}$ of (4.28) would be mutually orthogonal. Generally, such an orthogonality cannot be achieved by choosing orthogonal pilot vectors $\underline{\tilde{\mathbf{p}}}^{(k)}$ of (3.3), because the pilot vectors $\underline{\tilde{\mathbf{p}}}^{(k)}$ are transformed by the matrix $\underline{\tilde{\boldsymbol{\mathcal{F}}}}_{\mathrm{W}}$ in (4.24).

We conclude Section 4.3 by a rank consideration of $\underline{\tilde{\boldsymbol{\mathcal{G}}}}$ of (4.24). In order to guarantee that each component of $\underline{\mathbf{h}}$ of (4.22) is uniquely presented by $\underline{\tilde{\mathbf{r}}}$ of (4.24), $\underline{\tilde{\boldsymbol{\mathcal{G}}}}$ has to be of full rank KW. As an obvious condition for $\underline{\tilde{\boldsymbol{\mathcal{G}}}}$ having full rank KW, all K pilots $\underline{\tilde{\mathbf{p}}}^{(k)}$ of (3.3) have to be different. Intuitively, it should be required that all pilot vectors $\underline{\tilde{\mathbf{p}}}^{(k)}$ consist of only non-zero elements $\underline{\tilde{p}}_{n_{\mathrm{F}}}^{(k)}$. However, such a requirement does not exist. In each pilot vector $\underline{\tilde{\mathbf{p}}}^{(k)}$ only a number of W pilots $\underline{\tilde{p}}_{n_{\mathrm{F}}}^{(k)}$ have to be non-zero; these W non-zero pilots have to be chosen in such a way that they are exclusively used by MT k. For the case

$$\{N_{\mathrm{F}},\ K,\ W\} = \{8,\ 3,\ 2\} \tag{4.29}$$

Fig. 4.1 illustrates schematically one of the different possibilities of such an exclusive assignment of non-zero pilots. The total number of CIR values $\underline{h}_w^{(k)}$ is KW, which is equal to the number of required mutually exclusive non-zero pilots $\underline{\tilde{p}}_{n_{\mathrm{F}}}^{(k)}$.

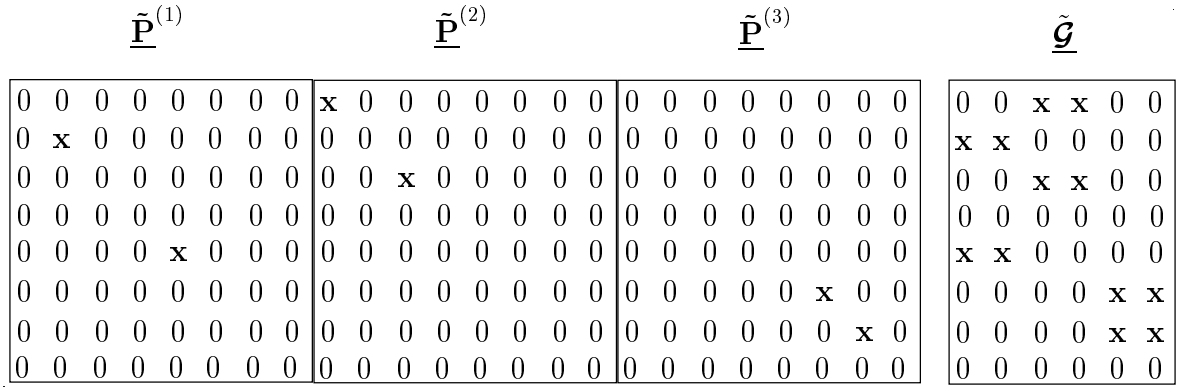

Fig. 4.1. Example of pilot matrices $\underline{\tilde{\mathbf{P}}}^{(k)}$ with mutually exclusive non-zero elements $\mathbf{x}$ leading to a non-singular matrix $\underline{\tilde{\mathcal{G}}}$; parameter set $\{N_\mathrm{F},\ K,\ W\} = \{8,\ 3,\ 2\}$

4.4 Joint Channel Estimation (JCE)

In order to perform JCE, we intend to utilize the Gauss–Markov estimator, which leads to an unbiased estimate of minimum variance [Fel94]. Let us assume that the noise $\underline{\tilde{\mathbf{n}}}$ of (4.4) is white with the covariance matrix

$$\underline{\mathbf{R}}_{\tilde{\mathbf{n}}} = \mathrm{E}\left\{ \underline{\tilde{\mathbf{n}}}\, \underline{\tilde{\mathbf{n}}}^{\mathsf{H}} \right\} = 2\sigma^2 \cdot \mathbf{I}^{(N_\mathrm{F} \times N_\mathrm{F})}, \tag{4.30}$$

and the variance σ^2 of real and imaginary parts. Then, with (4.24) the Gauss–Markov–estimate of the total CIR $\underline{\mathbf{h}}$ of (4.22) becomes [SMWB01]

$$\underline{\hat{\mathbf{h}}} = \left(\underline{\tilde{\mathcal{G}}}^{\mathsf{H}} \underline{\tilde{\mathcal{G}}} \right)^{-1} \underline{\tilde{\mathcal{G}}}^{\mathsf{H}}\, \underline{\tilde{\mathbf{r}}}\,. \tag{4.31}$$

With (4.23) the estimate

$$\underline{\hat{\tilde{\mathbf{h}}}} = \underline{\tilde{\boldsymbol{\mathcal{F}}}}_\mathrm{W} \underline{\hat{\mathbf{h}}} = \underbrace{\underline{\tilde{\boldsymbol{\mathcal{F}}}}_\mathrm{W} \left(\underline{\tilde{\mathcal{G}}}^{\mathsf{H}} \underline{\tilde{\mathcal{G}}} \right)^{-1} \underline{\tilde{\mathcal{G}}}^{\mathsf{H}}}_{\underline{\tilde{\mathbf{Z}}}}\, \underline{\tilde{\mathbf{r}}} \tag{4.32}$$

of the total CTF of (4.9) follows from (4.31). If the noise $\underline{\tilde{\mathbf{n}}}$ in addition to being white is Gaussian, then the estimates $\underline{\hat{\mathbf{h}}}$ of (4.31) and $\underline{\hat{\tilde{\mathbf{h}}}}$ of (4.32) are maximum likelihood (ML) estimates [Wha71, Hay01]. The estimator described by (4.32) could be particularly simply implemented, if $\underline{\tilde{\mathcal{G}}}^{\mathsf{H}} \underline{\tilde{\mathcal{G}}}$ would be a diagonal matrix.

Substitution of $\underline{\tilde{\mathbf{r}}}$ of (4.24) in (4.32) under consideration of (4.23) yields

$$\underline{\hat{\tilde{\mathbf{h}}}} = \underline{\tilde{\boldsymbol{\mathcal{F}}}}_\mathrm{W} \left(\underline{\tilde{\mathcal{G}}}^{\mathsf{H}} \underline{\tilde{\mathcal{G}}} \right)^{-1} \underline{\tilde{\mathcal{G}}}^{\mathsf{H}} \underline{\tilde{\mathcal{G}}}\, \underline{\mathbf{h}} + \underline{\tilde{\mathbf{Z}}}\, \underline{\tilde{\mathbf{n}}} = \underline{\tilde{\boldsymbol{\mathcal{F}}}}_\mathrm{W} \underline{\mathbf{h}} + \underline{\tilde{\mathbf{Z}}}\, \underline{\tilde{\mathbf{n}}} = \underline{\tilde{\mathbf{h}}} + \underline{\tilde{\mathbf{Z}}}\, \underline{\tilde{\mathbf{n}}}. \tag{4.33}$$

(4.33) shows that the estimate $\hat{\tilde{\underline{\mathbf{h}}}}$ is unbiased and is corrupted by a noise term $\tilde{\underline{\mathbf{Z}}}\,\tilde{\underline{\mathbf{n}}}$, which is in general non-white. According to (4.33) the desired part of the estimate $\hat{\tilde{\underline{\mathbf{h}}}}$ is $\tilde{\underline{\mathbf{h}}}$ and it is independent of the chosen pilot vectors $\tilde{\underline{\mathbf{p}}}^{(k)}$ of (3.3). However, this choice influences the effective noise $\tilde{\underline{\mathbf{Z}}}\,\tilde{\underline{\mathbf{n}}}$.

For given characteristics of the noise $\tilde{\underline{\mathbf{n}}}$ of (4.4) and of the CTF $\tilde{\underline{\mathbf{h}}}$ of (4.9) the effective noise $\tilde{\underline{\mathbf{Z}}}\,\tilde{\underline{\mathbf{n}}}$, that is the quality of the estimate $\hat{\tilde{\underline{\mathbf{h}}}}$ of (4.32) depend on the choice of the pilot vectors $\tilde{\underline{\mathbf{p}}}^{(k)}$ of (3.3). In the following Section 4.5 quality criteria to judge the suitability of the chosen pilot vectors $\tilde{\underline{\mathbf{p}}}^{(k)}$ are presented.

4.5 Quality criteria for JCE

4.5.1 SNR degradation

Let us consider (4.33). For each component $\hat{\tilde{\underline{h}}}^{(k)}_{n_\mathrm{F}}$ of the estimate $\hat{\tilde{\underline{\mathbf{h}}}}$ a signal-to-noise ratio (SNR) $\gamma^{(k)}_{n_\mathrm{F}}$ can be introduced. This SNR is given by the ratio of the desired energy

$$E^{(k)}_{n_\mathrm{F}} = \left|\tilde{\underline{h}}^{(k)}_{n_\mathrm{F}}\right|^2 \tag{4.34}$$

and the simultaneously present noise energy $N^{(k)}_{n_\mathrm{F}}$ as

$$\gamma^{(k)}_{n_\mathrm{F}} = \frac{E^{(k)}_{n_\mathrm{F}}}{N^{(k)}_{n_\mathrm{F}}} = \frac{\left|\tilde{\underline{h}}^{(k)}_{n_\mathrm{F}}\right|^2}{N^{(k)}_{n_\mathrm{F}}}. \tag{4.35}$$

Let us designate by $[\cdot]_{i,i}$ the diagonal element i of a square matrix in brackets. Then, under consideration of the definition of $\tilde{\underline{\mathbf{Z}}}$ of (4.32) and of the noise covariance matrix of (4.30)

$$\begin{aligned} N^{(k)}_{n_\mathrm{F}} &= \left[\mathrm{E}\left\{\tilde{\underline{\mathbf{Z}}}\,\tilde{\underline{\mathbf{n}}}\,\left(\tilde{\underline{\mathbf{Z}}}\,\tilde{\underline{\mathbf{n}}}\right)^{\mathsf{H}}\right\}\right]_{i,i} = \left[\tilde{\underline{\mathbf{Z}}}\,\mathbf{R}_{\tilde{\mathbf{n}}}\tilde{\underline{\mathbf{Z}}}^{\mathsf{H}}\right]_{i,i} = 2\sigma^2\cdot\left[\tilde{\underline{\mathbf{Z}}}\,\tilde{\underline{\mathbf{Z}}}^{\mathsf{H}}\right]_{i,i} \\ &= 2\sigma^2\cdot\left[\tilde{\underline{\boldsymbol{\mathcal{F}}}}_{\mathrm{W}}\left(\tilde{\underline{\boldsymbol{\mathcal{G}}}}^{\mathsf{H}}\tilde{\underline{\boldsymbol{\mathcal{G}}}}\right)^{-1}\tilde{\underline{\boldsymbol{\mathcal{G}}}}^{\mathsf{H}}\cdot\tilde{\underline{\boldsymbol{\mathcal{G}}}}\left(\tilde{\underline{\boldsymbol{\mathcal{G}}}}^{\mathsf{H}}\tilde{\underline{\boldsymbol{\mathcal{G}}}}\right)^{-1}\tilde{\underline{\boldsymbol{\mathcal{F}}}}^{\mathsf{H}}_{\mathrm{W}}\right]_{i,i} \\ &= 2\sigma^2\cdot\left[\tilde{\underline{\boldsymbol{\mathcal{F}}}}_{\mathrm{W}}\left(\tilde{\underline{\boldsymbol{\mathcal{G}}}}^{\mathsf{H}}\tilde{\underline{\boldsymbol{\mathcal{G}}}}\right)^{-1}\tilde{\underline{\boldsymbol{\mathcal{F}}}}^{\mathsf{H}}_{\mathrm{W}}\right]_{i,i},\ i=(k-1)N_\mathrm{F}+n_\mathrm{F}, \end{aligned} \tag{4.36}$$

follows from (4.33).

From the definition of $\tilde{\underline{\boldsymbol{\mathcal{G}}}}$ given in (4.24) and from (4.26) follows that with

$$i = (k-1)N_\mathrm{F} + n_\mathrm{F} \tag{4.37}$$

the norm of column i of $\underline{\tilde{\boldsymbol{\mathcal{G}}}}$ is equal to two times the pilot energy $E_{\mathrm{p}}^{(k)}$ of (3.4), that is

$$\left[\underline{\tilde{\boldsymbol{\mathcal{G}}}}^{\mathsf{H}}\underline{\tilde{\boldsymbol{\mathcal{G}}}}\right]_{(k-1)N_{\mathrm{F}}+n_{\mathrm{F}},(k-1)N_{\mathrm{F}}+n_{\mathrm{F}}} = 2E_{\mathrm{p}}^{(k)}. \tag{4.38}$$

It is known [Ste95, Kle96] that for given column norms, that is for given energies $2E_{\mathrm{p}}^{(k)}$, the noise energies $N_{n_{\mathrm{F}}}^{(k)}$ of (4.36) become minimum, if $\underline{\tilde{\boldsymbol{\mathcal{G}}}}^{\mathsf{H}}\underline{\tilde{\boldsymbol{\mathcal{G}}}}$ would be a diagonal matrix. In this case with the property

$$\left[\underline{\tilde{\boldsymbol{\mathcal{F}}}}_{\mathrm{W}}\underline{\tilde{\boldsymbol{\mathcal{F}}}}_{\mathrm{W}}^{\mathsf{H}}\right]_{j,j} = W,\ \forall j = 1\ \ldots\ KN_{\mathrm{F}}, \tag{4.39}$$

of the reduced Fourier matrix $\underline{\tilde{\boldsymbol{\mathcal{F}}}}_{\mathrm{W}}$ of (4.21),

$$N_{n_{\mathrm{F}}}^{(k)} = N_{\min,n_{\mathrm{F}}}^{(k)} = 2\sigma^2\frac{1}{2E_{\mathrm{p}}^{(k)}}\left[\underline{\tilde{\boldsymbol{\mathcal{F}}}}_{\mathrm{W}}\underline{\tilde{\boldsymbol{\mathcal{F}}}}_{\mathrm{W}}^{\mathsf{H}}\right]_{(k-1)N_{\mathrm{F}}+n_{\mathrm{F}},(k-1)N_{\mathrm{F}}+n_{\mathrm{F}}} = \frac{\sigma^2 W}{E_{\mathrm{p}}^{(k)}} \tag{4.40}$$

would result from (4.36). (4.38) and (4.39) can be easily verified by the reader for the exemplary parameter triplet of (4.12) under consideration of (3.4). At this point, it is still an open question how for given pilot energies $E_{\mathrm{p}}^{(k)}$ the pilot vectors $\underline{\tilde{\mathbf{p}}}^{(k)}$ of (3.3) should be chosen in order to make $\underline{\tilde{\boldsymbol{\mathcal{G}}}}^{\mathsf{H}}\underline{\tilde{\boldsymbol{\mathcal{G}}}}$ a diagonal matrix. (4.40) is valid under the assumption that such a choice would be possible and, therefore, at the moment it can yet not be considered as a practical possibility.

Substitution of $N_{\min,n_{\mathrm{F}}}^{(k)}$ in (4.35) leads to the maximum SNR

$$\gamma_{n_{\mathrm{F}}}^{(k)} = \gamma_{\max,n_{\mathrm{F}}}^{(k)} = \frac{\left|\underline{\tilde{h}}_{n_{\mathrm{F}}}^{(k)}\right|^2}{N_{\min,n_{\mathrm{F}}}^{(k)}} = \frac{E_{\mathrm{p}}^{(k)}}{\sigma^2 W}\left|\underline{\tilde{h}}_{n_{\mathrm{F}}}^{(k)}\right|^2. \tag{4.41}$$

In order to SNR-wise judge a chosen set of pilot vectors $\underline{\tilde{\mathbf{p}}}^{(k)}$ of (3.3), the author resorts to the conception of SNR degradations well known from the work on time slotted DS-CDMA [Kle96, Pap00] systems and adapts this conception to JOINT. We form with $\gamma_{n_{\mathrm{F}}}^{(k)}$ of (4.35) and $\gamma_{\max,n_{\mathrm{F}}}^{(k)}$ of (4.41) and under consideration of (4.36) and (4.40) the KN_{F} ratios

$$\delta_{n_{\mathrm{F}}}^{(k)} = \frac{\gamma_{\max,n_{\mathrm{F}}}^{(k)}}{\gamma_{n_{\mathrm{F}}}^{(k)}} = \frac{2E_{\mathrm{p}}^{(k)}}{W}\left[\underline{\tilde{\boldsymbol{\mathcal{F}}}}_{\mathrm{W}}\left(\underline{\tilde{\boldsymbol{\mathcal{G}}}}^{\mathsf{H}}\underline{\tilde{\boldsymbol{\mathcal{G}}}}\right)^{-1}\underline{\tilde{\boldsymbol{\mathcal{F}}}}_{\mathrm{W}}^{\mathsf{H}}\right]_{(k-1)N_{\mathrm{F}}+n_{\mathrm{F}},(k-1)N_{\mathrm{F}}+n_{\mathrm{F}}} \geq 1, \tag{4.42}$$

which are termed SNR degradations [Kle96, SMWB01] and should be as small as possible. They take on the lowest possible value of one if the Gram matrix $\underline{\tilde{\boldsymbol{\mathcal{G}}}}^{\mathsf{H}}\underline{\tilde{\boldsymbol{\mathcal{G}}}}$ is a diagonal matrix. Sets of pilot vectors $\underline{\tilde{\mathbf{p}}}^{(k)}$ by which these lowest possible SNR degradations $\delta_{n_{\mathrm{F}}}^{(k)}$ are reached are termed ideal sets of pilot vectors by the author. At first sight, the pilot energies $E_{\mathrm{p}}^{(k)}$ on the right hand side of (4.42) intimate that the SNR degradations $\delta_{n_{\mathrm{F}}}^{(k)}$ depend on these energies. However, this is not the case because the diagonal elements of $\underline{\tilde{\boldsymbol{\mathcal{G}}}}^{\mathsf{H}}\underline{\tilde{\boldsymbol{\mathcal{G}}}}$ in (4.42) are proportional to the corresponding pilot energies $E_{\mathrm{p}}^{(k)}$, see also (4.38). These factors $E_{\mathrm{p}}^{(k)}$ in the diagonal

elements of $\underline{\tilde{\mathcal{G}}}^{\mathsf{H}}\underline{\tilde{\mathcal{G}}}$ and the factors $E_{\mathrm{p}}^{(k)}$ in the denominator of $\delta_{n_{\mathrm{F}}}^{(k)}$ of (4.42) compensate each other. Therefore, the SNR degradations $\delta_{n_{\mathrm{F}}}^{(k)}$ of (4.42) only depend on the structural properties of the pilot vectors $\underline{\tilde{\mathbf{p}}}^{(k)}$ of (3.3).

In order to give a comprehensive impression of the SNR behavior of JCE for a given set of pilot vectors $\underline{\tilde{\mathbf{p}}}^{(k)}$, we may resort to the average SNR degradation

$$\delta = \frac{1}{KN_{\mathrm{F}}} \sum_{k=1}^{K} \sum_{n_{\mathrm{F}}=1}^{N_{\mathrm{F}}} \delta_{n_{\mathrm{F}}}^{(k)} \tag{4.43}$$

observed for this pilot vector set.

4.5.2 Variation coefficient

Up to now in Chapter 4 a single SA was considered. In practice it may occur that a communications network consists of several SAs, which are simultaneously active, see for instance the structure shown in Fig. 1.2. If SAs in such a multi-SA network use the same frequency band, inter-SA interference occurs between these SAs. Concerning JCE, it is desirable that the detrimental impact of inter-SA interference caused by pilot radiation in a certain SA is distributed as evenly as possible over the components of the CTF estimate $\underline{\hat{\tilde{\mathbf{h}}}}$ gained in any SA of the network. In this subsection the author proposes a method for evaluating pilot sets in this respect.

In what follows we consider the impact of inter-SA interference on JCE in a two-SA situation. We have a reference $\mathrm{SA}_{\mathrm{ref}}$ in which we study this impact and an interfering SA_{I} which causes interference in $\mathrm{SA}_{\mathrm{ref}}$. The number of MTs is assumed to be K both in $\mathrm{SA}_{\mathrm{ref}}$ and SA_{I}. The consideration of only one interfering SA can be justified by the fact that in practical situations often the mutual interference is particularly severe between pairs of closely adjacent SAs, whereas the interference from SAs further away from $\mathrm{SA}_{\mathrm{ref}}$ is of less importance. In case that more than one interfering SAs would cause considerable inter-SA interference in $\mathrm{SA}_{\mathrm{ref}}$, the following considerations could be extended to such situations by repeated pair-wise analysis of the inter-SA interference caused in $\mathrm{SA}_{\mathrm{ref}}$ by all the relevant interfering SAs.

Similarly to and in addition to $\underline{\mathbf{h}}$ of (4.22) assumed to be valid for $\mathrm{SA}_{\mathrm{ref}}$ we introduce the total CIR

$$\begin{aligned}
\underline{\mathbf{h}}_{\mathrm{I}} &= \left(\underline{\mathbf{h}}^{(1)^{\mathrm{T}}} \ \ldots \ \underline{\mathbf{h}}^{(k_{\mathrm{I}})^{\mathrm{T}}} \ \ldots \ \underline{\mathbf{h}}^{(K)^{\mathrm{T}}}\right)^{\mathrm{T}} \\
&= \left(\underline{h}_1^{(1)} \ \ldots \ \underline{h}_W^{(1)} \ \ldots \ \underline{h}_1^{(k_{\mathrm{I}})} \ \ldots \ \underline{h}_W^{(k_{\mathrm{I}})} \ \ldots \ \underline{h}_1^{(K)} \ \ldots \ \underline{h}_W^{(K)}\right)^{\mathrm{T}} \\
&= \left(\underline{h}_{\mathrm{I},1} \ \ldots \ \underline{h}_{\mathrm{I},KW}\right)^{\mathrm{T}}
\end{aligned} \tag{4.44}$$

constituted by the K CIRs $\underline{\mathbf{h}}^{(k_\mathrm{I})}$, $k_\mathrm{I} = 1 \ \ldots \ K$, of the channels between the K MTs of $\mathrm{SA_I}$ and the considered antenna in $\mathrm{SA_{ref}}$. We further introduce the pilot matrix $\underline{\tilde{\mathbf{P}}}_\mathrm{I}$ constituted by the pilot vectors $\underline{\tilde{\mathbf{p}}}^{(k_\mathrm{I})}$ used in $\mathrm{SA_I}$ and the system matrix

$$\underline{\tilde{\boldsymbol{\mathcal{G}}}}_\mathrm{I} = \underline{\tilde{\mathbf{P}}}_\mathrm{I} \underline{\tilde{\boldsymbol{\mathcal{F}}}}_\mathrm{W} \tag{4.45}$$

of $\mathrm{SA_I}$. Inter-SA interference caused by pilot radiation in $\mathrm{SA_I}$ causes an additional undesired term

$$\Delta\, \underline{\tilde{\mathbf{r}}} = \underline{\tilde{\mathbf{P}}}_\mathrm{I} \underline{\tilde{\boldsymbol{\mathcal{F}}}}_\mathrm{W} \underline{\mathbf{h}}_\mathrm{I} = \underline{\tilde{\boldsymbol{\mathcal{G}}}}_\mathrm{I} \underline{\mathbf{h}}_\mathrm{I} \tag{4.46}$$

in the receive signal $\underline{\tilde{\mathbf{r}}}$, see (4.24), of $\mathrm{SA_{ref}}$ so that we now obtain instead of (4.24)

$$\underline{\tilde{\mathbf{r}}} = \underline{\tilde{\boldsymbol{\mathcal{G}}}}\, \underline{\mathbf{h}} + \underline{\tilde{\mathbf{n}}} + \Delta\, \underline{\tilde{\mathbf{r}}} = \underline{\tilde{\boldsymbol{\mathcal{G}}}}\, \underline{\mathbf{h}} + \underline{\tilde{\mathbf{n}}} + \underline{\tilde{\boldsymbol{\mathcal{G}}}}_\mathrm{I} \underline{\mathbf{h}}_\mathrm{I}. \tag{4.47}$$

At the output of the joint channel estimator of $\mathrm{SA_{ref}}$, see (4.33), $\Delta\, \underline{\tilde{\mathbf{r}}}$ of (4.46) leads to an additional undesired term

$$\Delta \underline{\tilde{\mathbf{h}}} = \underbrace{\underline{\tilde{\boldsymbol{\mathcal{F}}}}_\mathrm{W} \left(\underline{\tilde{\boldsymbol{\mathcal{G}}}}^\mathsf{H} \underline{\tilde{\boldsymbol{\mathcal{G}}}} \right)^{-1} \underline{\tilde{\boldsymbol{\mathcal{G}}}}^\mathsf{H} \underline{\tilde{\boldsymbol{\mathcal{G}}}}_\mathrm{I}}_{\underline{\boldsymbol{\mathcal{I}}}} \underline{\mathbf{h}}_\mathrm{I}. \tag{4.48}$$

We designate the $(KN_\mathrm{F}) \times (KW)$ matrix $\underline{\boldsymbol{\mathcal{I}}}$ defined in (4.48) as inter-SA interference matrix. The impact of the element $\underline{h}_{\mathrm{I},j}$, $j = 1 \ \ldots \ KW$, of $\underline{\mathbf{h}}_\mathrm{I}$ of (4.44) on the element $\underline{\hat{\tilde{h}}}_i$, $i = 1 \ \ldots \ KN_\mathrm{F}$, of the estimate $\underline{\hat{\tilde{\mathbf{h}}}}$ of (4.33) is quantitatively given by the element $\left[\underline{\boldsymbol{\mathcal{I}}}\right]_{i,j}$ of the matrix $\underline{\boldsymbol{\mathcal{I}}}$. $\Delta \underline{\tilde{\mathbf{h}}}$ of (4.48) depends on the chosen pilot vectors $\underline{\tilde{\mathbf{p}}}^{(k)}$ and $\underline{\tilde{\mathbf{p}}}^{(k_\mathrm{I})}$ of $\mathrm{SA_{ref}}$ and $\mathrm{SA_I}$, respectively. These pilot vectors are given by their basic structures, that is by their directions in the N_F-dimensional space, and by their energies $E_\mathrm{p}^{(k)}$ and $E_{\mathrm{I,p}}^{(k)}$, respectively. In what follows we aspire that only the basic structures of the pilot vectors $\underline{\tilde{\mathbf{p}}}^{(k)}$ and $\underline{\tilde{\mathbf{p}}}^{(k_\mathrm{I})}$ play a role when judging the inter-SA interference situation, and, therefore, assume that all K pilot vectors $\underline{\tilde{\mathbf{p}}}^{(k)}$ of $\mathrm{SA_{ref}}$ and all K pilot vectors $\underline{\tilde{\mathbf{p}}}^{(k_\mathrm{I})}$ of $\mathrm{SA_I}$ have the same energies.

Let us first assume that all KW elements $\underline{h}_{\mathrm{I},j}$, $j = 1 \ \ldots \ KW$, of $\underline{\mathbf{h}}_\mathrm{I}$ of (4.44) have approximately the same magnitude. Then, in order to arrive at the desired even distribution of the impact of inter-SA interference, the variance σ_I^2 of the magnitudes $\left| \left[\underline{\boldsymbol{\mathcal{I}}}\right]_{i,j} \right|$ of the matrix elements $\left[\underline{\boldsymbol{\mathcal{I}}}\right]_{i,j}$, $i = 1 \ \ldots \ KN_\mathrm{F}$, $j = 1 \ \ldots \ KW$, should be as small as possible. With the mean value

$$\overline{\mathcal{I}} = \frac{1}{KN_\mathrm{F}KW} \sum_{i=1}^{KN_\mathrm{F}} \sum_{j=1}^{KW} \left| \left[\underline{\boldsymbol{\mathcal{I}}}\right]_{i,j} \right| \tag{4.49}$$

we obtain

$$\sigma_\mathrm{I}^2 = \frac{1}{KN_\mathrm{F}KW - 1} \sum_{i=1}^{KN_\mathrm{F}} \sum_{j=1}^{KW} \left(\left| \left[\underline{\boldsymbol{\mathcal{I}}}\right]_{i,j} \right| - \overline{\mathcal{I}} \right)^2 \geq 0. \tag{4.50}$$

We term σ_{I}^2 of (4.50) the total interference variance. Instead of σ_{I}^2 we can also resort to the quantity

$$\nu = \frac{\sigma_{\mathrm{I}}}{\overline{\mathcal{I}}}, \tag{4.51}$$

which we term total variation coefficient [Fis76, Sch90].

In the second paragraph of this subsection it was mentioned that in multi-SA networks the inter-SA interference from a certain interfering $\mathrm{SA_I}$ is prone to be dominant in $\mathrm{SA_{ref}}$. To carry on this argument, in each instant of time one specific MT k_{I}, $k_{\mathrm{I}} = 1 \ \ldots \ K$, out of the K MTs of the dominant $\mathrm{SA_I}$ may be the dominant interferer disturbing $\mathrm{SA_{ref}}$. In such a situation it would be desirable that the interference impact of this dominant interferer k_{I} alone is spread as evenly as possible over all KN_{F} estimates $\hat{\underline{h}}_{n_{\mathrm{F}}}^{(k)}$ gained in $\mathrm{SA_{ref}}$. We designate this dominant interferer by the index k_{I}, and instead of $\overline{\mathcal{I}}$ of (4.49) we now introduce the K interferer specific mean values

$$\overline{\mathcal{I}}^{(k_{\mathrm{I}})} = \frac{1}{KN_{\mathrm{F}}W} \sum_{i=1}^{KN_{\mathrm{F}}} \sum_{j=(k_{\mathrm{I}}-1)W+1}^{k_{\mathrm{I}}W} \left| [\underline{\boldsymbol{\mathcal{I}}}]_{i,j} \right|, \ k = 1 \ \ldots \ K, \tag{4.52}$$

and the K interferer specific variances

$$\sigma^{(k_{\mathrm{I}})^2} = \frac{1}{KN_{\mathrm{F}}W - 1} \sum_{i=1}^{KN_{\mathrm{F}}} \sum_{j=(k_{\mathrm{I}}-1)W+1}^{k_{\mathrm{I}}W} \left(\left| [\underline{\boldsymbol{\mathcal{I}}}]_{i,j} \right| - \overline{\mathcal{I}}^{(k_{\mathrm{I}})} \right)^2. \tag{4.53}$$

From (4.52) and (4.53) follow the interferer specific variation coefficients

$$\nu^{(k_{\mathrm{I}})} = \frac{\sigma^{(k_{\mathrm{I}})}}{\overline{\mathcal{I}}^{(k_{\mathrm{I}})}}, k = 1 \ \ldots \ K. \tag{4.54}$$

Now, instead of (4.51) another definition of the total variation coefficient would be

$$\nu = \frac{1}{K} \sum_{k=1}^{K} \nu^{(k_{\mathrm{I}})}. \tag{4.55}$$

In the further course of this thesis we use the total variation coefficient as defined by (4.52) to (4.55).

Chapter 5

Pilot vector design

5.1 Preliminary remarks

We consider a SA-based network consisting of N_{SA} SAs which all use the same frequency band. In order to enable JCE as described in Section 4.4 in each of these SAs, for each SA a total pilot matrix $\underline{\tilde{\mathbf{P}}}^{(n_{\mathrm{SA}})}$, $n_{\mathrm{SA}} = 1 \ldots N_{\mathrm{SA}}$, see (4.10), has to be introduced. From the standpoint of the individual SA, each of the N_{SA} total pilot matrices $\underline{\tilde{\mathbf{P}}}^{(n_{\mathrm{SA}})}$ should lead, when applying (4.32), to SNR degradations $\delta_{n_{\mathrm{F}}}^{(k,n_{\mathrm{SA}})}$ as small as possible. Considering the whole network, for each SA pair (n_{SA}, n'_{SA}), $n_{\mathrm{SA}} \neq n'_{\mathrm{SA}}$, a variation coefficient $\nu^{(n_{\mathrm{SA}},n'_{\mathrm{SA}})}$ can be defined following (4.52) to (4.55), and these variation coefficients should be as small as possible.

In the following sections the author presents and discusses a selection of four different methods to arrive at pilot sets for JCE, namely

- randomly generated pilot vectors,
- pilot vectors generated based on the approach of disjoint subcarriers,
- pilot vectors generated based on Walsh codes [Pro95], and
- pilot vectors generated based on the constant-amplitude-zero-autocorrelation (CAZAC) codes [Hei61, Mil83, KCWS03, Kan05].

In all these cases, (4.38) holds for the elements on the main diagonal of $\underline{\tilde{\boldsymbol{\mathcal{G}}}}^{\mathsf{H}}\underline{\tilde{\boldsymbol{\mathcal{G}}}}$ and, as stated in Subsection 4.5.2, we assume that the energies $E_{\mathrm{p}}^{(k)}$, $k = 1 \ \ldots \ K$, of all pilot vectors $\underline{\tilde{\mathbf{p}}}^{(k)}$ of (3.3) are equal, i. e.

$$E_{\mathrm{p}}^{(1)} = \ \ldots \ = E_{\mathrm{p}}^{(K)} = E_{\mathrm{p}}. \tag{5.1}$$

With (5.1), (4.38) now reads

$$\left[\underline{\tilde{\boldsymbol{\mathcal{G}}}}^{\mathsf{H}}\underline{\tilde{\boldsymbol{\mathcal{G}}}}\right]_{i,\,i} = 2E_{\mathrm{p}}, \ \forall \ i = 1 \ \ldots \ KW. \tag{5.2}$$

5.2 General considerations about the SNR degradation

In Subsection 4.5.1 it is stated that the SNR degradations $\delta_{n_{\mathrm{F}}}^{(k)}$, $k = 1 \ \ldots \ K$, $n_{\mathrm{F}} = 1 \ldots N_{\mathrm{F}}$, defined in (4.42) depend only on the structural properties of the applied pilot vectors $\underline{\tilde{\mathbf{p}}}^{(k)}$ of

(3.3). Further, it is said that the lowest value of $\delta_{n_\mathrm{F}}^{(k)}$ is one which is reached, when the Gram matrix $\tilde{\underline{\boldsymbol{\mathcal{G}}}}^{\mathsf{H}}\tilde{\underline{\boldsymbol{\mathcal{G}}}}$ in (4.42) is diagonal. In this case we would have an ideal set of pilot vectors $\tilde{\underline{\mathbf{p}}}^{(k)}$. Let us now take a more detailed look at said matrix $\tilde{\underline{\boldsymbol{\mathcal{G}}}}^{\mathsf{H}}\tilde{\underline{\boldsymbol{\mathcal{G}}}}$. Extending the component-wise representation of the system matrix $\tilde{\underline{\boldsymbol{\mathcal{G}}}}$ illustrated by the example of (4.27), and considering (4.7), (4.10), (4.18), (4.21) and (5.2), the general structure of the system matrix $\tilde{\underline{\boldsymbol{\mathcal{G}}}}$ reads

$$
\begin{aligned}
\tilde{\underline{\boldsymbol{\mathcal{G}}}} \;&=\; \tilde{\underline{\mathbf{P}}}\,\tilde{\underline{\boldsymbol{\mathcal{F}}}}_{\mathrm{W}} = \begin{pmatrix} \tilde{\underline{p}}_1^{(1)} & \cdots & 0 & & \tilde{\underline{p}}_1^{(K)} & \cdots & 0 \\ \vdots & \ddots & \vdots & \cdots & \vdots & \ddots & \vdots \\ 0 & \cdots & \tilde{\underline{p}}_{N_\mathrm{F}}^{(1)} & & 0 & \cdots & \tilde{\underline{p}}_{N_\mathrm{F}}^{(K)} \end{pmatrix} \cdot \\
&\qquad \begin{pmatrix} \tilde{\underline{f}}_{1,1} & \cdots & \tilde{\underline{f}}_{1,W} & & 0 & \cdots & 0 \\ \vdots & & \vdots & \cdots & \vdots & \ddots & \vdots \\ \tilde{\underline{f}}_{N_\mathrm{F},1} & \cdots & \tilde{\underline{f}}_{N_\mathrm{F},W} & & 0 & \cdots & 0 \\ & \vdots & & \ddots & & \vdots & \\ 0 & \cdots & 0 & & \tilde{\underline{f}}_{1,1} & \cdots & \tilde{\underline{f}}_{1,W} \\ \vdots & \ddots & \vdots & \cdots & \vdots & & \vdots \\ 0 & \cdots & 0 & & \tilde{\underline{f}}_{N_\mathrm{F},1} & \cdots & \tilde{\underline{f}}_{N_\mathrm{F},W} \end{pmatrix} \qquad (5.3) \\
&= \begin{pmatrix} \tilde{\underline{p}}_1^{(1)} \cdot \tilde{\underline{f}}_{1,1} & \cdots & \tilde{\underline{p}}_1^{(1)} \cdot \tilde{\underline{f}}_{1,W} & & \tilde{\underline{p}}_1^{(K)} \cdot \tilde{\underline{f}}_{1,1} & \cdots & \tilde{\underline{p}}_1^{(K)} \cdot \tilde{\underline{f}}_{1,W} \\ \vdots & & \vdots & \cdots & \vdots & & \vdots \\ \tilde{\underline{p}}_{N_\mathrm{F}}^{(1)} \cdot \tilde{\underline{f}}_{N_\mathrm{F},1} & \cdots & \tilde{\underline{p}}_{N_\mathrm{F}}^{(1)} \cdot \tilde{\underline{f}}_{N_\mathrm{F},W} & & \tilde{\underline{p}}_{N_\mathrm{F}}^{(K)} \cdot \tilde{\underline{f}}_{N_\mathrm{F},1} & \cdots & \tilde{\underline{p}}_{N_\mathrm{F}}^{(K)} \cdot \tilde{\underline{f}}_{N_\mathrm{F},W} \end{pmatrix} \\
&= \left(\tilde{\underline{\mathbf{p}}}^{(1)} \odot \tilde{\underline{\mathbf{f}}}_1 \;\cdots\; \tilde{\underline{\mathbf{p}}}^{(1)} \odot \tilde{\underline{\mathbf{f}}}_W \;\cdots\; \tilde{\underline{\mathbf{p}}}^{(K)} \odot \tilde{\underline{\mathbf{f}}}_1 \;\cdots\; \tilde{\underline{\mathbf{p}}}^{(K)} \odot \tilde{\underline{\mathbf{f}}}_W \right) \\
&= \left(\tilde{\underline{\boldsymbol{\mathcal{G}}}}^{(1)} \;\cdots\; \tilde{\underline{\boldsymbol{\mathcal{G}}}}^{(K)} \right),
\end{aligned}
$$

where "$\odot$" stands for the element-wise multiplication of vectors. With (5.2) and (5.3), the Gram matrix $\tilde{\underline{\boldsymbol{\mathcal{G}}}}^{\mathsf{H}}\tilde{\underline{\boldsymbol{\mathcal{G}}}}$ reads component-wise

$$
\tilde{\underline{\boldsymbol{\mathcal{G}}}}^{\mathsf{H}}\tilde{\underline{\boldsymbol{\mathcal{G}}}} = \begin{pmatrix} \tilde{\underline{\boldsymbol{\mathcal{G}}}}^{(1)^{\mathsf{H}}}\tilde{\underline{\boldsymbol{\mathcal{G}}}}^{(1)} & \cdots & \tilde{\underline{\boldsymbol{\mathcal{G}}}}^{(1)^{\mathsf{H}}}\tilde{\underline{\boldsymbol{\mathcal{G}}}}^{(K)} \\ \vdots & \ddots & \vdots \\ \tilde{\underline{\boldsymbol{\mathcal{G}}}}^{(K)^{\mathsf{H}}}\tilde{\underline{\boldsymbol{\mathcal{G}}}}^{(1)} & \cdots & \tilde{\underline{\boldsymbol{\mathcal{G}}}}^{(K)^{\mathsf{H}}}\tilde{\underline{\boldsymbol{\mathcal{G}}}}^{(K)} \end{pmatrix} \qquad (5.4)
$$

$$
\begin{pmatrix}
(\tilde{\underline{p}}_1^{(1)} \cdot \tilde{\underline{f}}_{1,1})^* & \cdots & (\tilde{\underline{p}}_{N_\mathrm{F}}^{(1)} \cdot \tilde{\underline{f}}_{N_\mathrm{F},1})^* \\
\vdots & & \vdots \\
(\tilde{\underline{p}}_1^{(1)} \cdot \tilde{\underline{f}}_{1,W})^* & \cdots & (\tilde{\underline{p}}_{N_\mathrm{F}}^{(1)} \cdot \tilde{\underline{f}}_{N_\mathrm{F},W})^* \\
\vdots & & \vdots \\
(\tilde{\underline{p}}_1^{(K)} \cdot \tilde{\underline{f}}_{1,1})^* & \cdots & (\tilde{\underline{p}}_{N_\mathrm{F}}^{(K)} \cdot \tilde{\underline{f}}_{N_\mathrm{F},1})^* \\
\vdots & & \vdots \\
(\tilde{\underline{p}}_1^{(K)} \cdot \tilde{\underline{f}}_{1,W})^* & \cdots & (\tilde{\underline{p}}_{N_\mathrm{F}}^{(K)} \cdot \tilde{\underline{f}}_{N_\mathrm{F},W})^*
\end{pmatrix}
\cdot
\begin{pmatrix}
\tilde{\underline{p}}_1^{(1)} \cdot \tilde{\underline{f}}_{1,1} & \cdots & \tilde{\underline{p}}_1^{(1)} \cdot \tilde{\underline{f}}_{1,W} & \cdots & \tilde{\underline{p}}_1^{(K)} \cdot \tilde{\underline{f}}_{1,1} & \cdots & \tilde{\underline{p}}_1^{(K)} \cdot \tilde{\underline{f}}_{1,W} \\
\vdots & & \vdots & & \vdots & & \vdots \\
\tilde{\underline{p}}_{N_\mathrm{F}}^{(1)} \cdot \tilde{\underline{f}}_{N_\mathrm{F},1} & \cdots & \tilde{\underline{p}}_{N_\mathrm{F}}^{(1)} \cdot \tilde{\underline{f}}_{N_\mathrm{F},W} & \cdots & \tilde{\underline{p}}_{N_\mathrm{F}}^{(K)} \cdot \tilde{\underline{f}}_{N_\mathrm{F},1} & \cdots & \tilde{\underline{p}}_{N_\mathrm{F}}^{(K)} \cdot \tilde{\underline{f}}_{N_\mathrm{F},W}
\end{pmatrix}
$$

$$
=
$$

$$
\begin{pmatrix}
2E_\mathrm{p} & \cdots & \sum_{i=1}^{N_\mathrm{F}} \left|\tilde{\underline{p}}_i^{(1)}\right|^2 \tilde{\underline{f}}_{i,1}^* \tilde{\underline{f}}_{i,W} & \cdots & \sum_{i=1}^{N_\mathrm{F}} \tilde{\underline{p}}_i^{(1)*} \tilde{\underline{p}}_i^{(K)} \left|\tilde{\underline{f}}_{i,1}\right|^2 & \cdots & \sum_{i=1}^{N_\mathrm{F}} (\tilde{\underline{p}}_i^{(1)} \cdot \tilde{\underline{f}}_{i,1})^* (\tilde{\underline{p}}_i^{(K)} \cdot \tilde{\underline{f}}_{i,W}) \\
\vdots & \ddots & \vdots & & \vdots & & \vdots \\
\sum_{i=1}^{N_\mathrm{F}} \left|\tilde{\underline{p}}_i^{(1)}\right|^2 \tilde{\underline{f}}_{i,W}^* \tilde{\underline{f}}_{i,1} & \cdots & 2E_\mathrm{p} & \cdots & \sum_{i=1}^{N_\mathrm{F}} (\tilde{\underline{p}}_i^{(1)} \cdot \tilde{\underline{f}}_{i,W})^* (\tilde{\underline{p}}_i^{(K)} \cdot \tilde{\underline{f}}_{i,1}) & \cdots & \sum_{i=1}^{N_\mathrm{F}} \tilde{\underline{p}}_i^{(1)*} \tilde{\underline{p}}_i^{(K)} \left|\tilde{\underline{f}}_{i,W}\right|^2 \\
\vdots & & \vdots & \ddots & \vdots & & \vdots \\
\sum_{i=1}^{N_\mathrm{F}} \tilde{\underline{p}}_i^{(K)*} \tilde{\underline{p}}_i^{(1)} \left|\tilde{\underline{f}}_{i,1}\right|^2 & \cdots & \sum_{i=1}^{N_\mathrm{F}} (\tilde{\underline{p}}_i^{(K)} \cdot \tilde{\underline{f}}_{i,1})^* (\tilde{\underline{p}}_i^{(1)} \cdot \tilde{\underline{f}}_{i,W}) & \cdots & 2E_\mathrm{p} & \cdots & \sum_{i=1}^{N_\mathrm{F}} \left|\tilde{\underline{p}}_i^{(K)}\right|^2 \tilde{\underline{f}}_{i,1}^* \tilde{\underline{f}}_{i,W} \\
\vdots & & \vdots & & \vdots & \ddots & \vdots \\
\sum_{i=1}^{N_\mathrm{F}} (\tilde{\underline{p}}_i^{(K)} \cdot \tilde{\underline{f}}_{i,W})^* (\tilde{\underline{p}}_i^{(1)} \cdot \tilde{\underline{f}}_{i,1}) & \cdots & \sum_{i=1}^{N_\mathrm{F}} \tilde{\underline{p}}_i^{(K)*} \tilde{\underline{p}}_i^{(1)} \left|\tilde{\underline{f}}_{i,W}\right|^2 & \cdots & \sum_{i=1}^{N_\mathrm{F}} \left|\tilde{\underline{p}}_i^{(K)}\right|^2 \tilde{\underline{f}}_{i,W}^* \tilde{\underline{f}}_{i,1} & \cdots & 2E_\mathrm{p}
\end{pmatrix}
.
$$

Let us now concentrate on the elements of $\underline{\tilde{\mathcal{G}}}^{\mathsf{H}}\underline{\tilde{\mathcal{G}}}$ off its main diagonal. With the view that $\delta_{n_{\mathrm{F}}}^{(k)}$ reaches the lowest possible value of one it is desired that all off-diagonal elements of $\underline{\tilde{\mathcal{G}}}^{\mathsf{H}}\underline{\tilde{\mathcal{G}}}$ are zero. In (5.4) we can distinguish between three different types of off-diagonal elements of $\underline{\tilde{\mathcal{G}}}^{\mathsf{H}}\underline{\tilde{\mathcal{G}}}$, namely:

Type I:
$$\sum_{i=1}^{N_{\mathrm{F}}} \left|\underline{\tilde{p}}_i^{(k)}\right|^2 \underline{\tilde{f}}_{i,w}^{*}\underline{\tilde{f}}_{i,w'},$$
$$k = 1 \ \ldots \ K,\ w, w' = 1 \ \ldots W, w \neq w',$$

Type II:
$$\sum_{i=1}^{N_{\mathrm{F}}} \underline{\tilde{p}}_i^{(k)^*}\underline{\tilde{p}}_i^{(k')} \left|\underline{\tilde{f}}_{i,w}\right|^2,$$
$$k, k' = 1 \ \ldots K,\ k \neq k',\ w = 1 \ \ldots W,$$

and

Type III:
$$\sum_{i=1}^{N_{\mathrm{F}}} \left(\underline{\tilde{p}}_i^{(k)} \cdot \underline{\tilde{f}}_{i,w}\right)^* \left(\underline{\tilde{p}}_i^{(k')} \cdot \underline{\tilde{f}}_{i,w'}\right),$$
$$k, k' = 1 \ \ldots K,\ k \neq k',\ w, w' = 1 \ \ldots W, w \neq w'.$$

All three types of off-diagonal elements of $\underline{\tilde{\mathcal{G}}}^{\mathsf{H}}\underline{\tilde{\mathcal{G}}}$ depend on the structural properties of the applied pilot vectors $\underline{\tilde{\mathbf{p}}}^{(k)}$ of (3.3) and on the coefficients $\underline{\tilde{f}}_{i,w}$, $i = 1 \ \ldots \ N_{\mathrm{F}}$, $w = 1 \ldots W$, of the Fourier matrix. In the following four sections, the Types I, II and III of the off-diagonal elements of $\underline{\tilde{\mathcal{G}}}^{\mathsf{H}}\underline{\tilde{\mathcal{G}}}$ are studied based on the applied method for pilot vector design.

5.3 Random pilot vectors

5.3.1 Generation

In the case of randomly generated pilot vectors $\underline{\tilde{\mathbf{p}}}^{(k)}$ all K MTs in the considered SA n_{SA} may use all N_{F} available subcarriers for pilot vector radiation, see Section 5.2. In the approach followed by the author, each of the KN_{F} elements $\underline{\tilde{p}}_{n_{\mathrm{F}}}^{(k)}$, $k = 1 \ \ldots \ K$, $n_{\mathrm{F}} = 1 \ldots N_{\mathrm{F}}$, of the pilot vectors $\underline{\tilde{\mathbf{p}}}^{(k)}$ of (3.3) is obtained by independently and randomly choosing one of the two values $\{-1,\ 1\}$. Based on this and on the assumption of (5.1) regarding the pilot energies, the MT-specific pilot vectors $\underline{\tilde{\mathbf{p}}}^{(k)}$ of (3.3) are of the form

$$\underline{\tilde{\mathbf{p}}}^{(k)} = \left(\underline{\tilde{p}}_1^{(k)}\underline{\tilde{p}}_2^{(k)} \ \ldots \ \underline{\tilde{p}}_{N_{\mathrm{F}}}^{(k)}\right)^{\mathrm{T}}, \underline{\tilde{p}}_{n_{\mathrm{F}}}^{(k)} \in \sqrt{\frac{2E_{\mathrm{p}}}{N_{\mathrm{F}}}}\{-1,\ 1\}. \tag{5.5}$$

According to (5.5) each of these pilot vectors can be written as the product of a factor $\sqrt{2E_{\mathrm{p}}/N_{\mathrm{F}}}$ and a random binary generating vector of dimension N_{F}, that is a vector the

elements of which take on the values +1 or -1 in a random fashion. A total amount of 2^{N_F} different pilot vectors $\underline{\tilde{\mathbf{p}}}^{(k)}$ of dimension N_F can be obtained. Further, $2^{N_\mathrm{F}}/K$ different pilot vector sets $\mathbb{P}^{(m)}$, $m = 1 \ \ldots \ 2^{N_\mathrm{F}}/K$, are obtained, each of them containing K different random pilot vectors $\underline{\tilde{\mathbf{p}}}^{(k)}$, $k = 1 \ \ldots \ K$, of (5.5). Random pilot vectors may be applied, if no particular effort shall be invested in pilot vector design.

5.3.2 SNR degradations

Based on the considerations given in Section 5.2 and also considering (5.5), the off-diagonal elements of Type I of $\underline{\tilde{\mathcal{G}}}^{\mathsf{H}}\underline{\tilde{\mathcal{G}}}$ can be written as

$$\sum_{i=1}^{N_\mathrm{F}} \left|\underline{\tilde{p}}_i^{(k)}\right|^2 \underline{\tilde{f}}_{i,w}^{*}\underline{\tilde{f}}_{i,w'}, = \frac{2E_\mathrm{p}}{N_\mathrm{F}} \cdot \sum_{i=1}^{N_\mathrm{F}} \underline{\tilde{f}}_{i,w}^{*}\underline{\tilde{f}}_{i,w'}, \ w, w' = 1 \ \ldots W, w \neq w'. \tag{5.6}$$

The sum on the right hand side of (5.6) represents the cross-correlation between two different column vectors $\underline{\tilde{\mathbf{f}}}_w$ and $\underline{\tilde{\mathbf{f}}}_{w'}$, $w \neq w'$, of the Fourier matrix $\underline{\tilde{\boldsymbol{\mathcal{F}}}}$ of (4.18) applied for the construction of the reduced blockdiagonal Fourier matrix $\underline{\tilde{\boldsymbol{\mathcal{F}}}}_\mathrm{W}$ of (4.21). Since all column vectors $\underline{\tilde{\mathbf{f}}}_{n_\mathrm{F}}$, $n_\mathrm{F} = 1 \ldots N_\mathrm{F}$, of the Fourier matrix $\underline{\tilde{\boldsymbol{\mathcal{F}}}}$ are orthogonal to each other [Rup93], it follows from (5.6) that all off-diagonal elements of Type I of $\underline{\tilde{\mathcal{G}}}^{\mathsf{H}}\underline{\tilde{\mathcal{G}}}$ are equal to zero.

Continuing with the off-diagonal elements of Type II of $\underline{\tilde{\mathcal{G}}}^{\mathsf{H}}\underline{\tilde{\mathcal{G}}}$, applying the property [Rup93]

$$\left|\underline{\tilde{f}}_{n_\mathrm{F},n_\mathrm{F}}\right|^2 = 1, \ \forall n_\mathrm{F} = 1 \ldots N_\mathrm{F}, \tag{5.7}$$

of the coefficients $\underline{\tilde{f}}_{n_\mathrm{F},n_\mathrm{F}}$ of the Fourier matrix, leads to

$$\sum_{i=1}^{N_\mathrm{F}} \underline{\tilde{p}}_i^{(k)^*}\underline{\tilde{p}}_i^{(k')} \left|\underline{\tilde{f}}_{i,w}\right|^2 = \sum_{i=1}^{N_\mathrm{F}} \underline{\tilde{p}}_i^{(k)^*}\underline{\tilde{p}}_i^{(k')}, \ k, k' = 1 \ \ldots K, k \neq k'. \tag{5.8}$$

(5.8) represents the cross-correlation between two different pilot vectors $\underline{\tilde{\mathbf{p}}}^{(k)}$ and $\underline{\tilde{\mathbf{p}}}^{(k')}$, $k \neq k'$. It is obvious from (5.8) that all off-diagonal elements of Type II of $\underline{\tilde{\mathcal{G}}}^{\mathsf{H}}\underline{\tilde{\mathcal{G}}}$ can be made equal to zero if orthogonal pilot vectors are applied. Since random pilot vectors $\underline{\tilde{\mathbf{p}}}^{(k)}$ according to (5.5) are in general non-orthogonal, the off-diagonal elements of Type II of the matrix $\underline{\tilde{\mathcal{G}}}^{\mathsf{H}}\underline{\tilde{\mathcal{G}}}$ are generally non-zero. This contributes to making the SNR degradations $\delta_{n_\mathrm{F}}^{(k)}$ larger than one.

Finally, the off-diagonal elements of Type III of $\underline{\tilde{\mathcal{G}}}^{\mathsf{H}}\underline{\tilde{\mathcal{G}}}$ are checked. The difference to the off-diagonal elements of Type I of $\underline{\tilde{\mathcal{G}}}^{\mathsf{H}}\underline{\tilde{\mathcal{G}}}$ lies in the fact that the two columns $\underline{\tilde{\mathbf{f}}}_w$ and $\underline{\tilde{\mathbf{f}}}_{w'}$ are weighted element-wise by two different pilot vectors $\underline{\tilde{\mathbf{p}}}^{(k)}$ and $\underline{\tilde{\mathbf{p}}}^{(k')}$, $k \neq k'$, respectively,

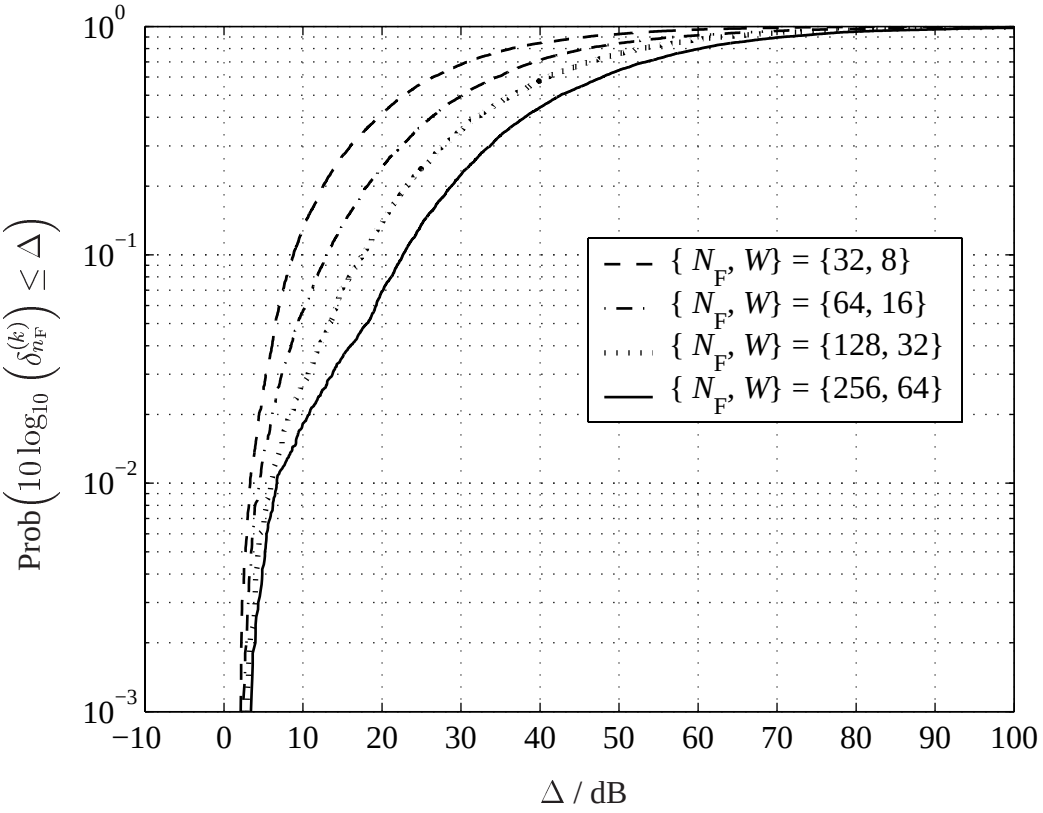

Fig. 5.1. Cdf of the SNR degradations $\delta_{n_\mathrm{F}}^{(k)}$ for random pilot vectors $\underline{\tilde{\mathbf{p}}}^{(k)}$; number of MTs: $K = 4$ (full system load)

by forming the direct products $\underline{\tilde{\mathbf{p}}}^{(k)} \odot \underline{\tilde{\mathbf{f}}}_w$ and $\underline{\tilde{\mathbf{p}}}^{(k')} \odot \underline{\tilde{\mathbf{f}}}_{w'}$ and then correlated. If these direct products are orthogonal to each other, then all off-diagonal elements of Type III of $\underline{\tilde{\mathcal{G}}}^{\mathsf{H}}\underline{\tilde{\mathcal{G}}}$ are equal to zero. Otherwise, the matrix $\underline{\tilde{\mathcal{G}}}^{\mathsf{H}}\underline{\tilde{\mathcal{G}}}$ also contains non-zero off-diagonal elements of type III. This again contributes to making the SNR degradations $\delta_{n_\mathrm{F}}^{(k)}$ of (4.42) larger than one.

For each set of K random pilot vectors $\underline{\tilde{\mathbf{p}}}^{(k)}$ we obtain a set of KN_F SNR degradations $\delta_{n_\mathrm{F}}^{(k)}$. If many experiments with different sets of random pilot vectors $\underline{\tilde{\mathbf{p}}}^{(k)}$ are performed, many different sets of KN_F SNR degradations $\delta_{n_\mathrm{F}}^{(k)}$ are obtained, all values being generally larger than one.

Now, in order to SNR-wise characterize the performance of random pilot vectors $\underline{\tilde{\mathbf{p}}}^{(k)}$, the author proposes to consider the cumulative distribution function (cdf) of the SNR degradations $\delta_{n_\mathrm{F}}^{(k)}$ of (4.42) under inclusion of all experiments and all values k, $k = 1 \ldots K$, and n_F, $n_\mathrm{F} = 1 \ldots N_\mathrm{F}$. Figs. 5.1 and 5.2 show the obtained cdf curves. For the curves shown in Fig. 5.1, the number K of MTs is kept equal to four, and the four different cases

$$\{N_\mathrm{F},\ W\} = \{32,\ 8\}\,,\ \{64,\ 16\}\,,\ \{128,\ 32\}\ \text{and}\ \{256,\ 64\} \tag{5.9}$$

of full system load are considered. The results of Fig. 5.1 show that the application of random pilot vectors $\underline{\tilde{\mathbf{p}}}^{(k)}$ leads to SNR degradations $\delta_{n_\mathrm{F}}^{(k)}$ larger than one or, equivalently, larger than

0 dB. For the curves shown in Fig. 5.2 the number N_{F} of subcarriers and the dimension W of the CIRs $\underline{\mathbf{h}}^{(k)}$ of (4.1) are fixed to 128 and 32, respectively, whereas the number K of MTs takes values from one till four. For the case of a single MT considered, it is evident from (4.35), (4.41) and (4.42) that the SNR degradations are equal to 0 dB. Although it seems that also for the case of two and three MTs the SNR degradations go towards 0 dB this is not the case, as illustrated in Fig. 5.3 for the magnification of the sector $-3 \ \ldots \ 4$ of the x-axis of Fig. 5.2. From Fig. 5.2 it can be observed that in the case of full system load, the variance of

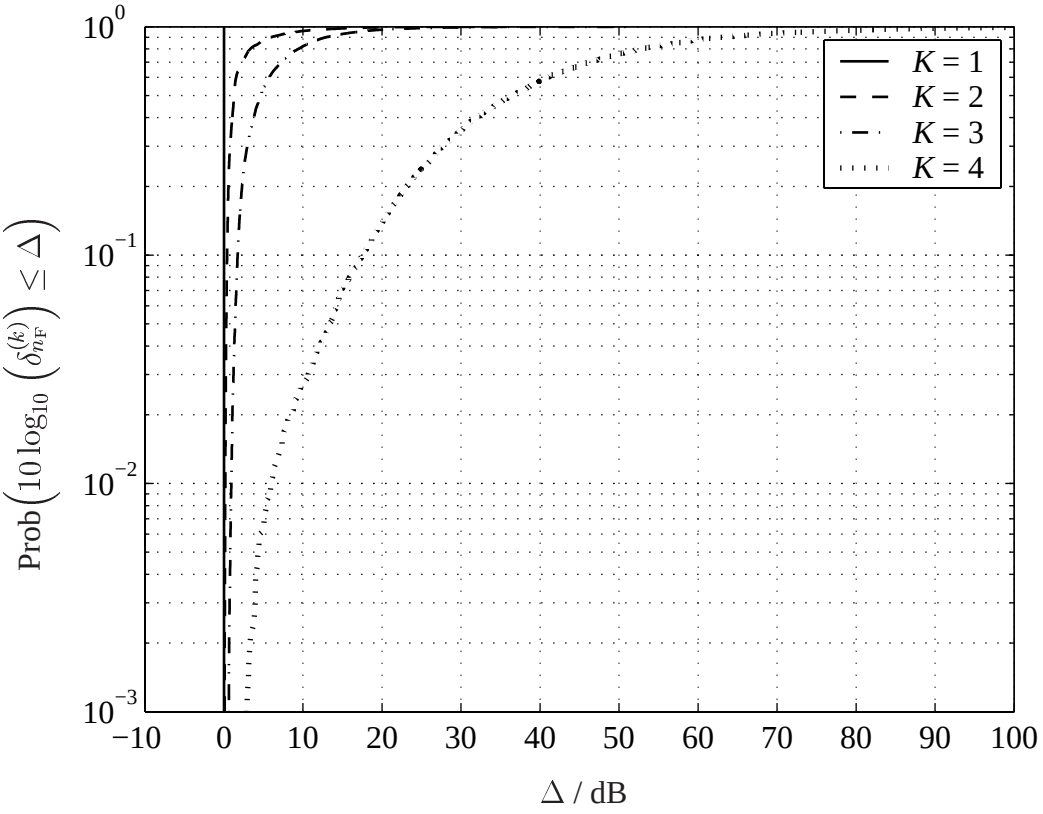

Fig. 5.2. Cdf of the SNR degradations $\delta_{n_{\mathrm{F}}}^{(k)}$ for random pilot vectors $\underline{\tilde{\mathbf{p}}}^{(k)}$; $N_{\mathrm{F}} = 128$, $W = 32$, $K = 1 \ \ldots \ 4$

the values $\delta_{n_{\mathrm{F}}}^{(k)}$ of the SNR degradations is much larger than in the other cases. In the cases, where the number N_{F} of subcarriers is smaller than the product of the number K of MTs and the length W of the CIRs $\underline{\mathbf{h}}^{(k)}$, the applied ML-JCE has more known values at its disposal than unknown values. This compensates up to a point the non-ideal performance of random pilots with respect to the variance of the SNR degradations $\delta_{n_{\mathrm{F}}}^{(k)}$.

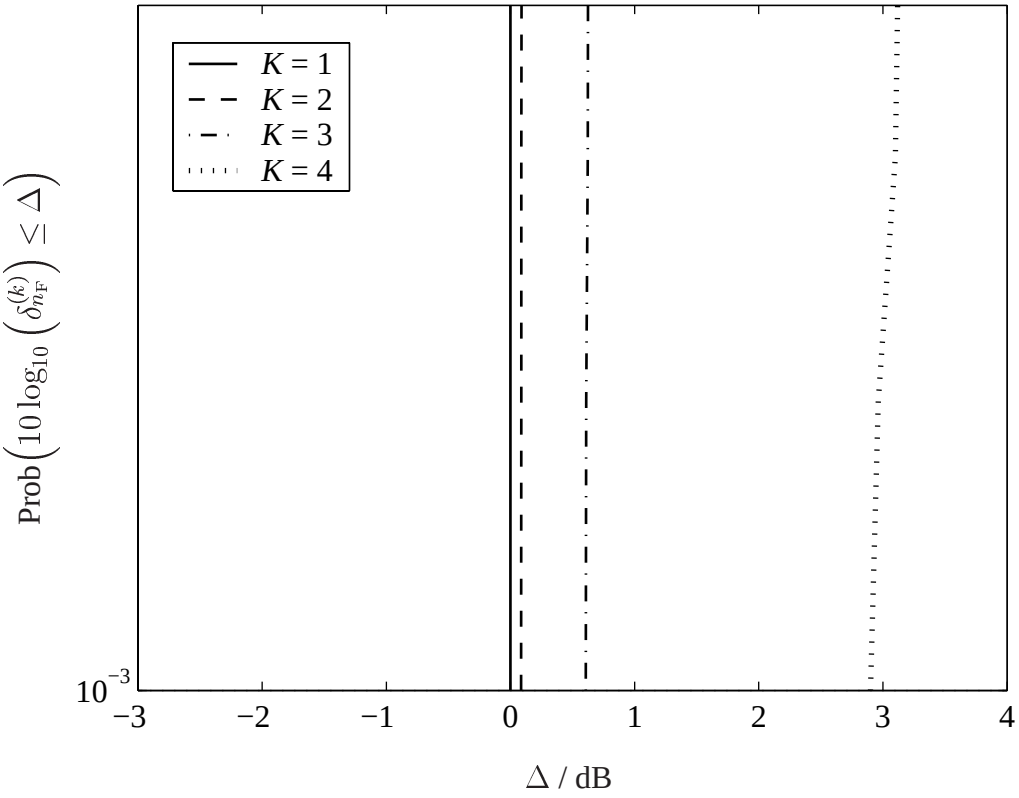

Fig. 5.3. Magnification of sector $-3 \ \ldots \ 4$ of the x-axis of Fig. 5.2

5.3.3 Variation coefficient

The performance of random pilot vectors $\underline{\tilde{\mathbf{p}}}^{(k)}$ with respect to the variation coefficient ν of (4.55) is shown in Fig. 5.4, where the cdf of ν for the number K of MTs equal to four and the four different cases of full system load given in (5.9) is displayed. One pair $(n_{\mathrm{SA}},\ n'_{\mathrm{SA}})$, $n_{\mathrm{SA}} \neq n'_{\mathrm{SA}}$, of adjacent SAs is considered, and the number of MTs in both SAs is equal to K. n_{SA} is considered as the reference $\mathrm{SA}_{\mathrm{ref}}$ and n'_{SA} is considered as the dominant interfering SA_{I}. As stated in Subsection 4.5.2, in each instant of time one specific MT k_{I}, $k_{\mathrm{I}} = 1 \ \ldots \ K$, out of the K MTs of the dominant interfering SA_{I} is considered as the dominant interferer disturbing $\mathrm{SA}_{\mathrm{ref}}$. Further, it is stated in Subsection 4.5.2 that it would be desirable for the interference impact of this dominant interferer alone to be spread as evenly as possible over all KN_{F} CTF estimates $\underline{\hat{\hat{h}}}^{(k)}_{n_{\mathrm{F}}}$ gained in $\mathrm{SA}_{\mathrm{ref}}$ [MWSL02]. To achieve this, the pilot vector set $\mathbb{P}^{(m)}$, $m = 1 \ \ldots \ 2^{N_{\mathrm{F}}}/K$, applied in $\mathrm{SA}_{\mathrm{ref}}$ should be different from the pilot vector set $\mathbb{P}^{(m')}$, $m' = 1 \ \ldots \ 2^{N_{\mathrm{F}}}/K$, $m' \neq m$, applied in SA_{I}. In the case of random pilot vectors $\underline{\tilde{\mathbf{p}}}^{(k)}$ this can be generally assured, since a large amount of different random pilot vectors $\underline{\tilde{\mathbf{p}}}^{(k)}$ can be generated, see Section 5.3.1. Another aspect observed in Fig. 5.4 is that with an increasing number N_{F} of available subcarriers, the variation coefficient ν also increases. The conjecture of the author is that by increasing N_{F}, i. e., increasing the dimension of the

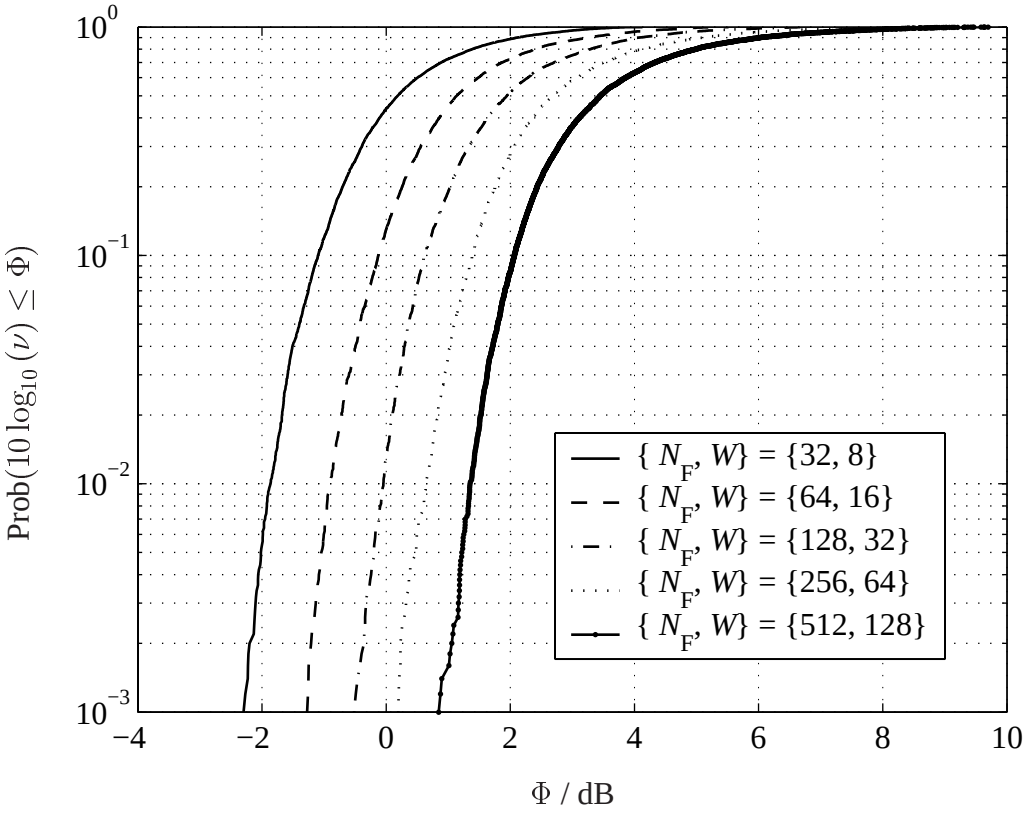

Fig. 5.4. Cdf of the variation coefficient ν of (4.55) for random pilot vectors $\underline{\tilde{\mathbf{p}}}^{(k)}$; number of MTs: $K = 4$ (full system load)

MT-specific pilot vectors $\underline{\tilde{\mathbf{p}}}^{(k)}$ of (5.5) and the total amount of possible pilot vectors, also increases the possibility of high inter-SA interference power caused in $\mathrm{SA}_{\mathrm{ref}}$. Consequently, the variance of the inter-SA power increases.

5.4 Pilot vectors based on the approach of disjoint subcarriers

5.4.1 Generation

In the previous section, the possibility of random pilot vectors for JCE is discussed, where all K MTs simultaneously use all N_{F} subcarriers for pilot vector radiation. In contrast to this concept, the generation of pilot vectors addressing disjoint subcarriers is based on the exclusive use of subcarrier subsets by each MT k, $k = 1 \ldots K$, in the considered SA n_{SA}. As mentioned at the end of Section 4.3, it is sufficient for the pilot vectors $\underline{\tilde{\mathbf{p}}}^{(k)}$ of (3.3) to have W non-zero elements. To this end, the N_{F} available subcarriers are divided in W subsets, each subset containing K pilot vectors $\underline{\tilde{\mathbf{p}}}^{(k)}$ of dimension N_{F}. Each of the pilot vectors $\underline{\tilde{\mathbf{p}}}^{(k)}$

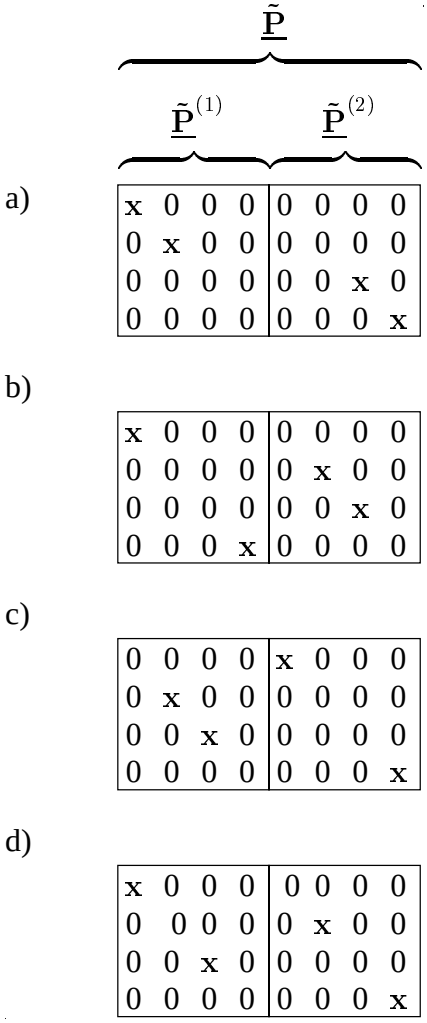

Fig. 5.5. Different options to place non-zero entries x in the total pilot matrix $\underline{\tilde{\mathbf{P}}}$; example: $\{N_{\mathrm{F}},\ K,\ W\} = \{4,\ 2,\ 2\}$
a) subcarrier assignment: MT 1 - subcarriers 1, 2; MT 2 - subcarriers 3, 4
b) subcarrier assignment: MT 1 - subcarriers 1, 4; MT 2 - subcarriers 2, 3
c) subcarrier assignment: MT 1 - subcarriers 2, 3; MT 2 - subcarriers 1, 4
d) subcarrier assignment: MT 1 - subcarriers 1, 3; MT 2 - subcarriers 2, 4

contains W non-zero elements $\underline{\tilde{p}}_{n_{\mathrm{F}}}^{(k)}$, see also Fig. 4.1. Due to the exclusive usage of subcarrier subsets by the MTs, the resulting disjoint pilot vectors are orthogonal to each other.

In order to illustrate these statements, we consider the exemplary case characterized by the parameter triplet

$$\{N_{\mathrm{F}},\ K,\ W\} = \{4,\ 2,\ 2\}\,, \tag{5.10}$$

where for convenience we assume all parameters to be powers of two in contrast to (4.29). Fig. 5.5a to d show four different possibilities of where the non-zero entries x of the total pilot matrix $\underline{\tilde{\mathbf{P}}}$ of (4.10) can be situated. In Fig. 5.5a, MT 1 is assigned the subset containing

subcarriers $n_{\mathrm{F}} = 1$ and 2, whereas MT 2 is assigned the subset containing subcarriers $n_{\mathrm{F}} = 3$ and 4. This assignment of subcarrier subsets leads to the MT-specific disjoint pilot vectors

$$\begin{aligned} \underline{\tilde{\mathbf{p}}}^{(1)} &= \left(\underline{\tilde{p}}_1^{(1)}\ \underline{\tilde{p}}_2^{(1)}\ 0\ 0\right)^{\mathrm{T}}, \\ \underline{\tilde{\mathbf{p}}}^{(2)} &= \left(0\ 0\ \underline{\tilde{p}}_3^{(2)}\ \underline{\tilde{p}}_4^{(2)}\right)^{\mathrm{T}}. \end{aligned} \tag{5.11}$$

With (5.10) and (5.11), (5.3) is rewritten as

$$\begin{aligned} \underline{\tilde{\mathcal{G}}} &= \underline{\tilde{\mathbf{P}}}\,\underline{\tilde{\mathcal{F}}}_{\mathrm{W}} = \left(\underline{\tilde{\mathcal{G}}}^{(1)}\ \cdots\ \underline{\tilde{\mathcal{G}}}^{(2)}\right) \\ &= \begin{pmatrix} \underline{\tilde{p}}_1^{(1)} & 0 & 0 & 0 & 0 & 0 & 0 & 0 \\ 0 & \underline{\tilde{p}}_2^{(1)} & 0 & 0 & 0 & 0 & 0 & 0 \\ 0 & 0 & 0 & 0 & 0 & 0 & \underline{\tilde{p}}_3^{(2)} & 0 \\ 0 & 0 & 0 & 0 & 0 & 0 & 0 & \underline{\tilde{p}}_4^{(2)} \end{pmatrix} \cdot \begin{pmatrix} \underline{\tilde{f}}_{1,1} & \underline{\tilde{f}}_{1,2} & 0 & 0 \\ \underline{\tilde{f}}_{2,1} & \underline{\tilde{f}}_{2,2} & 0 & 0 \\ \underline{\tilde{f}}_{3,1} & \underline{\tilde{f}}_{3,2} & 0 & 0 \\ \underline{\tilde{f}}_{4,1} & \underline{\tilde{f}}_{4,2} & 0 & 0 \\ 0 & 0 & \underline{\tilde{f}}_{1,1} & \underline{\tilde{f}}_{1,2} \\ 0 & 0 & \underline{\tilde{f}}_{2,1} & \underline{\tilde{f}}_{2,2} \\ 0 & 0 & \underline{\tilde{f}}_{3,1} & \underline{\tilde{f}}_{3,2} \\ 0 & 0 & \underline{\tilde{f}}_{4,1} & \underline{\tilde{f}}_{4,2} \end{pmatrix} \\ &= \begin{pmatrix} \underline{\tilde{p}}_1^{(1)}\underline{\tilde{f}}_{1,1} & \underline{\tilde{p}}_1^{(1)}\underline{\tilde{f}}_{1,2} & 0 & 0 \\ \underline{\tilde{p}}_2^{(1)}\underline{\tilde{f}}_{2,1} & \underline{\tilde{p}}_2^{(1)}\underline{\tilde{f}}_{2,2} & 0 & 0 \\ 0 & 0 & \underline{\tilde{p}}_3^{(2)}\underline{\tilde{f}}_{3,1} & \underline{\tilde{p}}_3^{(2)}\underline{\tilde{f}}_{3,2} \\ 0 & 0 & \underline{\tilde{p}}_4^{(2)}\underline{\tilde{f}}_{4,1} & \underline{\tilde{p}}_4^{(2)}\underline{\tilde{f}}_{4,2} \end{pmatrix}. \end{aligned} \tag{5.12}$$

Since the subcarrier subsets are used by the MTs in an exclusive manner and under consideration of (5.1), a special way to select the non-zero elements of the two MT-specific pilot vectors $\underline{\tilde{\mathbf{p}}}^{(k)}$, $k = 1,\ 2$, of (5.11) is

$$\begin{aligned} \underline{\tilde{\mathbf{p}}}^{(1)} &= \sqrt{\frac{2E_{\mathrm{p}}}{W}} \cdot (1\ 1\ 0\ 0)^{\mathrm{T}} \\ \underline{\tilde{\mathbf{p}}}^{(2)} &= \sqrt{\frac{2E_{\mathrm{p}}}{W}} \cdot (0\ 0\ 1\ 1)^{\mathrm{T}}. \end{aligned} \tag{5.13}$$

With (5.12) and (5.13), (5.4) is rewritten as

$$\underline{\tilde{\mathcal{G}}}^{\mathsf{H}}\underline{\tilde{\mathcal{G}}} = \begin{pmatrix} (\underline{\tilde{p}}_1^{(1)} \cdot \underline{\tilde{f}}_{1,1})^* & (\underline{\tilde{p}}_2^{(1)} \cdot \underline{\tilde{f}}_{2,1})^* & 0 & 0 \\ (\underline{\tilde{p}}_1^{(1)} \cdot \underline{\tilde{f}}_{1,2})^* & (\underline{\tilde{p}}_2^{(1)} \cdot \underline{\tilde{f}}_{2,2})^* & 0 & 0 \\ 0 & 0 & (\underline{\tilde{p}}_3^{(2)} \cdot \underline{\tilde{f}}_{3,1})^* & (\underline{\tilde{p}}_4^{(2)} \cdot \underline{\tilde{f}}_{4,1})^* \\ 0 & 0 & (\underline{\tilde{p}}_3^{(2)} \cdot \underline{\tilde{f}}_{3,2})^* & (\underline{\tilde{p}}_4^{(2)} \cdot \underline{\tilde{f}}_{4,2})^* \end{pmatrix} \cdot \tag{5.14}$$

$$
\begin{pmatrix}
\underline{\tilde{p}}_1^{(1)}\underline{\tilde{f}}_{1,1} & \underline{\tilde{p}}_1^{(1)}\underline{\tilde{f}}_{1,2} & 0 & 0 \\
\underline{\tilde{p}}_2^{(1)}\underline{\tilde{f}}_{2,1} & \underline{\tilde{p}}_2^{(1)}\underline{\tilde{f}}_{2,2} & 0 & 0 \\
0 & 0 & \underline{\tilde{p}}_3^{(2)}\underline{\tilde{f}}_{3,1} & \underline{\tilde{p}}_3^{(2)}\underline{\tilde{f}}_{3,2} \\
0 & 0 & \underline{\tilde{p}}_4^{(2)}\underline{\tilde{f}}_{4,1} & \underline{\tilde{p}}_4^{(2)}\underline{\tilde{f}}_{4,2}
\end{pmatrix}
$$

$$
= \begin{pmatrix}
\sum_{i=1}^{2}\left|\underline{\tilde{p}}_i^{(1)}\right|^2\left|\underline{\tilde{f}}_{i,1}\right|^2 & \sum_{i=1}^{2}\left|\underline{\tilde{p}}_i^{(1)}\right|^2\underline{\tilde{f}}_{i,1}^{*}\underline{\tilde{f}}_{i,2} & 0 & 0 \\
\sum_{i=1}^{2}\left|\underline{\tilde{p}}_i^{(1)}\right|^2\underline{\tilde{f}}_{i,2}^{*}\underline{\tilde{f}}_{i,1} & \sum_{i=1}^{2}\left|\underline{\tilde{p}}_i^{(1)}\right|^2\left|\underline{\tilde{f}}_{i,2}\right|^2 & 0 & 0 \\
0 & 0 & \sum_{j=3}^{4}\left|\underline{\tilde{p}}_j^{(2)}\right|^2\left|\underline{\tilde{f}}_{j,1}\right|^2 & \sum_{j=3}^{4}\left|\underline{\tilde{p}}_j^{(2)}\right|^2\underline{\tilde{f}}_{j,1}^{*}\underline{\tilde{f}}_{j,2} \\
0 & 0 & \sum_{j=3}^{4}\left|\underline{\tilde{p}}_j^{(2)}\right|^2\underline{\tilde{f}}_{j,2}^{*}\underline{\tilde{f}}_{j,1} & \sum_{j=3}^{4}\left|\underline{\tilde{p}}_j^{(2)}\right|^2\left|\underline{\tilde{f}}_{j,2}\right|^2
\end{pmatrix}
$$

$$
= \begin{pmatrix}
2E_\mathrm{p} & \frac{2E_\mathrm{p}}{W}\cdot\sum_{i=1}^{2}\underline{\tilde{f}}_{i,1}^{*}\underline{\tilde{f}}_{i,2} & 0 & 0 \\
\frac{2E_\mathrm{p}}{W}\cdot\sum_{i=1}^{2}\underline{\tilde{f}}_{i,2}^{*}\underline{\tilde{f}}_{i,1} & 1 & 0 & 0 \\
0 & 0 & 2E_\mathrm{p} & \frac{2E_\mathrm{p}}{W}\cdot\sum_{j=3}^{4}\underline{\tilde{f}}_{j,1}^{*}\underline{\tilde{f}}_{j,2} \\
0 & 0 & \frac{2E_\mathrm{p}}{W}\cdot\sum_{j=3}^{4}\underline{\tilde{f}}_{j,2}^{*}\underline{\tilde{f}}_{j,1} & 2E_\mathrm{p}
\end{pmatrix}.
$$

For the exemplary parameter triplet of (5.10) the reduced blockdiagonal Fourier matrix $\underline{\tilde{\boldsymbol{\mathcal{F}}}}_\mathrm{W}$ of (4.21) becomes

$$
\underline{\tilde{\boldsymbol{\mathcal{F}}}}_\mathrm{W} = \begin{pmatrix}
1 & 1 & 0 & 0 \\
1 & -\mathrm{j} & 0 & 0 \\
1 & -1 & 0 & 0 \\
1 & \mathrm{j} & 0 & 0 \\
0 & 0 & 1 & 1 \\
0 & 0 & 1 & -\mathrm{j} \\
0 & 0 & 1 & -1 \\
0 & 0 & 1 & \mathrm{j}
\end{pmatrix}, \tag{5.15}
$$

and with (5.15), (5.14) becomes

$$
\underline{\tilde{\boldsymbol{\mathcal{G}}}}^{\mathsf{H}}\underline{\tilde{\boldsymbol{\mathcal{G}}}} = \begin{pmatrix}
2E_\mathrm{p} & \frac{2E_\mathrm{p}}{2}\cdot(1-\mathrm{j}) & 0 & 0 \\
\frac{2E_\mathrm{p}}{2}\cdot(1+\mathrm{j}) & 2E_\mathrm{p} & 0 & 0 \\
0 & 0 & 2E_\mathrm{p} & \frac{2E_\mathrm{p}}{2}\cdot(-1+\mathrm{j}) \\
0 & 0 & \frac{2E_\mathrm{p}}{2}\cdot(-1-\mathrm{j}) & 2E_\mathrm{p}
\end{pmatrix}. \tag{5.16}
$$

Not all off-diagonal elements of this matrix are zero, and according to the considerations presented in Section 5.2, (5.16) leads to SNR degradations $\delta_{n_\mathrm{F}}^{(k)}$ larger than one. Applying

the assignments of subcarrier subsets illustrated in Fig. 5.5b and c also leads to non-zero off-diagonal elements of the matrix $\underline{\tilde{\boldsymbol{\mathcal{G}}}}^{\mathsf{H}}\underline{\tilde{\boldsymbol{\mathcal{G}}}}$.

In contrast to the assignments of subcarrier subsets illustrated in Fig. 5.5a, b and c, applying the assignment of subcarrier subsets illustrated in Fig. 5.5d leads to the MT-specific disjoint pilot vectors

$$\begin{aligned}\underline{\tilde{\mathbf{p}}}^{(1)} &= \left(\underline{\tilde{p}}_1^{(1)}\ 0\ \underline{\tilde{p}}_3^{(1)}\ 0\right)^{\mathrm{T}} = \sqrt{\frac{2E_{\mathrm{p}}}{W}}\cdot(1\ 0\ 1\ 0)^{\mathrm{T}},\\ \underline{\tilde{\mathbf{p}}}^{(2)} &= \left(0\ \underline{\tilde{p}}_2^{(2)}\ 0\ \underline{\tilde{p}}_4^{(2)}\right)^{\mathrm{T}} = \sqrt{\frac{2E_{\mathrm{p}}}{W}}\cdot(0\ 1\ 0\ 1)^{\mathrm{T}},\end{aligned} \tag{5.17}$$

and with (5.17), (5.12) leads to

$$\begin{aligned}\underline{\tilde{\boldsymbol{\mathcal{G}}}} &= \underline{\tilde{\mathbf{P}}}\,\underline{\tilde{\boldsymbol{\mathcal{F}}}}_{\mathrm{W}} = \left(\underline{\tilde{\boldsymbol{\mathcal{G}}}}^{(1)}\ \cdots\ \underline{\tilde{\boldsymbol{\mathcal{G}}}}^{(2)}\right)\\ &= \begin{pmatrix} \underline{\tilde{p}}_1^{(1)} & 0 & 0 & 0 & 0 & 0 & 0 & 0\\ 0 & 0 & 0 & 0 & 0 & \underline{\tilde{p}}_2^{(2)} & 0 & 0\\ 0 & 0 & \underline{\tilde{p}}_3^{(1)} & 0 & 0 & 0 & 0 & 0\\ 0 & 0 & 0 & 0 & 0 & 0 & 0 & \underline{\tilde{p}}_4^{(2)} \end{pmatrix} \cdot \begin{pmatrix} \underline{\tilde{f}}_{1,1} & \underline{\tilde{f}}_{1,2} & 0 & 0\\ \underline{\tilde{f}}_{2,1} & \underline{\tilde{f}}_{2,2} & 0 & 0\\ \underline{\tilde{f}}_{3,1} & \underline{\tilde{f}}_{3,2} & 0 & 0\\ \underline{\tilde{f}}_{4,1} & \underline{\tilde{f}}_{4,2} & 0 & 0\\ 0 & 0 & \underline{\tilde{f}}_{1,1} & \underline{\tilde{f}}_{1,2}\\ 0 & 0 & \underline{\tilde{f}}_{2,1} & \underline{\tilde{f}}_{2,2}\\ 0 & 0 & \underline{\tilde{f}}_{3,1} & \underline{\tilde{f}}_{3,2}\\ 0 & 0 & \underline{\tilde{f}}_{4,1} & \underline{\tilde{f}}_{4,2} \end{pmatrix}\\ &= \begin{pmatrix} \underline{\tilde{p}}_1^{(1)}\underline{\tilde{f}}_{1,1} & \underline{\tilde{p}}_1^{(1)}\underline{\tilde{f}}_{1,2} & 0 & 0\\ 0 & 0 & \underline{\tilde{p}}_2^{(2)}\underline{\tilde{f}}_{2,1} & \underline{\tilde{p}}_2^{(2)}\underline{\tilde{f}}_{2,2}\\ \underline{\tilde{p}}_3^{(1)}\underline{\tilde{f}}_{3,1} & \underline{\tilde{p}}_3^{(1)}\underline{\tilde{f}}_{3,2} & 0 & 0\\ 0 & 0 & \underline{\tilde{p}}_4^{(2)}\underline{\tilde{f}}_{4,1} & \underline{\tilde{p}}_4^{(2)}\underline{\tilde{f}}_{4,2} \end{pmatrix}.\end{aligned} \tag{5.18}$$

Now, with (5.15), (5.17) and (5.18), (5.4) can be rewritten as

$$\underline{\tilde{\boldsymbol{\mathcal{G}}}}^{\mathsf{H}}\underline{\tilde{\boldsymbol{\mathcal{G}}}} = \begin{pmatrix} (\underline{\tilde{p}}_1^{(1)}\cdot\underline{\tilde{f}}_{1,1})^* & 0 & (\underline{\tilde{p}}_3^{(1)}\cdot\underline{\tilde{f}}_{3,1})^* & 0\\ (\underline{\tilde{p}}_1^{(1)}\cdot\underline{\tilde{f}}_{1,2})^* & 0 & (\underline{\tilde{p}}_3^{(1)}\cdot\underline{\tilde{f}}_{3,2})^* & 0\\ 0 & (\underline{\tilde{p}}_2^{(2)}\cdot\underline{\tilde{f}}_{2,1})^* & 0 & (\underline{\tilde{p}}_4^{(2)}\cdot\underline{\tilde{f}}_{4,1})^*\\ 0 & (\underline{\tilde{p}}_2^{(2)}\cdot\underline{\tilde{f}}_{2,2})^* & 0 & (\underline{\tilde{p}}_4^{(2)}\cdot\underline{\tilde{f}}_{4,2})^* \end{pmatrix}\cdot$$

$$\begin{pmatrix} \underline{\tilde{p}}_1^{(1)}\underline{\tilde{f}}_{1,1} & \underline{\tilde{p}}_1^{(1)}\underline{\tilde{f}}_{1,2} & 0 & 0\\ 0 & 0 & \underline{\tilde{p}}_2^{(2)}\underline{\tilde{f}}_{2,1} & \underline{\tilde{p}}_2^{(2)}\underline{\tilde{f}}_{2,2}\\ \underline{\tilde{p}}_3^{(1)}\underline{\tilde{f}}_{3,1} & \underline{\tilde{p}}_3^{(1)}\underline{\tilde{f}}_{3,2} & 0 & 0\\ 0 & 0 & \underline{\tilde{p}}_4^{(2)}\underline{\tilde{f}}_{4,1} & \underline{\tilde{p}}_4^{(2)}\underline{\tilde{f}}_{4,2} \end{pmatrix}$$

$$= \begin{pmatrix} 2E_\mathrm{p} & \frac{2E_\mathrm{p}}{W} \cdot \sum\limits_{i=1,3} \underline{\tilde{f}}^*_{i,1} \underline{\tilde{f}}_{i,2} & 0 & 0 \\ \frac{2E_\mathrm{p}}{W} \cdot \sum\limits_{i=1,3} \underline{\tilde{f}}^*_{i,2} \underline{\tilde{f}}_{i,1} & 2E_\mathrm{p} & 0 & 0 \\ 0 & 0 & 2E_\mathrm{p} & \frac{2E_\mathrm{p}}{W} \cdot \sum\limits_{j=2,4} \underline{\tilde{f}}^*_{j,1} \underline{\tilde{f}}_{j,2} \\ 0 & 0 & \frac{2E_\mathrm{p}}{W} \cdot \sum\limits_{j=2,4} \underline{\tilde{f}}^*_{j,2} \underline{\tilde{f}}_{j,1} & 2E_\mathrm{p} \end{pmatrix}$$

$$= 2E_\mathrm{p} \cdot \begin{pmatrix} 1 & 0 & 0 & 0 \\ 0 & 1 & 0 & 0 \\ 0 & 0 & 1 & 0 \\ 0 & 0 & 0 & 1 \end{pmatrix} . \tag{5.19}$$

It can be seen from (5.14) and (5.19) that in the case of disjoint pilot vectors, only off-diagonal elements of Type I of $\underline{\tilde{\mathcal{G}}}^\mathsf{H} \underline{\tilde{\mathcal{G}}}$ are present. Due to the existing orthogonality between the K disjoint pilot vectors $\underline{\tilde{\mathbf{p}}}^{(k)}$, which can be verified by (5.11) and (5.17), the off-diagonal elements of Type II of $\underline{\tilde{\mathcal{G}}}^\mathsf{H} \underline{\tilde{\mathcal{G}}}$ are equal to zero, see also (5.8). Further, since the values of all non-zero elements $\underline{\tilde{p}}^{(k)}_{n_\mathrm{F}}$ of $\underline{\tilde{\mathbf{p}}}^{(k)}$ are equal to $\sqrt{2E_\mathrm{p}/W}$, see (5.11) and (5.17), the non-zero off-diagonal elements of Type III of $\underline{\tilde{\mathcal{G}}}^\mathsf{H} \underline{\tilde{\mathcal{G}}}$ are identical to those of Type I.

Because only W non-zero elements $\underline{\tilde{p}}^{(k)}_{n_\mathrm{F}}$ are contained in each MT-specific disjoint pilot vector $\underline{\tilde{\mathbf{p}}}^{(k)}$, also W non-zero elements of the corresponding column vector $\underline{\tilde{\mathbf{f}}}_w$, $w = 1 \ldots W$, of $\underline{\tilde{\mathcal{F}}}_\mathrm{W}$ are met in each column of $\underline{\tilde{\mathcal{G}}}$, see (5.12) and (5.18). Therefore, for the off-diagonal elements of Type I of $\underline{\tilde{\mathcal{G}}}^\mathsf{H} \underline{\tilde{\mathcal{G}}}$, there are not the column vectors $\underline{\tilde{\mathbf{f}}}_w$ and $\underline{\tilde{\mathbf{f}}}_{w'}$, $w \neq w'$, of the Fourier matrix $\underline{\tilde{\mathcal{F}}}$ which are cross-correlated, but the subvectors $\underline{\tilde{\mathbf{f}}}_m$ and $\underline{\tilde{\mathbf{f}}}_{m'}$, $m \neq m'$ of $\underline{\tilde{\mathbf{f}}}_w$ and $\underline{\tilde{\mathbf{f}}}_{w'}$, $w \neq w'$, respectively. The respective elements $\underline{\tilde{f}}_{m,n}$ and $\underline{\tilde{f}}_{m',n}$ of the subvectors $\underline{\tilde{\mathbf{f}}}_m$ and $\underline{\tilde{\mathbf{f}}}_{m'}$ are determined by the placement of the non-zero elements $\underline{\tilde{p}}^{(k)}_{n_\mathrm{F}}$ of $\underline{\tilde{\mathbf{p}}}^{(k)}$ on the main diagonal of the MT-specific pilot matrices $\underline{\tilde{\mathbf{P}}}^{(k)}$ of (4.7) and in the total pilot matrix $\underline{\tilde{\mathbf{P}}}$ of (4.10). If the elements $\underline{\tilde{f}}_{m,n}$ and $\underline{\tilde{f}}_{m',n}$ are chosen with the same mutual distance N_F/W from each other, then the resulting subvectors $\underline{\tilde{\mathbf{f}}}_m$ and $\underline{\tilde{\mathbf{f}}}_{m'}$ are orthogonal to each other. Any distance other than N_F/W leads to non-orthogonal subvectors $\underline{\tilde{\mathbf{f}}}_m$ and $\underline{\tilde{\mathbf{f}}}_{m'}$, as it can be verified by the examples of Fig. 5.5a, b and c. Therefore, the non-zero elements $\underline{\tilde{p}}^{(k)}_{n_\mathrm{F}}$ of $\underline{\tilde{\mathbf{p}}}^{(k)}$ should be placed with respect to the distance N_F/W from each other on the main diagonal of the MT-specific pilot matrices $\underline{\tilde{\mathbf{P}}}^{(k)}$ of (4.7). This leads to the MT-specific disjoint pilot vectors [SMWB01, MWSL02]

$$\underline{\tilde{\mathbf{p}}}^{(k)} = \sqrt{\frac{2E_\mathrm{p}}{W}} \cdot (\underbrace{0 \ \ldots \ 0}_{k-1} \, 1 \, \underbrace{0 \ \ldots \ 0}_{\frac{N_\mathrm{F}}{W}-k} \ \ldots \ \underbrace{0 \ \ldots \ 0}_{\frac{N_\mathrm{F}}{W}-1} \, 1 \, \underbrace{0 \ \ldots \ 0}_{\frac{N_\mathrm{F}}{W}-k})^\mathrm{T} , \ k = 1 \ \ldots \ K. \tag{5.20}$$

These pilot vectors form an ideal set of pilot vectors.

5.4.2 SNR degradations

Considering the exclusive subcarrier assignment demonstrated in Fig. 5.5d, for a fixed parameter triplet $\{N_\mathrm{F},\ K,\ W\}$ only K disjoint pilot vectors $\underline{\tilde{\mathbf{p}}}^{(k)}$ of dimension N_F result out of (5.20). With these K disjoint pilot vectors we can form via (4.7) and (4.10) the unique total pilot matrix $\underline{\tilde{\mathbf{P}}}$, which is applied in the considered SA. $\underline{\tilde{\mathbf{P}}}$ leads to SNR degradations $\delta_{n_\mathrm{F}}^{(k)}$ equal to one, as demonstrated for the exemplary scenario characterized by (5.10). Besides this benefit concerning the SNR degradations $\delta_{n_\mathrm{F}}^{(k)}$, the application of disjoint pilot vectors $\underline{\tilde{\mathbf{p}}}^{(k)}$ according to (5.20) leads to a reduced computational complexity for ML-JCE, since the effort required for inverting the matrix $\underline{\tilde{\mathcal{G}}}^{\mathsf{H}}\underline{\tilde{\mathcal{G}}}$ is relaxed. Unless stated otherwise, whenever disjoint pilot vectors are mentioned in the following, the pilot vectors $\underline{\tilde{\mathbf{p}}}^{(k)}$ of (5.20) leading to SNR degradations $\delta_{n_\mathrm{F}}^{(k)}$ equal to one are meant.

5.4.3 Variation coefficient

It is mentioned in Section 5.4.2 that the resulting unique set $\mathbb{P}^{(n_\mathrm{SA})}$ of disjoint pilot vectors $\underline{\tilde{\mathbf{p}}}^{(k)}$ of (5.20) leads to SNR degradations $\delta_{n_\mathrm{F}}^{(k)}$ equal to one. This means that the Gram matrix $\underline{\tilde{\mathcal{G}}}^{\mathsf{H}}\underline{\tilde{\mathcal{G}}}$ is a diagonal matrix, i. e.

$$\underline{\tilde{\mathcal{G}}}^{\mathsf{H}}\underline{\tilde{\mathcal{G}}} = 2E_\mathrm{p} \cdot \mathbf{I}^{(KW \times KW)} \tag{5.21}$$

holds. With (5.21), the inter-SA interference matrix $\underline{\mathcal{I}}$ of (4.48) can be rewritten as

$$\underline{\mathcal{I}} = \frac{1}{2E_\mathrm{p}} \cdot \underline{\tilde{\mathcal{F}}}_\mathrm{W}\underline{\tilde{\mathcal{G}}}^{\mathsf{H}}\underline{\tilde{\mathcal{G}}}_\mathrm{I} = \frac{1}{2E_\mathrm{p}} \cdot \underline{\mathcal{F}}_\mathrm{W} \begin{pmatrix} \underline{\tilde{\mathcal{G}}}^{(1)^{\mathsf{H}}} \\ \vdots \\ \underline{\tilde{\mathcal{G}}}^{(K)^{\mathsf{H}}} \end{pmatrix} \left(\underline{\tilde{\mathcal{G}}}_\mathrm{I}^{(1)} \ \ldots \ \underline{\tilde{\mathcal{G}}}_\mathrm{I}^{(K)} \right) \tag{5.22}$$

and depends on the cross-correlations of the pilot vectors $\underline{\tilde{\mathbf{p}}}^{(k)}$ and $\underline{\tilde{\mathbf{p}}}^{(k_\mathrm{I})}$ applied in the considered SA_ref and the adjacent SA_I, respectively. In the worst case that SA_ref and SA_I must both use the unique set of disjoint pilot vectors $\underline{\tilde{\mathbf{p}}}^{(k)}$ of (5.20), the K MTs in SA_ref and the K MTs in SA_I will be using the same disjoint pilot vectors pairwise. This means that in a certain time instant where one dominant interferer k_I of SA_I is considered, the impact of this dominant interferer is concentrated on the CTF estimates $\underline{\hat{\tilde{h}}}_{n_\mathrm{F}}^{(k)}$ of this MT k in SA_ref, which applies the same disjoint pilot vector $\underline{\tilde{\mathbf{p}}}^{(k)}$ as the dominant interferer k_I of SA_I. For the parameter triplet of (5.10) and applying the disjoint pilot vectors $\underline{\tilde{\mathbf{p}}}^{(1)}$ and $\underline{\tilde{\mathbf{p}}}^{(2)}$ of (5.17)

$$\underline{\tilde{\boldsymbol{\mathcal{G}}}}^{\mathsf{H}} = \begin{pmatrix} (\underline{\tilde{p}}_1^{(1)}\underline{\tilde{f}}_{1,1})^* & 0 & (\underline{\tilde{p}}_3^{(1)}\underline{\tilde{f}}_{3,1})^* & 0 \\ (\underline{\tilde{p}}_1^{(1)}\underline{\tilde{f}}_{1,2})^* & 0 & (\underline{\tilde{p}}_3^{(1)}\underline{\tilde{f}}_{3,2})^* & 0 \\ 0 & (\underline{\tilde{p}}_2^{(2)}\underline{\tilde{f}}_{2,1})^* & 0 & (\underline{\tilde{p}}_4^{(2)}\underline{\tilde{f}}_{4,1})^* \\ 0 & (\underline{\tilde{p}}_2^{(2)}\underline{\tilde{f}}_{2,2})^* & 0 & (\underline{\tilde{p}}_4^{(2)}\underline{\tilde{f}}_{4,2})^* \end{pmatrix} \tag{5.23}$$

holds. If, for instance, the dominant interferer k_I of $\mathrm{SA_I}$ uses the disjoint pilot vector $\underline{\tilde{\mathbf{p}}}^{(1)}$ of (5.17), then

$$\underline{\tilde{\boldsymbol{\mathcal{G}}}}_\mathrm{I}^{(k_\mathrm{I})} = \begin{pmatrix} \underline{\tilde{p}}_1^{(1)}\underline{\tilde{f}}_{1,1} & \underline{\tilde{p}}_1^{(1)}\underline{\tilde{f}}_{1,2} \\ 0 & 0 \\ \underline{\tilde{p}}_3^{(1)}\underline{\tilde{f}}_{3,1} & \underline{\tilde{p}}_3^{(1)}\underline{\tilde{f}}_{3,2} \\ 0 & 0 \end{pmatrix} \tag{5.24}$$

holds for the interferer specific system matrix of $\mathrm{SA_I}$, and with (5.15), (5.23) and (5.24), the interferer specific inter-SA matrix

$$\underline{\boldsymbol{\mathcal{I}}}^{(k_\mathrm{I})} = \begin{pmatrix} \underline{\boldsymbol{\mathcal{I}}}^{(k_\mathrm{I},1)} \\ \underline{\boldsymbol{\mathcal{I}}}^{(k_\mathrm{I},2)} \end{pmatrix} = \begin{pmatrix} \underline{\boldsymbol{\mathcal{I}}}^{(1,1)} \\ \underline{\boldsymbol{\mathcal{I}}}^{(1,2)} \end{pmatrix} = \frac{1}{2E_\mathrm{p}} \cdot \underline{\tilde{\boldsymbol{\mathcal{F}}}}_\mathrm{W} \underline{\tilde{\boldsymbol{\mathcal{G}}}}^{\mathsf{H}} \underline{\tilde{\boldsymbol{\mathcal{G}}}}_\mathrm{I}^{(k_\mathrm{I})} \tag{5.25}$$

$$= \frac{1}{2E_\mathrm{p}} \cdot \begin{pmatrix} \underline{\tilde{f}}_{1,1} & \underline{\tilde{f}}_{1,2} & 0 & 0 \\ \underline{\tilde{f}}_{2,1} & \underline{\tilde{f}}_{2,2} & 0 & 0 \\ \underline{\tilde{f}}_{3,1} & \underline{\tilde{f}}_{3,2} & 0 & 0 \\ \underline{\tilde{f}}_{4,1} & \underline{\tilde{f}}_{4,2} & 0 & 0 \\ 0 & 0 & \underline{\tilde{f}}_{1,1} & \underline{\tilde{f}}_{1,2} \\ 0 & 0 & \underline{\tilde{f}}_{2,1} & \underline{\tilde{f}}_{2,2} \\ 0 & 0 & \underline{\tilde{f}}_{3,1} & \underline{\tilde{f}}_{3,2} \\ 0 & 0 & \underline{\tilde{f}}_{4,1} & \underline{\tilde{f}}_{4,2} \end{pmatrix} \begin{pmatrix} 2E_\mathrm{p} & \sum_i \left|\underline{\tilde{p}}_i^{(1)}\right|^2 \underline{\tilde{f}}_{i,1}^* \underline{\tilde{f}}_{i,2} \\ \sum_i \left|\underline{\tilde{p}}_i^{(1)}\right|^2 \underline{\tilde{f}}_{i,2}^* \underline{\tilde{f}}_{i,1} & 2E_\mathrm{p} \\ 0 & 0 \\ 0 & 0 \end{pmatrix}$$

$$= \frac{1}{2E_\mathrm{p}} \cdot \begin{pmatrix} 2E_\mathrm{p}\left(\underline{\tilde{f}}_{1,1} + \frac{\underline{\tilde{f}}_{1,2}}{W} \cdot \sum_i \underline{\tilde{f}}_{i,2}^* \underline{\tilde{f}}_{i,1}\right) & 2E_\mathrm{p}\left(\frac{\underline{\tilde{f}}_{1,1}}{W} \cdot \sum_i \underline{\tilde{f}}_{i,1}^* \underline{\tilde{f}}_{i,2} + \underline{\tilde{f}}_{1,2}\right) \\ 2E_\mathrm{p}\left(\underline{\tilde{f}}_{2,1} + \frac{\underline{\tilde{f}}_{2,2}}{W} \cdot \sum_i \underline{\tilde{f}}_{i,2}^* \underline{\tilde{f}}_{i,1}\right) & 2E_\mathrm{p}\left(\frac{\underline{\tilde{f}}_{2,1}}{W} \cdot \sum_i \underline{\tilde{f}}_{i,1}^* \underline{\tilde{f}}_{i,2} + \underline{\tilde{f}}_{2,2}\right) \\ 2E_\mathrm{p}\left(\underline{\tilde{f}}_{3,1} + \frac{\underline{\tilde{f}}_{3,2}}{W} \cdot \sum_i \underline{\tilde{f}}_{i,2}^* \underline{\tilde{f}}_{i,1}\right) & 2E_\mathrm{p}\left(\frac{\underline{\tilde{f}}_{3,1}}{W} \cdot \sum_i \underline{\tilde{f}}_{i,1}^* \underline{\tilde{f}}_{i,2} + \underline{\tilde{f}}_{3,2}\right) \\ 2E_\mathrm{p}\left(\underline{\tilde{f}}_{4,1} + \frac{\underline{\tilde{f}}_{4,2}}{W} \cdot \sum_i \underline{\tilde{f}}_{i,2}^* \underline{\tilde{f}}_{i,1}\right) & 2E_\mathrm{p}\left(\frac{\underline{\tilde{f}}_{4,1}}{W} \cdot \sum_i \underline{\tilde{f}}_{i,1}^* \underline{\tilde{f}}_{i,2} + \underline{\tilde{f}}_{4,2}\right) \\ 0 & 0 \\ 0 & 0 \\ 0 & 0 \\ 0 & 0 \end{pmatrix}$$

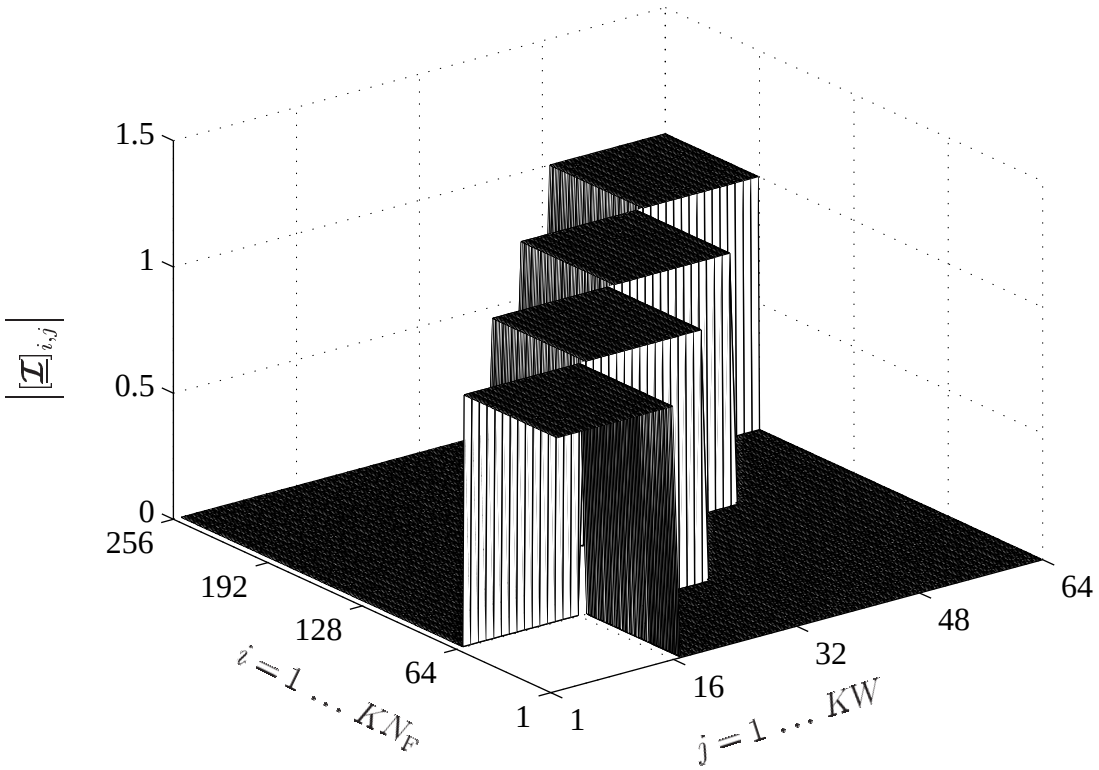

Fig. 5.6. Magnitudes $\left|[\underline{\underline{\mathcal{I}}}]_{i,j}\right|$, $i = 1 \ \ldots \ KN_{\mathrm{F}}$, $j = 1 \ \ldots \ KW$, of the inter-SA interference matrix $\underline{\underline{\mathcal{I}}}$ for the exemplary triplet $\{N_{\mathrm{F}},\ K,\ W\} = \{64,\ 4,\ 16\}$ and disjoint pilot vectors of (5.20)

$$= \begin{pmatrix} 1 & 1 \\ 1 & -\mathrm{j} \\ 1 & -1 \\ 1 & \mathrm{j} \\ 0 & 0 \\ 0 & 0 \\ 0 & 0 \\ 0 & 0 \end{pmatrix} = \begin{pmatrix} \underline{\tilde{f}}_{1,1} & \underline{\tilde{f}}_{1,2} \\ \underline{\tilde{f}}_{2,1} & \underline{\tilde{f}}_{2,2} \\ \underline{\tilde{f}}_{3,1} & \underline{\tilde{f}}_{3,2} \\ \underline{\tilde{f}}_{4,1} & \underline{\tilde{f}}_{4,2} \\ 0 & 0 \\ 0 & 0 \\ 0 & 0 \\ 0 & 0 \end{pmatrix}, \ i = 1,\ 3,$$

is obtained. (5.25) and (4.48) show that the interference originating in MT $k_{\mathrm{I}} = 1$ of SA_{I} will be spread only over the CTF estimates $\underline{\tilde{h}}_{n_{\mathrm{F}}}^{(1)}$ of MT 1 in $\mathrm{SA}_{\mathrm{ref}}$, which applies the same disjoint pilot vector $\underline{\tilde{\mathbf{p}}}^{(1)}$ as the dominant interferer $k_{\mathrm{I}} = 1$ of SA_{I}. With (5.25) and by applying (4.52) till (4.55), the variation ceofficient ν of (4.55) is equal to 0.73 for the exemplary parameter triplet of (5.10).

These considerations which are based on the numerical example of (5.10) can be extended in a straightforward manner to any fixed parameter triplet $\{N_{\mathrm{F}},\ K,\ W\}$. In this case, for the considered disjoint pilot vectors of (5.20), the interferer specific inter-SA interference matrix $\underline{\underline{\mathcal{I}}}^{(k_{\mathrm{I}})}$ is given by

$$\underline{\boldsymbol{\mathcal{I}}}^{(k_\mathrm{I})} = \begin{pmatrix} \underline{\boldsymbol{\mathcal{I}}}^{(k_\mathrm{I},1)} \\ \vdots \\ \underline{\boldsymbol{\mathcal{I}}}^{(k_\mathrm{I},K)} \end{pmatrix} = \begin{pmatrix} 0 & & 0 \\ \vdots & \cdots & \vdots \\ 0 & & 0 \end{pmatrix} \Bigg\} (k-1)N_\mathrm{F} \times (k-1)W$$
$$\vdots$$
$$\begin{pmatrix} \tilde{\underline{f}}_{1,1} & & \tilde{\underline{f}}_{1,W} \\ \vdots & \cdots & \vdots \\ \tilde{\underline{f}}_{N_\mathrm{F},1} & & \tilde{\underline{f}}_{N_\mathrm{F},W} \end{pmatrix} \Bigg\} N_\mathrm{F} \times W \tag{5.26}$$
$$\vdots$$
$$\begin{pmatrix} 0 & & 0 \\ \vdots & \cdots & \vdots \\ 0 & & 0 \end{pmatrix} \Bigg\} (K-k)N_\mathrm{F} \times (K-k)W,$$

and with (5.26) the inter-SA interference matrix of (4.48) and (5.25) reads

$$\underline{\boldsymbol{\mathcal{I}}} = \begin{pmatrix} \underline{\boldsymbol{\mathcal{I}}}^{(1,1)} & & \underline{\boldsymbol{\mathcal{I}}}^{(k_\mathrm{I},1)} & & \underline{\boldsymbol{\mathcal{I}}}^{(K,1)} \\ \vdots & \cdots & \vdots & \cdots & \vdots \\ \underline{\boldsymbol{\mathcal{I}}}^{(1,K)} & & \underline{\boldsymbol{\mathcal{I}}}^{(k_\mathrm{I},K)} & & \underline{\boldsymbol{\mathcal{I}}}^{(K,K)} \end{pmatrix}. \tag{5.27}$$

Fig. 5.6 illustrates the resulting structure of the inter-SA interference matrix $\underline{\boldsymbol{\mathcal{I}}}$ in the case of disjoint pilot vectors and demonstrates said pairwise impact of inter-SA interference. With (5.7) and (5.26) the interferer specific mean values $\overline{\mathcal{I}}^{(k_\mathrm{I})}$ of (4.52) are obtained as

$$\overline{\mathcal{I}}^{(k_\mathrm{I})} = \frac{WN_\mathrm{F}}{KN_\mathrm{F}W} = \frac{1}{K}. \tag{5.28}$$

The interferer specific variances $\sigma^{(k_\mathrm{I})^2}$ of (4.53) are gained by

$$\sigma^{(k_\mathrm{I})^2} = \frac{(1-1/K)^2 WN_\mathrm{F}}{KN_\mathrm{F}W-1}. \tag{5.29}$$

From (5.28) and (5.29), the interferer specific variation coefficients $\nu^{(k_\mathrm{I})}$ of (4.54) now read

$$\nu^{(k_\mathrm{I})} = (K-1)\sqrt{\frac{WN_\mathrm{F}}{KN_\mathrm{F}W-1}}. \tag{5.30}$$

The interferer specific variation coefficient $\nu^{(k_\mathrm{I})}$ of (5.30) holds for all K interferers present in $\mathrm{SA_I}$ for the considered case of disjoint pilot vectors. Therefore, considering (4.55), the variation coefficient ν of (4.55) reads

$$\nu = (K-1)\sqrt{\frac{WN_\mathrm{F}}{KN_\mathrm{F}W-1}}. \tag{5.31}$$

Table 5.1 shows the values of the variation coefficient ν of (5.31) valid for the case of disjoint pilot vectors $\underline{\tilde{\mathbf{p}}}^{(k)}$ of (5.20) for different parameter triplets $\{N_\mathrm{F},\ K,\ W\}$.

Table 5.1. Variation coefficent ν for the case of disjoint pilot vectors

$\{N_{\mathrm{F}},\ K,\ W\}$	ν	$10\log_{10}(\nu)$ / dB
$\{16,\ 4,\ 4\}$	1.5029	1.7694
$\{32,\ 4,\ 8\}$	1.5007	1.7629
$\{64,\ 4,\ 16\}$	1.5002	1.7615
$\{128,\ 4,\ 32\}$	1.5	1.7609
$\{256,\ 4,\ 64\}$	1.5	1.7609
$\{512,\ 4,\ 128\}$	1.5	1.7609
$\{256,\ 8,\ 32\}$	2.4749	3.9356
$\{256,\ 16,\ 16\}$	3.75	5.7403

It is observed from Table 5.1 that for a fixed number K of MTs the variation coefficient ν does not change significantly, if N_{F} and W vary. Comparing these values of ν with the curves plotted in Fig. 5.4 for the case of random pilot vectors $\underline{\tilde{\mathbf{p}}}^{(k)}$ shows that the performance of the disjoint pilot vectors with respect to the variation coefficient ν is worse as compared to the case of random pilot vectors. This occurs due to said uniqueness of the applied pilot set for the case of disjoint pilot vectors. What can also be observed from Table 5.1 is that, when the number K of MTs is increased, ν also increases.

5.5 Pilot vectors based on Walsh codes

5.5.1 Generation

Similarly to the random pilot vectors addressed in Section 5.3, also in the present section we consider pilot vectors based on binary generating vectors. However, in contrast to the situation considered in Section 5.3, these binary generating vectors are now not randomly chosen, but in a particular deterministic way, which leads to ideal sets of pilot vectors.

We assume that the number N_{F} of subcarriers, which is equal to the required dimension of the binary generating vectors, is a power of two. Now, in order to determine such generating vectors we resort to the Walsh codes of dimension N_{F}, which are the columns of the Hadamard matrix [Pro95]

$$\tilde{\mathbf{W}} = \left(\tilde{\mathbf{w}}^{(1)} \ \ldots \ \tilde{\mathbf{w}}^{(n_{\mathrm{F}})} \ \ldots \ \tilde{\mathbf{w}}^{(N_{\mathrm{F}})} \right),\ n_{\mathrm{F}} = 1 \ldots N_{\mathrm{F}}, \tag{5.32}$$

of dimension $N_{\mathrm{F}} \times N_{\mathrm{F}}$. Basically, in order to obtain K binary generating vectors, any set of K columns of $\tilde{\mathbf{W}}$ of (5.32) could be chosen. However, if this choice follows a certain scheme, it turns out that sets of pilot vectors $\underline{\tilde{\mathbf{p}}}^{(k)}$ can be obtained which are ideal. The

corresponding sets of K binary generating vectors are also termed ideal by the author. The optimum design of sets of pilot vectors $\underline{\tilde{\mathbf{p}}}^{(k)}$ based on Walsh codes was intuitively formed by the author, and its execution will be explained in what follows. In Appendix A it will be proven that this approach indeed yields ideal sets of pilot vectors $\underline{\tilde{\mathbf{p}}}^{(k)}$.

We assume that the number K of MTs is a divisor of N_{F} so that the ratio N_{F}/K is an integer, where for given values N_{F} and W one has to observe (4.15) when choosing K. Now, in order to obtain an ideal set of K binary generating vectors, we should choose the K consecutive columns

$$\mathbb{P}^{(m)} = \left(\underline{\tilde{\mathbf{p}}}_m^{(1)} \ \ldots \ \underline{\tilde{\mathbf{p}}}_m^{(K)} \right) = \sqrt{\frac{2E_{\mathrm{p}}}{N_{\mathrm{F}}}} \cdot \left(\tilde{\mathbf{w}}^{((m-1)K+1)} \ \ldots \ \tilde{\mathbf{w}}^{(mK)} \right), \ m = 1 \ \ldots \ \frac{N_{\mathrm{F}}}{K}, \quad (5.33)$$

of the Hadamard matrix $\tilde{\mathbf{W}}$ of (5.32). Obviously, this approach yields N_{F}/K different sets $\mathbb{P}^{(m)}$ of ideal binary generating vectors. This situation can be exploited to employ N_{F}/K different sets of ideal pilot vectors $\underline{\tilde{\mathbf{p}}}_m^{(k)}$, $m = 1 \ \ldots \ N_{\mathrm{F}}/K$, in different SAs, which will be illustrated by means of an example in Fig. 5.7. The availability of different sets of pilot vectors for different SAs is expected to be beneficial with respect to achieving a low variation coefficient ν. If the total number of SAs exceeds N_{F}/K, then the sets of pilot vectors have to be reused.

In the example illustrated in Fig. 5.7, N_{F} is set equal to eight. Four different cases are featured which differ by the dimension W of the CIRs, and, due to (4.15), by the number K of MTs per SA. It is shown in which way the Walsh codes $\tilde{\mathbf{w}}^{(n_{\mathrm{F}})}$, $n_{\mathrm{F}} = 1 \ldots N_{\mathrm{F}}$, are assigned as pilot vectors. For the one extreme case W equal to one, see Fig. 5.7a, only one set of eight ideal pilot vectors exists. For the other extreme case of $W = 8$, eight sets of pilot vectors exist with each set consisting of only one pilot vector.

5.5.2 SNR degradations

Following the considerations given in Section 5.2 let us take a closer look at the three different types of off-diagonal elements of $\underline{\tilde{\boldsymbol{\mathcal{G}}}}^{\mathsf{H}} \underline{\tilde{\boldsymbol{\mathcal{G}}}}$ for the case of pilot vectors based on Walsh codes. Considering (5.33)

$$\sum_{i=1}^{N_{\mathrm{F}}} \left| \underline{\tilde{p}}_i^{(k)} \right|^2 \underline{\tilde{f}}_{i,w}^{*} \underline{\tilde{f}}_{i,w'}, = \frac{2E_{\mathrm{p}}}{N_{\mathrm{F}}} \cdot \sum_{i=1}^{N_{\mathrm{F}}} \underline{\tilde{f}}_{i,w}^{*} \underline{\tilde{f}}_{i,w'} = 0, \ w, w' = 1 \ \ldots W, w \neq w', \quad (5.34)$$

holds for the off-diagonal elements of Type I of $\underline{\tilde{\boldsymbol{\mathcal{G}}}}^{\mathsf{H}} \underline{\tilde{\boldsymbol{\mathcal{G}}}}$, due to the orthogonality of the column vectors $\underline{\tilde{\mathbf{f}}}_w$ and $\underline{\tilde{\mathbf{f}}}_{w'}$, $w \neq w'$. Further, with (5.7) and due to the orthogonality of the Walsh

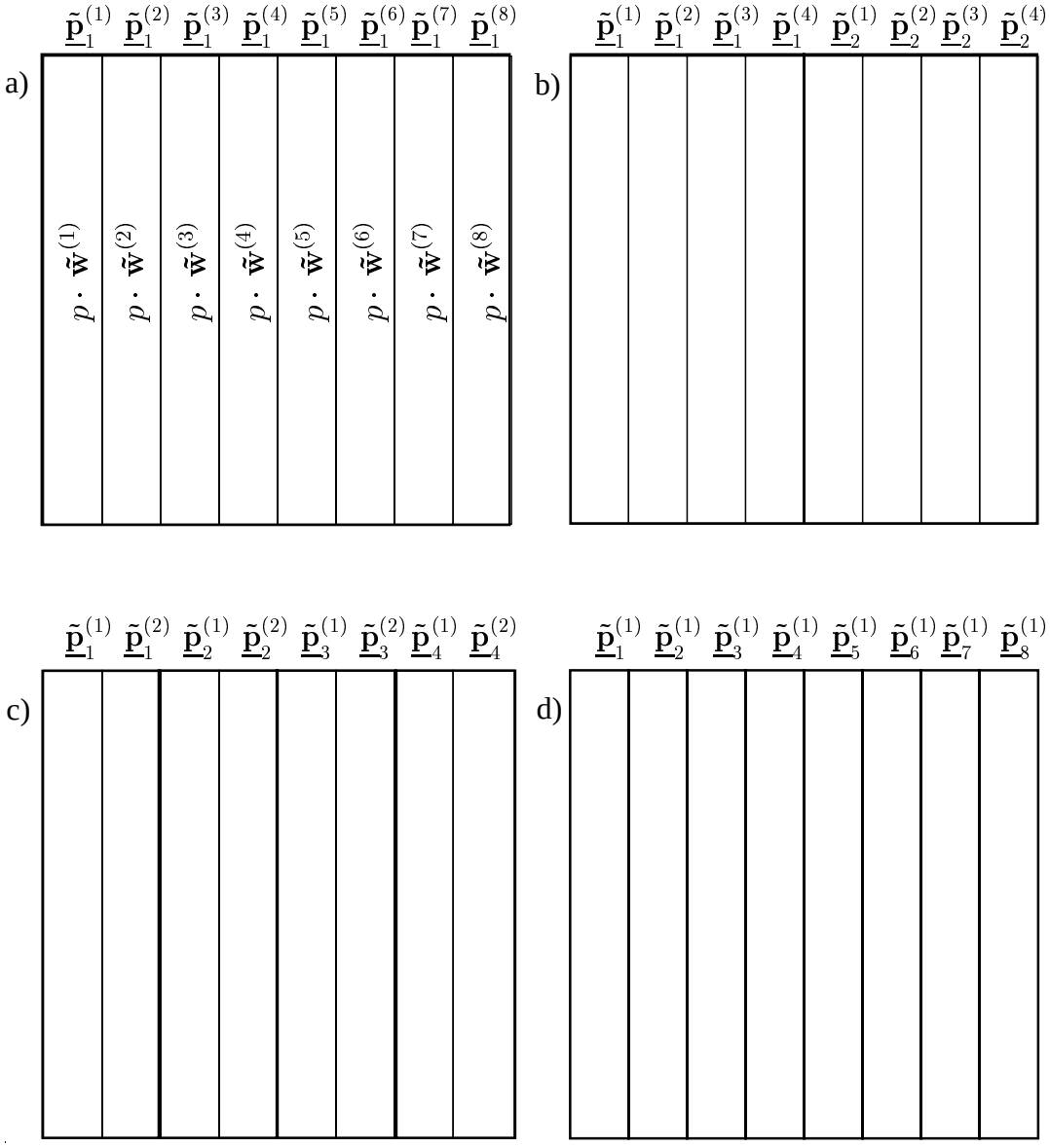

Fig. 5.7. Different options to generate sets of ideal pilot vectors $\underline{\tilde{\mathbf{p}}}^{(k)}$ based on Walsh codes in the case $N_{\mathrm{F}} = 8$; $p = \sqrt{2E_{\mathrm{p}}/N_{\mathrm{F}}}$
a) $W = 1,\ K = 8 \rightarrow$ 1 set of pilot vectors $\underline{\tilde{\mathbf{p}}}^{(k)}$
b) $W = 2,\ K = 8 \rightarrow$ 2 sets of pilot vectors $\underline{\tilde{\mathbf{p}}}^{(k)}$
c) $W = 4,\ K = 2 \rightarrow$ 4 sets of pilot vectors $\underline{\tilde{\mathbf{p}}}^{(k)}$
d) $W = 8,\ K = 1 \rightarrow$ 8 sets of pilot vectors $\underline{\tilde{\mathbf{p}}}^{(k)}$

codes $\tilde{\mathbf{w}}^{(n_{\mathrm{F}})}$, $n_{\mathrm{F}} = 1 \ldots N_{\mathrm{F}}$, of (5.32) [Pro95]

$$\sum_{i=1}^{N_{\mathrm{F}}} \underline{\tilde{p}}_i^{(k)^*}\, \underline{\tilde{p}}_i^{(k')} \left| \underline{\tilde{f}}_{i,w} \right|^2 = \sum_{i=1}^{N_{\mathrm{F}}} \underline{\tilde{p}}_i^{(k)^*}\, \underline{\tilde{p}}_i^{(k')} = 0,\ k, k' = 1\ \ldots K, k \neq k', \tag{5.35}$$

holds for the off-diagonal elements of Type II of $\underline{\tilde{\mathcal{G}}}^{\mathsf{H}}\underline{\tilde{\mathcal{G}}}$. Concerning the off-diagonal elements of Type III of $\underline{\tilde{\mathcal{G}}}^{\mathsf{H}}\underline{\tilde{\mathcal{G}}}$, simulations performed by the author unveiled that only for the N_{F}/K pilot sets $\mathbb{P}^{(m)}$, $m = 1 \ \ldots \ N_{\mathrm{F}}/K$, constructed according to (5.33) said elements are equal to zero. Any other construction of the pilot sets $\mathbb{P}^{(m)}$ with the Walsh codes $\tilde{\mathbf{w}}^{(n_{\mathrm{F}})}$ of (5.32) leads to non-zero off-diagonal elements of Type III of $\underline{\tilde{\mathcal{G}}}^{\mathsf{H}}\underline{\tilde{\mathcal{G}}}$ and, consequently, to SNR degradations $\delta_{n_{\mathrm{F}}}^{(k)}$ larger than one. In Appendix A this statement concerning the off-diagonal elements of Type III of $\underline{\tilde{\mathcal{G}}}^{\mathsf{H}}\underline{\tilde{\mathcal{G}}}$ is mathematically proven by means of induction.

5.5.3 Variation coefficient

Since the N_{F}/K pilot vector sets $\mathbb{P}^{(m)}$ of (5.33) lead to SNR degradations $\delta_{n_{\mathrm{F}}}^{(k)}$ equal to one, see Section 5.5.2 and Appendix A, (5.21) holds. As a consequence, (5.22) holds for the inter-SA interference matrix $\underline{\boldsymbol{\mathcal{I}}}$. Due to the fact that N_{F}/K different pilot vector sets $\mathbb{P}^{(m)}$ based on Walsh codes exist, in the considered interference scenario with the reference $\mathrm{SA}_{\mathrm{ref}}$ and the dominant interfering SA_{I} different pilot vector sets shall be assigned to said two SAs.

Let us consider the parameter triplet of (5.10) and the 4×4 Hadamard matrix

$$\tilde{\mathbf{W}} = \left(\begin{array}{cccc} \tilde{\mathbf{w}}^{(1)} & \tilde{\mathbf{w}}^{(2)} & \tilde{\mathbf{w}}^{(3)} & \tilde{\mathbf{w}}^{(4)} \end{array} \right) = \left(\begin{array}{rrrr} 1 & 1 & 1 & 1 \\ 1 & -1 & 1 & -1 \\ 1 & 1 & -1 & -1 \\ 1 & -1 & -1 & 1 \end{array} \right). \tag{5.36}$$

According to (5.33), the ideal pilot vector sets

$$\begin{aligned} \mathbb{P}^{(1)} &= \sqrt{\frac{2E_{\mathrm{p}}}{N_{\mathrm{F}}}} \left\{ \begin{array}{rr} 1 & 1 \\ 1 & -1 \\ 1 & 1 \\ 1 & -1 \end{array} \right\} = \left\{ \underline{\tilde{\mathbf{p}}}^{(1)} \ \underline{\tilde{\mathbf{p}}}^{(2)} \right\}, \\ \mathbb{P}^{(2)} &= \sqrt{\frac{2E_{\mathrm{p}}}{N_{\mathrm{F}}}} \left\{ \begin{array}{rr} 1 & 1 \\ 1 & -1 \\ -1 & -1 \\ -1 & 1 \end{array} \right\} = \left\{ \underline{\tilde{\mathbf{p}}}^{(3)} \ \underline{\tilde{\mathbf{p}}}^{(4)} \right\} \end{aligned} \tag{5.37}$$

are formed. We assign $\mathbb{P}^{(1)}$ to $\mathrm{SA}_{\mathrm{ref}}$ and $\mathbb{P}^{(2)}$ to SA_{I}. Further, let us consider the case where the dominant interferer k_{I} of SA_{I} applies the pilot vector $\underline{\tilde{\mathbf{p}}}^{(3)}$ of $\mathbb{P}^{(2)}$ of (5.37). With the reduced blockdiagonal Fourier matrix $\underline{\tilde{\boldsymbol{\mathcal{F}}}}_{\mathrm{W}}$ of (5.15), the Hermitian transpose of the system

matrix $\underline{\tilde{\mathcal{G}}}$ of $\mathrm{SA}_{\mathrm{ref}}$ reads

$$\begin{aligned}\underline{\tilde{\mathcal{G}}}^{\mathsf{H}} &= \begin{pmatrix} (\underline{\tilde{p}}_1^{(1)}\underline{\tilde{f}}_{11})^* & (\underline{\tilde{p}}_2^{(1)}\underline{\tilde{f}}_{21})^* & (\underline{\tilde{p}}_3^{(1)}\underline{\tilde{f}}_{31})^* & (\underline{\tilde{p}}_4^{(1)}\underline{\tilde{f}}_{41})^* \\ (\underline{\tilde{p}}_1^{(1)}\underline{\tilde{f}}_{12})^* & (\underline{\tilde{p}}_2^{(1)}\underline{\tilde{f}}_{22})^* & (\underline{\tilde{p}}_3^{(1)}\underline{\tilde{f}}_{32})^* & (\underline{\tilde{p}}_4^{(1)}\underline{\tilde{f}}_{42})^* \\ (\underline{\tilde{p}}_1^{(2)}\underline{\tilde{f}}_{11})^* & (\underline{\tilde{p}}_2^{(2)}\underline{\tilde{f}}_{21})^* & (\underline{\tilde{p}}_3^{(2)}\underline{\tilde{f}}_{31})^* & (\underline{\tilde{p}}_4^{(2)}\underline{\tilde{f}}_{41})^* \\ (\underline{\tilde{p}}_1^{(2)}\underline{\tilde{f}}_{12})^* & (\underline{\tilde{p}}_2^{(2)}\underline{\tilde{f}}_{22})^* & (\underline{\tilde{p}}_3^{(2)}\underline{\tilde{f}}_{32})^* & (\underline{\tilde{p}}_4^{(2)}\underline{\tilde{f}}_{42})^* \end{pmatrix} \\ &= \sqrt{\frac{2E_{\mathrm{p}}}{N_{\mathrm{F}}}} \cdot \begin{pmatrix} 1 & 1 & 1 & 1 \\ 1 & -\mathrm{j} & -1 & \mathrm{j} \\ 1 & -1 & 1 & -1 \\ 1 & \mathrm{j} & -1 & -\mathrm{j} \end{pmatrix},\end{aligned} \tag{5.38}$$

and with the pilot vector

$$\underline{\tilde{\mathbf{p}}}^{(k_{\mathrm{I}})} = \underline{\tilde{\mathbf{p}}}^{(3)} = \sqrt{\frac{2E_{\mathrm{p}}}{N_{\mathrm{F}}}} \cdot (1\,1\;\;-1\;\;-1)^{\mathrm{T}} \tag{5.39}$$

of the dominant interferer k_{I}, the interferer specific system matrix $\underline{\tilde{\mathcal{G}}}_{\mathrm{I}}^{(k_{\mathrm{I}})}$ of SA_{I} is given by

$$\underline{\tilde{\mathcal{G}}}_{\mathrm{I}}^{(k_{\mathrm{I}})} = \begin{pmatrix} \underline{\tilde{p}}_1^{(1)}\underline{\tilde{f}}_{11} & \underline{\tilde{p}}_1^{(1)}\underline{\tilde{f}}_{12} \\ \underline{\tilde{p}}_2^{(1)}\underline{\tilde{f}}_{21} & \underline{\tilde{p}}_2^{(1)}\underline{\tilde{f}}_{22} \\ \underline{\tilde{p}}_3^{(1)}\underline{\tilde{f}}_{31} & \underline{\tilde{p}}_3^{(1)}\underline{\tilde{f}}_{32} \\ \underline{\tilde{p}}_4^{(1)}\underline{\tilde{f}}_{41} & \underline{\tilde{p}}_4^{(1)}\underline{\tilde{f}}_{42} \end{pmatrix} = \sqrt{\frac{2E_{\mathrm{p}}}{N_{\mathrm{F}}}} \cdot \begin{pmatrix} 1 & 1 \\ 1 & -\mathrm{j} \\ -1 & 1 \\ -1 & -\mathrm{j} \end{pmatrix}. \tag{5.40}$$

With (5.38) and (5.40), the interferer specific inter-SA interference matrix $\underline{\boldsymbol{\mathcal{I}}}^{(k_{\mathrm{I}})}$ of (5.25) now reads

$$\underline{\boldsymbol{\mathcal{I}}}^{(k_{\mathrm{I}})} = \begin{pmatrix} \underline{\boldsymbol{\mathcal{I}}}^{(k_{\mathrm{I}},1)} \\ \underline{\boldsymbol{\mathcal{I}}}^{(k_{\mathrm{I}},2)} \end{pmatrix} = \begin{pmatrix} \underline{\boldsymbol{\mathcal{I}}}^{(1,1)} \\ \underline{\boldsymbol{\mathcal{I}}}^{(1,2)} \end{pmatrix} \tag{5.41}$$

$$= \frac{1}{2E_{\mathrm{p}}} \cdot \frac{2E_{\mathrm{p}}}{N_{\mathrm{F}}} \begin{pmatrix} 1 & 1 & 0 & 0 \\ 1 & -\mathrm{j} & 0 & 0 \\ 1 & -1 & 0 & 0 \\ 1 & \mathrm{j} & 0 & 0 \\ 0 & 0 & 1 & 1 \\ 0 & 0 & 1 & -\mathrm{j} \\ 0 & 0 & 1 & -1 \\ 0 & 0 & 1 & \mathrm{j} \end{pmatrix} \begin{pmatrix} 1 & 1 & 1 & 1 \\ 1 & -\mathrm{j} & -1 & \mathrm{j} \\ 1 & -1 & 1 & -1 \\ 1 & \mathrm{j} & -1 & -\mathrm{j} \end{pmatrix} \begin{pmatrix} 1 & 1 \\ 1 & -\mathrm{j} \\ -1 & 1 \\ -1 & -\mathrm{j} \end{pmatrix}$$

$$= \begin{pmatrix} 0.5+0.5\mathrm{j} & 0.5-0.5\mathrm{j} \\ 0.5-0.5\mathrm{j} & 0.5-0.5\mathrm{j} \\ -0.5-0.5\mathrm{j} & 0.5-0.5\mathrm{j} \\ -0.5+0.5\mathrm{j} & 0.5-0.5\mathrm{j} \\ 0.5-0.5\mathrm{j} & 0.5+0.5\mathrm{j} \\ -0.5-0.5\mathrm{j} & 0.5+0.5\mathrm{j} \\ -0.5+0.5\mathrm{j} & 0.5+0.5\mathrm{j} \\ 0.5+0.5\mathrm{j} & 0.5+0.5\mathrm{j} \end{pmatrix}.$$

Comparing (5.41) with the interferer specific inter-SA interference matrix of (5.25) for the case of disjoint pilot vectors, it is seen that the interference induced by the dominant interferer k_{I} is now spread over all MTs and subcarriers of $\mathrm{SA}_{\mathrm{ref}}$. With (5.41) and applying (4.52) till (4.55), the variation coefficient ν of (4.55) is equal to 0.1772, which is lower as compared to the respective exemplary case of the disjoint pilot vectors in Section 5.4.3.

With the pilot vector $\underline{\tilde{\mathbf{p}}}^{(k)}$ constructed according to (5.33) and for any fixed parameter triplet $\{N_{\mathrm{F}},\ K,\ W\}$, the element $[\underline{\boldsymbol{\mathcal{I}}}]_{p,q}$ on the p-th row and the q-th column of the inter-SA interference matrix of (4.48) is given by

$$\begin{aligned} [\underline{\boldsymbol{\mathcal{I}}}]_{p,q} &= [\underline{\boldsymbol{\mathcal{I}}}]_{(k-1)N_{\mathrm{F}}+n_{\mathrm{F}},(k_{\mathrm{I}}-1)W+w} = \frac{1}{2E_{\mathrm{p}}} \cdot \sum_{j=1}^{W} \sum_{i=1}^{N_{\mathrm{F}}} \underline{\tilde{f}}_{n_{\mathrm{F}},j} \left(\underline{\tilde{p}}_i^{(k)} \underline{\tilde{f}}_{i,j} \right)^* \left(\underline{\tilde{p}}_i^{(k_{\mathrm{I}})} \underline{\tilde{f}}_{i,w} \right) \\ &= \sum_{j=1}^{W} \sum_{i=1}^{N_{\mathrm{F}}} \underline{\tilde{f}}_{n_{\mathrm{F}},j} \left(\tilde{w}_i^{(k,m)} \underline{\tilde{f}}_{i,j} \right)^* \left(\tilde{w}_i^{(k_{\mathrm{I}},m')} \underline{\tilde{f}}_{i,w} \right), \qquad (5.42) \\ k,\ k_{\mathrm{I}} &= 1 \ldots K,\ \ w = 1 \ldots W,\ \ n_{\mathrm{F}} = 1 \ldots N_{\mathrm{F}},\ \ m, m' = 1 \ \ldots \ M, m \neq m'. \end{aligned}$$

Fig. 5.8 illustrates the resulting structure for the inter-SA interference matrix $\underline{\boldsymbol{\mathcal{I}}}$ in the case of pilot vectors based on Walsh codes. Again, out of the resulting pilot vector sets, it is assumed that $\mathbb{P}^{(1)}$ is assigned to $\mathrm{SA}_{\mathrm{ref}}$ and $\mathbb{P}^{(2)}$ is assigned to SA_{I}. Comparing Fig 5.8 and Fig. 5.6 it is seen that the inter-SA interference is spread more equally on the MTs of $\mathrm{SA}_{\mathrm{ref}}$ and that the absolute values of the induced interference are smaller in the case of pilot vectors based on Walsh codes.

Unfortunately, it is not possible to give any simple formulas for the calculation of the variation coefficient ν for the case of pilot vectors based on Walsh codes - as it is done for the

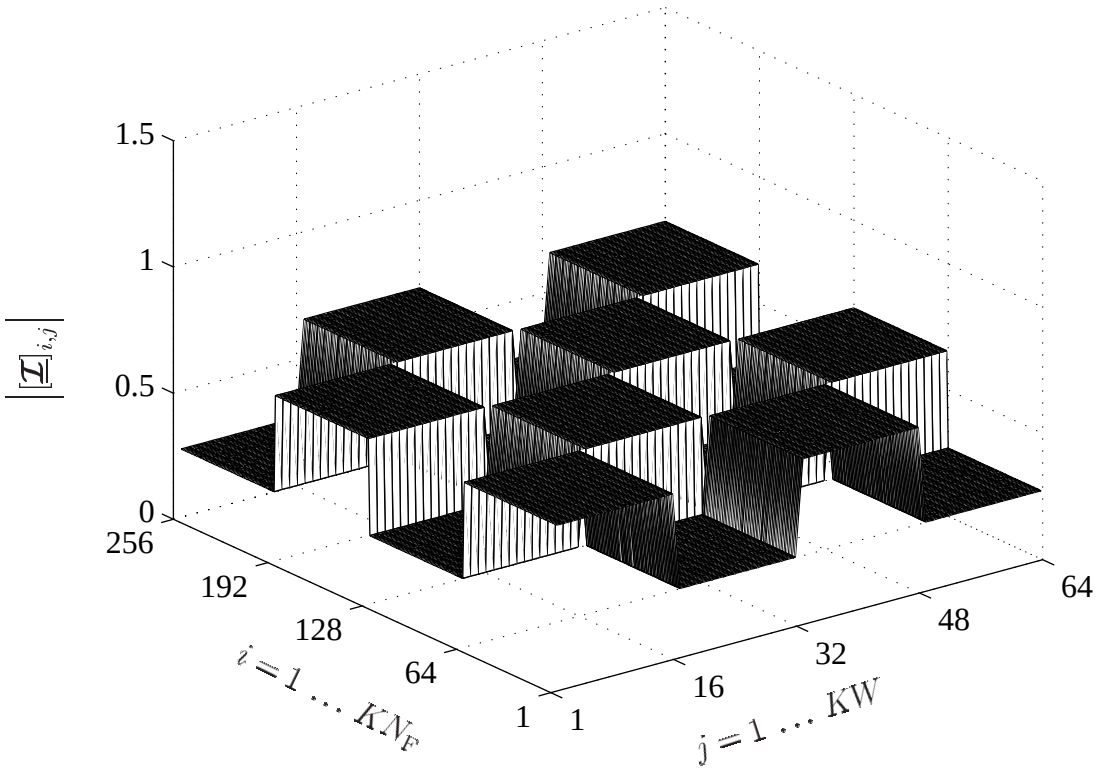

Fig. 5.8. Magnitudes $\left|[\underline{\underline{\mathcal{I}}}]_{i,j}\right|$, $i = 1 \ldots KN_{\mathrm{F}}$, $j = 1 \ldots KW$, of the inter-SA interference matrix $\underline{\underline{\mathcal{I}}}$ for the exemplary triplet $\{N_{\mathrm{F}},\ K,\ W\} = \{64,\ 4,\ 16\}$ and pilot vectors based on Walsh codes

case of disjoint pilot vectors, see (5.28) till (5.31) - due to the complexity of (5.42). Instead, numerical calculations performed for different parameter triplets $\{N_{\mathrm{F}},\ K,\ W\}$ are given in Table 5.2. For all calculations it is assumed that pilot set $\mathbb{P}^{(1)}$ of (5.33) is assigned in $\mathrm{SA}_{\mathrm{ref}}$ and pilot set $\mathbb{P}^{(2)}$ of (5.33) is assigned in SA_{I}. Further, in both SAs full system load is assumed. As in the case of the disjoint pilot vectors, see Table 5.1, it is observed from Table 5.2

Table 5.2. Variation coefficent ν for the case of pilot vectors based on Walsh codes

$\{N_{\mathrm{F}},\ K,\ W\}$	ν	$10\log_{10}(\nu)$ / dB
$\{16,\ 4,\ 4\}$	0.4144	-3.8256
$\{32,\ 4,\ 8\}$	0.4143	-3.8272
$\{64,\ 4,\ 16\}$	0.4142	-3.8277
$\{128,\ 4,\ 32\}$	0.4142	-3.8277
$\{256,\ 4,\ 64\}$	0.4142	-3.8277
$\{512,\ 4,\ 128\}$	0.4142	-3.8277
$\{256,\ 8,\ 32\}$	0.8335	-0.7912
$\{256,\ 16,\ 16\}$	1.3550	1.3194

that for a fixed number K of MTs the variation coefficient ν changes very little and takes values around -3.8 dB. Comparing these values with the cdf of ν illustrated in Fig. 5.4, it

is seen that the pilot vectors based on Walsh codes outperform random pilot vectors with respect to the variation coefficient.

When the number K of MTs is increased, ν also increases. For all parameter triplets of Table 5.2 the variation coefficient ν takes lower values as compared to the case of disjoint pilot vectors of Table 5.1.

5.6 Pilot vectors based on CAZAC codes

5.6.1 Generation

The fourth method for pilot vector design considered in the thesis is based on the constant-amplitude-zero-autocorrelation (CAZAC) codes [Hei61, Mil83, KCWS03, Kan05]. Due to these characteristics of a constant amplitude and zero autocorrelation, CAZAC codes are also known as polyphase sequences [FZ62, Chu72]. The attention of the author of the present thesis towards the CAZAC codes was first drawn by the author of [Kan05]. Following this hint, the concept of CAZAC code generation was applied for pilot vector design in JOINT and presented in what follows.

As a contrast to the elements of the codes considered in the previous three sections taken from the binary sets $\{0,\ 1\}$ and $\{-1,\ 1\}$, the elements of the CAZAC codes are roots of unity [Hei61, Mil83], i. e., roots of the form $\exp\left\{-\mathrm{j}\frac{2\pi}{N_\mathrm{F}}(n_\mathrm{F}-1)\right\}$, $n_\mathrm{F} = 1 \ldots N_\mathrm{F}$. The CAZAC codes are generated starting from a base code $\underline{\tilde{\mathbf{p}}}_\mathrm{b}$ of dimension N_F. From said base code $\underline{\tilde{\mathbf{p}}}_\mathrm{b}$, N_F different CAZAC codes $\underline{\tilde{\mathbf{c}}}^{(n_\mathrm{F})}$, $n_\mathrm{F} = 1 \ldots N_\mathrm{F}$, of dimension N_F can be obtained according to

$$\underline{\tilde{\mathbf{c}}}^{(n_\mathrm{F})} = \begin{pmatrix} \mathbf{0}^{(n_\mathrm{F}\times N_\mathrm{F}-l)} & \mathbf{I}^{(n_\mathrm{F}\times n_\mathrm{F})} \\ \mathbf{I}^{(N_\mathrm{F}-n_\mathrm{F}\times N_\mathrm{F}-n_\mathrm{F})} & \mathbf{0}^{(N_\mathrm{F}-n_\mathrm{F}\times n_\mathrm{F})} \end{pmatrix} \cdot \underline{\tilde{\mathbf{p}}}_\mathrm{b},\ n_\mathrm{F} = 1 \ldots N_\mathrm{F}. \tag{5.43}$$

In (5.43) $\mathbf{0}^{(n_\mathrm{F}\times N_\mathrm{F}-n_\mathrm{F})}$ denotes a zero matrix of dimension $n_\mathrm{F} \times (N_\mathrm{F} - n_\mathrm{F})$. Then, N_F/K different sets $\mathbb{P}^{(m)}$, $m = 1\ \ldots\ N_\mathrm{F}/K$, each set containing K different pilot vectors $\underline{\tilde{\mathbf{p}}}_m^{(k)}$, $k = 1\ \ldots\ K$, of dimension N_F are obtained according to [Kan05]

$$\begin{aligned} \mathbb{P}^{(m)} &= \left\{ \underline{\tilde{\mathbf{p}}}_m^{(1)}\ \ldots\ \underline{\tilde{\mathbf{p}}}_m^{(K)} \right\} = \sqrt{\frac{2E_\mathrm{p}}{N_\mathrm{F}}} \cdot \left\{ \underline{\tilde{\mathbf{c}}}^{((k-1)\frac{N_\mathrm{F}}{K}+m)} \right\}, \\ m &= 1\ \ldots\ N_\mathrm{F}/K,\ k = 1\ \ldots\ K. \end{aligned} \tag{5.44}$$

Regarding this procedure, it is observed that the generation of the pilot sets $\mathbb{P}^{(m)}$ of (5.44) is based on a single base code $\underline{\tilde{\mathbf{p}}}_\mathrm{b}$. For obtaining the base code $\underline{\tilde{\mathbf{p}}}_\mathrm{b}$ different methods exist,

which are featured in e. g. [Hei61, FZ62, Chu72, Mil83, KCWS03, Kan05]. Therefore, for a fixed value of N_{F} more than one base codes $\underline{\tilde{\mathbf{p}}}_{\mathrm{b}}$ can be obtained [FZ62, KCWS03]. Consequently, in the case of pilot vectors based on CAZAC codes a larger amount of different pilot vectors can be created as compared to the case of the pilot vectors based on Walsh codes.

One of the options for generating the base code $\underline{\tilde{\mathbf{p}}}_{\mathrm{b}}$ is to use the elements $\underline{\tilde{f}}_{n_{\mathrm{F}},n_{\mathrm{F}}}$ of the Fourier matrix $\underline{\tilde{\boldsymbol{\mathcal{F}}}}$ of (4.18). Let us define the variables

$$\begin{aligned} L &= N_{\mathrm{F}}, \\ M &= N_{\mathrm{F}}/K \end{aligned} \tag{5.45}$$

and consider the $\sqrt{L} \times \sqrt{L}$ Fourier matrix

$$\underline{\tilde{\boldsymbol{\mathcal{F}}}} = \begin{pmatrix} \underline{\tilde{f}}_{1,1} & \cdots & \underline{\tilde{f}}_{1,\sqrt{L}} \\ \vdots & & \vdots \\ \underline{\tilde{f}}_{\sqrt{L},1} & \cdots & \underline{\tilde{f}}_{\sqrt{L},\sqrt{L}} \end{pmatrix}, \tag{5.46}$$

the elements of which are roots of unity [Rup93]. The base code $\underline{\tilde{\mathbf{p}}}_{\mathrm{b}}$ of dimension N_{F} is then gained by stacking the columns of $\underline{\tilde{\boldsymbol{\mathcal{F}}}}$ of (5.46) one under the other, namely

$$\underline{\tilde{\mathbf{p}}}_{\mathrm{b}} = \left(\underline{\tilde{p}}_{\mathrm{b},1} \ \cdots \ \underline{\tilde{p}}_{\mathrm{b},N_{\mathrm{F}}} \right)^{\mathrm{T}} = \left(\underline{\tilde{f}}_{1,1} \ \cdots \ \underline{\tilde{f}}_{\sqrt{L},1} \ \cdots \ \underline{\tilde{f}}_{1,\sqrt{L}} \ \cdots \ \underline{\tilde{f}}_{\sqrt{L},\sqrt{L}} \right)^{\mathrm{T}}. \tag{5.47}$$

Now, according to (5.43), N_{F} different codes of dimension N_{F} are obtained from $\underline{\tilde{\mathbf{p}}}_{\mathrm{b}}$ of (5.47) according to

$$\begin{aligned} \underline{\tilde{\mathbf{c}}}^{(1)} &= \begin{pmatrix} \mathbf{0}^{(1\times N_{\mathrm{F}}-1)} & \mathbf{I}^{(1\times 1)} \\ \mathbf{I}^{(N_{\mathrm{F}}-1\times N_{\mathrm{F}}-1)} & \mathbf{0}^{(N_{\mathrm{F}}-1\times 1)} \end{pmatrix} \cdot \underline{\tilde{\mathbf{p}}}_{\mathrm{b}} \\ &= \left(\underline{\tilde{p}}_{\mathrm{b},N_{\mathrm{F}}} \ \underline{\tilde{p}}_{\mathrm{b},1} \ \cdots \ \underline{\tilde{p}}_{\mathrm{b},N_{\mathrm{F}}-1} \right)^{\mathrm{T}} \\ &\vdots \\ \underline{\tilde{\mathbf{c}}}^{(n_{\mathrm{F}})} &= \begin{pmatrix} \mathbf{0}^{(n_{\mathrm{F}}\times N_{\mathrm{F}}-n_{\mathrm{F}})} & \mathbf{I}^{(n_{\mathrm{F}}\times n_{\mathrm{F}})} \\ \mathbf{I}^{(N_{\mathrm{F}}-n_{\mathrm{F}}\times N_{\mathrm{F}}-n_{\mathrm{F}})} & \mathbf{0}^{(N_{\mathrm{F}}-n_{\mathrm{F}}\times n_{\mathrm{F}})} \end{pmatrix} \cdot \underline{\tilde{\mathbf{p}}}_{\mathrm{b}} \\ &= \left(\underline{\tilde{p}}_{\mathrm{b},N_{\mathrm{F}}-n_{\mathrm{F}}+1} \ \cdots \ \underline{\tilde{p}}_{\mathrm{b},N_{\mathrm{F}}} \ \underline{\tilde{p}}_{\mathrm{b},1} \ \cdots \ \underline{\tilde{p}}_{\mathrm{b},N_{\mathrm{F}}-n_{\mathrm{F}}} \right)^{\mathrm{T}} \\ &\vdots \\ \underline{\tilde{\mathbf{c}}}^{(N_{\mathrm{F}})} &= \underline{\tilde{\mathbf{p}}}_{\mathrm{b}}, \ n_{\mathrm{F}} = 1 \ldots N_{\mathrm{F}}. \end{aligned} \tag{5.48}$$

Based on (5.48) and following the procedure described by (5.44), the M pilot vector sets

$$\begin{aligned} \mathbb{P}^{(1)} &= \left\{ \underline{\tilde{\mathbf{p}}}_1^{(1)} \ \underline{\tilde{\mathbf{p}}}_1^{(2)} \ \cdots \ \underline{\tilde{\mathbf{p}}}_1^{(K)} \right\} = \sqrt{\frac{2E_{\mathrm{p}}}{N_{\mathrm{F}}}} \cdot \left\{ \underline{\tilde{\mathbf{c}}}^{(1)} \ \underline{\tilde{\mathbf{c}}}^{(M+1)} \ \cdots \ \underline{\tilde{\mathbf{c}}}^{((K-1)M+1)} \right\} \\ &\vdots \\ \mathbb{P}^{(M)} &= \left\{ \underline{\tilde{\mathbf{p}}}_M^{(1)} \ \underline{\tilde{\mathbf{p}}}_M^{(2)} \ \cdots \ \underline{\tilde{\mathbf{p}}}_M^{(K)} \right\} = \sqrt{\frac{2E_{\mathrm{p}}}{N_{\mathrm{F}}}} \cdot \left\{ \underline{\tilde{\mathbf{c}}}^{(M)} \ \underline{\tilde{\mathbf{c}}}^{(2M)} \ \cdots \ \underline{\tilde{\mathbf{c}}}^{(N_{\mathrm{F}})} \right\} \end{aligned} \tag{5.49}$$

are constructed.

5.6.2 SNR degradations

Investigations performed by the author of [Kan05] show that the pilot vectors based on the CAZAC codes lead to SNR degradations $\delta_{n_\mathrm{F}}^{(k)}$ equal to one, thus they are ideal pilot vectors. Therefore, in this thesis only an illustrative example will be given for the parameter triplet of (5.10) for the case that the base code $\underline{\tilde{\mathbf{p}}}_\mathrm{b}$ is gained from the elements of the Fourier matrix. With L of (5.45) equal to two, the 2×2 Fourier matrix reads

$$\underline{\tilde{\boldsymbol{\mathcal{F}}}} = \begin{pmatrix} 1 & 1 \\ 1 & -1 \end{pmatrix}. \tag{5.50}$$

From (5.50) the base code of dimension four is obtained as

$$\underline{\tilde{\mathbf{p}}}_\mathrm{b} = (1\,1\,1\,-1)^\mathrm{T}. \tag{5.51}$$

According to (5.43), we obtain the CAZAC codes

$$\begin{aligned} \underline{\tilde{\mathbf{c}}}^{(1)} &= (-1\,1\,1\,1)^\mathrm{T}, \\ \underline{\tilde{\mathbf{c}}}^{(2)} &= (1\,-1\,1\,1)^\mathrm{T}, \\ \underline{\tilde{\mathbf{c}}}^{(3)} &= (1\,1\,-1\,1)^\mathrm{T}, \\ \underline{\tilde{\mathbf{c}}}^{(4)} &= (1\,1\,1\,-1)^\mathrm{T} \end{aligned} \tag{5.52}$$

and from (5.52) the two pilot vector sets

$$\begin{aligned} \mathbb{P}^{(1)} &= \left\{ \underline{\tilde{\mathbf{p}}}_1^{(1)}\ \underline{\tilde{\mathbf{p}}}_1^{(2)} \right\} = \sqrt{\frac{2E_\mathrm{p}}{N_\mathrm{F}}} \cdot \left\{ \underline{\tilde{\mathbf{c}}}^{(1)} \underline{\tilde{\mathbf{c}}}^{(3)} \right\} \\ \mathbb{P}^{(2)} &= \left\{ \underline{\tilde{\mathbf{p}}}_2^{(1)}\ \underline{\tilde{\mathbf{p}}}_2^{(2)} \right\} = \sqrt{\frac{2E_\mathrm{p}}{N_\mathrm{F}}} \cdot \left\{ \underline{\tilde{\mathbf{c}}}^{(2)} \underline{\tilde{\mathbf{c}}}^{(4)} \right\} \end{aligned} \tag{5.53}$$

result. Considering the pilot vector set $\mathbb{P}^{(1)}$ of (5.53) and the reduced blockdiagonal Fourier matrix $\underline{\tilde{\boldsymbol{\mathcal{F}}}}_\mathrm{W}$ of (5.15), the system matrix $\underline{\tilde{\boldsymbol{\mathcal{G}}}}$ reads

$$\underline{\tilde{\boldsymbol{\mathcal{G}}}} = \sqrt{\frac{2E_\mathrm{p}}{N_\mathrm{F}}} \cdot \begin{pmatrix} -1 & 0 & 0 & 0 & -1 & 0 & 0 & 0 \\ 0 & 1 & 0 & 0 & 0 & 1 & 0 & 0 \\ 0 & 0 & 1 & 0 & 0 & 0 & -1 & 0 \\ 0 & 0 & 0 & 1 & 0 & 0 & 0 & 1 \end{pmatrix} \cdot \begin{pmatrix} 1 & 1 & 0 & 0 \\ 1 & -\mathrm{j} & 0 & 0 \\ 1 & -1 & 0 & 0 \\ 1 & \mathrm{j} & 0 & 0 \\ 0 & 0 & 1 & 1 \\ 0 & 0 & 1 & -\mathrm{j} \\ 0 & 0 & 1 & -1 \\ 0 & 0 & 1 & \mathrm{j} \end{pmatrix} \tag{5.54}$$

$$= \sqrt{\frac{2E_\mathrm{p}}{N_\mathrm{F}}} \cdot \begin{pmatrix} -1 & -1 & 1 & 1 \\ 1 & -\mathrm{j} & 1 & -\mathrm{j} \\ 1 & -1 & -1 & 1 \\ 1 & \mathrm{j} & 1 & \mathrm{j} \end{pmatrix},$$

and the respective Gram matrix $\underline{\tilde{\boldsymbol{\mathcal{G}}}}^{\mathsf{H}} \underline{\tilde{\boldsymbol{\mathcal{G}}}}$ is obtained as

$$\begin{aligned} \underline{\tilde{\boldsymbol{\mathcal{G}}}}^{\mathsf{H}} \underline{\tilde{\boldsymbol{\mathcal{G}}}} &= \sqrt{\frac{2E_\mathrm{p}}{N_\mathrm{F}}} \cdot \begin{pmatrix} -1 & 1 & 1 & 1 \\ -1 & \mathrm{j} & -1 & -\mathrm{j} \\ 1 & 1 & -1 & -1 \\ 1 & \mathrm{j} & 1 & -\mathrm{j} \end{pmatrix} \begin{pmatrix} -1 & -1 & 1 & 1 \\ 1 & -\mathrm{j} & 1 & -\mathrm{j} \\ 1 & -1 & -1 & 1 \\ 1 & \mathrm{j} & 1 & \mathrm{j} \end{pmatrix} \\ &= \frac{2E_\mathrm{p}}{4} \cdot \begin{pmatrix} 4 & 0 & 0 & 0 \\ 0 & 4 & 0 & 0 \\ 0 & 0 & 4 & 0 \\ 0 & 0 & 0 & 4 \end{pmatrix} = 2E_\mathrm{p} \cdot \mathbf{I}^{(4\times 4)}. \end{aligned} \tag{5.55}$$

With (5.55) one can verify that the Gram matrix $\underline{\tilde{\boldsymbol{\mathcal{G}}}}^{\mathsf{H}} \underline{\tilde{\boldsymbol{\mathcal{G}}}}$ is a diagonal matrix and along with the considerations given in Section 5.2 that all SNR degradations $\delta_{n_\mathrm{F}}^{(k)}$, $n_\mathrm{F} = 1 \ldots N_\mathrm{F}$, $k = 1 \ \ldots \ K$, are equal to one. In a similar way it can be seen that the Gram matrix $\underline{\tilde{\boldsymbol{\mathcal{G}}}}^{\mathsf{H}} \underline{\tilde{\boldsymbol{\mathcal{G}}}}$ is a diagonal matrix also for the pilot vector set $\mathbb{P}^{(2)}$ of (5.44) and, thus, all SNR degradations $\delta_{n_\mathrm{F}}^{(k)}$ are equal to one.

5.6.3 Variation coefficient

Since the N_F/K pilot sets $\mathbb{P}^{(i)}$ of (5.44) lead to SNR degradations $\delta_{n_\mathrm{F}}^{(k)}$ equal to one, see Section 5.6.2, (5.21) holds. As a consequence, (5.22) holds for the inter-SA interference matrix $\underline{\boldsymbol{\mathcal{I}}}$. The misfit when designing the pilot vectors $\underline{\tilde{\mathbf{p}}}^{(k)}$ based on the CAZAC codes of (5.48) comes from the fact that not all values of N_F can be considered. Starting from $L = N_\mathrm{F}$ for the construction of the respective Fourier matrix, see (5.46), and the construction of the base code $\underline{\tilde{\mathbf{p}}}_\mathrm{b}$, see (5.47), it becomes clear that only such values of N_F can be considered, which have an integer square root. In [Kan05] it is elaborated upon how to overcome this drawback.

Because of this, the results presented in Table 5.3 illustrating the performance of the variation coefficient with respect to pilot vectors based on CAZAC codes do not include the values 32, 128 and 512 for N_F, as it is the case in Table 5.1 and in Table 5.2. Similar to the case of pilot vectors based on Walsh codes, for all conducted calculations of Table 5.3 it is assumed that the pilot set $\mathbb{P}^{(1)}$ of (5.44) is applied in SA_ref and the pilot set $\mathbb{P}^{(2)}$ of (5.44) is applied in SA_I. Further, in both SAs full system load is assumed.

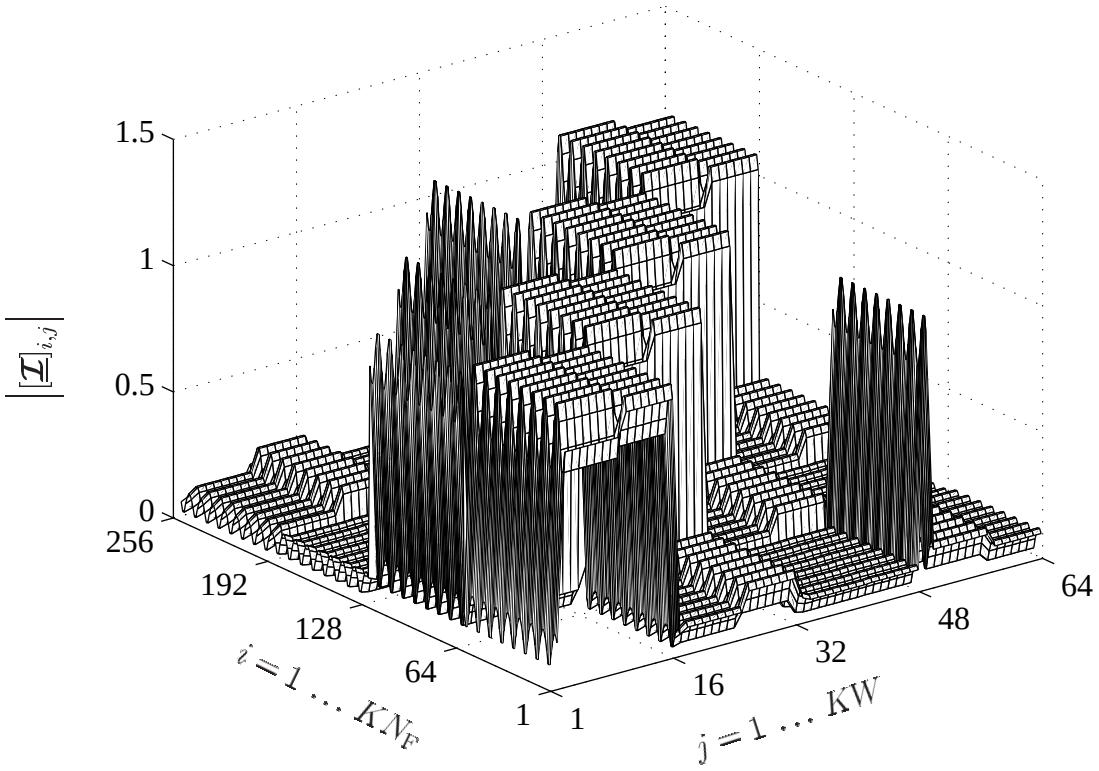

Fig. 5.9. Magnitudes $\left|[\underline{\underline{\mathcal{I}}}]_{i,j}\right|$, $i = 1 \ldots KN_{\mathrm{F}}$, $j = 1 \ldots KW$, of the inter-SA interference matrix $\underline{\underline{\mathcal{I}}}$ for the exemplary triplet $\{N_{\mathrm{F}},\ K,\ W\} = \{64,\ 4,\ 16\}$ and pilot vectors based on CAZAC codes

Table 5.3. Variation coefficent ν for the case of pilot vectors based on CAZAC codes

$\{N_{\mathrm{F}},\ K,\ W\}$	ν	$10\log_{10}(\nu)$ / dB
$\{16,\ 4,\ 4\}$	0.7291	-1.3721
$\{64,\ 4,\ 16\}$	1.2364	0.9271
$\{256,\ 4,\ 64\}$	1.5267	1.8376
$\{256,\ 8,\ 32\}$	2.1491	3.3226
$\{256,\ 16,\ 16\}$	2.7796	4.44

Finally, Fig. 5.9 illustrates the resulting structure for the inter-SA interference matrix $\underline{\underline{\mathcal{I}}}$ in the case of ideal pilot vectors based on CAZAC codes. The exemplary triplet $\{N_{\mathrm{F}},\ K,\ W\} = \{64,\ 4,\ 16\}$ is considered and the base code $\underline{\tilde{\mathbf{p}}}_{\mathrm{b}}$ is obtained from the elements of the 8×8 Fourier matrix, see (5.45) till (5.47). After constructing the sets of ideal pilot vectors, see (5.48) and (5.48), $\mathbb{P}^{(1)}$ is assigned to $\mathrm{SA}_{\mathrm{ref}}$ and $\mathbb{P}^{(2)}$ is assigned to SA_{I}. For the dominant interferer k_{I} of SA_{I}, the pilot vector $\underline{\tilde{\mathbf{p}}}_2^{(k_{\mathrm{I}})}$ is considered. Comparing Fig. 5.9 and the structure of the inter-SA interference matrix $\underline{\underline{\mathcal{I}}}$ for the case of ideal pilot vectors based on Walsh codes shown in Fig. 5.8, we can observe that the inter-SA interference is spread more evenly over the matrix $\underline{\underline{\mathcal{I}}}$ in the latter case of ideal pilot vectors.

Chapter 6

Enhancement of joint channel estimation by employing multi-element antennas at the APs

6.1 Preliminary remarks

Up to now it was assumed in this thesis that single-element antennas are employed at the APs. In the present Chapter 6 we now consider the case that each AP disposes of an array antenna with K_{A} antenna elements, whereas the MTs are equipped as before with single-element antennas. It is well known [FN94, God97, Rap98, Bla98, Pap00] that by using such multi-element antennas instead of single-element antennas the performance of data transmission can be improved. This improvement is due to the fact that the number of equations available for data estimation is increased by a factor K_{A}, whereas the number of data symbols to be estimated at the receiver remains unaltered [Bla98]. As a pre-condition of said improvement, the involved CIRs or CTFs have to be known. In the case of single-element antennas both at the MTs and the APs the channel between a MT k and an AP can be characterized by a single CTF $\underline{\tilde{\mathbf{h}}}^{(k)}$, see (4.2), that is by N_{F} complex quantities $\underline{\tilde{h}}_{n_{\mathrm{F}}}^{(k)}$, $n_{\mathrm{F}} = 1 \ldots N_{\mathrm{F}}$. If now each AP employs K_{A} antenna elements, then the radio propagation between a MT k and an AP has to be described by a set of K_{A} CTFs $\underline{\tilde{\mathbf{h}}}^{(k,k_{\mathrm{A}})}$, $k_{\mathrm{A}} = 1 \ \ldots \ K_{\mathrm{A}}$. This means that the number of required CTF values is increased by a factor of K_{A}. Because also the number of equations - see (4.11) - available for estimating these CTF values increases by the same factor K_{A}, generally, the quality of the CTF estimates cannot be enhanced by using $K_{\mathrm{A}} > 1$ antenna elements instead of only one. However, this statement is only generally true; there are exceptional situations in which the employment of multi-element antennas at the APs instead of single-element antennas can also improve the system performance with respect to channel estimation. Such exceptional situations are characterized by the facts that there exist known directional properties of

- the radio channels between the MTs and the APs, and/or
- of the disturbing signals impinging at the APs.

Based on the existence and knowledge of such directional properties, the original increase of the number of CTF values by a factor of K_{A} can be again mitigated, and/or the effective disturbance can be reduced.

In Chapter 6 the exploitation of said directional properties for JCE is presented. Besides the extension of the JCE algorithm from the single-element antenna case, see Section 4.4, to

the multi-element antenna case, the application of the minimum mean square error (MMSE) estimation principle for JCE is also presented in Chapter 6 for the case of array antennas utilized at the APs. Similar to the considerations given in Chapter 4, we shall focus on a single AP in the considered SA of JOINT.

6.2 Transmission model

Fig. 6.1 illustrates the considered UL scenario. K MTs are assumed to be contained in the SA, each of them applying a single-element omnidirectional antenna for the radiation of the MT-specific pilot vector $\underline{\tilde{\mathbf{p}}}^{(k)}$, $k = 1 \ \ldots \ K$, of (3.3). As mentioned before, the considered AP is equipped with an array antenna of K_{A} omnidirectional antenna elements. The radio channel between the antenna element of MT k, $k = 1 \ \ldots \ K$, and the antenna element k_{A}, $k_{\mathrm{A}} = 1 \ \ldots \ K_{\mathrm{A}}$, of the AP array antenna has the CTF

$$\underline{\tilde{\mathbf{h}}}^{(k,\ k_{\mathrm{A}})} = \left(\underline{\tilde{h}}_1^{(k,\ k_{\mathrm{A}})} \ \ldots \ \underline{\tilde{h}}_{N_{\mathrm{F}}}^{(k,\ k_{\mathrm{A}})}\right)^{\mathrm{T}}. \tag{6.1}$$

The radiated pilot vectors $\underline{\tilde{\mathbf{p}}}^{(k)}$ reach the element k_{A} of the AP array antenna over a radio channel characterized by $\underline{\tilde{\mathbf{h}}}^{(k,\ k_{\mathrm{A}})}$ of (6.1). The subcarrier radiated by MT k at subcarrier frequency n_{F} with the complex amplitude $\underline{\tilde{p}}_{n_{\mathrm{F}}}^{(k)}$ leads at antenna element k_{A} to a subcarrier with the same frequency and the complex amplitude $\underline{\tilde{e}}_{n_{\mathrm{F}}}^{(k,k_{\mathrm{A}})}$, see also Section 3.3. The total signal originating in MT k and received at antenna element k_{A} can be written as

$$\underline{\tilde{\mathbf{e}}}^{(k,k_{\mathrm{A}})} = \left(\underline{\tilde{e}}_1^{(k,k_{\mathrm{A}})} \ \ldots \ \underline{\tilde{e}}_{N_{\mathrm{F}}}^{(k,k_{\mathrm{A}})}\right)^{\mathrm{T}}, \tag{6.2}$$

see also (3.5). The K signals $\underline{\tilde{\mathbf{e}}}^{(k,k_{\mathrm{A}})}$ of (6.2) are now superimposed to form the antenna element specific undisturbed receive signal

$$\underline{\tilde{\mathbf{e}}}^{(k_{\mathrm{A}})} = \sum_{k=1}^{K} \underline{\tilde{\mathbf{e}}}^{(k,k_{\mathrm{A}})} = \left(\underline{\tilde{e}}_1^{(k_{\mathrm{A}})} \ \ldots \ \underline{\tilde{e}}_{N_{\mathrm{F}}}^{(k_{\mathrm{A}})}\right)^{\mathrm{T}} \tag{6.3}$$

of antenna element k_{A}. If noise

$$\underline{\tilde{\mathbf{n}}}^{(k_{\mathrm{A}})} = \left(\underline{\tilde{n}}_1^{(k_{\mathrm{A}})} \ \ldots \ \underline{\tilde{n}}_{N_{\mathrm{F}}}^{(k_{\mathrm{A}})}\right)^{\mathrm{T}} \tag{6.4}$$

is superimposed on $\underline{\tilde{\mathbf{e}}}^{(k_{\mathrm{A}})}$ of (6.3), then the antenna element specific noise corrupted receive signal

$$\underline{\tilde{\mathbf{r}}}^{(k_{\mathrm{A}})} = \underline{\tilde{\mathbf{e}}}^{(k_{\mathrm{A}})} + \underline{\tilde{\mathbf{n}}}^{(k_{\mathrm{A}})} \tag{6.5}$$

is obtained, see also (3.8). The K_{A} signals $\underline{\tilde{\mathbf{r}}}^{(k_{\mathrm{A}})}$ of (6.5) received by the antenna elements of the AP are stacked in the signal

$$\underline{\tilde{\mathbf{r}}}_{\mathrm{tot}} = \left(\underline{\tilde{\mathbf{r}}}^{(1)^{\mathrm{T}}} \ \ldots \ \underline{\tilde{\mathbf{r}}}^{(K_{\mathrm{A}})^{\mathrm{T}}}\right)^{\mathrm{T}} \tag{6.6}$$

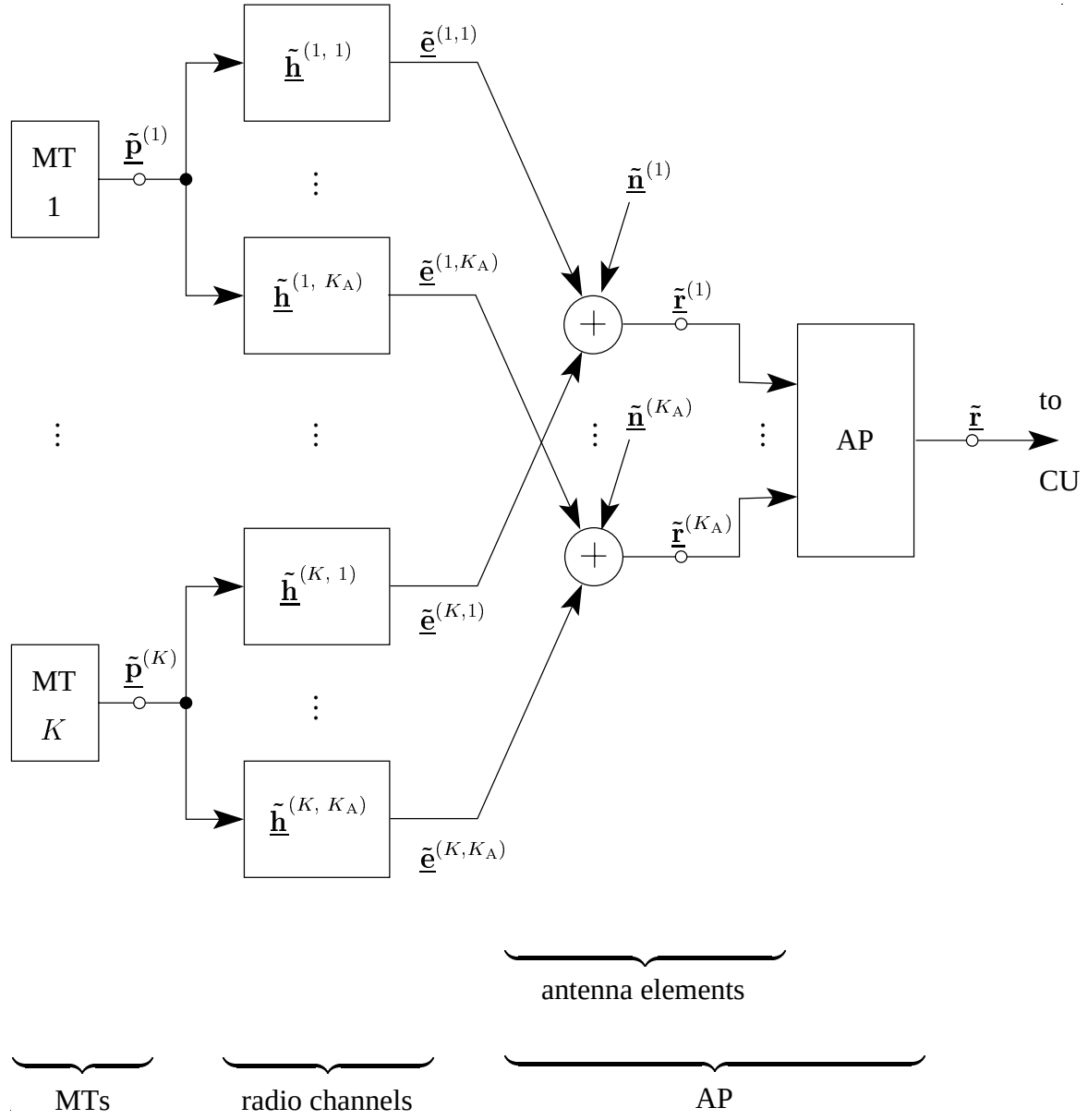

Fig. 6.1. Uplink transmission situation in a SA of JOINT with an array antenna at the considered AP

of dimension $K_{\mathrm{A}}N_{\mathrm{F}}$, which is termed total noise corrupted receive signal. $\underline{\tilde{\mathbf{r}}}_{\mathrm{tot}}$ of (6.6) is forwarded to the CU.

Stacking the total pilot matrix $\underline{\tilde{\mathbf{P}}}$ of (4.10) in a blockdiagonal manner leads to the total pilot matrix

$$\underline{\tilde{\mathbf{P}}}_{\mathrm{tot}} = \mathrm{blkdiag}\Big(\underbrace{\underline{\tilde{\mathbf{P}}} \ \ldots \ \underline{\tilde{\mathbf{P}}}}_{K_{\mathrm{A}} \text{ times}}\Big) \tag{6.7}$$

of dimension $(K_{\mathrm{A}}N_{\mathrm{F}}) \times (K_{\mathrm{A}}KN_{\mathrm{F}})$. With $\underline{\tilde{\mathbf{P}}}_{\mathrm{tot}}$ of (6.7), the total CTF

$$\underline{\tilde{\mathbf{h}}}_{\mathrm{tot}} = \left(\underline{\tilde{\mathbf{h}}}^{(1,\,1)^{\mathrm{T}}} \ \ldots \ \underline{\tilde{\mathbf{h}}}^{(K,\,1)^{\mathrm{T}}} \ \ldots \ \underline{\tilde{\mathbf{h}}}^{(1,\,K_{\mathrm{A}})^{\mathrm{T}}} \ \ldots \ \underline{\tilde{\mathbf{h}}}^{(K,\,K_{\mathrm{A}})^{\mathrm{T}}} \right)^{\mathrm{T}} \tag{6.8}$$

of dimension $K_{\mathrm{A}}KN_{\mathrm{F}}$ and the total noise signal

$$\underline{\tilde{\mathbf{n}}}_{\mathrm{tot}} = \left(\underline{\tilde{\mathbf{n}}}^{(1)^{\mathrm{T}}} \ \ldots \ \underline{\tilde{\mathbf{n}}}^{(K_{\mathrm{A}})^{\mathrm{T}}} \right)^{\mathrm{T}} \tag{6.9}$$

of dimension $K_{\mathrm{A}}N_{\mathrm{F}}$, $\underline{\tilde{\mathbf{r}}}_{\mathrm{tot}}$ of (6.6) can be expressed as

$$\underline{\tilde{\mathbf{r}}}_{\mathrm{tot}} = \underline{\tilde{\mathbf{P}}}_{\mathrm{tot}} \underline{\tilde{\mathbf{h}}}_{\mathrm{tot}} + \underline{\tilde{\mathbf{n}}}_{\mathrm{tot}} . \tag{6.10}$$

Based on the $K_{\mathrm{A}}N_{\mathrm{F}}$ known components $\underline{\tilde{r}}_{n_{\mathrm{F}}}^{(k_{\mathrm{A}})}$, $n_{\mathrm{F}} = 1 \ldots N_{\mathrm{F}}$, $k_{\mathrm{A}} = 1 \ \ldots \ K_{\mathrm{A}}$, of $\underline{\tilde{\mathbf{r}}}_{\mathrm{tot}}$ of (6.10) and the knowledge of the complex amplitudes $\underline{\tilde{p}}_{n_{\mathrm{F}}}^{(k)}$ of (3.3) constituting the total pilot matrix $\underline{\tilde{\mathbf{P}}}_{\mathrm{tot}}$ of (6.7), the CU has the task to estimate the $K_{\mathrm{A}}KN_{\mathrm{F}}$ unknown components $\underline{\tilde{h}}_{n_{\mathrm{F}}}^{(k,k_{\mathrm{A}})}$ of the total CTF $\underline{\tilde{\mathbf{h}}}_{\mathrm{tot}}$ of (6.8). In general, the matrix $\underline{\tilde{\mathbf{P}}}_{\mathrm{tot}}$ in (6.10) is a wide matrix, which means that the number $K_{\mathrm{A}}KN_{\mathrm{F}}$ of unknown CTF components $\underline{\tilde{h}}_{n_{\mathrm{F}}}^{(k,k_{\mathrm{A}})}$ exceeds the number $K_{\mathrm{A}}N_{\mathrm{F}}$ of equations. Therefore, similarly to the case of single-element AP antennas, see Section 4.2, the number of unknown components to be estimated needs to be reduced. How such a reduction can be performed is shown in the following.

6.3 Reduction of the number of unknowns

In order to reduce the number of unknown CTF components $\underline{\tilde{h}}_{n_{\mathrm{F}}}^{(k,k_{\mathrm{A}})}$ of (6.1) to be estimated, directional information concerning the desired received signals $\underline{\tilde{\mathbf{e}}}^{(k,k_{\mathrm{A}})}$ of (6.2) can be exploited [Pap00, Wec02]. This information concerns the directions of arrival (DOAs) from which the signals $\underline{\tilde{\mathbf{e}}}^{(k,k_{\mathrm{A}})}$ impinge at the AP array antenna. For the array antennas the narrowband assumption [MM80, RK89] is made, i. e., time shifts of the same signal received at different antenna elements of the array which are smaller than the inverse of the system bandwidth lead only to changes of the argument of the complex signal envelope [MM80, Pap00]. These changes depend on the DOA of the impinging signal and the array geometry [MM80, RK89, Pap00].

The number and the distribution of the DOAs depend on the propagation environment. In this thesis we consider environments where a single DOA per desired signal is assumed [vdVTP97, Pap00]. Therefore, a total of K DOAs are considered. The K DOAs are assumed to be perfectly known at the CU.

The geometry of the AP array antenna considered in this thesis is illustrated in Fig. 6.2a. A circular antenna element arrangement is assumed, where the AP antenna elements are

equidistantly placed on the perimeter of a circle with the radius r. The center of the circle is termed the reference point (RP) of the array and lies on the reference line (RL) of the array. The distance between adjacent AP antenna elements is marked by l. The position of each AP antenna element k_{A}, $k_{\mathrm{A}} = 1 \ldots K_{\mathrm{A}}$, is given by the radius r of the array and the azimuth angle $\alpha^{(k_{\mathrm{A}})}$ of the antenna element relative to the RL. The K MTs in the SA are assumed to be in the far field of the array. Consequently, the pilot vector $\underline{\tilde{\mathbf{p}}}^{(k)}$ radiated by MT k impinges at the AP array in the form of a planar wave with the MT-specific DOA $\varphi^{(k)}$ [RK89] as illustrated in Fig. 6.2b. Since the narrowband assumption is made, only the phases and not the amplitudes of the received signals vary from array element to array element [Pap00]. Considering a wave front impinging at the array antenna element k_{A}, $k_{\mathrm{A}} = 1 \ldots K_{\mathrm{A}}$, from

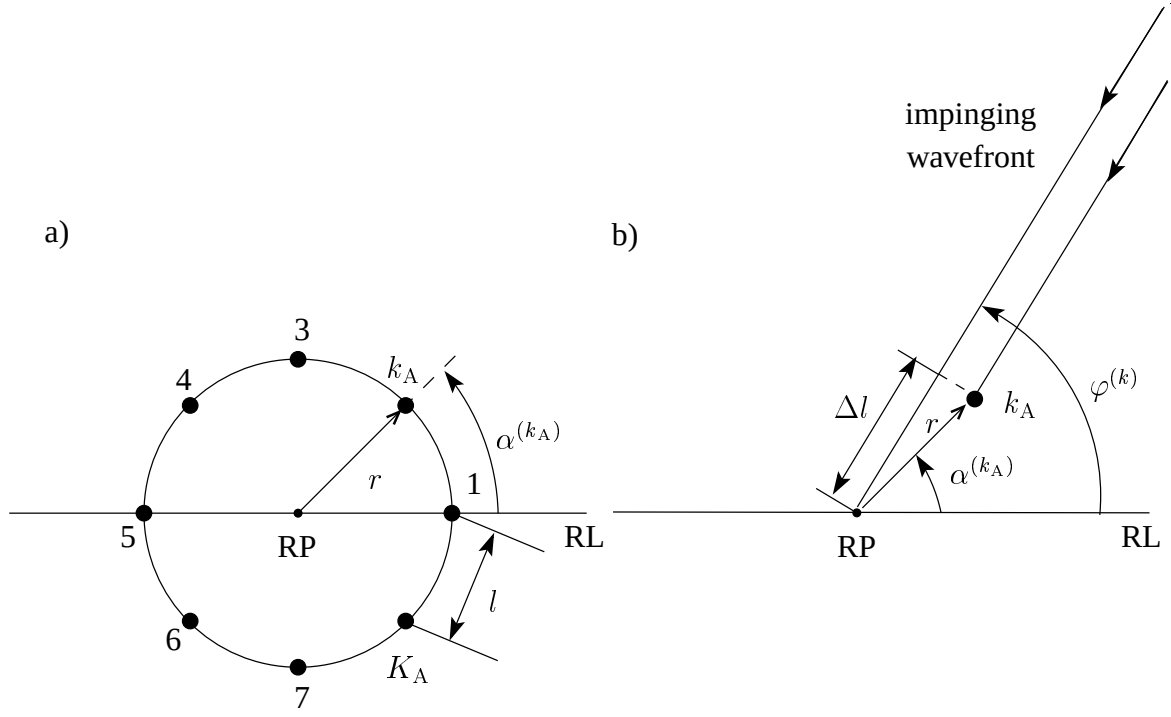

RP: reference point

RL: reference line

Fig. 6.2. Array geometry
a) circular antenna arrangement at the APs of JOINT
b) impinging wave front

the MT-specific DOA $\varphi^{(k)}$, see Fig. 6.2b, the path from MT k to the array antenna element k_{A} is shorter by

$$\Delta l = r \cdot \cos\left(\varphi^{(k)} - \alpha^{(k_{\mathrm{A}})}\right) \tag{6.11}$$

than the path from MT k to the RP [Pap00]. Due to the path length difference Δl of (6.11), a time delay of the signal received at a virtual antenna element at the RP results relative to the reception of this signal at the considered AP antenna element k_{A}, $k_{\mathrm{A}} = 1 \ \ldots \ K_{\mathrm{A}}$. With the carrier wavelength λ, this time delay corresponds to a phase lag [Pap00]

$$\psi^{(k,k_{\mathrm{A}})} = 2\pi \frac{r}{\lambda} \cos\left(\varphi^{(k)} - \alpha^{(k_{\mathrm{A}})}\right), \ k = 1 \ \ldots \ K, \ k_{\mathrm{A}} = 1 \ \ldots \ K_{\mathrm{A}}, \tag{6.12}$$

of the signal received at a virtual antenna element at the RP as compared to the same signal received at the array antenna element k_{A}. With the K_{A} MT-specific phase lags $\psi^{(k,k_{\mathrm{A}})}$ of (6.12), the MT-specific vectors

$$\underline{\tilde{\mathbf{a}}}^{(k)} = \left(\underline{\tilde{a}}^{(k,1)} \ \ldots \ \underline{\tilde{a}}^{(k,K_{\mathrm{A}})}\right)^{\mathrm{T}} = \left(\mathrm{e}^{\mathrm{j}\psi^{(k,1)}} \ \ldots \ \mathrm{e}^{\mathrm{j}\psi^{(k,K_{\mathrm{A}})}}\right)^{\mathrm{T}}, \ k = 1 \ \ldots \ K, \tag{6.13}$$

termed steering vectors of the array [MM80, Haa97] are obtained.

The radio channel between the antenna element of MT k, $k = 1 \ \ldots \ K$, and the array antenna element k_{A}, $k_{\mathrm{A}} = 1 \ \ldots \ K_{\mathrm{A}}$, represented by the CTF vector $\underline{\tilde{\mathbf{h}}}^{(k,k_{\mathrm{A}})}$ of (6.1), can be described by a directional CTF

$$\underline{\tilde{\mathbf{h}}}_{\mathrm{d}}^{(k)} = \left(\underline{\tilde{h}}_{\mathrm{d},1}^{(k)} \ \ldots \ \underline{\tilde{h}}_{\mathrm{d},N_{\mathrm{F}}}^{(k)}\right)^{\mathrm{T}} \tag{6.14}$$

of the radio channel between the antenna element of the same MT k and a virtual antenna element at the RP of the AP array [Pap00, MWW03, MW03]. With the corresponding element $\mathrm{e}^{\mathrm{j}\psi^{(k,k_{\mathrm{A}})}}$ of the MT-specific steering vector $\underline{\tilde{\mathbf{a}}}^{(k)}$ of (6.13) and $\underline{\tilde{\mathbf{h}}}_{\mathrm{d}}^{(k)}$ of (6.14), (6.1) can be rewritten as

$$\underline{\tilde{\mathbf{h}}}^{(k,k_{\mathrm{A}})} = \mathrm{e}^{\mathrm{j}\psi^{(k,k_{\mathrm{A}})}} \underline{\tilde{\mathbf{h}}}_{\mathrm{d}}^{(k)} \ . \tag{6.15}$$

With the elements $\underline{\tilde{a}}^{(k,k_{\mathrm{A}})}$, $k = 1 \ \ldots \ K$, $k_{\mathrm{A}} = 1 \ \ldots \ K_{\mathrm{A}}$, of the MT-specific steering vectors $\underline{\tilde{\mathbf{a}}}^{(k)}$, $k = 1 \ \ldots \ K$, of (6.13), the blockdiagonal antenna element specific steering matrices

$$\begin{aligned} \underline{\tilde{\mathbf{A}}}^{(k_{\mathrm{A}})} &= \mathrm{blkdiag}\left(\underline{\tilde{a}}^{(1,k_{\mathrm{A}})} \cdot \mathbf{I}^{(N_{\mathrm{F}} \times N_{\mathrm{F}})} \ \ldots \ \underline{\tilde{a}}^{(K,k_{\mathrm{A}})} \cdot \mathbf{I}^{(N_{\mathrm{F}} \times N_{\mathrm{F}})}\right) \\ &= \mathrm{blkdiag}\left(\underline{\tilde{\mathbf{A}}}^{(1,k_{\mathrm{A}})} \ \ldots \ \underline{\tilde{\mathbf{A}}}^{(K,k_{\mathrm{A}})}\right) \end{aligned} \tag{6.16}$$

of dimension $(KN_{\mathrm{F}}) \times (KN_{\mathrm{F}})$ are formed. Now, stacking the matrices $\underline{\tilde{\mathbf{A}}}^{(k_{\mathrm{A}})}$, $k_{\mathrm{A}} = 1 \ \ldots \ K_{\mathrm{A}}$, of (6.16) one under the other yields the total steering matrix

$$\underline{\tilde{\mathbf{A}}} = \begin{pmatrix} \underline{\tilde{\mathbf{A}}}^{(1)} \\ \vdots \\ \underline{\tilde{\mathbf{A}}}^{(K_{\mathrm{A}})} \end{pmatrix} \tag{6.17}$$

of dimension $(K_{\mathrm{A}} K N_{\mathrm{F}}) \times (K N_{\mathrm{F}})$. Stacking the K vectors $\underline{\tilde{\mathbf{h}}}_{\mathrm{d}}^{(k)}$ of (6.14) one under the other yields the total directional CTF

$$\underline{\tilde{\mathbf{h}}}_{\mathrm{d}} = \left(\underline{\tilde{\mathbf{h}}}_{\mathrm{d}}^{(1)^{\mathrm{T}}} \ \ldots \ \underline{\tilde{\mathbf{h}}}_{\mathrm{d}}^{(K)^{\mathrm{T}}}\right)^{\mathrm{T}} \tag{6.18}$$

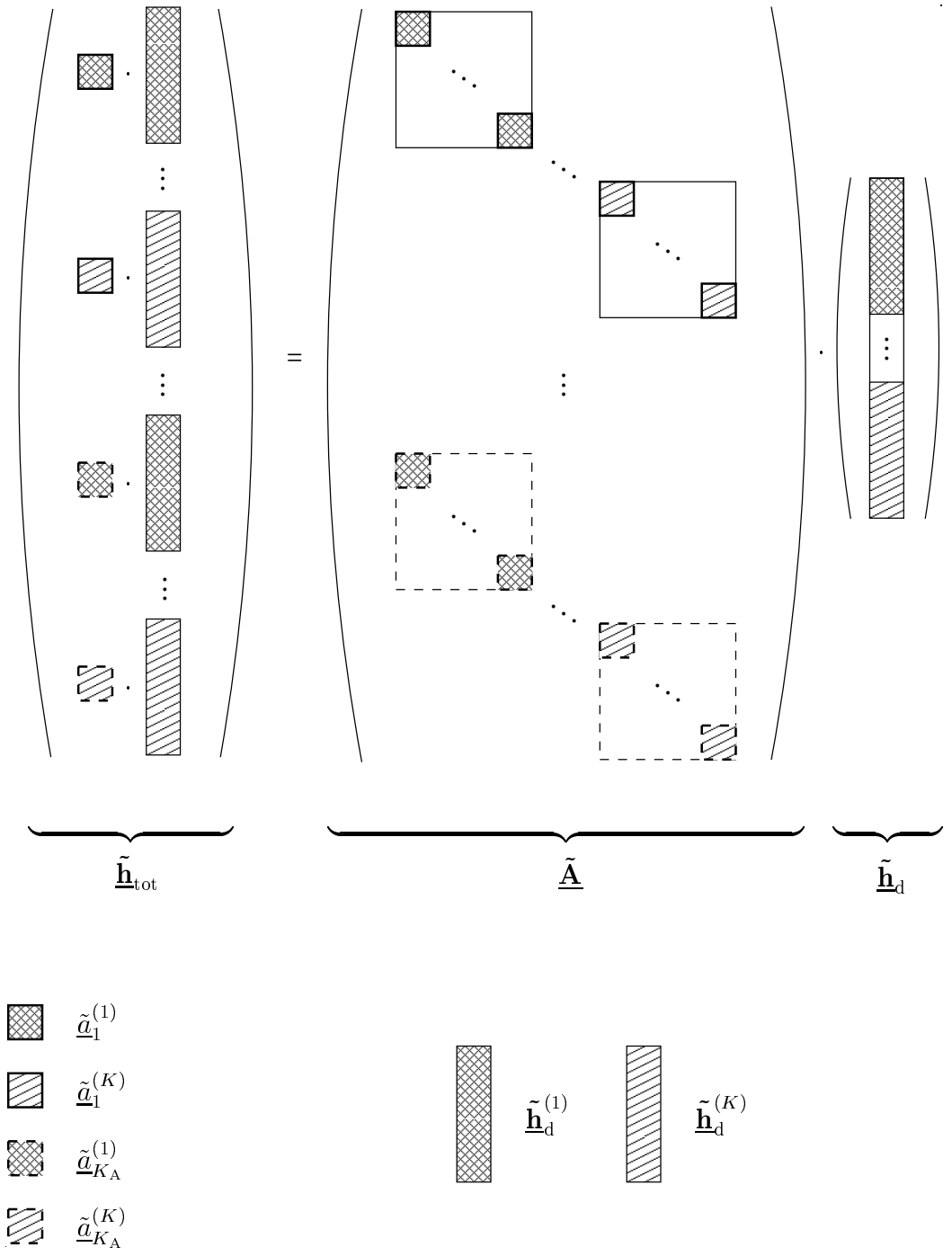

Fig. 6.3. Illustration of the derivation of $\underline{\tilde{\mathbf{h}}}_{\mathrm{tot}}$ according to (6.19)

of dimension KN_{F}. With (6.17) and (6.18), the total CTF of (6.8) now reads

$$\underline{\tilde{\mathbf{h}}}_{\mathrm{tot}} = \underline{\tilde{\mathbf{A}}}\,\underline{\tilde{\mathbf{h}}}_{\mathrm{d}}\ . \tag{6.19}$$

(6.19) is illustrated in Fig. 6.3. Via (6.19) the $K_{\mathrm{A}}KN_{\mathrm{F}}$ components of $\underline{\tilde{\mathbf{h}}}_{\mathrm{tot}}$ of (6.8) are expressed by the KN_{F} components of $\underline{\tilde{\mathbf{h}}}_{\mathrm{d}}$ of (6.18). This observation is the key to the reduction

of the number of unknowns aspired in the present Section 6.3.

With the reduced blockdiagonal Fourier matrix $\underline{\tilde{\boldsymbol{\mathcal{F}}}}_{\mathrm{W}}$ of (4.21), the total directional CTF $\underline{\tilde{\mathbf{h}}}_{\mathrm{d}}$ of (6.18) is related to the total directional CIR

$$\begin{aligned} \underline{\mathbf{h}}_{\mathrm{d}} &= \left(\underline{\mathbf{h}}_{\mathrm{d}}^{(1)^{\mathrm{T}}} \ \ldots \ \underline{\mathbf{h}}_{\mathrm{d}}^{(K)^{\mathrm{T}}} \right)^{\mathrm{T}} \\ &= \left(\underline{h}_{\mathrm{d},1}^{(1)} \ \ldots \ \underline{h}_{\mathrm{d},W}^{(1)} \ \ldots \ \underline{h}_{\mathrm{d},1}^{(K)} \ \ldots \ \underline{h}_{\mathrm{d},W}^{(K)} \right)^{\mathrm{T}} \end{aligned} \tag{6.20}$$

of dimension KW by

$$\underline{\tilde{\mathbf{h}}}_{\mathrm{d}} = \underline{\tilde{\boldsymbol{\mathcal{F}}}}_{\mathrm{W}} \underline{\mathbf{h}}_{\mathrm{d}} \ , \tag{6.21}$$

see also (4.23). With (6.21), (6.19) finally reads

$$\underline{\tilde{\mathbf{h}}}_{\mathrm{tot}} = \underline{\tilde{\mathbf{A}}} \, \underline{\tilde{\boldsymbol{\mathcal{F}}}}_{\mathrm{W}} \underline{\mathbf{h}}_{\mathrm{d}}, \tag{6.22}$$

and by substituting (6.22) into (6.10)

$$\underline{\tilde{\mathbf{r}}}_{\mathrm{tot}} = \underbrace{\underline{\tilde{\mathbf{P}}}_{\mathrm{tot}} \, \underline{\tilde{\mathbf{A}}} \, \underline{\tilde{\boldsymbol{\mathcal{F}}}}_{\mathrm{W}}}_{\underline{\tilde{\boldsymbol{\mathcal{G}}}}_{\mathrm{d}}} \underline{\mathbf{h}}_{\mathrm{d}} + \ \underline{\tilde{\mathbf{n}}}_{\mathrm{tot}} \tag{6.23}$$

follows for the total noise corrupted receive signal at the considered AP. The matrix $\underline{\tilde{\boldsymbol{\mathcal{G}}}}_{\mathrm{d}}$ is the system matrix valid for the multi-element receive antenna case under consideration and has the dimension $(K_{\mathrm{A}} N_{\mathrm{F}}) \times (KW)$. Now, as observed from (6.10) and (6.23), after the exploitation of the information concerning the DOAs of the impinging desired signals and of the array geometry, the number of unknown components to be estimated has been reduced from $K_{\mathrm{A}} K N_{\mathrm{F}}$ components of the total CTF $\underline{\tilde{\mathbf{h}}}_{\mathrm{tot}}$ in (6.10) to KW components of the total directional CIR $\underline{\mathbf{h}}_{\mathrm{d}}$ in (6.23). Also, comparing (6.23) with (4.24) shows that under the existence of DOA knowledge, the number of unknown components to be estimated remains the same, namely KW, in both multi-element and single-element receive antenna cases, whereas the number of known components available has increased in the multi-element antenna case by the number K_{A} of array antenna elements.

6.4 Channel estimation

Following the procedure described in Section 4.4 and introducing the total noise covariance matrix

$$\underline{\mathbf{R}}_{\tilde{\mathbf{n}}_{\mathrm{tot}}} = \mathrm{E} \left\{ \underline{\tilde{\mathbf{n}}}_{\mathrm{tot}} \, \underline{\tilde{\mathbf{n}}}_{\mathrm{tot}}^{\mathsf{H}} \right\} \tag{6.24}$$

of dimension $(K_{\mathrm{A}}N_{\mathrm{F}}) \times (K_{\mathrm{A}}N_{\mathrm{F}})$, the estimate $\hat{\underline{\tilde{\mathbf{h}}}}_{\mathrm{tot}}$ of the total CTF $\underline{\tilde{\mathbf{h}}}_{\mathrm{tot}}$ of (6.8) is obtained by

$$\hat{\underline{\tilde{\mathbf{h}}}}_{\mathrm{tot}} = \overbrace{\underbrace{\underline{\tilde{\mathbf{A}}}\,\underline{\tilde{\boldsymbol{\mathcal{F}}}}_{\mathrm{W}}\underbrace{\left(\underline{\tilde{\boldsymbol{\mathcal{G}}}}_{\mathrm{d}}^{\mathsf{H}}\underline{\mathbf{R}}_{\tilde{\mathbf{n}}_{\mathrm{tot}}}^{-1}\underline{\tilde{\boldsymbol{\mathcal{G}}}}_{\mathrm{d}}\right)^{-1}\underline{\tilde{\boldsymbol{\mathcal{G}}}}_{\mathrm{d}}^{\mathsf{H}}\underline{\mathbf{R}}_{\tilde{\mathbf{n}}_{\mathrm{tot}}}^{-1}}_{\tilde{\underline{\mathbf{Z}}}_{\mathrm{d}}} \cdot\, \underline{\tilde{\mathbf{r}}}_{\mathrm{tot}}}^{\hat{\underline{\mathbf{h}}}_{\mathrm{d}}\ (\text{channel estimator})}}^{\hat{\hat{\underline{\mathbf{h}}}}_{\mathrm{d}}\ (\text{Fourier transformer})} = \tilde{\underline{\mathbf{Z}}}_{\mathrm{d}} \cdot\, \underline{\tilde{\mathbf{r}}}_{\mathrm{tot}}, \tag{6.25}$$

where the estimation matrix $\tilde{\underline{\mathbf{Z}}}_{\mathrm{d}}$ valid for the considered multi-element receive antenna case has the dimension $(K_{\mathrm{A}}KN_{\mathrm{F}}) \times (K_{\mathrm{A}}N_{\mathrm{F}})$. It is seen in (6.25) that the channel estimator applies the pilot vector knowledge and the directional information to gain the estimate $\hat{\underline{\mathbf{h}}}_{\mathrm{d}}$ of the total directional CIR $\underline{\mathbf{h}}_{\mathrm{d}}$ of (6.20). Following this, the Fourier transformer is applied to deliver the CTF estimate $\hat{\underline{\tilde{\mathbf{h}}}}_{\mathrm{d}}$ of the total directional CTF $\underline{\tilde{\mathbf{h}}}_{\mathrm{d}}$ of (6.18). Finally, the directional information is once again invoked by the total steering matrix $\underline{\tilde{\mathbf{A}}}$ of (6.17), and the CTF estimate $\hat{\underline{\tilde{\mathbf{h}}}}_{\mathrm{tot}}$ of the total CTF $\underline{\tilde{\mathbf{h}}}_{\mathrm{tot}}$ of (6.8) is gained.

6.5 Exploiting directional properties of the impinging undesired signals

At each AP antenna element k_{A}, along with the desired undisturbed receive signal $\underline{\tilde{\mathbf{e}}}^{(k_{\mathrm{A}})}$ of (6.3) undesired signals are received as well. These signals originate in the thermal noise present at the AP array antenna and in other radio sources inside and/or outside the considered SA. The impact of the undesired signals originating in radio sources inside the considered SA, i. e., intra-SA interference, is eliminated by the application of joint signal processing at the CU of the SA, that is in this case JCE. Therefore, only the impact of thermal noise and of the undesired signals originating in radio sources outside the considered SA, i. e., inter-SA interference, remain to be dealt with. In what follows, these two sources of undesired signals shall be referred to as noise at the AP array antenna. The statistical information on this noise is contained in the total noise covariance matrix $\underline{\mathbf{R}}_{\tilde{\mathbf{n}}_{\mathrm{tot}}}$ of (6.24). Similar to investigations conducted in [Wec02], the impinging noise is assumed to be directionally uncorrelated. We shall focus on the cases of the noise comprising [Wec02]

- directionally homogeneous signals, which constitute an omnidirectional noise scenario, and
- a combination of directionally discrete and homogeneous signals, which constitute a mixed noise scenario.

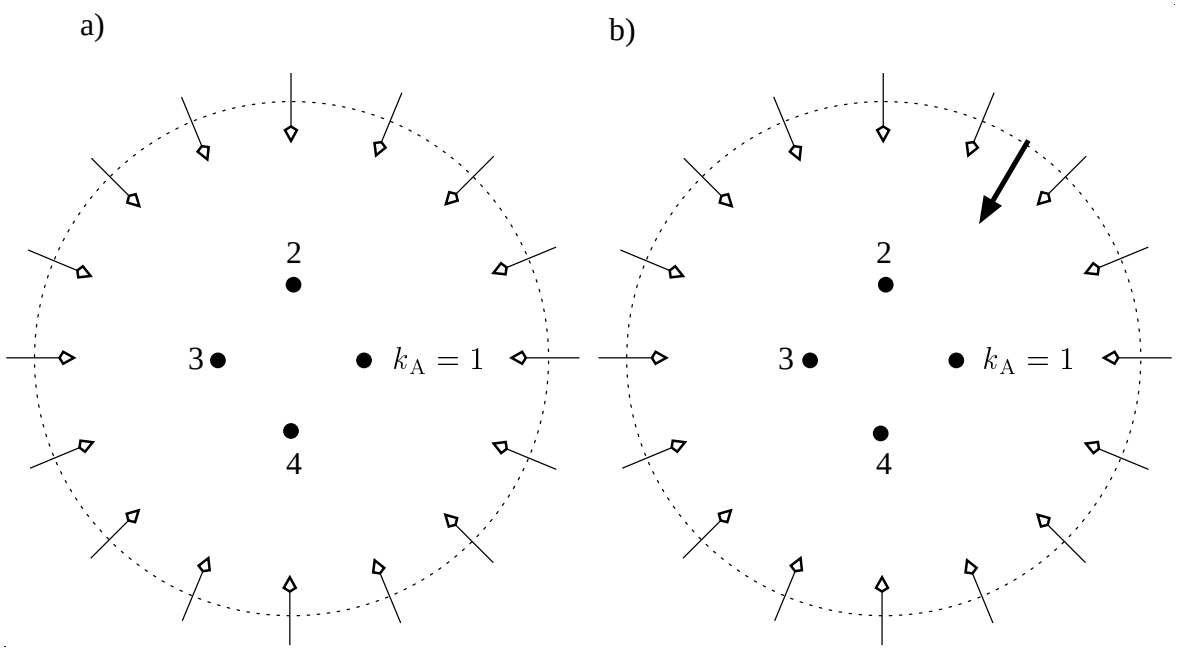

Fig. 6.4. Noise scenarios considered in the thesis for the exemplary case of $K_{\mathrm{A}} = 4$ antenna elements at the AP array
a) omnidirectional noise scenario
b) mixed noise scenario

Both noise scenarios are illustrated in Fig. 6.4 and will be explained in detail in the following.

The information contained in the total noise covariance matrix $\underline{\mathbf{R}}_{\tilde{\mathbf{n}}_{\mathrm{tot}}}$ of (6.24) concerns both the temporal and the spatial correlations of the noise signals impinging at the AP array antenna [Bla98, Wec02]. The temporal correlations of the K_{A} noise signals $\underline{\tilde{\mathbf{n}}}^{(k_{\mathrm{A}})}$, $k_{\mathrm{A}} = 1 \ldots K_{\mathrm{A}}$, of (6.4) are assumed to be the same for each of these signals. Following [Wec02] these correlations can be characterized by a temporal covariance matrix $\underline{\mathbf{R}}_{\mathrm{t}}$. For the sake of simplicity we assume that the noise is spectrally white, which can be considered by choosing the temporal covariance matrix [MW03]

$$\underline{\mathbf{R}}_{\mathrm{t}} = \mathbf{I}^{(N_{\mathrm{F}} \times N_{\mathrm{F}})}. \tag{6.26}$$

With $\underline{\mathbf{R}}_{\mathrm{t}}$ of (6.26), with the Kronecker product operator $\otimes$ [Gra81] and by introducing the spatial covariance matrix $\underline{\mathbf{R}}_{\mathrm{s}}$ of dimension $K_{\mathrm{A}} \times K_{\mathrm{A}}$ containing the spatial correlations of the impinging noise signals $\underline{\tilde{\mathbf{n}}}^{(k_{\mathrm{A}})}$ [Wec02], the total noise covariance matrix $\underline{\mathbf{R}}_{\tilde{\mathbf{n}}_{\mathrm{tot}}}$ of (6.24) can be displayed as [Bla98, Wec02]

$$\underline{\mathbf{R}}_{\tilde{\mathbf{n}}_{\mathrm{tot}}} = \underline{\mathbf{R}}_{\mathrm{s}} \otimes \underline{\mathbf{R}}_{\mathrm{t}} = \underline{\mathbf{R}}_{\mathrm{s}} \otimes \mathbf{I}^{(N_{\mathrm{F}} \times N_{\mathrm{F}})}. \tag{6.27}$$

Based on the assumption of (6.26) only the spatial covariance matrix $\underline{\mathbf{R}}_{\mathrm{s}}$ of (6.27) needs to be determined in order to get the covariance matrix $\underline{\mathbf{R}}_{\tilde{\mathbf{n}}_{\mathrm{tot}}}$ of (6.24).

Let us now assume that a total of K_{I} noise sources exist with each of the K_{I} noise signals impinging at the array antenna from a single specific DOA $\varphi^{(k_{\mathrm{I}})}$, $k_{\mathrm{I}} = 1 \ \ldots \ K_{\mathrm{I}}$. With the power $\sigma^{(k_{\mathrm{I}})^2}$ of the k_{I}-th noise source, the noise signal at the RP of the considered AP array antenna is expressed by [WPE98, WPS99]

$$\sigma^{(k_{\mathrm{I}})^2}\ \underline{\tilde{\mathbf{n}}}^{(k_{\mathrm{I}})} = \sigma^{(k_{\mathrm{I}})^2}\left(\underline{\tilde{n}}^{(k_{\mathrm{I}},1)}\ \ldots\ \underline{\tilde{n}}^{(k_{\mathrm{I}},N_{\mathrm{F}})}\right)^{\mathrm{T}}, \tag{6.28}$$

where the components $\underline{\tilde{n}}^{(k_{\mathrm{I}},n_{\mathrm{F}})}$ of (6.28) are considered to be Gaussian with zero mean and unit variance of the real and the imaginary parts. The noise signal $\underline{\tilde{\mathbf{n}}}^{(k_{\mathrm{A}})}$ impinging at the array antenna element k_{A}, see (6.4), can be associated with the noise signal $\underline{\tilde{\mathbf{n}}}^{(k_{\mathrm{I}})}$ of (6.28) impinging at the imaginary antenna element at the RP by [Bla98, Wec02]

$$\begin{aligned}\underline{\tilde{\mathbf{n}}}^{(k_{\mathrm{A}})} &= \sum_{k_{\mathrm{I}}=1}^{K_{\mathrm{I}}} \sigma^{(k_{\mathrm{I}})^2}\ \underline{\tilde{\mathbf{n}}}^{(k_{\mathrm{I}})} \cdot \exp\left\{\mathrm{j}2\pi\frac{l^{(k_{\mathrm{A}})}}{\lambda}\ \cos\left(\varphi^{(k_{\mathrm{I}})} - \alpha^{(k_{\mathrm{A}})}\right)\right\} \\ &= \sum_{k_{\mathrm{I}}=1}^{K_{\mathrm{I}}} \sigma^{(k_{\mathrm{I}})^2}\ \underline{\tilde{\mathbf{n}}}^{(k_{\mathrm{I}})} \cdot \exp\left\{\mathrm{j}2\pi\frac{r}{\lambda}\ \cos\left(\varphi^{(k_{\mathrm{I}})} - \alpha^{(k_{\mathrm{A}})}\right)\right\},\end{aligned} \tag{6.29}$$

where $l^{(k_{\mathrm{A}})}$ marks the distance of the array antenna element k_{A} to the RP of the array antenna, and for the considered array antenna configuration of Fig. 6.2a is equal to the array radius r. With (6.29) and the total noise signal $\underline{\tilde{\mathbf{n}}}_{\mathrm{tot}}$ of (6.9), the total noise covariance matrix $\underline{\mathbf{R}}_{\tilde{\mathbf{n}}_{\mathrm{tot}}}$ of (6.24) is given by [Wec02]

$$\begin{aligned}\underline{\mathbf{R}}_{\tilde{\mathbf{n}}_{\mathrm{tot}}} &= \begin{bmatrix} \mathrm{E}\left\{\underline{\tilde{\mathbf{n}}}^{(1)}\ \underline{\tilde{\mathbf{n}}}^{(1)^{\mathsf{H}}}\right\} & \cdots & \mathrm{E}\left\{\underline{\tilde{\mathbf{n}}}^{(1)}\ \underline{\tilde{\mathbf{n}}}^{(K_{\mathrm{A}})^{\mathsf{H}}}\right\} \\ \vdots & & \vdots \\ \mathrm{E}\left\{\underline{\tilde{\mathbf{n}}}^{(K_{\mathrm{A}})}\ \underline{\tilde{\mathbf{n}}}^{(1)^{\mathsf{H}}}\right\} & \cdots & \mathrm{E}\left\{\underline{\tilde{\mathbf{n}}}^{(K_{\mathrm{A}})}\ \underline{\tilde{\mathbf{n}}}^{(K_{\mathrm{A}})^{\mathsf{H}}}\right\} \end{bmatrix} \\ &= \begin{bmatrix} \underline{\mathbf{R}}_{\tilde{\mathbf{n}}}^{(1,1)} & \cdots & \underline{\mathbf{R}}_{\tilde{\mathbf{n}}}^{(1,K_{\mathrm{A}})} \\ \vdots & & \vdots \\ \underline{\mathbf{R}}_{\tilde{\mathbf{n}}}^{(K_{\mathrm{A}},1)} & \cdots & \underline{\mathbf{R}}_{\tilde{\mathbf{n}}}^{(K_{\mathrm{A}},K_{\mathrm{A}})} \end{bmatrix}.\end{aligned} \tag{6.30}$$

Assuming pairwise uncorrelated noise vectors $\underline{\tilde{\mathbf{n}}}^{(k_{\mathrm{I}})}$ of (6.28) and applying (6.29) and (6.30), the element matrices $\underline{\mathbf{R}}_{\tilde{\mathbf{n}}}^{(m,n)}$, $m = 1 \ \ldots \ K_{\mathrm{A}}$, $n = 1 \ \ldots \ K_{\mathrm{A}}$, of (6.30) are obtained by

$$\underline{\mathbf{R}}_{\tilde{\mathbf{n}}}^{(m,n)} = \mathrm{E}\left\{\underline{\tilde{\mathbf{n}}}^{(k_{\mathrm{I}})}\ \underline{\tilde{\mathbf{n}}}^{(k_{\mathrm{I}})^{\mathsf{H}}}\right\} \cdot \tag{6.31}$$

$$\sum_{k_{\mathrm{I}}=1}^{K_{\mathrm{I}}} \sigma^{(k_{\mathrm{I}})^2} \cdot \exp\left\{\mathrm{j}\frac{2\pi}{\lambda}\left(l^{(m)}\cos(\varphi^{(k_{\mathrm{I}})} - \alpha^{(m)}) - l^{(n)}\cos(\varphi^{(k_{\mathrm{I}})} - \alpha^{(n)})\right)\right\}$$

$$= \mathrm{E}\left\{\underline{\tilde{\mathbf{n}}}^{(k_{\mathrm{I}})}\ \underline{\tilde{\mathbf{n}}}^{(k_{\mathrm{I}})^{\mathsf{H}}}\right\} \cdot \sum_{k_{\mathrm{I}}=1}^{K_{\mathrm{I}}} \sigma^{(k_{\mathrm{I}})^2} \cdot \exp\left\{\mathrm{j}\frac{2\pi}{\lambda}r\left(\cos(\varphi^{(k_{\mathrm{I}})} - \alpha^{(m)}) - \cos(\varphi^{(k_{\mathrm{I}})} - \alpha^{(n)})\right)\right\},$$

$$m = 1 \ \ldots \ K_{\mathrm{A}},\ n = 1 \ \ldots \ K_{\mathrm{A}}.$$

In the omnidirectional noise scenario of Fig. 6.4a the number K_{I} of noise sources is regarded as infinitely large, and the distribution of the DOAs $\varphi^{(k_{\mathrm{I}})}$ of the impinging noise signals is regarded as uniform over the total azimuthal range $[0,\ 2\pi[$. Furthermore, it is assumed that each noise source k_{I} has the same power $\sigma^{(k_{\mathrm{I}})^2}$ and that all K_{I} noise sources together produce the total noise power σ^2 [Wec02, MWW03]. For such a case it is shown in [Bla98] that the element matrices $\underline{\mathbf{R}}_{\tilde{\mathbf{n}}}^{(m,n)}$, $m,\ n = 1\ \ldots\ K_{\mathrm{A}}$, of (6.31) depend on the total noise power σ^2 and on the distance $l^{(m,n)}$, $m,\ n = 1\ \ldots\ K_{\mathrm{A}}$, between the array antenna elements m and n. With $\mathrm{J}_0(\cdot)$ denoting the Bessel function of the 1^{st} kind and 0^{th} order [BS79], the element matrices $\underline{\mathbf{R}}_{\tilde{\mathbf{n}}}^{(m,n)}$ of (6.31) are obtained by [Bla98]

$$\underline{\mathbf{R}}_{\tilde{\mathbf{n}}}^{(m,\ n)} = \sigma^2 \cdot \mathrm{J}_0\left(\frac{2\pi}{\lambda} l^{(m,\ n)}\right) \cdot \mathbf{I}^{(N_{\mathrm{F}} \times N_{\mathrm{F}})},\ m = 1\ \ldots\ K_{\mathrm{A}},\ n = 1\ \ldots\ K_{\mathrm{A}}. \tag{6.32}$$

Comparing (6.26), (6.27), (6.30) and (6.32) it can be seen that the spatial covariance matrix $\underline{\mathbf{R}}_{\mathrm{s}}$ of (6.27) is given by

$$\begin{aligned} \underline{\mathbf{R}}_{\mathrm{s,omni}} &= \begin{pmatrix} \underline{r}_{\mathrm{s,omni}}^{(1,1)} & \cdots & \underline{r}_{\mathrm{s,omni}}^{(1,K_{\mathrm{A}})} \\ \vdots & & \vdots \\ \underline{r}_{\mathrm{s,omni}}^{(K_{\mathrm{A}},1)} & \cdots & \underline{r}_{\mathrm{s,omni}}^{(K_{\mathrm{A}},K_{\mathrm{A}})} \end{pmatrix} \\ &= \sigma^2 \cdot \begin{pmatrix} \mathrm{J}_0\left(\frac{2\pi}{\lambda} l^{(1,1)}\right) & \cdots & \mathrm{J}_0\left(\frac{2\pi}{\lambda} l^{(1,K_{\mathrm{A}})}\right) \\ \vdots & & \vdots \\ \mathrm{J}_0\left(\frac{2\pi}{\lambda} l^{(K_{\mathrm{A}},1)}\right) & \cdots & \mathrm{J}_0\left(\frac{2\pi}{\lambda} l^{(K_{\mathrm{A}},K_{\mathrm{A}})}\right) \end{pmatrix} \end{aligned} \tag{6.33}$$

for the omnidirectional noise scenario. With (6.27), (6.32) and (6.33), the total noise covariance matrix $\underline{\mathbf{R}}_{\tilde{\mathbf{n}}_{\mathrm{tot}}}$ of (6.30) becomes

$$\underline{\mathbf{R}}_{\tilde{\mathbf{n}}_{\mathrm{tot}}} = \underline{\mathbf{R}}_{\mathrm{s,omni}} \otimes \mathbf{I}^{(N_{\mathrm{F}} \times N_{\mathrm{F}})} \tag{6.34}$$

$$= \sigma^2 \cdot \begin{pmatrix} \mathrm{J}_0\left(\frac{2\pi}{\lambda} l^{(1,\ 1)}\right) \cdot \mathbf{I}^{(N_{\mathrm{F}} \times N_{\mathrm{F}})} & \cdots & \mathrm{J}_0\left(\frac{2\pi}{\lambda} l^{(1,\ K_{\mathrm{A}})}\right) \cdot \mathbf{I}^{(N_{\mathrm{F}} \times N_{\mathrm{F}})} \\ \vdots & & \vdots \\ \mathrm{J}_0\left(\frac{2\pi}{\lambda} l^{(K_{\mathrm{A}},\ 1)}\right) \cdot \mathbf{I}^{(N_{\mathrm{F}} \times N_{\mathrm{F}})} & \cdots & \mathrm{J}_0\left(\frac{2\pi}{\lambda} l^{(K_{\mathrm{A}},\ K_{\mathrm{A}})}\right) \cdot \mathbf{I}^{(N_{\mathrm{F}} \times N_{\mathrm{F}})} \end{pmatrix}$$

for the omnidirectional scenario of Fig. 6.4a.

Investigations concerning the assignment of the noise power to the existing noise sources performed in [Ste96] and [Wec02] showed that most of the noise power impinging at the RP of the considered AP array antenna originates in a small number of noise sources. The

remaining part of the total noise power σ^2 accounts to a large number of noise signals each contributing only a small part to σ^2. Based on this investigation it can be assumed that the combination of a directionally discrete and a directionally homogeneous noise yields a quite realistic noise scenario [Wec02]. Fig. 6.4b illustrates this mixed noise scenario, where the total noise power received at the AP array antenna is the sum of two components [Wec02]. One component consists of a single noise signal marked by the thick arrow in Fig. 6.4b, which impinges at the AP array antenna from the discrete DOA $\varphi^{(k_\mathrm{I})}$ and contributes the part $x_\mathrm{dir}\sigma^2$, $0 < x_\mathrm{dir} < 1$, to the total noise power σ^2. This component is referred to as the directional noise component. The second component consists of the directionally homogeneous noise signals described before and contributes the remaining part $x_\mathrm{omni}\sigma^2 = (1 - x_\mathrm{dir})\sigma^2$, $0 < x_\mathrm{omni} < 1$, to the total noise power σ^2. This component is referred to as the omnidirectional noise component. Under the assumption of directional uncorrelatedness between all noise signals impinging at the AP array antenna

$$\sigma^2 = \sigma^2_\mathrm{dir} + \sigma^2_\mathrm{omni} = (x_\mathrm{dir} + x_\mathrm{omni})\,\sigma^2 \tag{6.35}$$

holds for the total noise power.

Applying the considerations of (6.28) till (6.32) to the case of a single noise signal impinging at the array antenna element k_A from the single DOA $\varphi^{(k_\mathrm{I})}$ together with the considered circular array antenna configuration illustrated in Fig. 6.2a, the spatial covariance matrix $\underline{\mathbf{R}}_\mathrm{s,dir}$ of the directional noise component is obtained by [Wec02]

$$\underline{\mathbf{R}}_\mathrm{s,dir} = \begin{pmatrix} \underline{r}^{(1,1)}_\mathrm{s,dir} & \cdots & \underline{r}^{(1,K_\mathrm{A})}_\mathrm{s,dir} \\ \vdots & & \vdots \\ \underline{r}^{(K_\mathrm{A},1)}_\mathrm{s,dir} & \cdots & \underline{r}^{(K_\mathrm{A},K_\mathrm{A})}_\mathrm{s,dir} \end{pmatrix} \tag{6.36}$$

$$= \sigma^2 \cdot \begin{pmatrix} \exp\left\{\mathrm{j}2\pi\frac{r}{\lambda}\left(\cos(\varphi^{(k_\mathrm{I})} - \alpha^{(1)}) - \cos(\varphi^{(k_\mathrm{I})} - \alpha^{(1)})\right)\right\} & \cdots \\ \vdots & \\ \exp\left\{\mathrm{j}2\pi\frac{r}{\lambda}\left(\cos(\varphi^{(k_\mathrm{I})} - \alpha^{(K_\mathrm{A})}) - \cos(\varphi^{(k_\mathrm{I})} - \alpha^{(1)})\right)\right\} & \cdots \end{pmatrix}$$

$$\begin{pmatrix} \cdots & \exp\left\{\mathrm{j}2\pi\frac{r}{\lambda}\left(\cos(\varphi^{(k_\mathrm{I})} - \alpha^{(1)}) - \cos(\varphi^{(k_\mathrm{I})} - \alpha^{(K_\mathrm{A})})\right)\right\} \\ & \vdots \\ \cdots & \exp\left\{\mathrm{j}2\pi\frac{r}{\lambda}\left(\cos(\varphi^{(k_\mathrm{I})} - \alpha^{(K_\mathrm{A})}) - \cos(\varphi^{(k_\mathrm{I})} - \alpha^{(K_\mathrm{A})})\right)\right\} \end{pmatrix}.$$

With (6.36), the $(K_\mathrm{A}N_\mathrm{F}) \times (K_\mathrm{A}N_\mathrm{F})$ noise covariance matrix

$$\underline{\mathbf{R}}_{\check{\mathbf{n}},\mathrm{dir}} = \underline{\mathbf{R}}_\mathrm{s,dir} \otimes \mathbf{I}^{(N_\mathrm{F}\times N_\mathrm{F})} \tag{6.37}$$

of the directional noise component is obtained. Analogously, with (6.33), the $(K_{\mathrm{A}}N_{\mathrm{F}}) \times (K_{\mathrm{A}}N_{\mathrm{F}})$ noise covariance matrix

$$\underline{\mathbf{R}}_{\tilde{\mathbf{n}},\mathrm{omni}} = \underline{\mathbf{R}}_{\mathrm{s,omni}} \otimes \mathbf{I}^{(N_{\mathrm{F}} \times N_{\mathrm{F}})} \tag{6.38}$$

of the omnidirectional noise component is obtained. Both (6.37) and (6.38) are valid for the case of purely directionally noise and for the case of purely directionally homogenous noise, respectively. Considering (6.35) together with (6.37), (6.38) and the property [Gra81]

$$(\underline{\mathbf{A}} + \underline{\mathbf{B}}) \otimes \underline{\mathbf{C}} = \underline{\mathbf{A}} \otimes \underline{\mathbf{C}} + \underline{\mathbf{B}} \otimes \underline{\mathbf{C}} \tag{6.39}$$

of the Kronecker product, the total noise covariance matrix $\underline{\mathbf{R}}_{\tilde{\mathbf{n}}_{\mathrm{tot}}}$ of (6.27) reads

$$\underline{\mathbf{R}}_{\tilde{\mathbf{n}}_{\mathrm{tot}}} = \left(x_{\mathrm{dir}} \cdot \underline{\mathbf{R}}_{\mathrm{s,dir}} + x_{\mathrm{omni}} \cdot \underline{\mathbf{R}}_{\mathrm{s,omni}}\right) \otimes \mathbf{I}^{(N_{\mathrm{F}} \times N_{\mathrm{F}})} \tag{6.40}$$

for the mixed noise scenario of Fig. 6.4b.

6.6 Simulations

Based on the considerations regarding the inclusion of directional information about the desired and the undesired signals impinging at the AP array presented in the previous three sections, the present section gives simulation results concerning the performance of JCE of (6.25). Due to the assumption of zero mean Gaussian noise components $\underline{\tilde{n}}^{(k_{\mathrm{I}},n_{\mathrm{F}})}$ of (6.28), the antenna element specific noise signals $\underline{\tilde{\mathbf{n}}}^{(k_{\mathrm{A}})}$ of (6.29) are also zero mean and Gaussian. Therefore, the estimate $\underline{\hat{\tilde{\mathbf{h}}}}_{\mathrm{tot}}$ of (6.25) is a ML estimate of the CTF $\underline{\tilde{\mathbf{h}}}_{\mathrm{tot}}$ of (6.8). The considered simulation scenarios, which are based on the two noise scenarios presented in Section 6.5, are illustrated in Fig. 6.5 for the exemplary case of $K = 4$ MTs and $K_{\mathrm{A}} = 4$ array antenna elements at the AP. The distance l between adjacent antenna elements, see Fig. 6.2a, is set equal to $\lambda/2$. The MTs are placed on the perimeter of a circle, the center of which is the RP of the AP array antenna. In the conducted simulations, the DOAs $\varphi^{(k)}$, $k = 1 \ \ldots \ K$, are varied simultaneously for all K MTs by the angle φ, $\varphi \in [0, \pi/2]$, i. e.

$$\varphi^{(k)} = \frac{2\pi}{K}(k-1) + \varphi, \ k = 1 \ \ldots \ K, \tag{6.41}$$

holds. One may argue that a symmetric DOA scenario such as the one in Fig. 6.5 is rather unlikely to occur in the real world. Nevertheless, the applied scenario is sufficient in order to gain qualitative and quantitative impressions about the performance of ML–JCE. For both simulation scenarios of Fig. 6.5 the pilot vectors based on Walsh codes defined in Section 5.5 are considered.

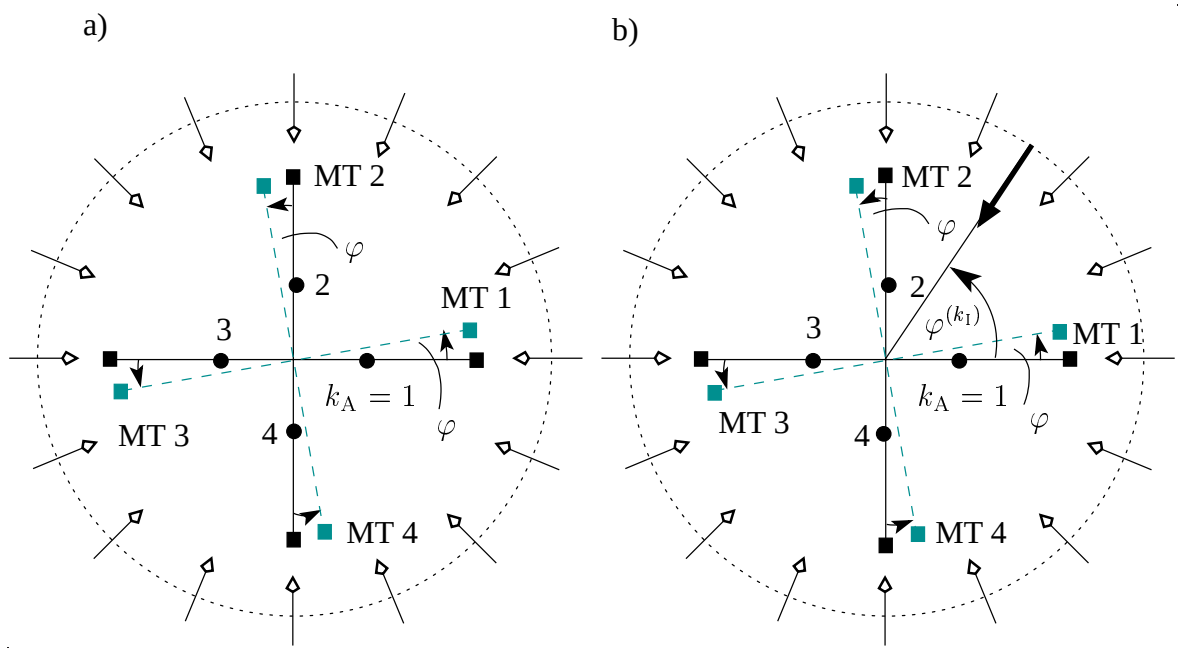

Fig. 6.5. Simulation scenarios considered in the thesis for the exemplary case of $K = 4$ MTs and $K_{\mathrm{A}} = 4$ antenna elements at the AP array
a) omnidirectional noise scenario
b) mixed noise scenario

As the performance criterion, the SNR degradations [MWW03, MW03]

$$\begin{aligned} \delta_{n_{\mathrm{F}}}^{(k,\,k_{\mathrm{A}})} &= \frac{2E_{\mathrm{p}}}{\sigma^2 \cdot W} \left[\underline{\tilde{\mathbf{Z}}}_{\mathrm{d}}\, \underline{\mathbf{R}}_{\tilde{\mathbf{n}}_{\mathrm{tot}}} \underline{\tilde{\mathbf{Z}}}_{\mathrm{d}}^{\mathsf{H}} \right]_{i,\,i} , \\ i &= (k_{\mathrm{A}} - 1) K_{\mathrm{A}} N_{\mathrm{F}} + (k-1) N_{\mathrm{F}} + n_{\mathrm{F}}, \\ k_{\mathrm{A}} &= 1 \,\ldots\, K_{\mathrm{A}},\; k = 1 \,\ldots\, K,\; n_{\mathrm{F}} = 1 \ldots N_{\mathrm{F}}, \end{aligned} \tag{6.42}$$

for the multi-element receive antenna case of JOINT – defined in (6.42) based on the considerations presented in Subsection 4.5.1 – are adopted. In (6.42) the assumption stated in (5.1) is made. Further, although the total noise power σ^2 at the AP array appears in (6.42), the SNR degradations $\delta_{n_{\mathrm{F}}}^{(k,\,k_{\mathrm{A}})}$ are independent of σ^2. As a matter of fact, σ^2 is eliminated from (6.42) due to its presence in the total noise covariance matrix $\underline{\mathbf{R}}_{\tilde{\mathbf{n}}_{\mathrm{tot}}}$, see (6.34) and (6.40).

In Fig. 6.6 the simulation curves obtained for the omnidirectional noise scenario of Fig. 6.5a are shown. The SNR degradations $\delta_{n_{\mathrm{F}}}^{(1,\,k_{\mathrm{A}})}$, obtained for MT 1 according to (6.42), are plotted versus the MT-specific DOA $\varphi^{(1)}$ of (6.41) for the cases of the number K_{A} of array antenna elements equal to two, four and eight. Due to the mentioned symmetry of the simulation scenario of Fig. 6.5a the curves in Fig. 6.6 hold for all values of k_{A} and n_{F}. Furthermore,

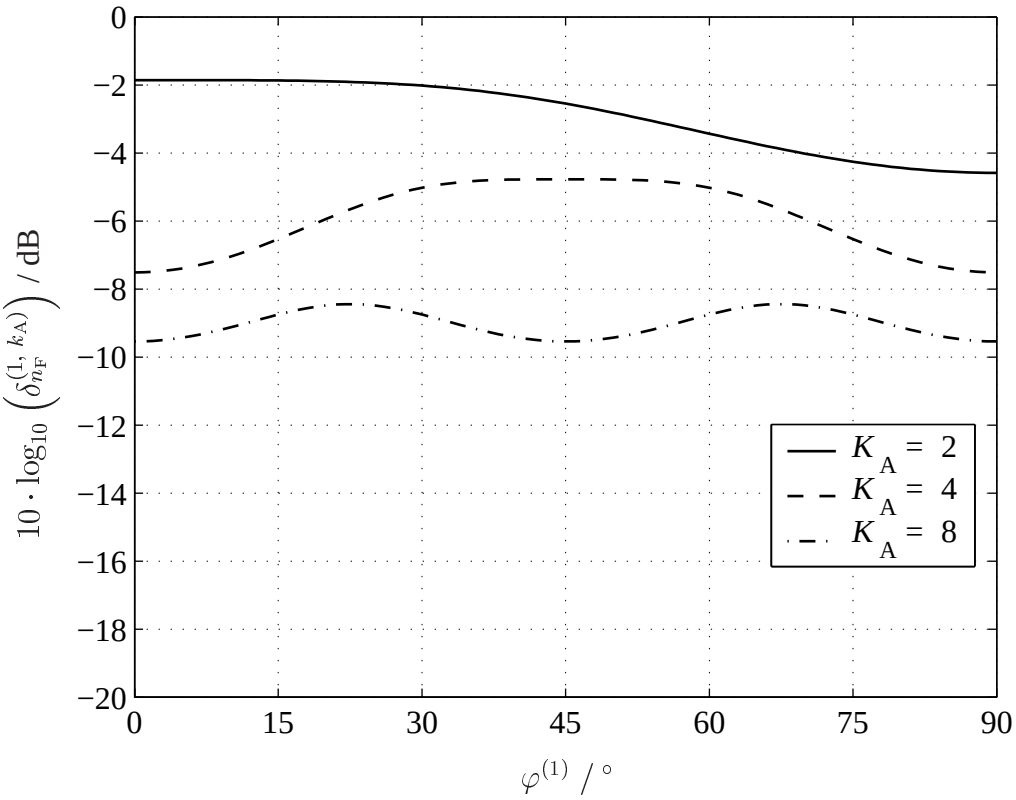

Fig. 6.6. SNR degradation $\delta_{n_\mathrm{F}}^{(1,\,k_\mathrm{A})}$ of MT 1 versus the MT-specific DOA $\varphi^{(1)}$ for different numbers K_A of antenna elements of the AP array; omnidirectional noise scenario

the curves of Fig. 6.6 hold for all K MTs of the considered scenario. In the case of a single-element receive antenna, the SNR degradations $\delta_{n_\mathrm{F}}^{(k)}$ of (4.42) are equal to 0 dB for all K MTs due to the application of the pilot vectors based on Walsh codes, see Subsection 5.5.2. In Fig. 6.6 it is seen that the SNR degradations $\delta_{n_\mathrm{F}}^{(1,\,k_\mathrm{A})}$ of (6.42) drop to values lower than 0 dB due to the application of array antennas and the involved exploitation of DOA knowledge. For the omnidirectional noise scenario of Fig. 6.5a the SNR degradations $\delta_{n_\mathrm{F}}^{(1,\,k_\mathrm{A})}$ in Fig. 6.6 are decreased by 3 dB in the mean each time the number K_A of antenna elements is doubled.

Figs. 6.7 to 6.10 show the results obtained for the mixed noise scenario of Fig. 6.5b. Figs. 6.7 and 6.8 show the SNR degradations $\delta_{n_\mathrm{F}}^{(1,\,k_\mathrm{A})}$ versus the MT-specific DOA $\varphi^{(1)}$ of MT 1 for the cases of the number K_A of array antenna elements equal to two, four and eight. The percentages x_dir and x_omni of (6.35) take on the values 0.8 and 0.2, respectively. In the case of Fig. 6.7 the DOA $\varphi^{(k_\mathrm{I})}$ of the directional noise component is equal to $0°$, whereas in the case of Fig. 6.8 $\varphi^{(k_\mathrm{I})}$ equals $30°$. As expected, the increase of the number K_A of array antenna elements leads to a decrease of $\delta_{n_\mathrm{F}}^{(1,\,k_\mathrm{A})}$. In both Fig. 6.7 and Fig. 6.8 it can be seen that when the DOA $\varphi^{(k_\mathrm{I})}$ of the directional noise component is close to or identical with the MT-specific DOA $\varphi^{(1)}$ of MT 1, the achieved decrease of $\delta_{n_\mathrm{F}}^{(1,\,k_\mathrm{A})}$ is rather low. In contrast to this, when $\varphi^{(k_\mathrm{I})}$ and $\varphi^{(1)}$ are further away from each other, the achieved decrease of $\delta_{n_\mathrm{F}}^{(1,\,k_\mathrm{A})}$

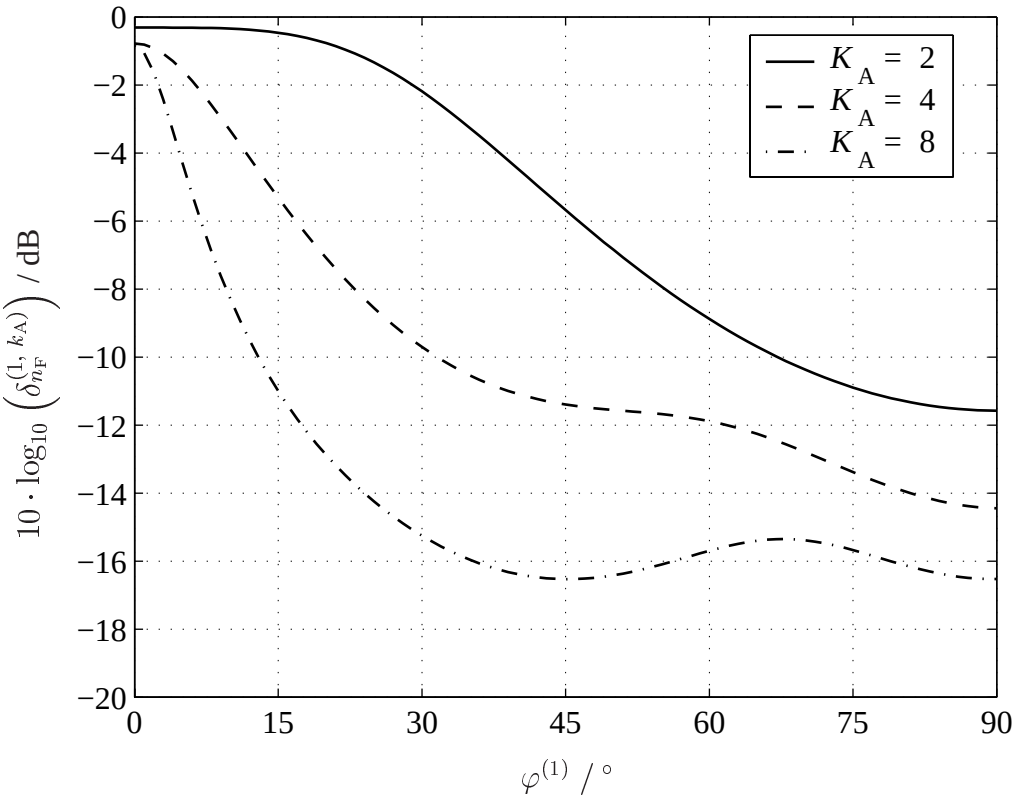

Fig. 6.7. SNR degradation $\delta_{n_\mathrm{F}}^{(1,\,k_\mathrm{A})}$ of MT 1 versus the MT-specific DOA $\varphi^{(1)}$ for different numbers K_A of antenna elements of the AP array; mixed noise model, $\varphi^{(k_\mathrm{I})} = 0°$

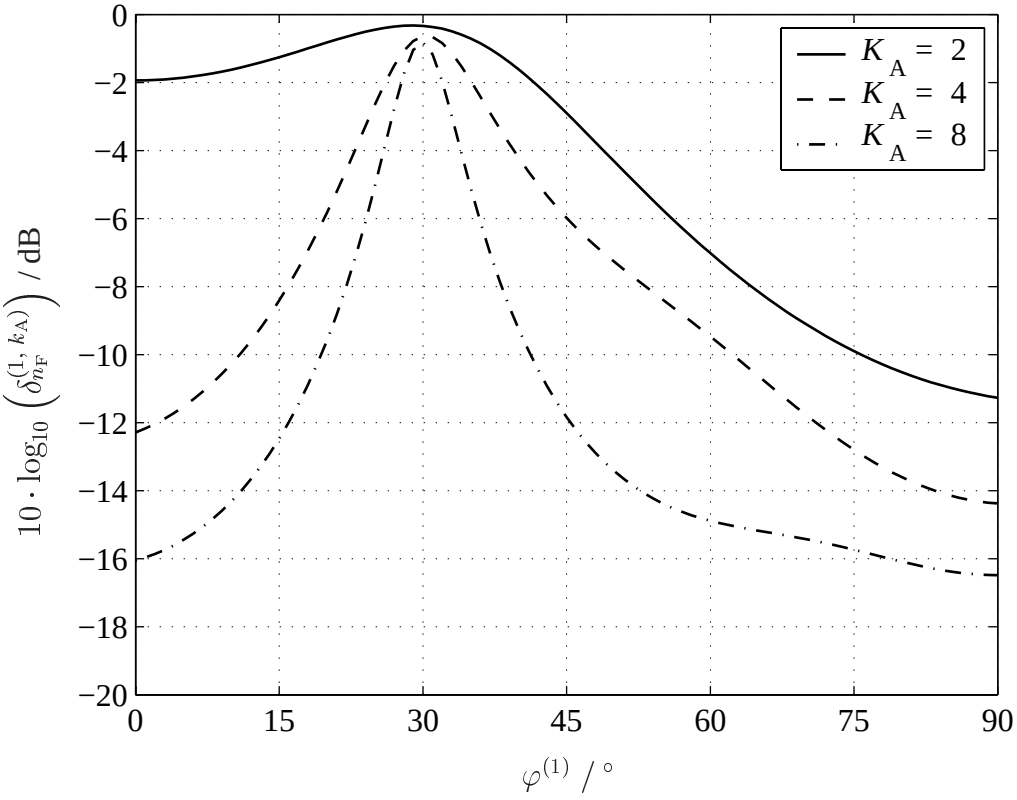

Fig. 6.8. SNR degradation $\delta_{n_\mathrm{F}}^{(1,\,k_\mathrm{A})}$ of MT 1 versus the MT-specific DOA $\varphi^{(1)}$ for different numbers K_A of antenna elements of the AP array; mixed noise model, $\varphi^{(k_\mathrm{I})} = 30°$

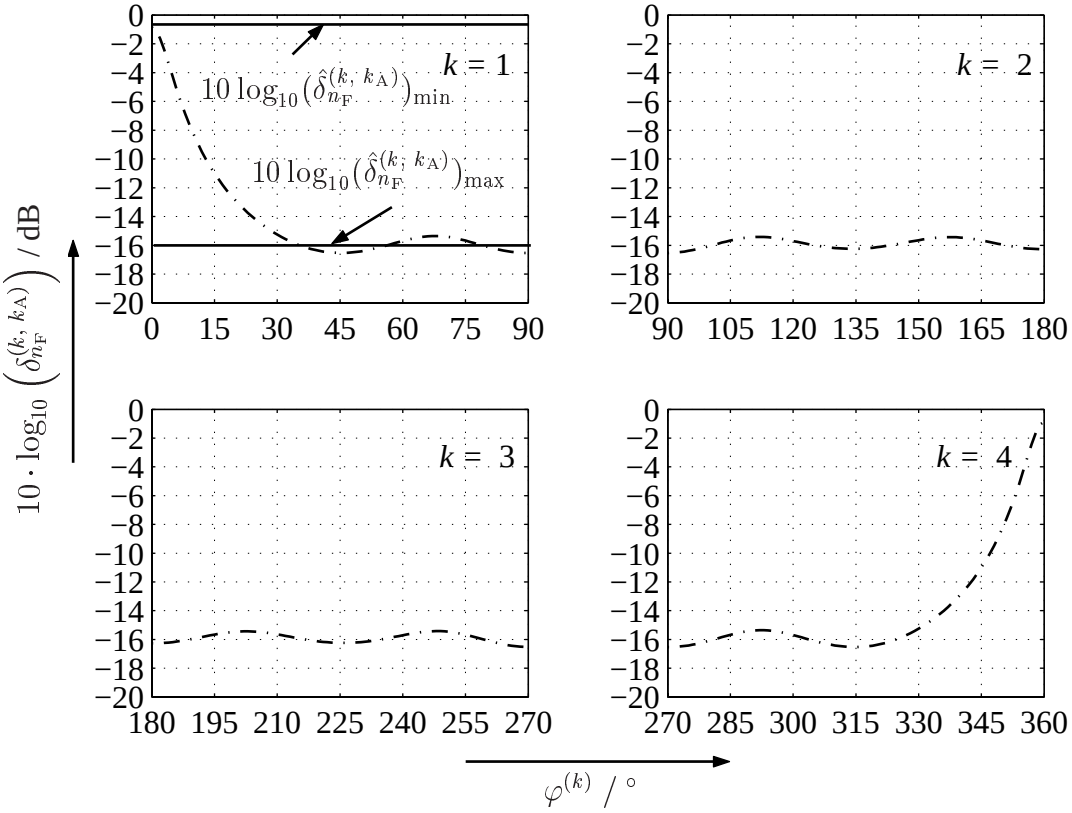

Fig. 6.9. SNR degradation $\delta_{n_\mathrm{F}}^{(k,\,k_\mathrm{A})}$ versus the MT-specific DOA $\varphi^{(k)}$, $k = 1 \ \ldots \ K$; $K_\mathrm{A} = 8$ antenna elements; mixed noise model, $\varphi^{(k_\mathrm{I})} = 0°$

is higher than in the case of Fig. 6.6 for the omnidirectional noise scenario. This is shown by the curves in Fig. 6.9, where the SNR degradations $\delta_{n_\mathrm{F}}^{(k,\,k_\mathrm{A})}$, for all K MTs are plotted versus the MT-specific DOA $\varphi^{(k)}$, $k = 1 \ \ldots \ K$, for the case of eight array antenna elements and $\varphi^{(k_\mathrm{I})}$ equal to $0°$. For MTs two and three, the DOAs of which are spatial farther from $\varphi^{(k_\mathrm{I})}$, $\delta_{n_\mathrm{F}}^{(k,\,k_\mathrm{A})}$, $k = 2, 3$, are decreased to -16 dB in the mean as compared to -9 dB in Fig. 6.6. In the cases of MTs two and three, the applied array antenna at the considered AP is able to suppress the directional noise component. Therefore, only the impact of the omnidirectional noise component remains to be dealt with. However, in the mixed noise scenario of Fig. 6.5b the power of the omnidirectional noise component is only 20% of the total noise power, i. e., x_omni is equal to 0.2, as compared to the omnidirectional noise scenario of Fig. 6.5a. For this reason, the SNR degradations $\delta_{n_\mathrm{F}}^{(2,k_\mathrm{A})}$ and $\delta_{n_\mathrm{F}}^{(3,k_\mathrm{A})}$ of MTs two and three are lower than in the case of Fig. 6.6.

Rough estimates $\hat{\delta}_{n_\mathrm{F}}^{(k,\,k_\mathrm{A})}$ of the SNR degradations $\delta_{n_\mathrm{F}}^{(k,\,k_\mathrm{A})}$ for the worst case where

$$\varphi^{(k_\mathrm{I})} \equiv \varphi^{(k)} \tag{6.43}$$

holds can be given by

$$10\log_{10}\left(\hat{\delta}_{n_{\mathrm{F}}}^{(k,\,k_{\mathrm{A}})}\right)_{\min} \approx 10\log_{10}\left(x_{\mathrm{dir}}\right). \tag{6.44}$$

The approximation of (6.44) is based on the thought that when (6.43) holds, it can be assumed that only the directional noise component has an impact on $\delta_{n_{\mathrm{F}}}^{(k,\,k_{\mathrm{A}})}$. As the directional noise component and the desired signals impinge at the AP array antenna from the same direction, no suppression of the undesired signal by the applied array antenna is possible. Thus, the only performance improvement as compared to the single-element receive antenna case comes from the fact that the directional noise component contributes only a part $x_{\mathrm{dir}} < 1$ to the total noise power σ^2 of (6.35). For the considered value of 0.8 for x_{dir}, $10\log_{10}\left(\hat{\delta}_{n_{\mathrm{F}}}^{(k,\,k_{\mathrm{A}})}\right)_{\min}$ is equal to -0.97 dB. The quality of the estimate $\left(\hat{\delta}_{n_{\mathrm{F}}}^{(k,\,k_{\mathrm{A}})}\right)_{\min}$ of (6.44) of $\delta_{n_{\mathrm{F}}}^{(k,\,k_{\mathrm{A}})}$ of (6.42) is influenced by the fact that the omnidirectional noise component is also present in the case of (6.43).

In analogy to the worse case of (6.44), a rough estimate $\left(\hat{\delta}_{n_{\mathrm{F}}}^{(k,\,k_{\mathrm{A}})}\right)_{\max}$ of $\delta_{n_{\mathrm{F}}}^{(k,\,k_{\mathrm{A}})}$ can be obtained also for the best case of the mixed noise scenario of Fig. 6.5b, where $\varphi^{(k_{\mathrm{I}})}$ and $\varphi^{(1)}$ are spatial farther from each other. In this case the directional noise component can be suppressed by the applied array antenna leaving only the omnidirectional noise component to be dealt with. With the average performance improvement by a factor of K_{A} due to the use of array antennas, see Fig. 6.6, and the fact that the omnidirectional noise component contributes only a fraction x_{omni} to the total noise power σ^2 of (6.35), the approximation

$$10\log_{10}\left(\hat{\delta}_{n_{\mathrm{F}}}^{(k,\,k_{\mathrm{A}})}\right)_{\max} \approx 10\log_{10}\left(\frac{x_{\mathrm{omni}}}{K_{\mathrm{A}}}\right) \tag{6.45}$$

can be made, which for the scenario of Fig. 6.9 is equal to -16 dB. The quality of the estimates $\left(\hat{\delta}_{n_{\mathrm{F}}}^{(k,\,k_{\mathrm{A}})}\right)_{\max}$ of (6.45) of the SNR degradations $\delta_{n_{\mathrm{F}}}^{(k,\,k_{\mathrm{A}})}$ of (6.42) is influenced by the fact that in real world applications the array antenna cannot completely eliminate the impact of the directional noise component.

Finally, Fig. 6.10 gives an impression concerning the impact of the percentage x_{dir}, with which the directional noise component contributes to the total noise power σ^2 of (6.35), on the SNR degradation $\delta_{n_{\mathrm{F}}}^{(k,\,k_{\mathrm{A}})}$, of MT k, $k = 1 \ldots K$. The value x_{dir} is varied within the interval $[0,\ 0.9]$ in steps of 0.1. It is observed from the curves in Fig. 6.10 that the SNR degradation $\delta_{n_{\mathrm{F}}}^{(k,\,k_{\mathrm{A}})}$ is decreased at the most when x_{dir} is equal to 0.9. The case of 100% directional noise is not displayed in Fig. 6.10, because in this case the SNR degradation $\delta_{n_{\mathrm{F}}}^{(k,\,k_{\mathrm{A}})}$ would decrease to $-\infty$ except for the case where the DOAs $\varphi^{(k_{\mathrm{I}})}$ and $\varphi^{(1)}$ of the directional noise component and the desired signal, respectively, are identical with each other. In this case, i. e., when the desired and the noise signals impinge at the AP array from the same DOA, the SNR degradation $\delta_{n_{\mathrm{F}}}^{(k,\,k_{\mathrm{A}})}$ would be equal to 0 dB.

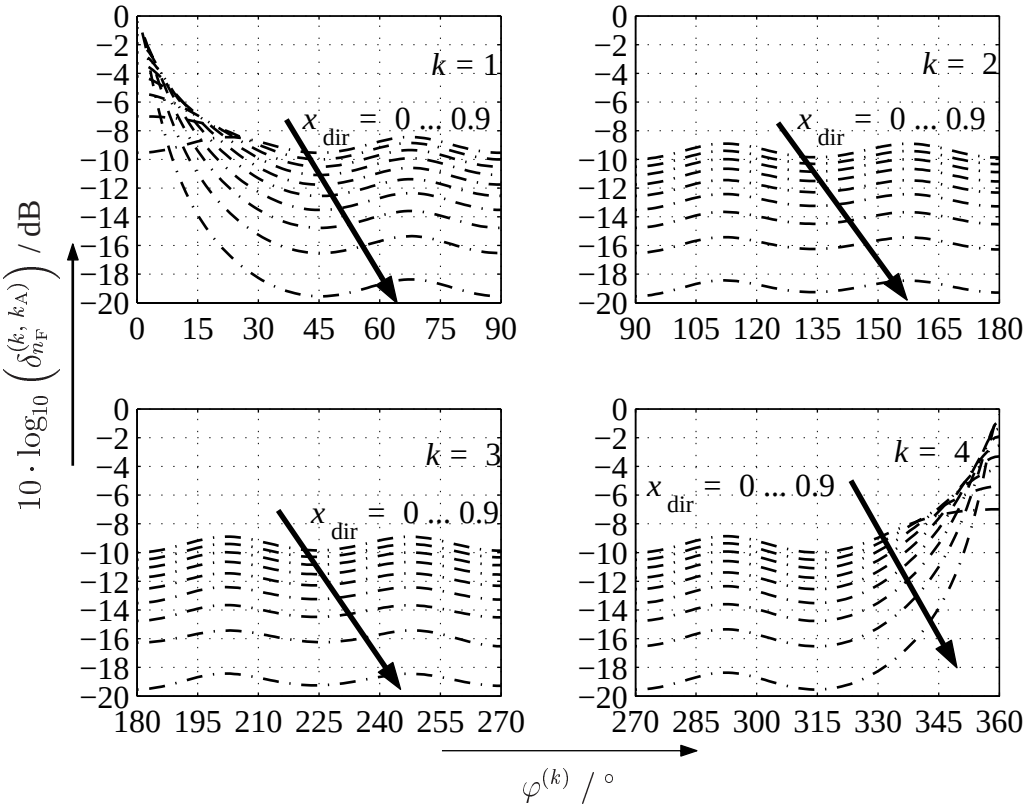

Fig. 6.10. SNR degradation $\delta_{n_\mathrm{F}}^{(k,\,k_\mathrm{A})}$ versus the MT-specific DOA $\varphi^{(k)}$, $k = 1 \ldots K$; $K_\mathrm{A} = 8$ antenna elements; mixed noise model, $\varphi^{(k_\mathrm{I})} = 0°$, $x_\mathrm{dir} = 0,\ 0.1,\ \ldots\ 0.9$

6.7 Minimum Mean Square Error JCE (MMSE–JCE)

So far in the thesis, the ML estimation principle [Wha71, Hay01] is applied for JCE. In order to apply ML–JCE, the number of unknown CTF values $\underline{\tilde{h}}_{n_\mathrm{F}}^{(k,\,k_\mathrm{A})}$ to be estimated needs to be reduced for both the single-element and the multi-element receive antenna cases, see Section 4.3 and Section 6.3. An alternative to the ML estimation principle is the minimum mean square error (MMSE) estimation principle [Wha71, Hay01]. Applying MMSE–JCE, said reduction is no longer necessary, because additional a-priori information about the mobile radio channel is included in the estimation process as presented in what follows.

The scenario of Fig. 6.1 with multi-element receive antennas is considered. The case of single-element receive antennas is included as a special case in the considerations. The a-priori information concerning the mobile radio channel described by the total CTF $\underline{\tilde{\mathbf{h}}}_\mathrm{tot}$ of (6.8) is contained in the total channel covariance matrix

$$\underline{\mathbf{R}}_{\tilde{\mathbf{h}}_\mathrm{tot}} = \mathrm{E}\left\{\underline{\tilde{\mathbf{h}}}_\mathrm{tot}\ \underline{\tilde{\mathbf{h}}}_\mathrm{tot}^\mathsf{H}\right\} \tag{6.46}$$

of dimension $(K_{\mathrm{A}}KN_{\mathrm{F}}) \times (K_{\mathrm{A}}KN_{\mathrm{F}})$. Applying the considerations and assumptions made in Section 6.3 for the exploitation of the directional properties of the radio channels between the MTs and the AP leading to (6.22), (6.46) is rewritten as [MWW03, MW03]

$$\begin{aligned} \underline{\mathbf{R}}_{\tilde{\mathbf{h}}_{\mathrm{tot}}} &= \mathrm{E}\left\{\left(\underline{\tilde{\mathbf{A}}}\,\underline{\tilde{\boldsymbol{\mathcal{F}}}}_{\mathrm{W}}\underline{\mathbf{h}}_{\mathrm{d}}\right)\left(\underline{\tilde{\mathbf{A}}}\,\underline{\tilde{\boldsymbol{\mathcal{F}}}}_{\mathrm{W}}\underline{\mathbf{h}}_{\mathrm{d}}\right)^{\mathsf{H}}\right\} \\ &= \underline{\tilde{\mathbf{A}}}\,\underline{\tilde{\boldsymbol{\mathcal{F}}}}_{\mathrm{W}}\underbrace{\mathrm{E}\left\{\underline{\mathbf{h}}_{\mathrm{d}}\,\underline{\mathbf{h}}_{\mathrm{d}}^{\mathsf{H}}\right\}}_{\underline{\mathbf{R}}_{\mathbf{h}_{\mathrm{d}}}}\underline{\tilde{\boldsymbol{\mathcal{F}}}}_{\mathrm{W}}^{\mathsf{H}}\underline{\tilde{\mathbf{A}}}^{\mathsf{H}}. \end{aligned} \tag{6.47}$$

The $(KW) \times (KW)$ matrix $\underline{\mathbf{R}}_{\mathbf{h}_{\mathrm{d}}}$ in (6.47) is the channel covariance matrix of the total directional CIR $\underline{\mathbf{h}}_{\mathrm{d}}$ of (6.20). $\underline{\mathbf{R}}_{\mathbf{h}_{\mathrm{d}}}$ is a diagonal matrix and contains the values of the power delay profile (PDP) of the considered channel model. It is seen from (6.47) that besides said information about the PDP, $\underline{\mathbf{R}}_{\tilde{\mathbf{h}}_{\mathrm{tot}}}$ also contains the directional information about the desired signals stacked in the total steering matrix $\underline{\tilde{\mathbf{A}}}$ of (6.17). With $\underline{\mathbf{R}}_{\tilde{\mathbf{h}}_{\mathrm{tot}}}$ of (6.47) and $\underline{\tilde{\mathbf{r}}}_{\mathrm{tot}}$ of (6.10) the biased estimate [Wha71, MWW03]

$$\begin{aligned} \hat{\underline{\tilde{\mathbf{h}}}}_{\mathrm{tot}} &= \underline{\mathbf{R}}_{\tilde{\mathbf{h}}_{\mathrm{tot}}}\,\underline{\tilde{\mathbf{P}}}_{\mathrm{tot}}^{\mathsf{H}}\left(\underline{\mathbf{R}}_{\tilde{\mathbf{n}}_{\mathrm{tot}}} + \underline{\tilde{\mathbf{P}}}_{\mathrm{tot}}\,\underline{\mathbf{R}}_{\tilde{\mathbf{h}}_{\mathrm{tot}}}\,\underline{\tilde{\mathbf{P}}}_{\mathrm{tot}}^{\mathsf{H}}\right)^{-1}\underline{\tilde{\mathbf{r}}}_{\mathrm{tot}} \\ &= \underbrace{\underbrace{\underline{\tilde{\mathbf{A}}}\,\underline{\tilde{\boldsymbol{\mathcal{F}}}}_{\mathrm{W}}\underbrace{\underline{\mathbf{R}}_{\mathbf{h}_{\mathrm{d}}}\underline{\tilde{\boldsymbol{\mathcal{G}}}}_{\mathrm{d}}^{\mathsf{H}}\left(\underline{\mathbf{R}}_{\tilde{\mathbf{n}}_{\mathrm{tot}}} + \underline{\tilde{\boldsymbol{\mathcal{G}}}}_{\mathrm{d}}\underline{\mathbf{R}}_{\mathbf{h}_{\mathrm{d}}}\underline{\tilde{\boldsymbol{\mathcal{G}}}}_{\mathrm{d}}^{\mathsf{H}}\right)^{-1}\underline{\tilde{\mathbf{r}}}_{\mathrm{tot}}}_{\hat{\underline{\mathbf{h}}}_{\mathrm{d}}\ \text{(MMSE estimator)}}}_{\hat{\hat{\underline{\mathbf{h}}}}_{\mathrm{d}}\ \text{(Fourier transformer)}}} \end{aligned} \tag{6.48}$$

of the total CTF $\underline{\tilde{\mathbf{h}}}_{\mathrm{tot}}$ of (6.8) is obtained at the output of MMSE–JCE. In analogy to the case of ML–JCE, the MMSE estimator of (6.48) applies the pilot vector knowledge, the directional information and the a-priori PDP information to gain the estimate $\hat{\underline{\mathbf{h}}}_{\mathrm{d}}$ of the total directional CIR $\underline{\mathbf{h}}_{\mathrm{d}}$ of (6.20). Then, the Fourier transformer is applied to deliver the estimate $\hat{\hat{\underline{\mathbf{h}}}}_{\mathrm{d}}$ of the total directional CTF $\underline{\tilde{\mathbf{h}}}_{\mathrm{d}}$ of (6.18). Finally, the directional information is once again invoked in the form of the total steering matrix $\underline{\tilde{\mathbf{A}}}$, and the CTF estimate $\hat{\hat{\underline{\mathbf{h}}}}_{\mathrm{tot}}$ of the total CTF $\underline{\tilde{\mathbf{h}}}_{\mathrm{tot}}$ of (6.8) is gained.

6.8 Simulations

In Section 6.6 the performance of ML–JCE is investigated with respect to the SNR degradations $\delta_{n_{\mathrm{F}}}^{(k,\,k_{\mathrm{A}})}$ defined in (6.42). In contrast to the ML estimate $\hat{\hat{\underline{\mathbf{h}}}}_{\mathrm{tot}}$ of (6.25), which is unbiased, the MMSE estimate $\hat{\hat{\underline{\mathbf{h}}}}_{\mathrm{tot}}$ of (6.48) is biased [Wha71, Kle96]. This means that in order to evaluate the performance of MMSE–JCE with respect to $\delta_{n_{\mathrm{F}}}^{(k,\,k_{\mathrm{A}})}$, we need to redefine $\delta_{n_{\mathrm{F}}}^{(k,\,k_{\mathrm{A}})}$ for the case of MMSE–JCE.

The MMSE estimator of (6.48) is represented by the $(K_{\mathrm{A}}KN_{\mathrm{F}}) \times (K_{\mathrm{A}}N_{\mathrm{F}})$ estimation matrix

$$\underline{\tilde{\mathbf{Z}}}_{\mathrm{d}} = \underline{\tilde{\mathbf{A}}}\, \underline{\tilde{\boldsymbol{\mathcal{F}}}}_{\mathrm{W}} \underline{\mathbf{R}}_{\mathbf{h}_{\mathrm{d}}} \underline{\tilde{\boldsymbol{\mathcal{G}}}}_{\mathrm{d}}^{\mathsf{H}} \left(\underline{\mathbf{R}}_{\tilde{\mathbf{n}}_{\mathrm{tot}}} + \underline{\tilde{\boldsymbol{\mathcal{G}}}}_{\mathrm{d}} \underline{\mathbf{R}}_{\mathbf{h}_{\mathrm{d}}} \underline{\tilde{\boldsymbol{\mathcal{G}}}}_{\mathrm{d}}^{\mathsf{H}} \right)^{-1}. \tag{6.49}$$

The part of $\underline{\tilde{\mathbf{Z}}}_{\mathrm{d}}$ yielding the estimate $\underline{\hat{\mathbf{h}}}_{\mathrm{d}}$ of the total directional CIR $\underline{\mathbf{h}}_{\mathrm{d}}$, see (6.48), can be alternatively expressed as a concatenation of a ML estimator and a Wiener estimator represented by the $(KW) \times (KW)$ matrix $\underline{\mathbf{W}}_{\mathbf{0}}$ [Kle96] leading to

$$\underline{\tilde{\mathbf{Z}}}_{\mathrm{d}} = \underline{\tilde{\mathbf{A}}}\, \underline{\tilde{\boldsymbol{\mathcal{F}}}}_{\mathrm{W}} \underbrace{\left(\mathbf{I}^{(KW \times KW)} + \left(\underline{\mathbf{R}}_{\mathbf{h}_{\mathrm{d}}} \underline{\tilde{\boldsymbol{\mathcal{G}}}}_{\mathrm{d}}^{\mathsf{H}} \underline{\mathbf{R}}_{\tilde{\mathbf{n}}_{\mathrm{tot}}}^{-1} \underline{\tilde{\boldsymbol{\mathcal{G}}}}_{\mathrm{d}} \right)^{-1} \right)^{-1}}_{\underline{\mathbf{W}}_{\mathbf{0}} \text{ (Wiener estimator)}} \underbrace{\left(\underline{\tilde{\boldsymbol{\mathcal{G}}}}_{\mathrm{d}}^{\mathsf{H}} \underline{\mathbf{R}}_{\tilde{\mathbf{n}}_{\mathrm{tot}}}^{-1} \underline{\tilde{\boldsymbol{\mathcal{G}}}}_{\mathrm{d}} \right)^{-1} \underline{\tilde{\boldsymbol{\mathcal{G}}}}_{\mathrm{d}}^{\mathsf{H}} \underline{\mathbf{R}}_{\tilde{\mathbf{n}}_{\mathrm{tot}}}^{-1}}_{\text{ML estimator}}. \tag{6.50}$$

The derivation of the matrix $\underline{\mathbf{W}}_{\mathbf{0}}$ in (6.50) is given in Appendix B.

As a consequence of the bias of the MMSE estimator, the CTF estimate $\underline{\hat{\tilde{\mathbf{h}}}}_{\mathrm{tot}}$ of (6.48) consists of three components [Kle96]:

- The true CTF (desired component),
- a MAI component, and
- the noise component.

Following this consideration and applying (6.50), (6.48) reads [Kle96]

$$\begin{aligned}
\underline{\hat{\tilde{\mathbf{h}}}}_{\mathrm{tot}} &= \underline{\tilde{\mathbf{A}}}\, \underline{\tilde{\boldsymbol{\mathcal{F}}}}_{\mathrm{W}} \underline{\mathbf{W}}_{\mathbf{0}} \left(\underline{\tilde{\boldsymbol{\mathcal{G}}}}_{\mathrm{d}}^{\mathsf{H}} \underline{\mathbf{R}}_{\tilde{\mathbf{n}}_{\mathrm{tot}}}^{-1} \underline{\tilde{\boldsymbol{\mathcal{G}}}}_{\mathrm{d}} \right)^{-1} \underline{\tilde{\boldsymbol{\mathcal{G}}}}_{\mathrm{d}}^{\mathsf{H}} \underline{\mathbf{R}}_{\tilde{\mathbf{n}}_{\mathrm{tot}}}^{-1} \underline{\tilde{\mathbf{r}}}_{\mathrm{tot}} \qquad (6.51) \\
&= \underline{\tilde{\mathbf{A}}}\, \underline{\tilde{\boldsymbol{\mathcal{F}}}}_{\mathrm{W}} \underline{\mathbf{W}}_{\mathbf{0}} \underline{\hat{\mathbf{h}}}_{\mathrm{d}} + \underline{\tilde{\mathbf{A}}}\, \underline{\tilde{\boldsymbol{\mathcal{F}}}}_{\mathrm{W}} \underline{\mathbf{W}}_{\mathbf{0}} \left(\underline{\tilde{\boldsymbol{\mathcal{G}}}}_{\mathrm{d}}^{\mathsf{H}} \underline{\mathbf{R}}_{\tilde{\mathbf{n}}_{\mathrm{tot}}}^{-1} \underline{\tilde{\boldsymbol{\mathcal{G}}}}_{\mathrm{d}} \right)^{-1} \underline{\tilde{\boldsymbol{\mathcal{G}}}}_{\mathrm{d}}^{\mathsf{H}} \underline{\mathbf{R}}_{\tilde{\mathbf{n}}_{\mathrm{tot}}}^{-1} \underline{\tilde{\mathbf{n}}}_{\mathrm{tot}} \\
&= \underbrace{\underline{\tilde{\mathbf{A}}}\, \underline{\tilde{\boldsymbol{\mathcal{F}}}}_{\mathrm{W}} \mathrm{diag}\left(\underline{\mathbf{W}}_{\mathbf{0}} \right) \underline{\mathbf{h}}_{\mathrm{d}}}_{\text{desired component}} + \underbrace{\underline{\tilde{\mathbf{A}}}\, \underline{\tilde{\boldsymbol{\mathcal{F}}}}_{\mathrm{W}} \left(\underline{\mathbf{W}}_{\mathbf{0}} - \mathrm{diag}\left(\underline{\mathbf{W}}_{\mathbf{0}} \right) \right) \underline{\mathbf{h}}_{\mathrm{d}}}_{\text{MAI component}} + \\
&\quad \underbrace{\underline{\tilde{\mathbf{A}}}\, \underline{\tilde{\boldsymbol{\mathcal{F}}}}_{\mathrm{W}} \underline{\mathbf{W}}_{\mathbf{0}} \left(\underline{\tilde{\boldsymbol{\mathcal{G}}}}_{\mathrm{d}}^{\mathsf{H}} \underline{\mathbf{R}}_{\tilde{\mathbf{n}}_{\mathrm{tot}}}^{-1} \underline{\tilde{\boldsymbol{\mathcal{G}}}}_{\mathrm{d}} \right)^{-1} \underline{\tilde{\boldsymbol{\mathcal{G}}}}_{\mathrm{d}}^{\mathsf{H}} \underline{\mathbf{R}}_{\tilde{\mathbf{n}}_{\mathrm{tot}}}^{-1} \underline{\tilde{\mathbf{n}}}_{\mathrm{tot}}}_{\text{noise component}},
\end{aligned}$$

where $\mathrm{diag}\left(\underline{\mathbf{W}}_{\mathbf{0}} \right)$ represents a diagonal matrix containing the elements of the main diagonal of the matrix $\underline{\mathbf{W}}_{\mathbf{0}}$. The SNR $\gamma_{n_{\mathrm{F}}}^{(k,k_{\mathrm{A}})}$ of the estimated CTF components $\underline{\hat{\tilde{h}}}_{n_{\mathrm{F}}}^{(k,k_{\mathrm{A}})}$ is given by the ratio of the desired energy $E_{n_{\mathrm{F}}}^{(k,k_{\mathrm{A}})}$ of the estimated CTF components $\underline{\hat{\tilde{h}}}_{n_{\mathrm{F}}}^{(k,k_{\mathrm{A}})}$ over the undesired energy $N_{n_{\mathrm{F}}}^{(k,k_{\mathrm{A}})}$, namely

$$\gamma_{n_{\mathrm{F}}}^{(k,k_{\mathrm{A}})} = \frac{E_{n_{\mathrm{F}}}^{(k,k_{\mathrm{A}})}}{N_{n_{\mathrm{F}}}^{(k,k_{\mathrm{A}})}}, \tag{6.52}$$

see also (4.35). Since MAI is also present in addition to noise, see (6.51), (6.52) can be written as

$$\gamma_{n_{\mathrm{F}}}^{(k,k_{\mathrm{A}})} = \frac{E_{n_{\mathrm{F}}}^{(k,k_{\mathrm{A}})}}{N_{\mathrm{MAI},n_{\mathrm{F}}}^{(k,k_{\mathrm{A}})} + N_{\mathrm{noise},n_{\mathrm{F}}}^{(k,k_{\mathrm{A}})}}. \tag{6.53}$$

Due to (6.53), we shall refer to $\gamma_{n_{\mathrm{F}}}^{(k,k_{\mathrm{A}})}$ in the following as the signal-to-noise-and-interference-ratio (SNIR) of the MMSE estimates. The desired energy $E_{n_{\mathrm{F}}}^{(k,k_{\mathrm{A}})}$ in (6.53) is obtained by

$$\begin{aligned} E_{n_{\mathrm{F}}}^{(k,k_{\mathrm{A}})} &= \left[\mathrm{E}\left\{\underline{\tilde{\mathbf{A}}}\,\underline{\tilde{\boldsymbol{\mathcal{F}}}}_{\mathrm{W}}\mathrm{diag}\left(\underline{\mathbf{W_0}}\right)\underline{\mathbf{h}}_{\mathrm{d}}\cdot\underline{\mathbf{h}}_{\mathrm{d}}^{\mathsf{H}}\mathrm{diag}\left(\underline{\mathbf{W_0}}^{\mathsf{H}}\right)\underline{\tilde{\boldsymbol{\mathcal{F}}}}_{\mathrm{W}}^{\mathsf{H}}\underline{\tilde{\mathbf{A}}}^{\mathsf{H}}\right\}\right]_{i,i} \\ &= \left[\underline{\tilde{\mathbf{A}}}\,\underline{\tilde{\boldsymbol{\mathcal{F}}}}_{\mathrm{W}}\mathrm{diag}\left(\underline{\mathbf{W_0}}\right)\mathrm{E}\left\{\underline{\mathbf{h}}_{\mathrm{d}}\cdot\underline{\mathbf{h}}_{\mathrm{d}}^{\mathsf{H}}\right\}\mathrm{diag}\left(\underline{\mathbf{W_0}}^{\mathsf{H}}\right)\underline{\tilde{\boldsymbol{\mathcal{F}}}}_{\mathrm{W}}^{\mathsf{H}}\underline{\tilde{\mathbf{A}}}^{\mathsf{H}}\right]_{i,i} \\ &= \left[\underline{\tilde{\mathbf{A}}}\,\underline{\tilde{\boldsymbol{\mathcal{F}}}}_{\mathrm{W}}\mathrm{diag}\left(\underline{\mathbf{W_0}}\right)\underline{\mathbf{R}}_{\mathbf{h}_{\mathrm{d}}}\mathrm{diag}\left(\underline{\mathbf{W_0}}^{\mathsf{H}}\right)\underline{\tilde{\boldsymbol{\mathcal{F}}}}_{\mathrm{W}}^{\mathsf{H}}\underline{\tilde{\mathbf{A}}}^{\mathsf{H}}\right]_{i,i}, \end{aligned} \tag{6.54}$$

$$\begin{aligned} &i = (k_{\mathrm{A}}-1)KN_{\mathrm{F}} + (k-1)N_{\mathrm{F}} + n_{\mathrm{F}},\ k_{\mathrm{A}} = 1\ \ldots\ K_{\mathrm{A}}, \\ &k = 1\ \ldots\ K,\ n_{\mathrm{F}} = 1\ldots N_{\mathrm{F}}. \end{aligned}$$

The undesired energy part originating in MAI is given by

$$\begin{aligned} N_{\mathrm{MAI},n_{\mathrm{F}}}^{(k,k_{\mathrm{A}})} &= \left[\mathrm{E}\left\{\underline{\tilde{\mathbf{A}}}\,\underline{\tilde{\boldsymbol{\mathcal{F}}}}_{\mathrm{W}}\left(\underline{\mathbf{W_0}} - \mathrm{diag}\left(\underline{\mathbf{W_0}}\right)\right)\underline{\mathbf{h}}_{\mathrm{d}}\cdot\underline{\mathbf{h}}_{\mathrm{d}}^{\mathsf{H}}\left(\underline{\mathbf{W_0}} - \mathrm{diag}\left(\underline{\mathbf{W_0}}\right)\right)^{\mathsf{H}}\underline{\tilde{\boldsymbol{\mathcal{F}}}}_{\mathrm{W}}^{\mathsf{H}}\underline{\tilde{\mathbf{A}}}^{\mathsf{H}}\right\}\right]_{i,i} \\ &= \left[\underline{\tilde{\mathbf{A}}}\,\underline{\tilde{\boldsymbol{\mathcal{F}}}}_{\mathrm{W}}\left(\underline{\mathbf{W_0}} - \mathrm{diag}\left(\underline{\mathbf{W_0}}\right)\right)\underline{\mathbf{R}}_{\mathbf{h}_{\mathrm{d}}}\left(\underline{\mathbf{W_0}} - \mathrm{diag}\left(\underline{\mathbf{W_0}}\right)\right)^{\mathsf{H}}\underline{\tilde{\boldsymbol{\mathcal{F}}}}_{\mathrm{W}}^{\mathsf{H}}\underline{\tilde{\mathbf{A}}}^{\mathsf{H}}\right]_{i,i}, \end{aligned} \tag{6.55}$$

$$\begin{aligned} &i = (k_{\mathrm{A}}-1)KN_{\mathrm{F}} + (k-1)N_{\mathrm{F}} + n_{\mathrm{F}},\ k_{\mathrm{A}} = 1\ \ldots\ K_{\mathrm{A}}, \\ &k = 1\ \ldots\ K,\ n_{\mathrm{F}} = 1\ldots N_{\mathrm{F}}, \end{aligned}$$

and the undesired energy originating in noise is obtained by

$$\begin{aligned} N_{\mathrm{noise},n_{\mathrm{F}}}^{(k,k_{\mathrm{A}})} &= \Bigg[\mathrm{E}\Bigg\{\underline{\tilde{\mathbf{A}}}\,\underline{\tilde{\boldsymbol{\mathcal{F}}}}_{\mathrm{W}}\underline{\mathbf{W_0}}\left(\underline{\tilde{\boldsymbol{\mathcal{G}}}}_{\mathrm{d}}^{\mathsf{H}}\underline{\mathbf{R}}_{\tilde{\mathbf{n}}_{\mathrm{tot}}}^{-1}\underline{\tilde{\boldsymbol{\mathcal{G}}}}_{\mathrm{d}}\right)^{-1}\underline{\tilde{\boldsymbol{\mathcal{G}}}}_{\mathrm{d}}^{\mathsf{H}}\underline{\mathbf{R}}_{\tilde{\mathbf{n}}_{\mathrm{tot}}}^{-1}\,\underline{\tilde{\mathbf{n}}}_{\mathrm{tot}}\cdot \\ &\qquad \underline{\tilde{\mathbf{n}}}_{\mathrm{tot}}^{\mathsf{H}}\underline{\mathbf{R}}_{\tilde{\mathbf{n}}_{\mathrm{tot}}}^{-1}\underline{\tilde{\boldsymbol{\mathcal{G}}}}_{\mathrm{d}}\left(\underline{\tilde{\boldsymbol{\mathcal{G}}}}_{\mathrm{d}}^{\mathsf{H}}\underline{\mathbf{R}}_{\tilde{\mathbf{n}}_{\mathrm{tot}}}^{-1}\underline{\tilde{\boldsymbol{\mathcal{G}}}}_{\mathrm{d}}\right)^{-1}\underline{\mathbf{W}}_0^{\mathsf{H}}\underline{\tilde{\boldsymbol{\mathcal{F}}}}_{\mathrm{W}}^{\mathsf{H}}\underline{\tilde{\mathbf{A}}}^{\mathsf{H}}\Bigg\}\Bigg]_{i,i} \end{aligned} \tag{6.56}$$

$$\begin{aligned} &= \Bigg[\underline{\tilde{\mathbf{A}}}\,\underline{\tilde{\boldsymbol{\mathcal{F}}}}_{\mathrm{W}}\underline{\mathbf{W}}_0\left(\underline{\tilde{\boldsymbol{\mathcal{G}}}}_{\mathrm{d}}^{\mathsf{H}}\underline{\mathbf{R}}_{\tilde{\mathbf{n}}_{\mathrm{tot}}}^{-1}\underline{\tilde{\boldsymbol{\mathcal{G}}}}_{\mathrm{d}}\right)^{-1}\underline{\tilde{\boldsymbol{\mathcal{G}}}}_{\mathrm{d}}^{\mathsf{H}}\underline{\mathbf{R}}_{\tilde{\mathbf{n}}_{\mathrm{tot}}}^{-1}\underline{\mathbf{R}}_{\tilde{\mathbf{n}}}\underline{\mathbf{R}}_{\tilde{\mathbf{n}}_{\mathrm{tot}}}^{-1}\underline{\tilde{\boldsymbol{\mathcal{G}}}}_{\mathrm{d}} \\ &\qquad \left(\underline{\tilde{\boldsymbol{\mathcal{G}}}}_{\mathrm{d}}^{\mathsf{H}}\underline{\mathbf{R}}_{\tilde{\mathbf{n}}_{\mathrm{tot}}}^{-1}\underline{\tilde{\boldsymbol{\mathcal{G}}}}_{\mathrm{d}}\right)^{-1}\underline{\mathbf{W}}_0^{\mathsf{H}}\underline{\tilde{\boldsymbol{\mathcal{F}}}}_{\mathrm{W}}^{\mathsf{H}}\underline{\tilde{\mathbf{A}}}^{\mathsf{H}}\Bigg]_{i,i} \end{aligned} \tag{6.57}$$

$$= \left[\underline{\tilde{\mathbf{A}}}\,\underline{\tilde{\boldsymbol{\mathcal{F}}}}_{\mathrm{W}}\underline{\mathbf{W_0}}\left(\underline{\tilde{\boldsymbol{\mathcal{G}}}}_{\mathrm{d}}^{\mathsf{H}}\underline{\mathbf{R}}_{\tilde{\mathbf{n}}_{\mathrm{tot}}}^{-1}\underline{\tilde{\boldsymbol{\mathcal{G}}}}_{\mathrm{d}}\right)^{-1}\underline{\mathbf{W}}_0^{\mathsf{H}}\underline{\tilde{\boldsymbol{\mathcal{F}}}}_{\mathrm{W}}^{\mathsf{H}}\underline{\tilde{\mathbf{A}}}^{\mathsf{H}}\right]_{i,i},$$

$$i = (k_{\mathrm{A}}-1)KN_{\mathrm{F}} + (k-1)N_{\mathrm{F}} + n_{\mathrm{F}},\ k_{\mathrm{A}} = 1\ \ldots\ K_{\mathrm{A}},$$
$$k = 1\ \ldots\ K,\ n_{\mathrm{F}} = 1\ldots N_{\mathrm{F}}.$$

Now, substituting (6.54), (6.55) and (6.56) in (6.53) leads to

$$\gamma_{n_{\mathrm{F}}}^{(k,k_{\mathrm{A}})} = \frac{\left[\underline{\tilde{\mathbf{A}}}\,\underline{\tilde{\boldsymbol{\mathcal{F}}}}_{\mathrm{W}}\mathrm{diag}\left(\underline{\mathbf{W_0}}\right)\underline{\mathbf{R}}_{\mathbf{h}_{\mathrm{d}}}\mathrm{diag}\left(\underline{\mathbf{W_0}}^{\mathsf{H}}\right)\underline{\tilde{\boldsymbol{\mathcal{F}}}}_{\mathrm{W}}^{\mathsf{H}}\underline{\tilde{\mathbf{A}}}^{\mathsf{H}}\right]_{i,i}}{\left[\underline{\tilde{\mathbf{A}}}\,\underline{\tilde{\boldsymbol{\mathcal{F}}}}_{\mathrm{W}}\left(\underline{\mathbf{W_0}} - \mathrm{diag}\left(\underline{\mathbf{W_0}}\right)\right)\underline{\mathbf{R}}_{\mathbf{h}_{\mathrm{d}}}\left(\underline{\mathbf{W_0}} - \mathrm{diag}\left(\underline{\mathbf{W_0}}\right)\right)^{\mathsf{H}}\underline{\tilde{\boldsymbol{\mathcal{F}}}}_{\mathrm{W}}^{\mathsf{H}}\underline{\tilde{\mathbf{A}}}^{\mathsf{H}}\right]_{i,i} + \overline{\left[\underline{\tilde{\mathbf{A}}}\,\underline{\tilde{\boldsymbol{\mathcal{F}}}}_{\mathrm{W}}\underline{\mathbf{W_0}}\left(\underline{\tilde{\boldsymbol{\mathcal{G}}}}_{\mathrm{d}}^{\mathsf{H}}\underline{\mathbf{R}}_{\tilde{\mathbf{n}}_{\mathrm{tot}}}^{-1}\underline{\tilde{\boldsymbol{\mathcal{G}}}}_{\mathrm{d}}\right)^{-1}\underline{\mathbf{W}}_0^{\mathsf{H}}\underline{\tilde{\boldsymbol{\mathcal{F}}}}_{\mathrm{W}}^{\mathsf{H}}\underline{\tilde{\mathbf{A}}}^{\mathsf{H}}\right]_{i,i}}}, \tag{6.58}$$

$$i = (k_{\mathrm{A}}-1)KN_{\mathrm{F}} + (k-1)N_{\mathrm{F}} + n_{\mathrm{F}},\ k_{\mathrm{A}} = 1\ \ldots\ K_{\mathrm{A}},$$
$$k = 1\ \ldots\ K,\ n_{\mathrm{F}} = 1\ldots N_{\mathrm{F}}.$$

Comparing the SNIR $\gamma_{n_{\mathrm{F}}}^{(k,k_{\mathrm{A}})}$ of (6.58) with the maximum SNR $\gamma_{\mathrm{max},n_{\mathrm{F}}}^{(k)}$ of (4.41) leads to the SNIR degradation

$$\delta_{n_{\mathrm{F}}}^{(k,\,k_{\mathrm{A}})} = \frac{\gamma_{\mathrm{max},n_{\mathrm{F}}}^{(k)}}{\gamma_{n_{\mathrm{F}}}^{(k,k_{\mathrm{A}})}} = \gamma_{\mathrm{max},n_{\mathrm{F}}}^{(k)} \cdot \frac{\left[\underline{\tilde{\mathbf{A}}}\,\underline{\tilde{\boldsymbol{\mathcal{F}}}}_{\mathrm{W}}\mathrm{diag}\left(\underline{\mathbf{W_0}}\right)\underline{\mathbf{R}}_{\mathbf{h}_{\mathrm{d}}}\mathrm{diag}\left(\underline{\mathbf{W_0}}^{\mathsf{H}}\right)\underline{\tilde{\boldsymbol{\mathcal{F}}}}_{\mathrm{W}}^{\mathsf{H}}\underline{\tilde{\mathbf{A}}}^{\mathsf{H}}\right]_{i,i}}{\left[\underline{\tilde{\mathbf{A}}}\,\underline{\tilde{\boldsymbol{\mathcal{F}}}}_{\mathrm{W}}\left(\underline{\mathbf{W_0}} - \mathrm{diag}\left(\underline{\mathbf{W_0}}\right)\right)\underline{\mathbf{R}}_{\mathbf{h}_{\mathrm{d}}}\left(\underline{\mathbf{W_0}} - \mathrm{diag}\left(\underline{\mathbf{W_0}}\right)\right)^{\mathsf{H}}\underline{\tilde{\boldsymbol{\mathcal{F}}}}_{\mathrm{W}}^{\mathsf{H}}\underline{\tilde{\mathbf{A}}}^{\mathsf{H}}\right]_{i,i} + \overline{\left[\underline{\tilde{\mathbf{A}}}\,\underline{\tilde{\boldsymbol{\mathcal{F}}}}_{\mathrm{W}}\underline{\mathbf{W_0}}\left(\underline{\tilde{\boldsymbol{\mathcal{G}}}}_{\mathrm{d}}^{\mathsf{H}}\underline{\mathbf{R}}_{\tilde{\mathbf{n}}_{\mathrm{tot}}}^{-1}\underline{\tilde{\boldsymbol{\mathcal{G}}}}_{\mathrm{d}}\right)^{-1}\underline{\mathbf{W}}_0^{\mathsf{H}}\underline{\tilde{\boldsymbol{\mathcal{F}}}}_{\mathrm{W}}^{\mathsf{H}}\underline{\tilde{\mathbf{A}}}^{\mathsf{H}}\right]_{i,i}}},$$

$$i = (k-1)K_{\mathrm{A}}N_{\mathrm{F}} + (k_{\mathrm{A}}-1)N_{\mathrm{F}} + n_{\mathrm{F}}, \tag{6.59}$$
$$k = 1\ \ldots\ K,\ k_{\mathrm{A}} = 1\ \ldots\ K_{\mathrm{A}},\ n_{\mathrm{F}} = 1\ldots N_{\mathrm{F}},$$

for the case of MMSE–JCE. As compared to $\delta_{n_{\mathrm{F}}}^{(k,\,k_{\mathrm{A}})}$ of (6.42) valid for the case of ML–JCE, $\delta_{n_{\mathrm{F}}}^{(k,\,k_{\mathrm{A}})}$ of (6.59) additionally depends on the total noise power σ^2, which is present in the total noise covariance matrix $\underline{\mathbf{R}}_{\tilde{\mathbf{n}}_{\mathrm{tot}}}$, in the matrix $\underline{\mathbf{W_0}}$ and in the maximum SNR $\gamma_{\mathrm{max},n_{\mathrm{F}}}^{(k)}$ of (4.41). Further, the PDP of the considered mobile radio channel included in the channel covariance matrix $\underline{\mathbf{R}}_{\mathbf{h}_{\mathrm{d}}}$ has an impact on $\delta_{n_{\mathrm{F}}}^{(k,\,k_{\mathrm{A}})}$ of (6.59).

Accurate knowledge concerning the PDP of the mobile radio channel is hard to obtain in reality. One way to get it consists in observing the mobile radio channel for a period of time

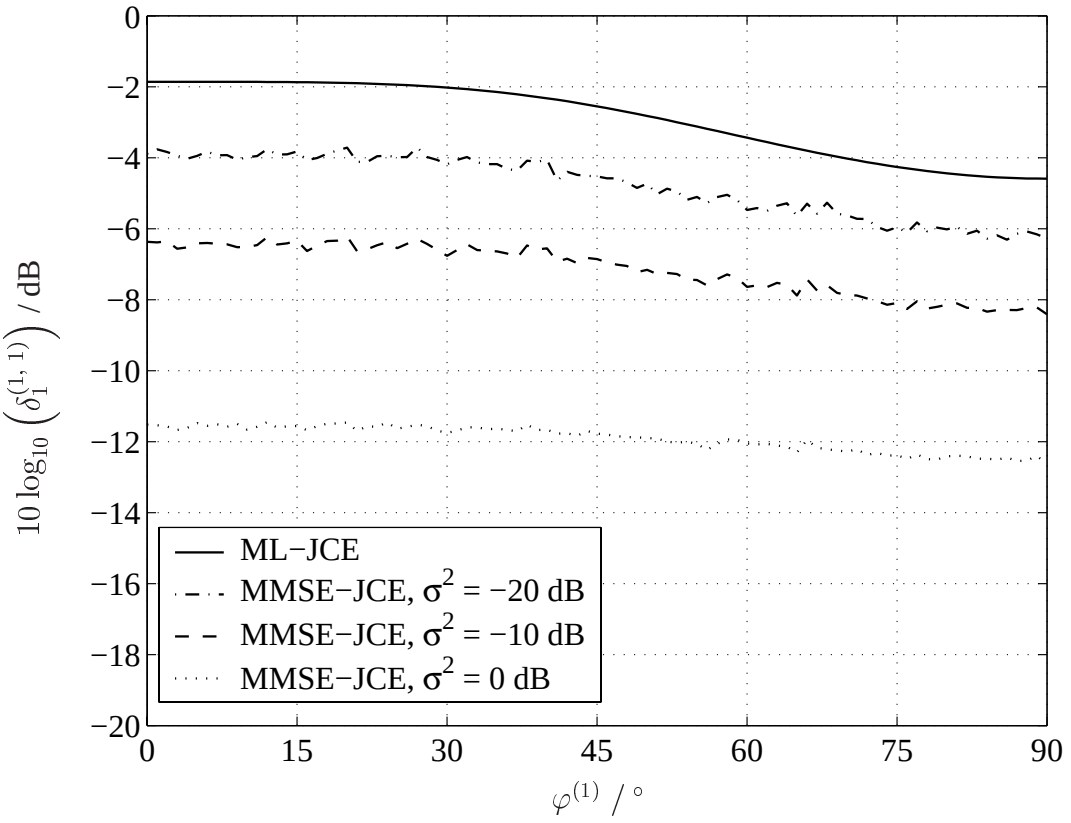

Fig. 6.11. SNIR degradation $\delta_1^{(1,\,1)}$ of MT one versus the MT-specific DOA $\varphi^{(1)}$ for MMSE–JCE; $K_{\mathrm{A}} = 2$ antenna elements; omnidirectional noise model, $\sigma^2 = 0,\ -10,\ -20$ dB

and then building the channel covariance matrix $\underline{\mathbf{R}}_{\tilde{\mathbf{h}}_{\mathrm{tot}}}$ applying the expectation operation over all observations, as seen in (6.46), (6.47) and (6.54). However, forming the expectation would require an infinitely long observation time period, which cannot be met in real mobile radio applications. In the simulations conducted in order to evaluate the MMSE–JCE performance, the PDP included in the estimation process by the channel covariance matrix $\underline{\mathbf{R}}_{\mathbf{h}_{\mathrm{d}}}$ of the total directional CIR $\underline{\mathbf{h}}_{\mathrm{d}}$, see (6.47), is assumed to be perfectly at hand at the CU. The COST 207 RA channel model [COS89] is adopted, and a MT-velocity v equal to 50 km/h is considered. Further, the simulation scenarios depicted in Fig. 6.5 are considered. As in the case of ML–JCE, the pilot vectors based on Walsh codes, see Section 5.5, are applied by the MTs of the SA under investigation. The case of full system load with the parameter triplet

$$\{N_{\mathrm{F}},\ K,\ W\} = \{128,\ 4,\ 32\} \tag{6.60}$$

is considered.

Figs. 6.11, 6.12 and 6.13 show the simulation results obtained for the omnidirectional noise scenario of Fig. 6.5a for the cases of two, four and eight antenna elements at the AP array. The SNIR degradation $\delta_1^{(1,\,1)}$ of (6.59) of MT one for subcarrier $n_{\mathrm{F}} = 1$ and array antenna element $k_{\mathrm{A}} = 1$ is plotted versus the MT-specific DOA $\varphi^{(1)}$ of (6.41). Three different curves

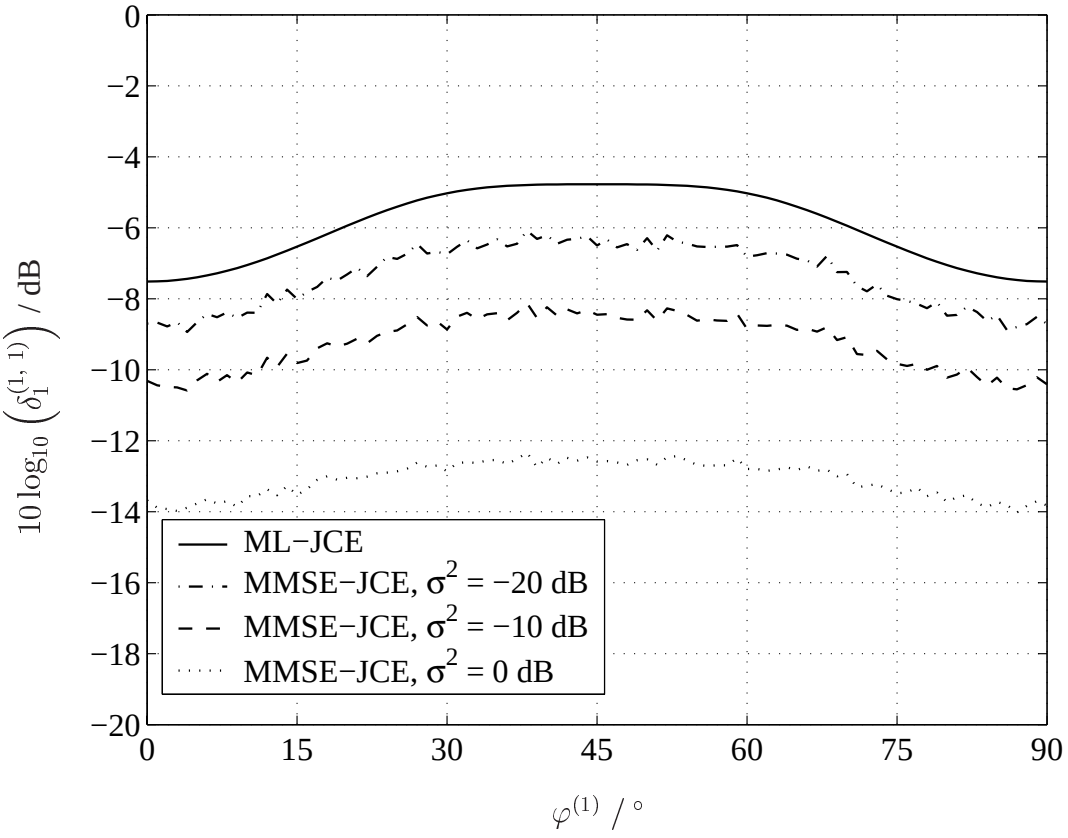

Fig. 6.12. SNIR degradation $\delta_1^{(1,\,1)}$ of MT one versus the MT-specific $\varphi^{(1)}$ for MMSE–JCE; $K_{\mathrm{A}} = 4$ antenna elements; omnidirectional noise model, $\sigma^2 = 0,\ -10,\ -20$ dB

for MMSE–JCE are shown in Figs. 6.11 till 6.13 corresponding to the values

$$\sigma^2/\mathrm{dB} = 0,\ -10,\ -20 \tag{6.61}$$

of the total noise power σ^2. For the purpose of comparison, the respective curves of $\delta_1^{(1,\,1)}$ of (6.42) for the ML–JCE performance, which are independent of the total noise power σ^2, see Section 6.6, are plotted in Figs. 6.11, 6.12 and 6.13 as well. For all numbers K_{A} of antenna elements at the AP array, MMSE–JCE outperforms ML–JCE in the considered scenario. Although both estimators include directional information about the desired signals and the noise signals in the estimation process, MMSE–JCE experiences better performance due to the additionally exploited PDP information contained in the channel covariance matrix $\underline{\mathbf{R}}_{\mathbf{h}_{\mathrm{d}}}$, see (6.48). Figs. 6.11, 6.12 and 6.13 also show that with decreasing total noise power σ^2, the performance of MMSE–JCE converges to the performance of ML–JCE. The randomness of the included radio channel, which in general influences the SNIR degradations $\delta_{n_{\mathrm{F}}}^{(k,\,k_{\mathrm{A}})}$ of (6.59), becomes obvious in the shape of the illustrated MMSE–JCE performance curves, which are not as smooth as in the case of ML–JCE.

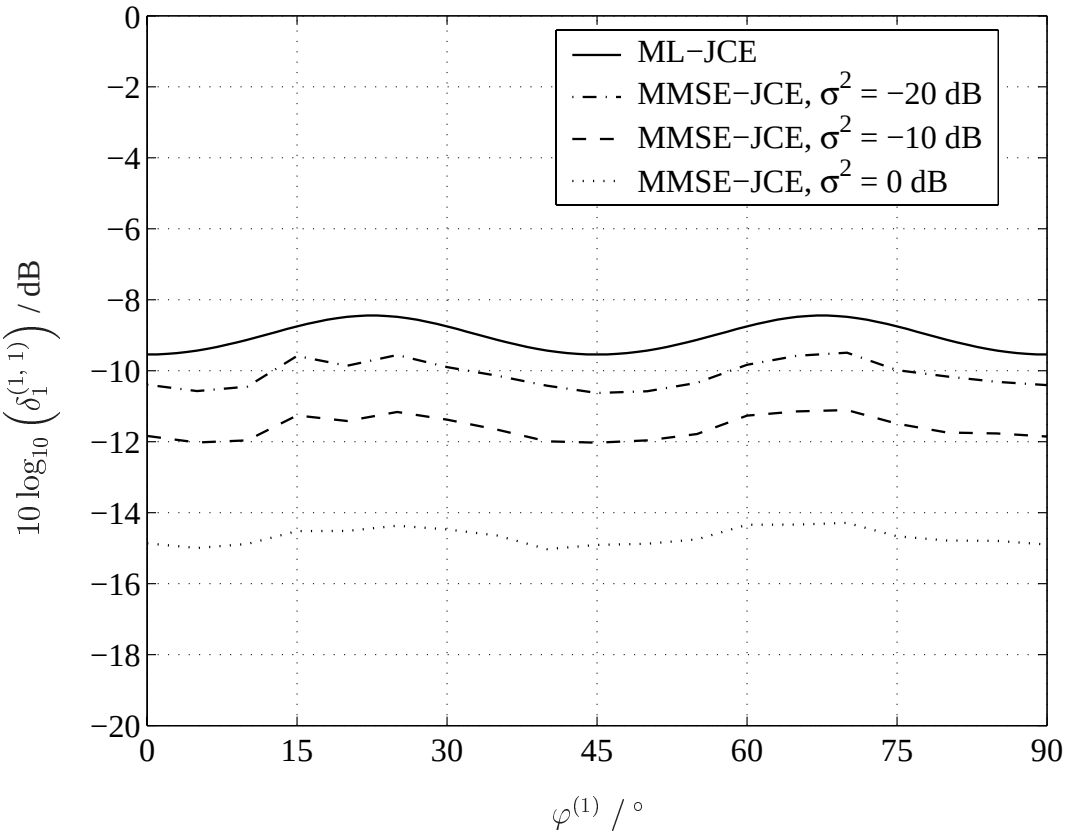

Fig. 6.13. SNIR degradation $\delta_1^{(1,\,1)}$ of MT one versus the MT-specific $\varphi^{(1)}$ for MMSE–JCE; $K_{\mathrm{A}} = 8$ antenna elements; omnidirectional noise model, $\sigma^2 = 0,\ -10,\ -20$ dB

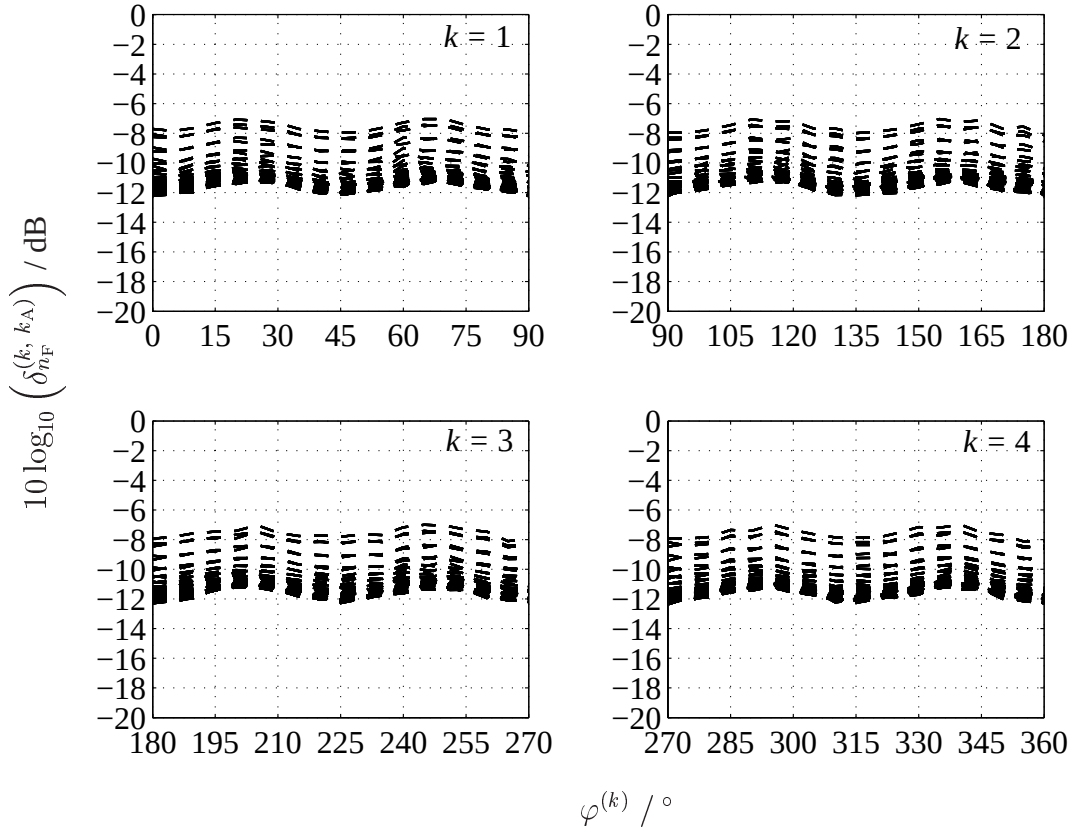

Fig. 6.14. SNIR degradation $\delta_{n_{\mathrm{F}}}^{(k,\,k_{\mathrm{A}})}$ versus the MT-specific DOA $\varphi^{(k)}$, $k = 1 \ \ldots \ K$, for MMSE–JCE; $K_{\mathrm{A}} = 8$ antenna elements; omnidirectional noise model, $\sigma^2 = -10$ dB

In order to gain a quantitative impression about the SNIR degradation of all four MTs of the scenario in Fig. 6.5a, all $K_{\mathrm{A}}KN_{\mathrm{F}}$ curves of the SNIR degradations $\delta_{n_{\mathrm{F}}}^{(k,\,k_{\mathrm{A}})}$ of (6.59) are plotted in Fig. 6.14 versus the MT-specific DOA $\varphi^{(k)}$ of (6.41). In Fig. 6.14, the total noise power σ^2 and the number K_{A} of AP array antenna elements are equal to -10 dB and eight, respectively. The influence of the included channel state information on the performance of MMSE–JCE, see (6.59), becomes obvious in Fig. 6.14, where the fluctuating SNIR degradations $\delta_{n_{\mathrm{F}}}^{(k,\,k_{\mathrm{A}})}$ take values between -8 dB and -12 dB, in contrast to the case of ML–JCE in the considered omnidirectional noise scenario, where the values of $\delta_{n_{\mathrm{F}}}^{(k,\,k_{\mathrm{A}})}$ are the same for all MTs, all subcarriers and all antenna elements.

Figs. 6.15 till 6.22 show the results obtained for the SNIR degradations $\delta_{n_{\mathrm{F}}}^{(k,\,k_{\mathrm{A}})}$ of (6.59) in the case of the mixed noise scenario of Fig. 6.5b. As in the simulations conducted for ML–JCE, see Section 6.6, the directional noise component contributes 80% to the total noise power σ^2 of (6.35), and the remaining 20% originate in the omnidirectional noise component. Further, the parameter triplet of (6.60) is considered. In the curves displayed in Figs. 6.15, 6.16 and 6.17, where the SNIR degradation $\delta_1^{(1,\,1)}$ of MT one is displayed, the DOA $\varphi^{(k_{\mathrm{I}})}$ of the directional noise component is set equal to 0°, and the number K_{A} of array antenna elements is chosen equal to two, four and eight, respectively. In the curves in Figs. 6.19, 6.20 and 6.21, the DOA $\varphi^{(k_{\mathrm{I}})}$ of the directional noise component is set equal to 30°, and again the number K_{A} of array antenna elements is chosen equal to two, four and eight, respectively. The total noise power σ^2 takes the values given in (6.61).

Similarly to the omnidirectional noise case, MMSE–JCE outperforms ML–JCE due to the additional information about the PDP of the mobile radio channel included in the estimation process. It is observed that the performance improvement suffers whenever the MT-specific DOA $\varphi^{(1)}$ and the DOA $\varphi^{(k_{\mathrm{I}})}$ of the directional noise component are close to or identical with each other. This is shown in Fig. 6.18, where all $K_{\mathrm{A}}KN_{\mathrm{F}}$ SNIR degradations $\delta_{n_{\mathrm{F}}}^{(k,\,k_{\mathrm{A}})}$ of (6.59) are plotted for $K_{\mathrm{A}} = 8$ array antenna elements, the total noise power $\sigma^2 = -10$ dB and the DOA $\varphi^{(k_{\mathrm{I}})} = 0^\circ$ of the directional noise component.

Finally, the influence of the composition of the total noise power σ^2 on the performance of MMSE–JCE is illustrated in Fig. 6.22 for the total noise power σ^2 equal to -10 dB and the DOA $\varphi^{(k_{\mathrm{I}})}$ of the directional noise component equal to 0°. As in the case of ML–JCE, see Fig. 6.10, the fraction x_{dir} of the contribution of the directional noise component to the total noise power σ^2 is varied in the interval $[0\ 0.9]$ in steps of 0.1. The run of the SNIR degradation value $\delta_1^{(k,1)}$ for MT k, $k = 1\ \ldots\ K$, at antenna element $k_{\mathrm{A}} = 1$ and on subcarrier $n_{\mathrm{F}} = 1$ is plotted versus the MT-specific DOA $\varphi^{(k)}$, $k = 1\ \ldots\ K$. MMSE–JCE exhibits an analog behavior to ML–JCE, where the SNIR degradation $\delta_1^{(k,1)}$ decreases further with an increasing x_{dir}. The same behavior was observed by the author for all $K_{\mathrm{A}}KN_{\mathrm{F}}$ SNIR degradation values $\delta_{n_{\mathrm{F}}}^{(k,\,k_{\mathrm{A}})}$.

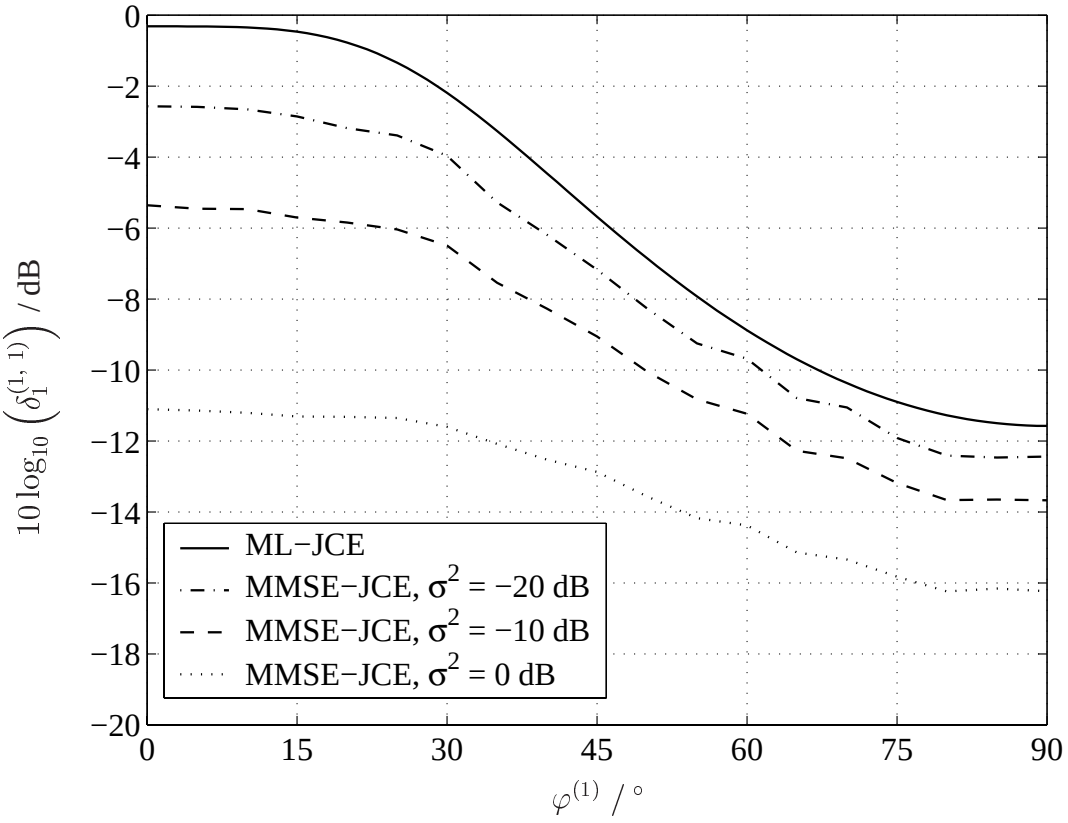

Fig. 6.15. SNIR degradation $\delta_1^{(1,\,1)}$ of MT one versus the MT-specific $\varphi^{(1)}$ for MMSE–JCE; $K_{\mathrm{A}} = 2$ antenna elements; mixed noise model, $\sigma^2 = 0,\ -10,\ -20$ dB, $\varphi^{(k_{\mathrm{I}})} = 0°$

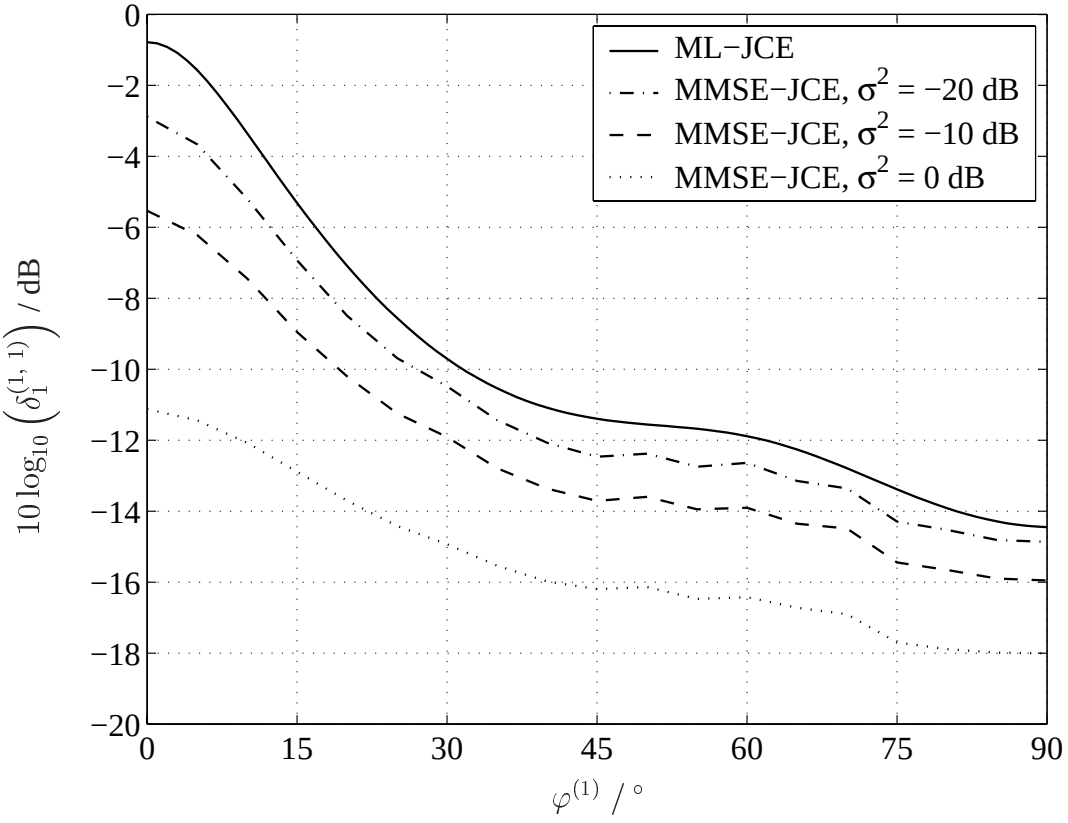

Fig. 6.16. SNIR degradation $\delta_1^{(1,\,1)}$ of MT one versus the MT-specific $\varphi^{(1)}$ for MMSE–JCE; $K_{\mathrm{A}} = 4$ antenna elements; mixed noise model, $\sigma^2 = 0,\ -10,\ -20$ dB, $\varphi^{(k_{\mathrm{I}})} = 0°$

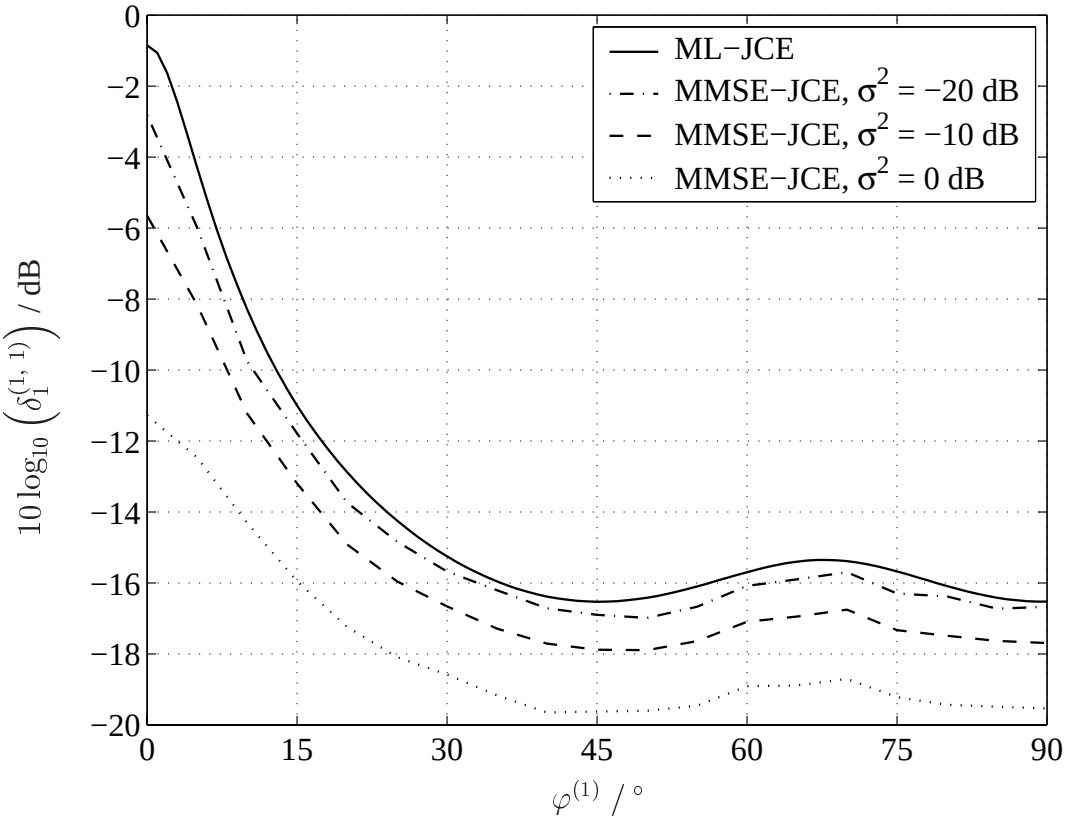

Fig. 6.17. SNIR degradation $\delta_1^{(1,\,1)}$ of MT one versus the MT-specific $\varphi^{(1)}$ for MMSE–JCE; $K_{\mathrm{A}} = 8$ antenna elements; mixed noise model, $\sigma^2 = 0,\ -10,\ -20$ dB, $\varphi^{(k_{\mathrm{I}})} = 0°$

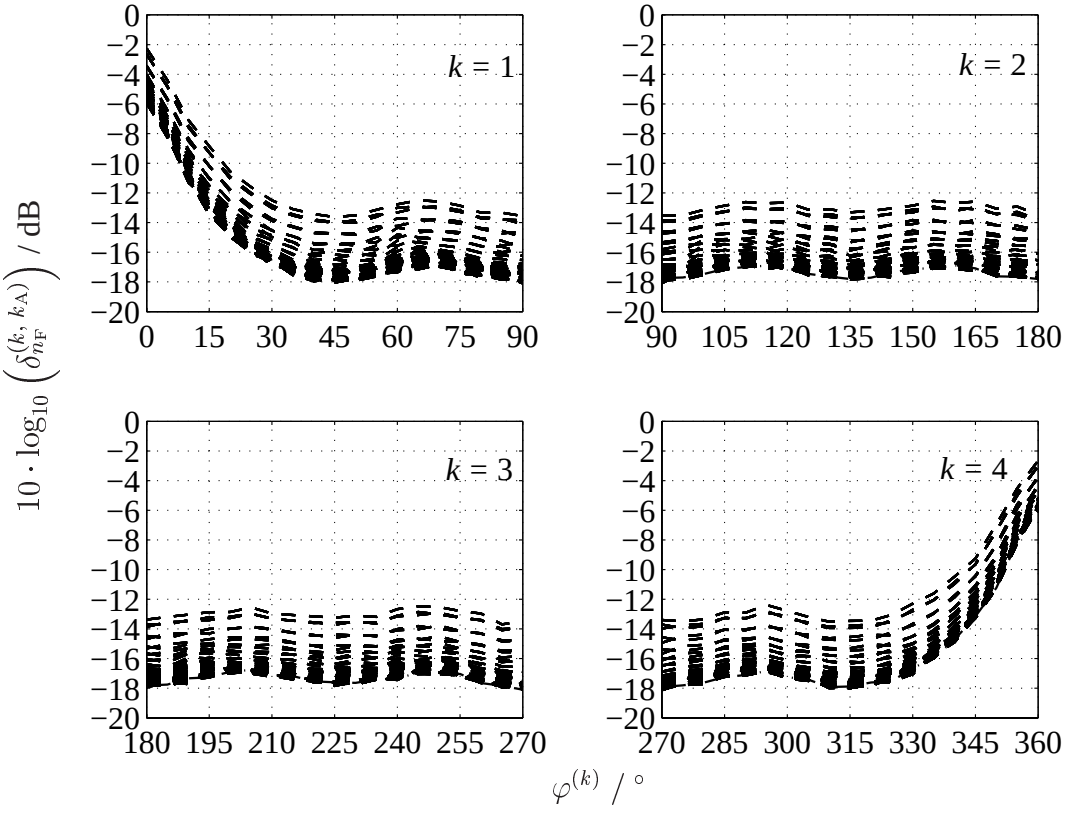

Fig. 6.18. SNIR degradation $\delta_1^{(1,\,1)}$ versus the MT-specific DOA $\varphi^{(k)}$, $k = 1\ \ldots\ K$, for MMSE–JCE; $K_{\mathrm{A}} = 8$; mixed noise model, $\sigma^2 = -10$ dB, $\varphi^{(k_{\mathrm{I}})} = 0°$

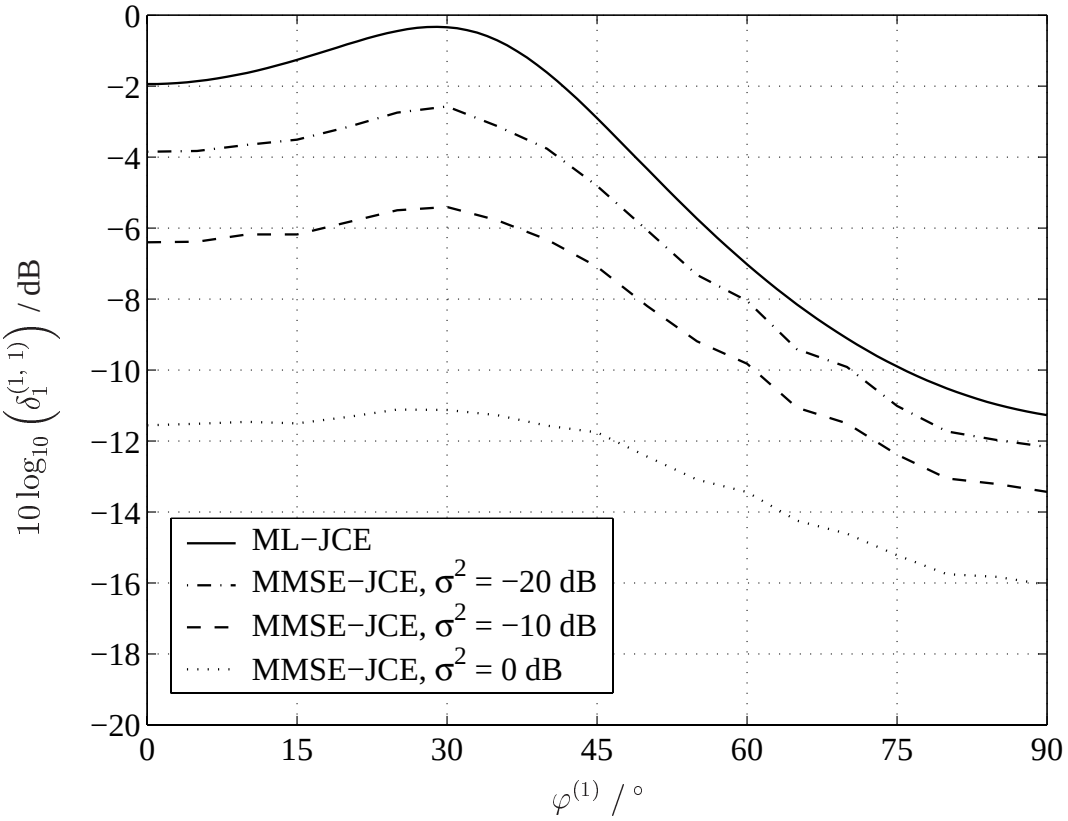

Fig. 6.19. SNIR degradation $\delta_1^{(1,\,1)}$ of MT one versus the MT-specific $\varphi^{(1)}$ for MMSE–JCE; $K_{\mathrm{A}} = 2$ antenna elements; mixed noise model, $\sigma^2 = 0,\ -10,\ -20$ dB, $\varphi^{(k_{\mathrm{I}})} = 30°$

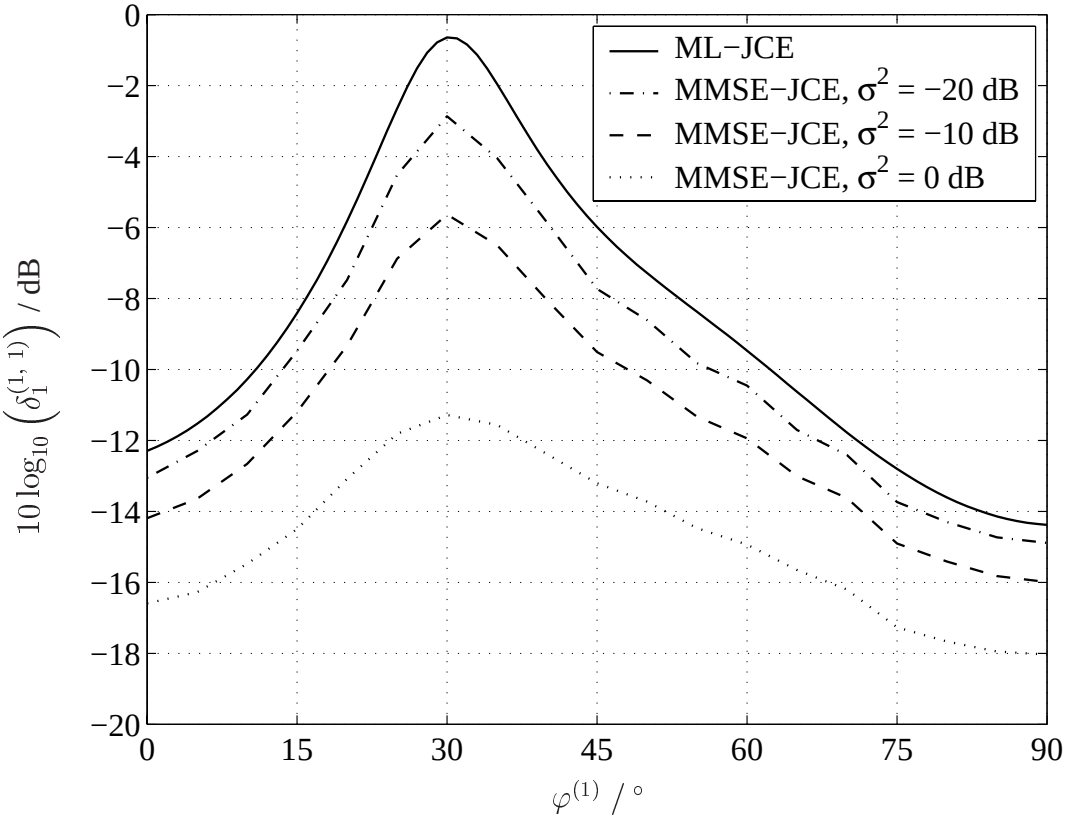

Fig. 6.20. SNIR degradation $\delta_1^{(1,\,1)}$ of MT one versus the MT-specific $\varphi^{(1)}$ for MMSE–JCE; $K_{\mathrm{A}} = 4$ antenna elements; mixed noise model, $\sigma^2 = 0,\ -10,\ -20$ dB, $\varphi^{(k_{\mathrm{I}})} = 30°$

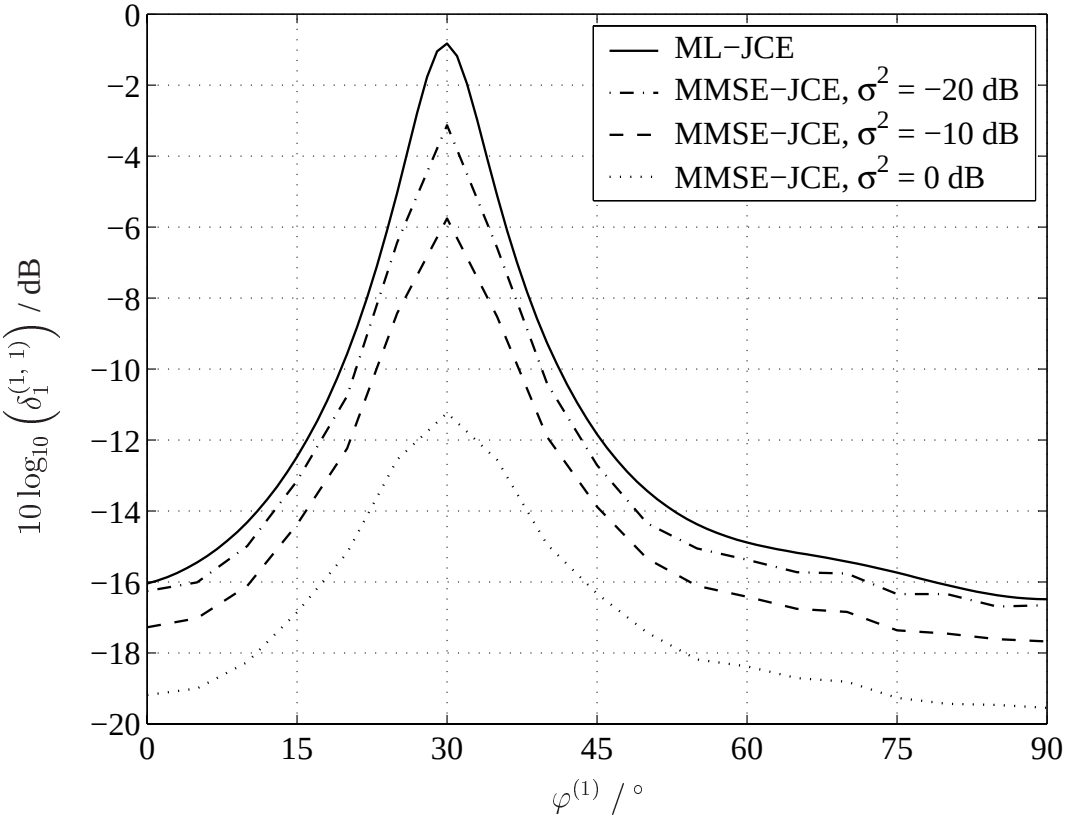

Fig. 6.21. SNIR degradation $\delta_1^{(1,\,1)}$ of MT one versus the MT-specific $\varphi^{(1)}$ for MMSE–JCE; $K_{\mathrm{A}} = 8$ antenna elements; mixed noise model, $\sigma^2 = 0,\ -10,\ -20$ dB, $\varphi^{(k_{\mathrm{I}})} = 30°$

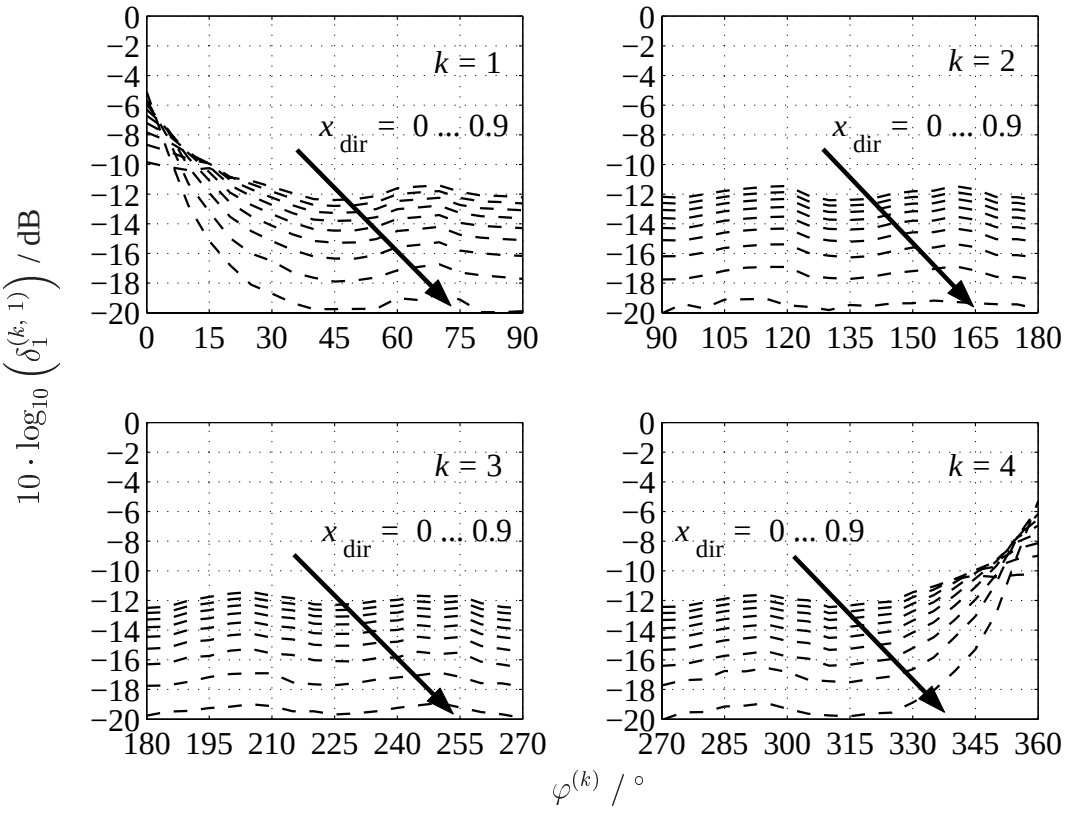

Fig. 6.22. SNIR degradation $\delta_1^{(k,\,1)}$ versus the MT-specific DOA $\varphi^{(k)}$, $k = 1\ \ldots\ K$, for MMSE–JCE; $K_{\mathrm{A}} = 8$ antenna elements; mixed noise model, $\sigma^2 = -10$ dB, $\varphi^{(k_{\mathrm{I}})} = 0°$, $x_{\mathrm{dir}} = 0,\ 0.1,\ \ldots\ 0.9$

6.9 Impact of non-perfect DOA knowledge on JCE

In the present Chapter 6 the application of multi-element receive antennas at the APs of JOINT is presented as an enhancement of the JCE performance. Both algorithms described, ML–JCE in Section 6.4 and MMSE–JCE in Section 6.7, lead to decreased SN(I)R degradations $\delta_{n_\mathrm{F}}^{(k,\,k_\mathrm{A})}$ as compared to the single-element receive antenna case, see Sections 6.6 and 6.8. A basic assumption made for the considerations presented in said sections is the perfect knowledge of the MT-specific DOAs $\varphi^{(k)}$, $k = 1 \ \ldots \ K$, of the desired signals impinging at the AP array antenna. In reality these MT-specific DOAs $\varphi^{(k)}$ must be estimated, and the applied DOA estimation algorithms, like e. g., MUSIC [Sch79, Sch86], ESPRIT [RK89, HN95, Haa97] or SAGE [THT98, FTH$^+$99], do not produce error free DOA estimates.

The present Section 6.9 and the following Section 6.10 discuss the impact of non-perfect DOA knowledge on the performance of JCE. To this end, the ML–JCE algorithm described in Section 6.4 is considered, and the noise free case is investigated. Further, the UL transmission situation shown in Fig. 6.1 is considered. In the absence of noise and with the considerations made in Section 6.3 the total received signal vector $\underline{\tilde{\mathbf{r}}}_\mathrm{tot}$ of (6.23) can be rewritten as

$$\underline{\tilde{\mathbf{r}}}_\mathrm{tot} \;=\; \underline{\tilde{\mathbf{e}}}_\mathrm{tot} \;=\; \underline{\tilde{\mathbf{P}}}_\mathrm{tot}\underline{\tilde{\mathbf{h}}}_\mathrm{tot} \;=\; \underline{\tilde{\mathbf{P}}}_\mathrm{tot}\underline{\tilde{\mathbf{A}}}\,\underline{\tilde{\boldsymbol{\mathcal{F}}}}_\mathrm{W}\underline{\mathbf{h}}_\mathrm{d} = \underline{\tilde{\boldsymbol{\mathcal{G}}}}_\mathrm{d}\underline{\mathbf{h}}_\mathrm{d}, \tag{6.62}$$

where the DOA knowledge is included in the total steering matrix $\underline{\tilde{\mathbf{A}}}$ of (6.17). As stated in Section 6.3 a single DOA is assumed per impinging signal. In the presence of DOA estimation errors $\Delta\varphi^{(k)}$ the MT-specific steering vectors $\underline{\tilde{\mathbf{a}}}^{(k)}$ of (6.13) are corrupted, since the CU applies the false MT-specific DOAs $\varphi^{(k)} + \Delta\varphi^{(k)}$ instead of $\varphi^{(k)}$. The false MT-specific steering vectors are given by

$$\begin{aligned}\underline{\tilde{\mathbf{a}}}_\mathrm{F}^{(k)} \;&=\; \left(\underline{\tilde{a}}_\mathrm{F}^{(k,1)} \ \ldots \ \underline{\tilde{a}}_\mathrm{F}^{(k,K_\mathrm{A})}\right)^\mathrm{T} \\ &=\; \left(\exp\left\{-\mathrm{j}\frac{2\pi}{\lambda}r\cos\left(\varphi^{(k)} + \Delta\varphi^{(k)} - \alpha^{(1)}\right)\right\} \ \ldots \right. \\ &\qquad \left. \exp\left\{-\mathrm{j}\frac{2\pi}{\lambda}r\cos\left(\varphi^{(k)} + \Delta\varphi^{(k)} - \alpha^{(K_\mathrm{A})}\right)\right\}\right)^\mathrm{T}.\end{aligned} \tag{6.63}$$

The subscript F will be used to distinguish between the cases of perfect and non-perfect DOA knowledge. With (6.16), (6.17), (6.63) and the false steering submatrices

$$\underline{\tilde{\mathbf{A}}}_\mathrm{F}^{(k,k_\mathrm{A})} = \underline{\tilde{a}}_\mathrm{F}^{(k,k_\mathrm{A})} \cdot \mathbf{I}^{(N_\mathrm{F}\times N_\mathrm{F})}, \tag{6.64}$$

the false total steering matrix

$$\underline{\tilde{\mathbf{A}}}_{\mathrm{F}} = \begin{pmatrix} \mathrm{blkdiag}\left(\underline{\tilde{\mathbf{A}}}_{\mathrm{F}}^{(1,1)} \ \ldots \ \underline{\tilde{\mathbf{A}}}_{\mathrm{F}}^{(K,1)}\right) \\ \vdots \\ \mathrm{blkdiag}\left(\underline{\tilde{\mathbf{A}}}_{\mathrm{F}}^{(1,K_{\mathrm{A}})} \ \ldots \ \underline{\tilde{\mathbf{A}}}_{\mathrm{F}}^{(K,K_{\mathrm{A}})}\right) \end{pmatrix} \tag{6.65}$$

results. Applying $\underline{\tilde{\mathbf{A}}}_{\mathrm{F}}$ of (6.65) for building the estimation matrix $\underline{\tilde{\mathbf{Z}}}_{\mathrm{d}}$ of (6.25) yields the false estimation matrix

$$\underline{\tilde{\mathbf{Z}}}_{\mathrm{d,F}} = \underline{\tilde{\mathbf{A}}}_{\mathrm{F}} \underline{\tilde{\boldsymbol{\mathcal{F}}}}_{\mathrm{W}} \Big(\underbrace{\underline{\tilde{\boldsymbol{\mathcal{F}}}}_{\mathrm{W}}^{\mathsf{H}} \underline{\tilde{\mathbf{A}}}_{\mathrm{F}}^{\mathsf{H}} \underline{\tilde{\mathbf{P}}}_{\mathrm{tot}}}_{\underline{\tilde{\boldsymbol{\mathcal{G}}}}_{\mathrm{d,F}}^{\mathsf{H}}} \ {}^{\mathsf{H}} \underbrace{\underline{\tilde{\mathbf{P}}}_{\mathrm{tot}} \underline{\tilde{\mathbf{A}}}_{\mathrm{F}} \underline{\tilde{\boldsymbol{\mathcal{F}}}}_{\mathrm{W}}}_{\underline{\tilde{\boldsymbol{\mathcal{G}}}}_{\mathrm{d,F}}} \Big)^{-1} \underline{\tilde{\boldsymbol{\mathcal{F}}}}_{\mathrm{W}}^{\mathsf{H}} \underline{\tilde{\mathbf{A}}}_{\mathrm{F}}^{\mathsf{H}} \ \underline{\tilde{\mathbf{P}}}_{\mathrm{tot}}^{\ \mathsf{H}} \tag{6.66}$$

for the noise free case under investigation. Processing the total receive signal vector $\underline{\tilde{\mathbf{r}}}_{\mathrm{tot}}$ of (6.62) with $\underline{\tilde{\mathbf{Z}}}_{\mathrm{d,F}}$ of (6.66) leads to the estimate

$$\underline{\hat{\tilde{\mathbf{h}}}}_{\mathrm{tot}} = \underline{\tilde{\mathbf{Z}}}_{\mathrm{d,F}} \, \underline{\tilde{\mathbf{r}}}_{\mathrm{tot}} = \underline{\tilde{\mathbf{h}}}_{\mathrm{tot}} + \Delta\underline{\tilde{\mathbf{h}}}_{\mathrm{tot}} \tag{6.67}$$

of the total CTF $\underline{\tilde{\mathbf{h}}}_{\mathrm{tot}}$ of (6.8), see also (6.25). In the absence of noise the estimation error $\Delta\underline{\tilde{\mathbf{h}}}_{\mathrm{tot}}$ on the right side of (6.67) is given by

$$\begin{aligned} \Delta\underline{\tilde{\mathbf{h}}}_{\mathrm{tot}} &= \underline{\hat{\tilde{\mathbf{h}}}}_{\mathrm{tot}} - \underline{\tilde{\mathbf{h}}}_{\mathrm{tot}} = \left(\underline{\tilde{\mathbf{Z}}}_{\mathrm{d,F}} \, \underline{\tilde{\mathbf{P}}}_{\mathrm{tot}} - \mathbf{I}^{(K_{\mathrm{A}} K N_{\mathrm{F}} \times K_{\mathrm{A}} K N_{\mathrm{F}})} \right) \underline{\tilde{\mathbf{h}}}_{\mathrm{tot}} \\ &= \left(\underline{\tilde{\mathbf{Z}}}_{\mathrm{d,F}} \, \underline{\tilde{\mathbf{P}}}_{\mathrm{tot}} - \mathbf{I}^{(K_{\mathrm{A}} K N_{\mathrm{F}} \times K_{\mathrm{A}} K N_{\mathrm{F}})} \right) \underline{\tilde{\mathbf{A}}} \, \underline{\tilde{\mathbf{h}}}_{\mathrm{d}} \\ &= \left(\underline{\tilde{\mathbf{Z}}}_{\mathrm{d,F}} \, \underline{\tilde{\mathbf{P}}}_{\mathrm{tot}} - \mathbf{I}^{(K_{\mathrm{A}} K N_{\mathrm{F}} \times K_{\mathrm{A}} K N_{\mathrm{F}})} \right) \underline{\tilde{\mathbf{A}}} \, \underline{\tilde{\boldsymbol{\mathcal{F}}}}_{\mathrm{W}} \underline{\mathbf{h}}_{\mathrm{d}} \\ &= \underline{\tilde{\mathbf{Z}}}_{\mathrm{d,F}} \, \underline{\tilde{\mathbf{P}}}_{\mathrm{tot}} \underline{\tilde{\mathbf{A}}} \, \underline{\tilde{\boldsymbol{\mathcal{F}}}}_{\mathrm{W}} \underline{\mathbf{h}}_{\mathrm{d}} - \underline{\tilde{\mathbf{A}}} \, \underline{\tilde{\boldsymbol{\mathcal{F}}}}_{\mathrm{W}} \underline{\mathbf{h}}_{\mathrm{d}}. \end{aligned} \tag{6.68}$$

With the system matrix $\underline{\tilde{\boldsymbol{\mathcal{G}}}}_{\mathrm{d}}$ of (6.23) for the case of perfect DOA knowledge and (6.66) the minuend of (6.68) can be rewritten as

$$\underline{\tilde{\mathbf{Z}}}_{\mathrm{d,F}} \, \underline{\tilde{\mathbf{P}}}_{\mathrm{tot}} \underline{\tilde{\mathbf{A}}} \, \underline{\tilde{\boldsymbol{\mathcal{F}}}}_{\mathrm{W}} \underline{\mathbf{h}}_{\mathrm{d}} = \underline{\tilde{\mathbf{Z}}}_{\mathrm{d,F}} \underline{\tilde{\boldsymbol{\mathcal{G}}}}_{\mathrm{d}} \underline{\mathbf{h}}_{\mathrm{d}} = \underline{\tilde{\mathbf{A}}}_{\mathrm{F}} \underline{\tilde{\boldsymbol{\mathcal{F}}}}_{\mathrm{W}} \left(\underline{\tilde{\boldsymbol{\mathcal{G}}}}_{\mathrm{d,F}}^{\mathsf{H}} \underline{\tilde{\boldsymbol{\mathcal{G}}}}_{\mathrm{d,F}} \right)^{-1} \underline{\tilde{\boldsymbol{\mathcal{G}}}}_{\mathrm{d,F}}^{\mathsf{H}} \underline{\tilde{\boldsymbol{\mathcal{G}}}}_{\mathrm{d}} \underline{\mathbf{h}}_{\mathrm{d}}. \tag{6.69}$$

Let us now take a closer look at the system matrix products $\underline{\tilde{\boldsymbol{\mathcal{G}}}}_{\mathrm{d,F}}^{\mathsf{H}} \underline{\tilde{\boldsymbol{\mathcal{G}}}}_{\mathrm{d,F}}$ and $\underline{\tilde{\boldsymbol{\mathcal{G}}}}_{\mathrm{d,F}}^{\mathsf{H}} \underline{\tilde{\boldsymbol{\mathcal{G}}}}_{\mathrm{d}}$ in (6.69). With the total pilot matrix $\underline{\tilde{\mathbf{P}}}_{\mathrm{tot}}$ of (6.7), the false total steering matrix $\underline{\tilde{\mathbf{A}}}_{\mathrm{F}}$ of (6.65) and the blockdiagonal reduced Fourier matrix $\underline{\tilde{\boldsymbol{\mathcal{F}}}}_{\mathrm{W}}$ of (4.21), the analytical representation of the false system matrix $\underline{\tilde{\boldsymbol{\mathcal{G}}}}_{\mathrm{d,F}}$ yields

$$\begin{aligned} \underline{\tilde{\boldsymbol{\mathcal{G}}}}_{\mathrm{d,F}} &= \underline{\tilde{\mathbf{P}}}_{\mathrm{tot}} \underline{\tilde{\mathbf{A}}}_{\mathrm{F}} \underline{\tilde{\boldsymbol{\mathcal{F}}}}_{\mathrm{W}} \\ &= \begin{pmatrix} \underline{\tilde{\mathbf{P}}}^{(1)} \underline{\tilde{\mathbf{A}}}_{\mathrm{F}}^{(1,1)} \left[\underline{\tilde{\boldsymbol{\mathcal{F}}}} \right]_{N_{\mathrm{F}},W}^{1,1} & \cdots & \underline{\tilde{\mathbf{P}}}^{(K)} \underline{\tilde{\mathbf{A}}}_{\mathrm{F}}^{(K,1)} \left[\underline{\tilde{\boldsymbol{\mathcal{F}}}} \right]_{N_{\mathrm{F}},W}^{1,1} \\ \vdots & & \vdots \\ \underline{\tilde{\mathbf{P}}}^{(1)} \underline{\tilde{\mathbf{A}}}_{\mathrm{F}}^{(1,K_{\mathrm{A}})} \left[\underline{\tilde{\boldsymbol{\mathcal{F}}}} \right]_{N_{\mathrm{F}},W}^{1,1} & \cdots & \underline{\tilde{\mathbf{P}}}^{(K)} \underline{\tilde{\mathbf{A}}}_{\mathrm{F}}^{(K,K_{\mathrm{A}})} \left[\underline{\tilde{\boldsymbol{\mathcal{F}}}} \right]_{N_{\mathrm{F}},W}^{1,1} \end{pmatrix}. \end{aligned} \tag{6.70}$$

With the false steering submatrices $\underline{\tilde{\mathbf{A}}}_{\mathrm{F}}^{(k,k_{\mathrm{A}})}$ of (6.64) and the MT-specific $N_{\mathrm{F}} \times W$ system submatrices

$$\underline{\tilde{\boldsymbol{\mathcal{G}}}}^{(k)} = \underline{\tilde{\mathbf{P}}}^{(k)} \left[\underline{\tilde{\boldsymbol{\mathcal{F}}}}\right]_{N_{\mathrm{F}},W}^{1,1} \tag{6.71}$$

valid for the single-element receive antenna case, see also (5.3), (6.70) is rewritten as

$$\underline{\tilde{\boldsymbol{\mathcal{G}}}}_{\mathrm{d,F}} = \begin{pmatrix} \underline{\tilde{a}}_{\mathrm{F}}^{(1,1)} \cdot \underline{\tilde{\boldsymbol{\mathcal{G}}}}^{(1)} & \cdots & \underline{\tilde{a}}_{\mathrm{F}}^{(K,1)} \cdot \underline{\tilde{\boldsymbol{\mathcal{G}}}}^{(K)} \\ \vdots & & \vdots \\ \underline{\tilde{a}}_{\mathrm{F}}^{(1,K_{\mathrm{A}})} \cdot \underline{\tilde{\boldsymbol{\mathcal{G}}}}^{(1)} & \cdots & \underline{\tilde{a}}_{\mathrm{F}}^{(K,K_{\mathrm{A}})} \cdot \underline{\tilde{\boldsymbol{\mathcal{G}}}}^{(K)} \end{pmatrix}. \tag{6.72}$$

With (6.72) the Gram matrix $\underline{\tilde{\boldsymbol{\mathcal{G}}}}_{\mathrm{d,F}}^{\mathsf{H}} \underline{\tilde{\boldsymbol{\mathcal{G}}}}_{\mathrm{d,F}}$ to be inverted in (6.69) takes the form

$$\begin{aligned} \underline{\tilde{\boldsymbol{\mathcal{G}}}}_{\mathrm{d,F}}^{\mathsf{H}} \underline{\tilde{\boldsymbol{\mathcal{G}}}}_{\mathrm{d,F}} &= \begin{pmatrix} \underline{\tilde{a}}_{\mathrm{F}}^{(1,1)*} \cdot \underline{\tilde{\boldsymbol{\mathcal{G}}}}^{(1)\mathsf{H}} & \cdots & \underline{\tilde{a}}_{\mathrm{F}}^{(1,K_{\mathrm{A}})*} \cdot \underline{\tilde{\boldsymbol{\mathcal{G}}}}^{(1)\mathsf{H}} \\ \vdots & & \vdots \\ \underline{\tilde{a}}_{\mathrm{F}}^{(K,1)*} \cdot \underline{\tilde{\boldsymbol{\mathcal{G}}}}^{(K)\mathsf{H}} & \cdots & \underline{\tilde{a}}_{\mathrm{F}}^{(K,K_{\mathrm{A}})*} \cdot \underline{\tilde{\boldsymbol{\mathcal{G}}}}^{(K)\mathsf{H}} \end{pmatrix} \cdot \\ &\quad \begin{pmatrix} \underline{\tilde{a}}_{\mathrm{F}}^{(1,1)} \cdot \underline{\tilde{\boldsymbol{\mathcal{G}}}}^{(1)} & \cdots & \underline{\tilde{a}}_{\mathrm{F}}^{(K,1)} \cdot \underline{\tilde{\boldsymbol{\mathcal{G}}}}^{(K)} \\ \vdots & & \vdots \\ \underline{\tilde{a}}_{\mathrm{F}}^{(1,K_{\mathrm{A}})} \cdot \underline{\tilde{\boldsymbol{\mathcal{G}}}}^{(1)} & \cdots & \underline{\tilde{a}}_{\mathrm{F}}^{(K,K_{\mathrm{A}})} \cdot \underline{\tilde{\boldsymbol{\mathcal{G}}}}^{(K)} \end{pmatrix} \\ &= \begin{pmatrix} \sum\limits_{k_{\mathrm{A}}=1}^{K_{\mathrm{A}}} \left|\underline{\tilde{a}}_{\mathrm{F}}^{(1,k_{\mathrm{A}})}\right|^2 \cdot \underline{\tilde{\boldsymbol{\mathcal{G}}}}^{(1)\mathsf{H}} \underline{\tilde{\boldsymbol{\mathcal{G}}}}^{(1)} & \cdots & \sum\limits_{k_{\mathrm{A}}=1}^{K_{\mathrm{A}}} \underline{\tilde{a}}_{\mathrm{F}}^{(1,k_{\mathrm{A}})*} \underline{\tilde{a}}_{\mathrm{F}}^{(K,k_{\mathrm{A}})} \cdot \underline{\tilde{\boldsymbol{\mathcal{G}}}}^{(1)\mathsf{H}} \underline{\tilde{\boldsymbol{\mathcal{G}}}}^{(K)} \\ \vdots & & \vdots \\ \sum\limits_{k_{\mathrm{A}}=1}^{K_{\mathrm{A}}} \underline{\tilde{a}}_{\mathrm{F}}^{(K,k_{\mathrm{A}})*} \underline{\tilde{a}}_{\mathrm{F}}^{(1,k_{\mathrm{A}})} \cdot \underline{\tilde{\boldsymbol{\mathcal{G}}}}^{(K)\mathsf{H}} \underline{\tilde{\boldsymbol{\mathcal{G}}}}^{(1)} & \cdots & \sum\limits_{k_{\mathrm{A}}=1}^{K_{\mathrm{A}}} \left|\underline{\tilde{a}}_{\mathrm{F}}^{(K,k_{\mathrm{A}})}\right|^2 \cdot \underline{\tilde{\boldsymbol{\mathcal{G}}}}^{(K)\mathsf{H}} \underline{\tilde{\boldsymbol{\mathcal{G}}}}^{(K)} \end{pmatrix}. \end{aligned} \tag{6.73}$$

Applying ideal pilot vectors based on Walsh codes as described in Section 5.5 together with (5.1) leads to

$$\underline{\tilde{\boldsymbol{\mathcal{G}}}}^{(k)\mathsf{H}} \underline{\tilde{\boldsymbol{\mathcal{G}}}}^{(k')} = \begin{cases} 2E_{\mathrm{p}} \cdot \mathbf{I}^{(W \times W)}, & k = k' \\ \mathbf{0}^{(W \times W)}, & k \neq k' \end{cases}, \; k, k' = 1 \; \ldots \; K, \tag{6.74}$$

which together with

$$\left|\underline{\tilde{a}}_{\mathrm{F}}^{(k,k_{\mathrm{A}})}\right|^2 = 1, \; \forall k, \; k_{\mathrm{A}}, \tag{6.75}$$

yields the real valued diagonal Gram matrix

$$\underline{\tilde{\boldsymbol{\mathcal{G}}}}_{\mathrm{d,F}}^{\mathsf{H}} \underline{\tilde{\boldsymbol{\mathcal{G}}}}_{\mathrm{d,F}} = 2E_{\mathrm{p}} K_{\mathrm{A}} \cdot \mathbf{I}^{(KW \times KW)}. \tag{6.76}$$

Analogously to (6.73) to (6.76), the system matrix product $\underline{\tilde{\boldsymbol{\mathcal{G}}}}_{\mathrm{d,F}}^{\mathsf{H}} \underline{\tilde{\boldsymbol{\mathcal{G}}}}_{\mathrm{d}}$ also produces a diagonal matrix

$$\underline{\tilde{\boldsymbol{\mathcal{G}}}}_{\mathrm{d,F}}^{\mathsf{H}} \underline{\tilde{\boldsymbol{\mathcal{G}}}}_{\mathrm{d}} = \begin{pmatrix} \sum\limits_{k_{\mathrm{A}}=1}^{K_{\mathrm{A}}} \underline{\tilde{a}}_{\mathrm{F}}^{(1,k_{\mathrm{A}})*} \underline{\tilde{a}}^{(1,k_{\mathrm{A}})} \cdot \underline{\tilde{\boldsymbol{\mathcal{G}}}}^{(1)\mathsf{H}} \underline{\tilde{\boldsymbol{\mathcal{G}}}}^{(1)} & \cdots & \sum\limits_{k_{\mathrm{A}}=1}^{K_{\mathrm{A}}} \underline{\tilde{a}}_{\mathrm{F}}^{(1,k_{\mathrm{A}})*} \underline{\tilde{a}}^{(K,k_{\mathrm{A}})} \cdot \underline{\tilde{\boldsymbol{\mathcal{G}}}}^{(1)\mathsf{H}} \underline{\tilde{\boldsymbol{\mathcal{G}}}}^{(K)} \\ \vdots & & \vdots \\ \sum\limits_{k_{\mathrm{A}}=1}^{K_{\mathrm{A}}} \underline{\tilde{a}}_{\mathrm{F}}^{(K,k_{\mathrm{A}})*} \underline{\tilde{a}}^{(1,k_{\mathrm{A}})} \cdot \underline{\tilde{\boldsymbol{\mathcal{G}}}}^{(K)\mathsf{H}} \underline{\tilde{\boldsymbol{\mathcal{G}}}}^{(1)} & \cdots & \sum\limits_{k_{\mathrm{A}}=1}^{K_{\mathrm{A}}} \underline{\tilde{a}}_{\mathrm{F}}^{(K,k_{\mathrm{A}})*} \underline{\tilde{a}}^{(K,k_{\mathrm{A}})} \cdot \underline{\tilde{\boldsymbol{\mathcal{G}}}}^{(K)\mathsf{H}} \underline{\tilde{\boldsymbol{\mathcal{G}}}}^{(K)} \end{pmatrix}$$

$$= \begin{pmatrix} 2E_{\mathrm{p}} \sum\limits_{k_{\mathrm{A}}=1}^{K_{\mathrm{A}}} \underline{\tilde{a}}_{\mathrm{F}}^{(1,k_{\mathrm{A}})*} \underline{\tilde{a}}^{(1,k_{\mathrm{A}})} & \cdots & 0 \\ \vdots & & \vdots \\ 0 & \cdots & 2E_{\mathrm{p}} \sum\limits_{k_{\mathrm{A}}=1}^{K_{\mathrm{A}}} \underline{\tilde{a}}_{\mathrm{F}}^{(K,k_{\mathrm{A}})*} \underline{\tilde{a}}^{(K,k_{\mathrm{A}})} \end{pmatrix}. \tag{6.77}$$

With (6.76) and (6.77)

$$\left(\underline{\tilde{\boldsymbol{\mathcal{G}}}}_{\mathrm{d,F}}^{\mathsf{H}} \underline{\tilde{\boldsymbol{\mathcal{G}}}}_{\mathrm{d,F}}\right)^{-1} \underline{\tilde{\boldsymbol{\mathcal{G}}}}_{\mathrm{d,F}}^{\mathsf{H}} \underline{\tilde{\boldsymbol{\mathcal{G}}}}_{\mathrm{d}} =$$

$$\begin{pmatrix} \underbrace{\frac{1}{K_{\mathrm{A}}} \sum\limits_{k_{\mathrm{A}}=1}^{K_{\mathrm{A}}} \underline{\tilde{a}}_{\mathrm{F}}^{(1,k_{\mathrm{A}})*} \underline{\tilde{a}}^{(1,k_{\mathrm{A}})}}_{\Delta\underline{\tilde{a}}^{(1)}} \cdot \mathbf{I}^{(W\times W)} & \cdots & 0 \\ \vdots & \ddots & \vdots \\ 0 & \cdots & \underbrace{\frac{1}{K_{\mathrm{A}}} \sum\limits_{k_{\mathrm{A}}=1}^{K_{\mathrm{A}}} \underline{\tilde{a}}_{\mathrm{F}}^{(K,k_{\mathrm{A}})*} \underline{\tilde{a}}^{(K,k_{\mathrm{A}})}}_{\Delta\underline{\tilde{a}}^{(K)}} \cdot \mathbf{I}^{(W\times W)} \end{pmatrix} =$$

$$\mathrm{blkdiag}\left(\Delta\underline{\tilde{a}}^{(1)} \cdot \mathbf{I}^{(W\times W)} \ \ldots \ \Delta\underline{\tilde{a}}^{(K)} \cdot \mathbf{I}^{(W\times W)}\right) \tag{6.78}$$

holds, and with (6.78), (6.69) can be rewritten as

$$\underline{\tilde{\mathbf{Z}}}_{\mathrm{d,F}}\, \underline{\tilde{\mathbf{P}}}_{\mathrm{tot}} \underline{\tilde{\mathbf{A}}}\, \underline{\tilde{\boldsymbol{\mathcal{F}}}}_{\mathrm{W}} \underline{\mathbf{h}}_{\mathrm{d}} = \underline{\tilde{\mathbf{A}}}_{\mathrm{F}} \cdot \mathrm{blkdiag}\left(\Delta\underline{\tilde{a}}^{(1)} \cdot \mathbf{I}^{(W\times W)} \ \ldots \ \Delta\underline{\tilde{a}}^{(K)} \cdot \mathbf{I}^{(W\times W)}\right) \cdot \underline{\tilde{\mathbf{h}}}_{\mathrm{d}}. \tag{6.79}$$

Applying (6.79) leads to the JCE error

$$\begin{aligned} \Delta\underline{\tilde{\mathbf{h}}}_{\mathrm{tot}} &= \underline{\tilde{\mathbf{A}}}_{\mathrm{F}} \cdot \mathrm{blkdiag}\left(\Delta\underline{\tilde{a}}^{(1)} \cdot \mathbf{I}^{(W\times W)} \ \ldots \ \Delta\underline{\tilde{a}}^{(K)} \cdot \mathbf{I}^{(W\times W)}\right) \cdot \underline{\tilde{\mathbf{h}}}_{\mathrm{d}} - \underline{\tilde{\mathbf{A}}}\, \underline{\tilde{\mathbf{h}}}_{\mathrm{d}} \qquad (6.80) \\ &= \left(\underline{\tilde{\mathbf{A}}}_{\mathrm{F}} \cdot \mathrm{blkdiag}\left(\Delta\underline{\tilde{a}}^{(1)} \cdot \mathbf{I}^{(W\times W)} \ \ldots \ \Delta\underline{\tilde{a}}^{(K)} \cdot \mathbf{I}^{(W\times W)}\right) - \underline{\tilde{\mathbf{A}}}\right) \underline{\tilde{\mathbf{h}}}_{\mathrm{d}}, \end{aligned}$$

and from (6.80) the component $\Delta\underline{\tilde{h}}_{\mathrm{tot},n_{\mathrm{F}}}^{(k,k_{\mathrm{A}})}$ of the JCE error $\Delta\underline{\tilde{\mathbf{h}}}_{\mathrm{tot}}$ is obtained as

$$\begin{aligned} \Delta\underline{\tilde{h}}_{\mathrm{tot},n_{\mathrm{F}}}^{(k,k_{\mathrm{A}})} &= \left(\Delta\underline{\tilde{a}}^{(k)} \cdot \underline{\tilde{a}}_{\mathrm{F}}^{(k,k_{\mathrm{A}})} - \underline{\tilde{a}}^{(k,k_{\mathrm{A}})}\right) \cdot \underline{\tilde{h}}_{\mathrm{d},n_{\mathrm{F}}}^{(k)} \qquad (6.81) \\ &\quad k_{\mathrm{A}} = 1 \ \ldots \ K_{\mathrm{A}},\ k = 1 \ \ldots \ K,\ n_{\mathrm{F}} = 1 \ldots N_{\mathrm{F}}, \end{aligned}$$

for the noise free case. Providing (6.76) and (6.77) hold, what can be seen from (6.81) is that in the absence of noise the component $\Delta\underline{\tilde{h}}_{\mathrm{tot},n_{\mathrm{F}}}^{(k,k_{\mathrm{A}})}$ of the JCE error $\Delta\underline{\tilde{\mathbf{h}}}_{\mathrm{tot}}$ depends on the true

MT-specific DOAs $\varphi^{(k)}$, the DOA estimation error $\Delta\varphi^{(k)}$ and the actual state of the mobile radio channel characterized by the component $\underline{\tilde{h}}_{\mathrm{d},n_\mathrm{F}}^{(k)}$ of the directional CTF $\underline{\tilde{\mathbf{h}}}_\mathrm{d}$ of (6.18). Further, through the application of ideal pilot vectors based on Walsh codes, see Section 5.5, MAI is avoided despite the non-perfect DOA knowledge. This avoidance of MAI is also achieved by the application of the ideal pilot vectors based on disjoint subcarriers, see Section 5.4, and of the ideal pilot vectors based on CAZAC codes, see Section 5.6. Finally, the component $\Delta\underline{\tilde{h}}_{\mathrm{tot},n_\mathrm{F}}^{(k,k_\mathrm{A})}$ of the JCE error of MT k is affected only by the DOA estimation error $\Delta\varphi^{(k)}$ of the same MT k.

In order to avoid the dependence of the JCE performance on the actual state of the mobile radio channel, we define the normalized square error (NSE)

$$\begin{aligned}\underline{\tilde{\varepsilon}}_{n_\mathrm{F}}^{(k,k_\mathrm{A})} &= \frac{\left|\Delta\underline{\tilde{h}}_{\mathrm{tot},n_\mathrm{F}}^{(k,k_\mathrm{A})}\right|^2}{\left|\underline{\tilde{h}}_{n_\mathrm{F}}^{(k,k_\mathrm{A})}\right|^2} = \frac{\left|\Delta\underline{\tilde{h}}_{\mathrm{tot},n_\mathrm{F}}^{(k,k_\mathrm{A})}\right|^2}{\left|\underline{\tilde{a}}^{(k,k_\mathrm{A})}\right|^2\left|\underline{\tilde{h}}_{\mathrm{d},n_\mathrm{F}}^{(k)}\right|^2} = \frac{\left|\Delta\underline{\tilde{h}}_{\mathrm{tot},n_\mathrm{F}}^{(k,k_\mathrm{A})}\right|^2}{\left|\underline{\tilde{h}}_{\mathrm{d},n_\mathrm{F}}^{(k)}\right|^2} \\ &= 1 + \left(\Delta\underline{\tilde{a}}^{(k)}\right)^2 - 2\cdot\Delta\underline{\tilde{a}}^{(k)}\cdot\mathrm{Re}\left\{\underline{\tilde{a}}_\mathrm{F}^{(k,k_\mathrm{A})*}\underline{\tilde{a}}^{(k,k_\mathrm{A})}\right\},\end{aligned} \tag{6.82}$$

$$k_\mathrm{A} = 1\ \ldots\ K_\mathrm{A},\ k = 1\ \ldots\ K,\ \forall n_\mathrm{F} = 1\ldots N_\mathrm{F},$$

normalized by the square absolute value $\left|\underline{\tilde{h}}_{\mathrm{d},n_\mathrm{F}}^{(k)}\right|^2$ of the component $\underline{\tilde{h}}_{\mathrm{d},n_\mathrm{F}}^{(k)}$ of the directional CTF as the performance criterion for the case of non-perfect DOA knowledge. $\underline{\tilde{\varepsilon}}_{n_\mathrm{F}}^{(k,k_\mathrm{A})}$ of (6.82) depends on the MT-specific DOA $\varphi^{(k)}$ and the DOA estimation error $\Delta\varphi^{(k)}$, and it has the same value for all N_F subcarriers. Nevertheless, the subscript n_F will be kept for the NSE $\underline{\tilde{\varepsilon}}_{n_\mathrm{F}}^{(k,k_\mathrm{A})}$ in order to denote/remind said normalization by $\left|\underline{\tilde{h}}_{\mathrm{d},n_\mathrm{F}}^{(k)}\right|^2$.

For the circular array antenna configuration assumed in the present investigations, see Fig. 6.2, $\underline{\tilde{\varepsilon}}_{n_\mathrm{F}}^{(k,k_\mathrm{A})}$ is real valued for an even number K_A of antenna elements, as it will demonstrated in the following. It can be seen from (6.82) that $\underline{\tilde{\varepsilon}}_{n_\mathrm{F}}^{(k,k_\mathrm{A})}$ is real valued if $\Delta\underline{\tilde{a}}^{(k)}$ of (6.78) is real valued. In the case of $K_\mathrm{A} = 2$ antenna elements $\Delta\underline{\tilde{a}}^{(k)}$ of (6.78) is given by

$$\Delta\underline{\tilde{a}}^{(k)} = \frac{1}{K_\mathrm{A}}\sum_{k_\mathrm{A}=1}^{K_\mathrm{A}}\underline{\tilde{a}}_\mathrm{F}^{(k,k_\mathrm{A})*}\underline{\tilde{a}}^{(k,k_\mathrm{A})}$$

$$\begin{aligned}&= \frac{1}{2}\left(\exp\left\{\mathrm{j}\frac{2\pi\cdot r}{\lambda}\left[\cos(\varphi^{(k)}+\Delta\varphi^{(k)}-\alpha^{(1)})-\cos(\varphi^{(k)}-\alpha^{(1)})\right]\right\}+\right. \\ &\qquad \left.\exp\left\{\mathrm{j}\frac{2\pi\cdot r}{\lambda}\left[\cos(\varphi^{(k)}+\Delta\varphi^{(k)}-\alpha^{(2)})-\cos(\varphi^{(k)}-\alpha^{(2)})\right]\right\}\right).\end{aligned} \tag{6.83}$$

With

$$\alpha^{(1)} = 0^\circ,\ \alpha^{(2)} = \pi \tag{6.84}$$

valid for the case of $K_{\mathrm{A}} = 2$ antenna elements and the property

$$\cos(x - \pi) = -\cos(x) \tag{6.85}$$

of the cosine function, (6.83) can be rewritten as

$$\begin{aligned}
\Delta\underline{\tilde{a}}^{(k)} &= \frac{1}{2}\left(\exp\left\{\mathrm{j}\frac{2\pi\cdot r}{\lambda}\left[\cos(\varphi^{(k)}+\Delta\varphi^{(k)})-\cos(\varphi^{(k)})\right]\right\}+\right. \\
&\qquad \left.\exp\left\{\mathrm{j}\frac{2\pi\cdot r}{\lambda}\left[\cos(\varphi^{(k)}+\Delta\varphi^{(k)}-\pi)-\cos(\varphi^{(k)}-\pi)\right]\right\}\right) \\
&= \frac{1}{2}\left(\exp\left\{\mathrm{j}\frac{2\pi\cdot r}{\lambda}\left[\cos(\varphi^{(k)}+\Delta\varphi^{(k)})-\cos(\varphi^{(k)})\right]\right\}+\right. \\
&\qquad \left.\exp\left\{-\mathrm{j}\frac{2\pi\cdot r}{\lambda}\left[\cos(\varphi^{(k)}+\Delta\varphi^{(k)})-\cos(\varphi^{(k)})\right]\right\}\right) \\
&= \cos\left(\frac{2\pi\cdot r}{\lambda}\left[\cos(\varphi^{(k)}+\Delta\varphi^{(k)})-\cos(\varphi^{(k)})\right]\right).
\end{aligned} \tag{6.86}$$

(6.86) holds for any pair of array antenna elements separated angularly by 180° from each other. Therefore, for a circular array antenna with an even number K_{A} of antenna elements, the NSE $\underline{\tilde{\varepsilon}}_{n_{\mathrm{F}}}^{(k,k_{\mathrm{A}})}$ of (6.82) is real valued.

6.10 Investigation results

Since the NSE $\underline{\tilde{\varepsilon}}_{n_{\mathrm{F}}}^{(k,k_{\mathrm{A}})}$ of (6.82) of MT k is affected only by the DOA estimation error $\Delta\varphi^{(k)}$ of the same MT k, it is sufficient to consider the case of a single MT in order to demonstrate the impact of non-perfect DOA knowledge on the performance of JCE. Figs. 6.23 till 6.29 illustrate the resulting curves calculated based on (6.82). In Figs. 6.23 and 6.24 the NSE $\underline{\tilde{\varepsilon}}_{n_{\mathrm{F}}}^{(1,k_{\mathrm{A}})}$ of (6.82) of the considered MT one is depicted versus the DOA estimation error $\Delta\varphi^{(1)}$. $\Delta\varphi^{(1)}$ is varied in the interval $[0^\circ \ \ldots \ 90^\circ]$, and the actual MT-specific DOA $\varphi^{(1)}$ of the desired impinging signal is fixed to 0°. Fig. 6.23 shows the results for the cases of two and four antenna elements and Fig. 6.24 for the case of eight antenna elements at the AP array. As presented in the previous section, for the considered cases of two, four and eight antenna elements at the AP array the NSE $\underline{\tilde{\varepsilon}}_{n_{\mathrm{F}}}^{(k,k_{\mathrm{A}})}$ of (6.82) is real valued. In both figures it can be seen that $\underline{\tilde{\varepsilon}}_{n_{\mathrm{F}}}^{(1,k_{\mathrm{A}})}$ rises rather fast with an increasing DOA estimation error $\Delta\varphi^{(1)}$. Also, the statement made at the end of the previous section is verified by the curves in Figs. 6.23 and 6.24, where it is seen that antenna elements spaced by 180° from each other deliver the same results. As a further result, the mean NSE (MNSE)

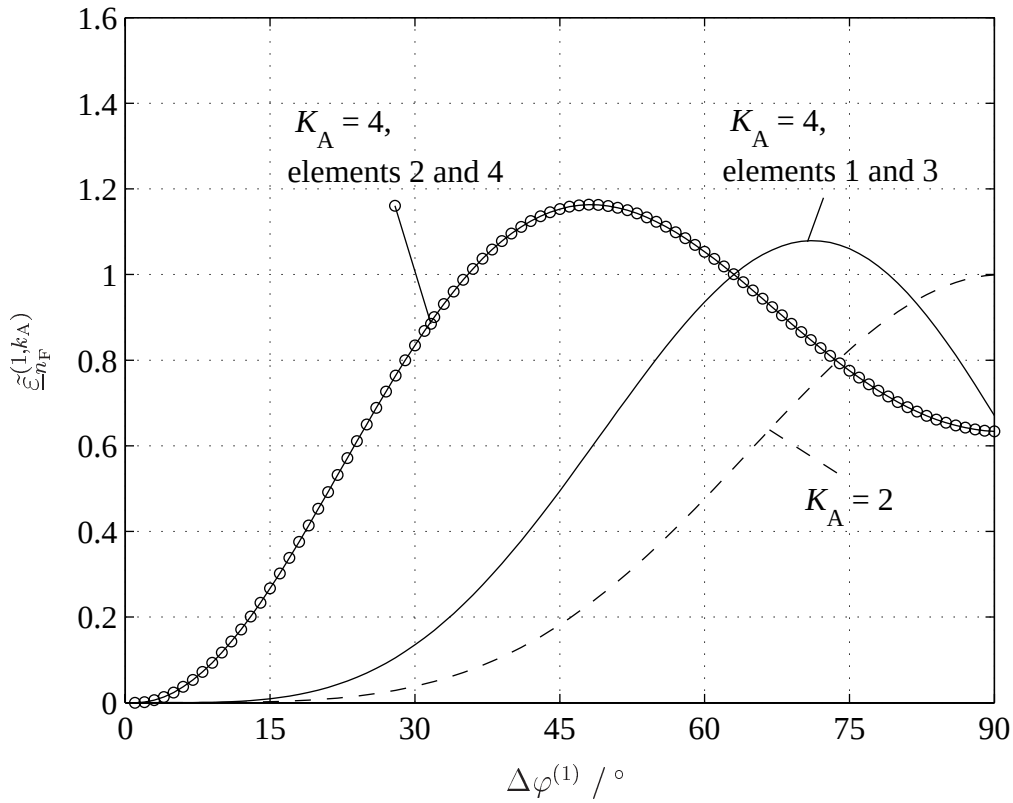

Fig. 6.23. Normalized square error $\tilde{\underline{\varepsilon}}_{n_\mathrm{F}}^{(1,k_\mathrm{A})}$ of MT $k = 1$ versus the MT-specific DOA estimation error $\Delta\varphi^{(1)}$; $K_\mathrm{A} = 2$, 4 antenna elements, $\varphi^{(1)} = 0°$

$$\overline{\tilde{\underline{\varepsilon}}_{n_\mathrm{F}}^{(1)}} = \frac{1}{K_\mathrm{A}} \sum_{k_\mathrm{A}=1}^{K_\mathrm{A}} \tilde{\underline{\varepsilon}}_{n_\mathrm{F}}^{(1,k_\mathrm{A})} \tag{6.87}$$

over all K_A array antenna elements is given in Fig. 6.25 for increasing K_A. The more antenna elements the array antenna consists of, the higher the accuracy of the array antenna in direction of the DOA $\varphi^{(1)}$, i. e., the array resolution, and the narrower the main lobe of the array antenna become. This increases the sensitivity of the array antenna to DOA estimation errors with the result that the MNSE of (6.87) rises faster for larger numbers K_A of array antenna elements. Similar results are obtained for the NSE and the MNSE also for other values of the MT-specific DOA $\varphi^{(1)}$. Finally, Figs. 6.26 till 6.29 show the curves calculated from (6.82) for the case of a fixed DOA estimation error $\Delta\varphi^{(1)}$. The NSE $\tilde{\underline{\varepsilon}}_{n_\mathrm{F}}^{(1,k_\mathrm{A})}$ of MT $k = 1$ is plotted in all figures versus the MT-specific DOA $\varphi^{(1)}$. Five different values $10°,\ 15°,\ 20°,\ 25°$ and $30°$ are considered for $\Delta\varphi^{(1)}$. Again, the cases of two, four and eight antenna elements are considered. The symmetry of the array antenna is reflected on the periodicity of the curves. The rather fast increase of the NSE $\tilde{\underline{\varepsilon}}_{n_\mathrm{F}}^{(1,k_\mathrm{A})}$ is clearly seen for an increasing DOA estimation error $\Delta\varphi^{(1)}$.

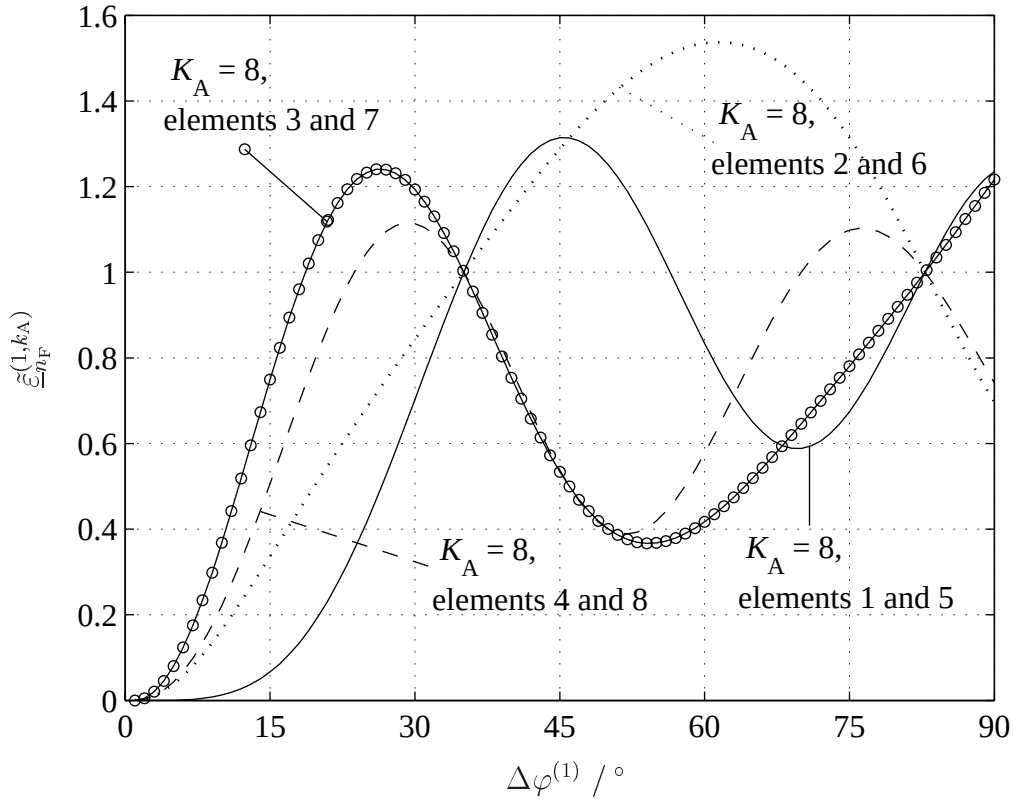

Fig. 6.24. Normalized square error $\tilde{\underline{\varepsilon}}_{n_\mathrm{F}}^{(1,k_\mathrm{A})}$ of MT $k = 1$ versus the MT-specific DOA estimation error $\Delta\varphi^{(1)}$; $K_\mathrm{A} = 8$ antenna elements, $\varphi^{(1)} = 0°$

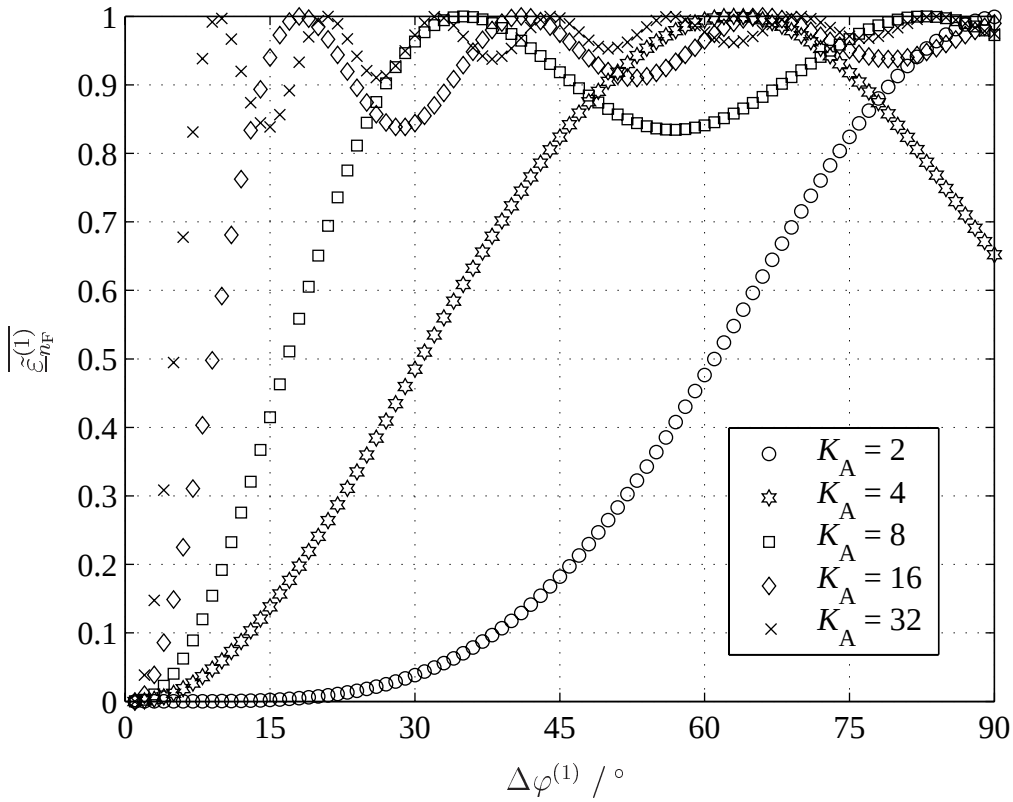

Fig. 6.25. Mean normalized square error $\overline{\tilde{\underline{\varepsilon}}_{n_\mathrm{F}}^{(1)}}$ of MT $k = 1$ versus the DOA estimation error $\Delta\varphi^{(1)}$; $\varphi^{(1)} = 0°$

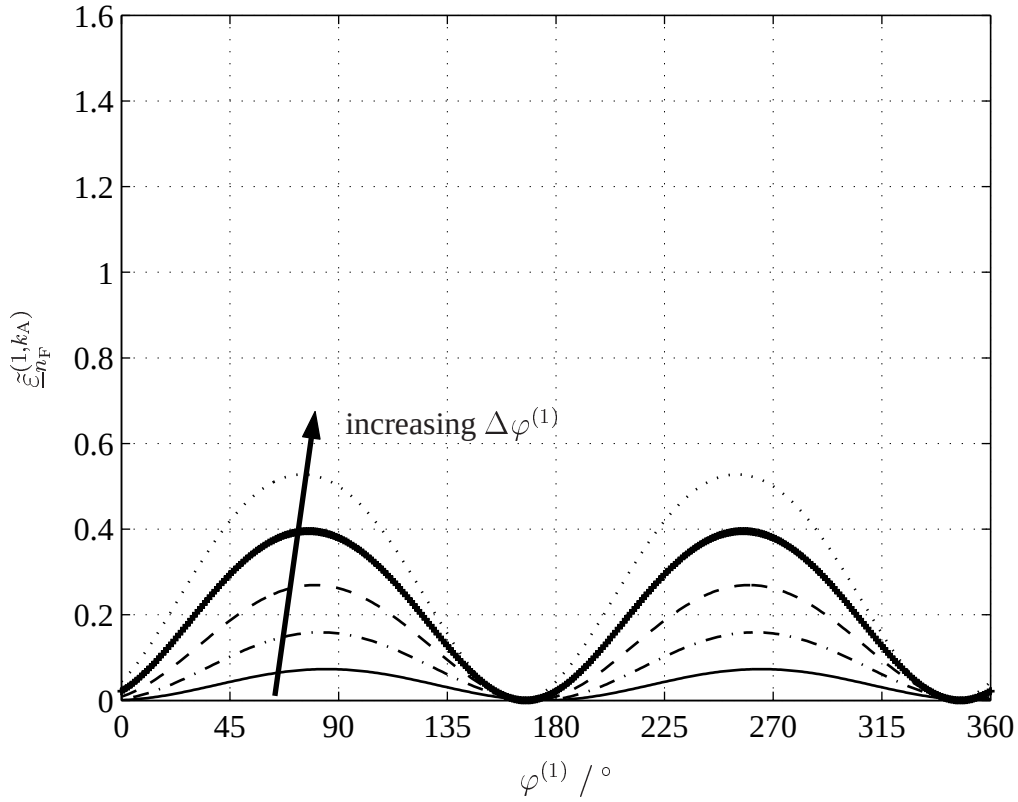

Fig. 6.26. Normalized square error $\tilde{\underline{\varepsilon}}_{n_\mathrm{F}}^{(1,k_\mathrm{A})}$ of MT $k = 1$ versus the MT-specific DOA $\varphi^{(1)}$; $K_\mathrm{A} = 2$ antenna elements, $\Delta\varphi^{(1)} = 10°,\ 15°,\ 20°,\ 25°,\ 30°$

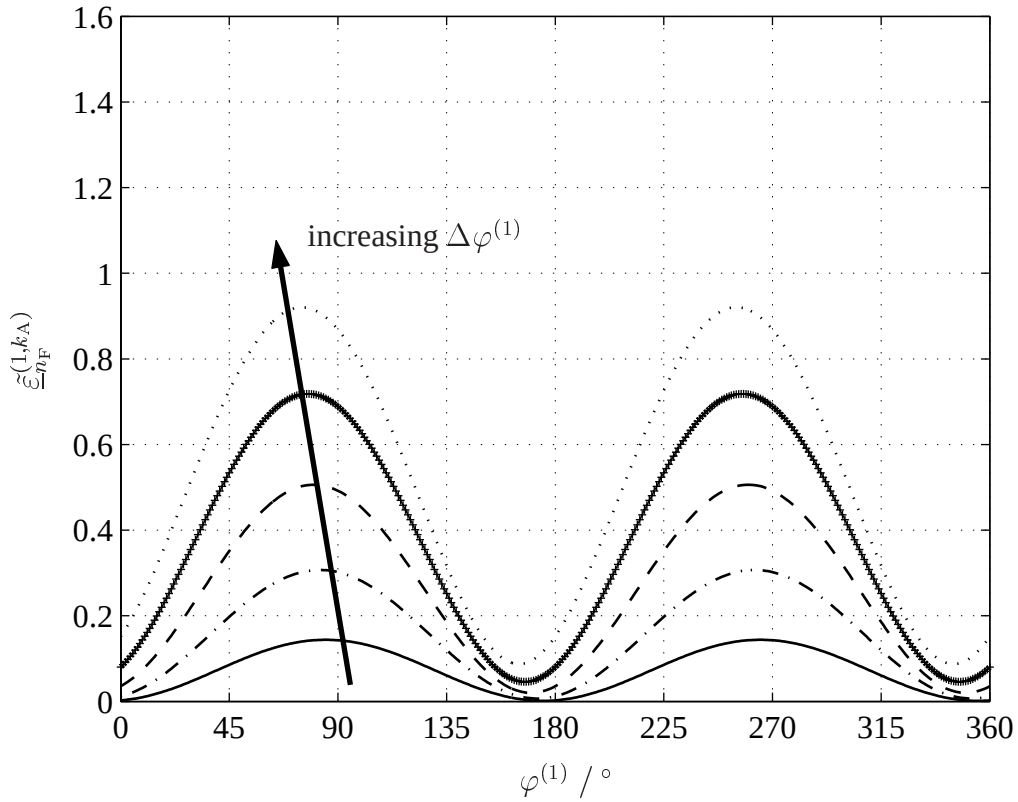

Fig. 6.27. Normalized square error $\tilde{\underline{\varepsilon}}_{n_\mathrm{F}}^{(1,k_\mathrm{A})}$ of MT $k = 1$ versus the MT-specific DOA $\varphi^{(1)}$; $K_\mathrm{A} = 2$ antenna elements, $\Delta\varphi^{(1)} = 10°,\ 15°,\ 20°,\ 25°,\ 30°$; antenna elements $k_\mathrm{A} = 1$ and $k_\mathrm{A} = 3$

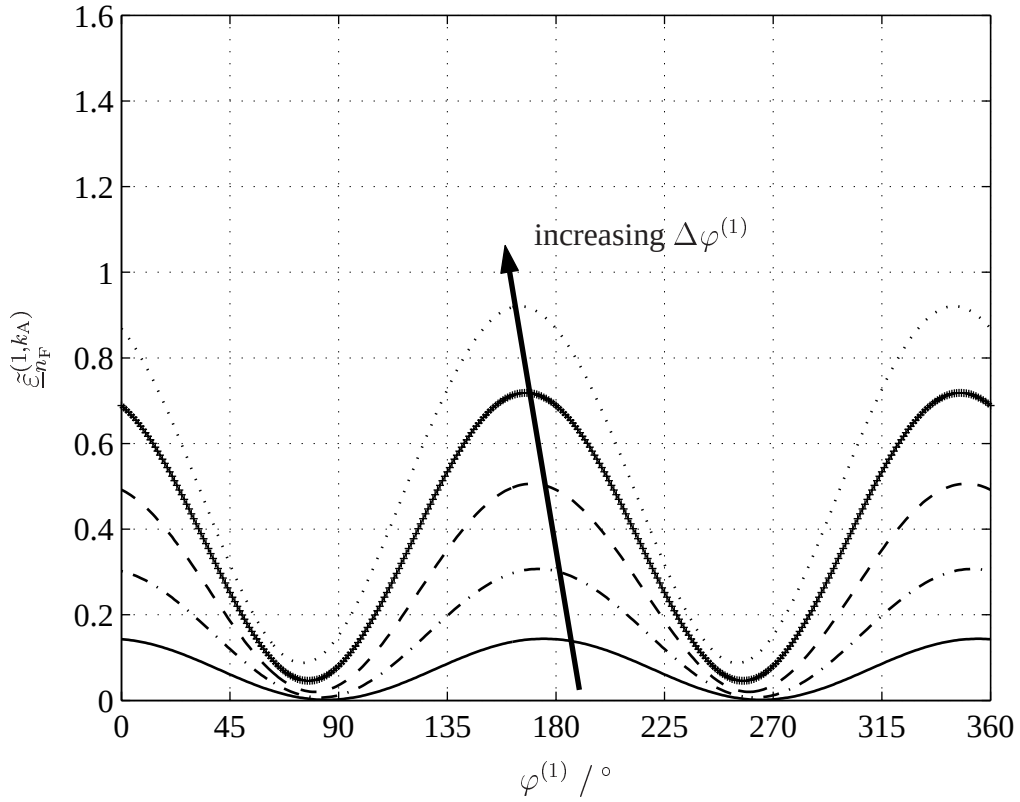

Fig. 6.28. Normalized square error $\tilde{\underline{\varepsilon}}^{(1,k_\mathrm{A})}_{n_\mathrm{F}}$ of MT $k = 1$ versus the MT-specific DOA $\varphi^{(1)}$; $K_\mathrm{A} = 4$ antenna elements, $\Delta\varphi^{(1)} = 10°,\ 15°,\ 20°,\ 25°,\ 30°$; antenna elements $k_\mathrm{A} = 2$ and $k_\mathrm{A} = 4$

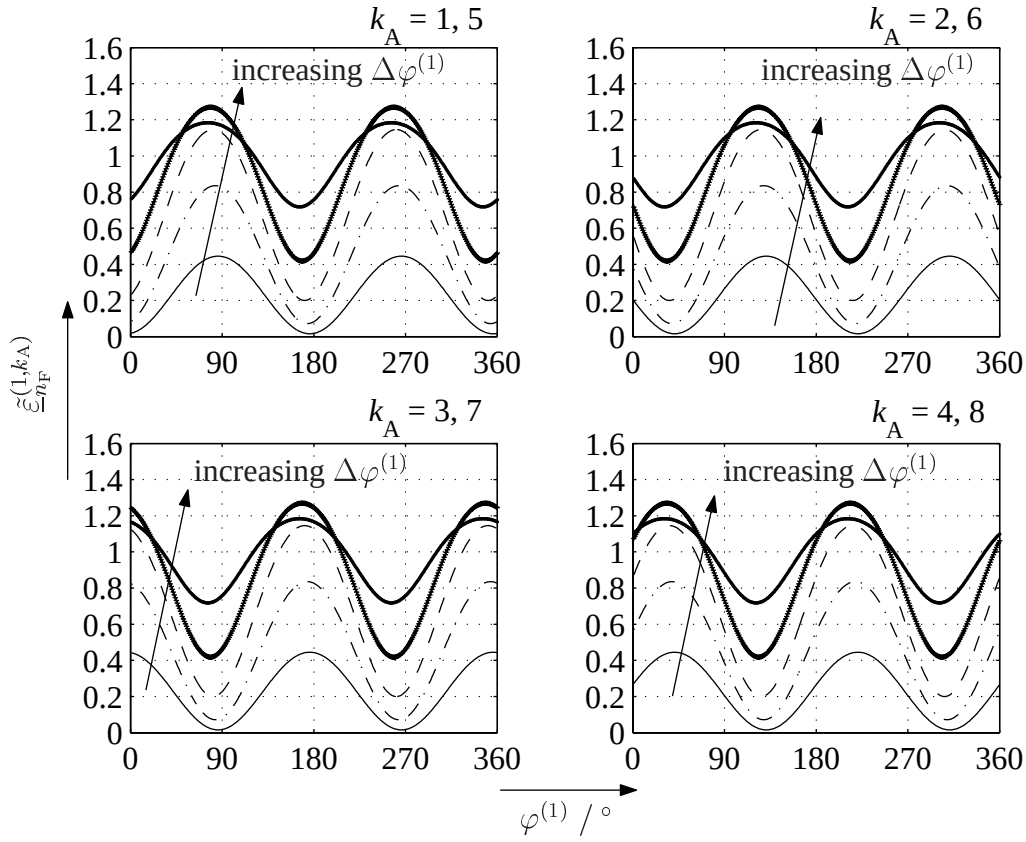

Fig. 6.29. Normalized square error $\tilde{\underline{\varepsilon}}^{(1,k_\mathrm{A})}_{n_\mathrm{F}}$ of MT $k = 1$ versus the MT-specific DOA $\varphi^{(1)}$; $K_\mathrm{A} = 8$ antenna elements, $\Delta\varphi^{(1)} = 10°,\ 15°,\ 20°,\ 25°,\ 30°$

Chapter 7

Exploitation of temporal correlations for JCE

7.1 Two dimensional joint channel estimation (2D–JCE)

Following the considerations given in Chapter 4, the enhancement of the JCE performance presented in Chapter 6 features the application of multi-element antennas at the APs of JOINT, based on which the exploitation of the directional properties of the mobile radio channel becomes feasible. In addition to directional properties, a-priori channel state information can be included in the estimation process by the application of MMSE–JCE, see Section 6.7. JCE, as described in Chapters 4 and 6, is an one dimensional channel estimation technique (1D–JCE) performed over the subcarriers of an OFDM symbol slot dedicated to channel estimation. However, there exists also the possibility of performing JCE over two dimensions, that is over the subcarriers and over the OFDM symbol slots.

Let us a look at the frame structure applied in JOINT illustrated in Fig. 7.1. One frame contains N_{B} OFDM symbol slots in the time dimension, each symbol slot n_{B}, $n_{\mathrm{B}} = 1 \ldots N_{\mathrm{B}}$, containing the N_{F} available subcarriers in the frequency dimension. Within a frame one or more OFDM symbol slots may be dedicated to channel estimation. After performing JCE over the subcarriers - either for the single-element or for the multi-element antenna case - the estimated CTF components $\underline{\hat{\hat{h}}}_{n_{\mathrm{F}}}^{(k)}$ are used to perform JD in the following UL OFDM symbol slots or to perform JT in the following DL OFDM symbol slots [Skl04] until the next OFDM symbol slot dedicated to channel estimation comes up. The temporal distance between two consecutive OFDM symbol slots dedicated to channel estimation is dictated by the maximum Doppler frequency $f_{\mathrm{D,max}}$, i. e., by the MT velocity v, see (2.13). Although the estimated CTF components $\underline{\hat{\hat{h}}}_{n_{\mathrm{F}}}^{(k)}$ gained during 1D–JCE are of optimum quality and the radio channels are considered to vary only slowly for the number of OFDM symbol slots between two consecutive channel estimations, applying the same estimates for JD or JT will eventually lead to data estimation errors due to the time variance of the mobile radio channel. To restrict these errors and, hence, to improve the JCE performance, 2D–JCE can be applied in JOINT.

As it is known from literature [Pra72, HKR97b, HKR97a, vNP00, FK03], the optimum filter for channel estimation in both time and frequency is the 2D Wiener filter, which minimizes the mean square channel estimation error. Although optimum, the filter is prohibitively complex to realize, and, therefore, two cascaded 1D filters are preferred instead. In JOINT,

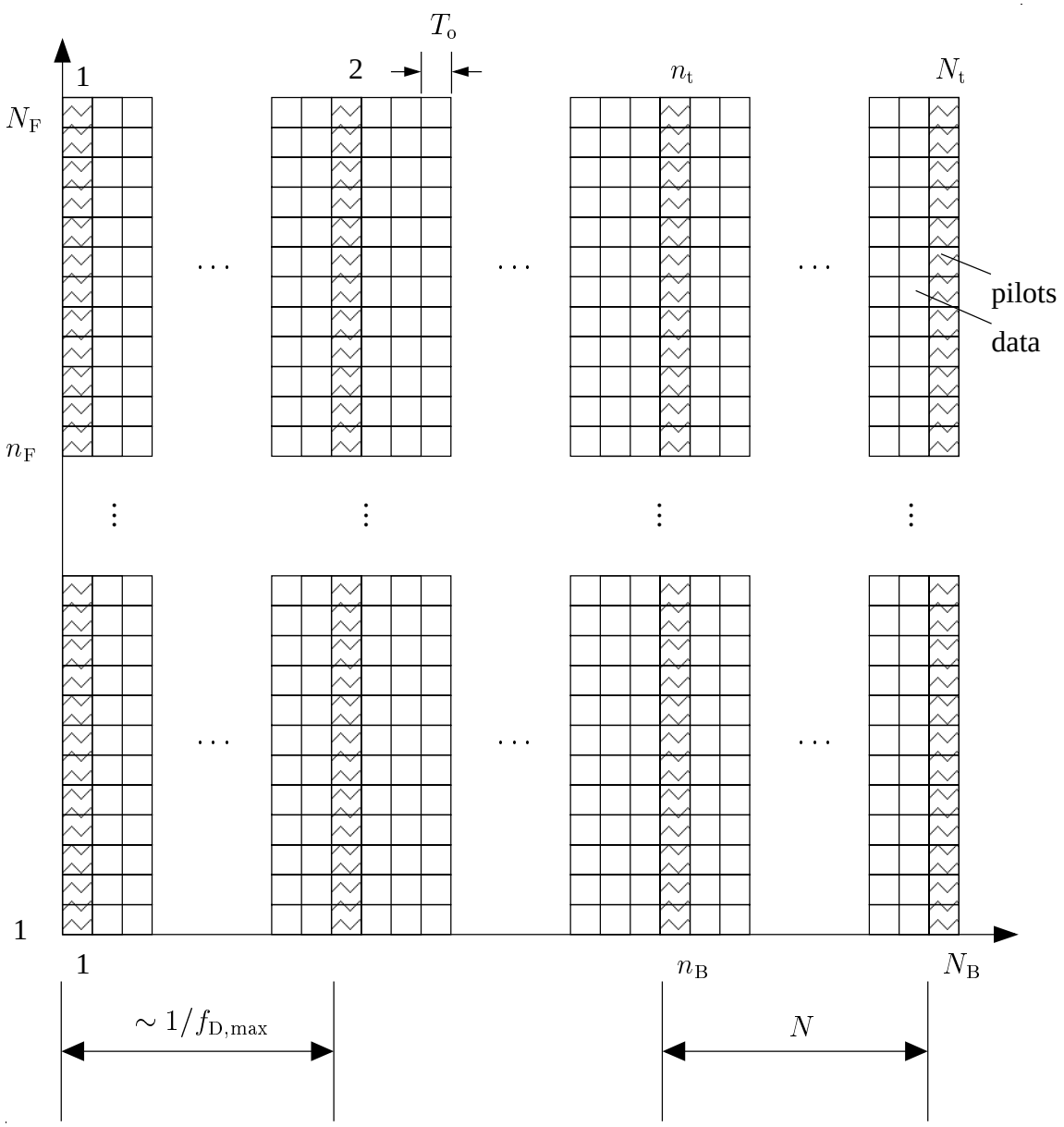

Fig. 7.1. Frame structure applied in JOINT

channel estimation over the subcarriers can be performed by ML–JCE as described in Sections 4.4 and 6.4. In the second step, an interpolation is performed over the N_B OFDM symbol slots of the frame, where the OFDM symbol slots dedicated to channel estimation are used as interpolation bases. Three different interpolation methods are considered in the thesis:

- sinc interpolation,
- linear interpolation of real and imaginary parts, and
- linear interpolation of absolute values and arguments.

The investigations conducted in this chapter shall focus on the impact of time variance on the performance of 2D–JCE. To this end, the noise free case of JOINT will be considered. For the noise free case in a SA of JOINT

$$\hat{\tilde{\underline{\mathbf{h}}}}^{(k)} = \tilde{\underline{\mathbf{h}}}^{(k)} \tag{7.1}$$

holds for ML–JCE, see also (4.33) and (6.25). Therefore, it is sufficient to consider the case of a single MT in the SA without any loss of generality.

The OFDM symbol slots dedicated to channel estimation and applied as interpolation bases are denoted by n_t, $n_\mathrm{t} = 1 \ldots N_\mathrm{t}$, see Fig. 7.1. With the duration T_o of an OFDM symbol slot and the number N of symbol slots from one interpolation base to the other, see Fig. 7.1, the unbiased CTF estimates for subcarrier n_F, $n_\mathrm{F} = 1 \ldots N_\mathrm{F}$, on all N_t interpolation bases are given by the sequence

$$\hat{\tilde{\underline{h}}}^{(1)}_{n_\mathrm{F}}(n_\mathrm{t}) = \tilde{\underline{h}}^{(1)}_{n_\mathrm{F}}(n_\mathrm{t}) = \tilde{\underline{h}}^{(1)}_{n_\mathrm{F}}\left([n_\mathrm{t}-1]N\ T_\mathrm{o} + T_\mathrm{o}\right)\ , n_\mathrm{t} = 1 \ldots N_\mathrm{t}. \tag{7.2}$$

For sinc interpolation the sequence $\tilde{\underline{h}}^{(1)}_{n_\mathrm{F}}(n_\mathrm{t})$ of (7.2) is convolved with the sequence

$$g(mT_\mathrm{o}) = \mathrm{sinc}\left(2\pi f_{\mathrm{D,max}}\ mT_\mathrm{o}\right), m = 0\ \ldots\ N_\mathrm{B}, \tag{7.3}$$

of the sinc function to yield the sequence

$$\hat{\tilde{\underline{h}}}^{(1)}_{n_\mathrm{F}}(mT_\mathrm{o}) = \tilde{\underline{h}}^{(1)}_{n_\mathrm{F}}(n_\mathrm{t}) \star g(mT_\mathrm{o}),\ m = 0\ \ldots\ N_\mathrm{B}, \tag{7.4}$$

of the sinc interpolated CTF sequence over all N_B OFDM symbol slots for subcarrier n_F.

For linear interpolation two options are considered. In the first one, the real and the imaginary parts of the estimated CTF component $\hat{\tilde{\underline{h}}}^{(1)}_{n_\mathrm{F},\ n_\mathrm{B}}$ on subcarrier n_F and OFDM symbol slot n_B between two consecutive interpolation bases n_t and $n_\mathrm{t}+1$ are interpolated separately according to

$$\begin{aligned}
\mathrm{Re}\left\{\hat{\tilde{\underline{h}}}^{(1)}_{n_\mathrm{F},\ n_\mathrm{B}}\right\} &= \mathrm{Re}\left\{\tilde{\underline{h}}^{(1)}_{n_\mathrm{F},\ n_\mathrm{t}}\right\} + \frac{n_\mathrm{B}-n_\mathrm{t}}{N} \cdot \left(\mathrm{Re}\left\{\tilde{\underline{h}}^{(1)}_{n_\mathrm{F},\ n_\mathrm{t}+1}\right\} - \mathrm{Re}\left\{\tilde{\underline{h}}^{(1)}_{n_\mathrm{F},\ n_\mathrm{t}}\right\}\right) \\
\mathrm{Im}\left\{\hat{\tilde{\underline{h}}}^{(1)}_{n_\mathrm{F},\ n_\mathrm{B}}\right\} &= \mathrm{Im}\left\{\tilde{\underline{h}}^{(1)}_{n_\mathrm{F},\ n_\mathrm{t}}\right\} + \frac{n_\mathrm{B}-n_\mathrm{t}}{N} \cdot \left(\mathrm{Im}\left\{\tilde{\underline{h}}^{(1)}_{n_\mathrm{F},\ n_\mathrm{t}+1}\right\} - \mathrm{Im}\left\{\tilde{\underline{h}}^{(1)}_{n_\mathrm{F},\ n_\mathrm{t}}\right\}\right)\ .
\end{aligned} \tag{7.5}$$

In the second option, the absolute value and the argument of the estimated CTF component $\hat{\tilde{\underline{h}}}^{(1)}_{n_\mathrm{F},\ n_\mathrm{B}}$ on subcarrier n_F and OFDM symbol slot n_B between two consecutive interpolation bases n_t and $n_\mathrm{t}+1$ are interpolated separately according to

$$\left|\hat{\tilde{\underline{h}}}^{(1)}_{n_\mathrm{F},\ n_\mathrm{B}}\right| = \left|\tilde{\underline{h}}^{(1)}_{n_\mathrm{F},\ n_\mathrm{t}}\right| + \frac{n_\mathrm{B}-n_\mathrm{t}}{N} \cdot \left(\left|\tilde{\underline{h}}^{(1)}_{n_\mathrm{F},\ n_\mathrm{t}+1}\right| - \left|\tilde{\underline{h}}^{(1)}_{n_\mathrm{F},\ n_\mathrm{t}}\right|\right) \tag{7.6}$$

and

$$\arg\left\{\hat{\tilde{\underline{h}}}^{(1)}_{n_\mathrm{F},\ n_\mathrm{B}}\right\} = \arg\left\{\tilde{\underline{h}}^{(1)}_{n_\mathrm{F},\ n_\mathrm{t}}\right\} + \frac{n_\mathrm{B}-n_\mathrm{t}}{N} \cdot \left(\arg\left\{\tilde{\underline{h}}^{(1)}_{n_\mathrm{F},\ n_\mathrm{t}+1}\right\} - \arg\left\{\tilde{\underline{h}}^{(1)}_{n_\mathrm{F},\ n_\mathrm{t}}\right\}\right). \tag{7.7}$$

7.2 Performance of 2D–JCE

Based on the considerations presented in Section 7.1, this section discusses the performance of 2D–JCE in JOINT. The adopted performance criterion is the square error

$$\varepsilon^{(1)}_{n_\mathrm{F},\,n_\mathrm{B}} = \frac{\left|\hat{\underline{\tilde{h}}}^{(1)}_{n_\mathrm{F},\,n_\mathrm{B}} - \underline{\tilde{h}}^{(1)}_{n_\mathrm{F},\,n_\mathrm{B}}\right|^2}{\mathrm{E}\left\{\left|\underline{\tilde{h}}^{(1)}_{n_\mathrm{F},\,n_\mathrm{B}}\right|^2\right\}} \tag{7.8}$$

normalized to the energy $\mathrm{E}\left\{\left|\underline{\tilde{h}}^{(1)}_{n_\mathrm{F},\,n_\mathrm{B}}\right|^2\right\}$ of the true CTF component $\underline{\tilde{h}}^{(1)}_{n_\mathrm{F},\,n_\mathrm{B}}$ in OFDM symbol slot n_B, $n_\mathrm{B} = 1 \ldots N_\mathrm{B}$. The parameters of the conducted simulations are listed in Table 7.1. As mentioned in Section 7.1, the single MT case is considered. The velocities of

Table 7.1. Simulation parameters

bandwidth B	20 MHz	
carrier frequency f_c	5.5 GHz	
OFDM symbol slot duration T_o	32 μs	
number of subcarriers N_F	256	
channel model	COST 207 RA	
MT velocity v	25 km/h	120 km/h
max. Doppler frequency $f_{\mathrm{D},\,\max}$	127 Hz	611 Hz
number N of symbol slots from one interpolation base to the other	50	20
number N_t of interpolation bases	11	
number N_B of OFDM symbol slots in a frame	501	201

v equal to 25 km/h and 120 km/h of the MT are chosen in the simulations. With the corresponding maximum Doppler frequencies $f_{\mathrm{D},\,\max}$ and the duration T_o of the OFDM symbol slot, the number N_tv of symbol slots after which the impact of time variance can no longer be neglected is calculated by

$$N_\mathrm{tv} = \frac{1}{2 f_{\mathrm{D},\,\max} T_\mathrm{o}}\,. \tag{7.9}$$

The number N of OFDM symbol slots from one interpolation base to the other is set equal to 50 and 25, respectively. The number N_t of interpolation bases is set equal to 11 for both MT velocities, which results in the number

$$N_\mathrm{B} = N \cdot (N_\mathrm{t} - 1) + 1 = \begin{cases} 201 & \text{for } N = 20, \\ 501 & \text{for } N = 50 \end{cases} \tag{7.10}$$

of considered OFDM symbol slots.

Figs. 7.2 and 7.3 show the run of the real part $\mathrm{Re}\left\{\hat{\underline{\tilde{h}}}^{(1)}_{n_\mathrm{F},\,n_\mathrm{B}}\right\}$ and the imaginary part $\mathrm{Im}\left\{\hat{\underline{\tilde{h}}}^{(1)}_{n_\mathrm{F},\,n_\mathrm{B}}\right\}$ of the estimated CTF component $\hat{\underline{\tilde{h}}}^{(1)}_{n_\mathrm{F},\,n_\mathrm{B}}$ in OFDM symbol slot n_B, $n_\mathrm{B} = 1 \ldots N_\mathrm{B}$, respectively, for the MT velocity $v = 25$ km/h. The resulting curves for 2D–JCE applying the three interpolation schemes mentioned in Section 7.1 are shown together with the curves for the true CTF component $\underline{\tilde{h}}^{(1)}_{n_\mathrm{F},\,n_\mathrm{B}}$ in OFDM symbol slot n_B, $n_\mathrm{B} = 1 \ldots N_\mathrm{B}$. In addition, the curves for conventional 1D–ML–JCE as described in Section 4.4 are shown as well, where the N_t estimated CTF components $\hat{\underline{\tilde{h}}}^{(1)}_{n_\mathrm{F},\,n_\mathrm{t}}$, each obtained at the respective interpolation base n_t, $n_\mathrm{t} = 1 \ldots N_\mathrm{t}$, are applied for JD or JT in the following N OFDM symbol slots. As it can be seen from Figs. 7.2 and 7.3, 2D–JCE exhibits a solid performance for all three interpolation techniques due to the fact that the number N of OFDM symbol slots from one interpolation base to the other is smaller than N_tv of (7.9) for the considered velocity. According to (7.9), at a MT speed of 25 km/h time variance has an impact after the duration of 123 OFDM symbol slots. Despite the fact that within the duration of 123 OFDM symbol slots there exist three OFDM symbol slots dedicated to channel estimation, performing 1D–ML–JCE every 50 OFDM symbol slots proves insufficient. It can be seen in Figs. 7.2 and 7.3 that the performance of 1D–ML–JCE between two consecutive interpolation bases differs by far from the performance of the applied 2D–JCE techniques. This results to an increased relative square error $\varepsilon^{(1)}_{n_\mathrm{F},\,n_\mathrm{B}}$ of (7.8) as it can be seen in Fig. 7.6.

The respective results obtained for the MT speed of $v = 120$ km/h are shown in Figs. 7.4 7.5. According to (7.9), at a velocity of $v = 120$ km/h time variance has an impact after the duration of 25 OFDM symbol slots. The results show that 2D–JCE with sinc interpolation performs best. Although the interpolation bases are placed at every 20th OFDM symbol slot, the two linear interpolation schemes exhibit worse performance as compared to sinc interpolation. Conventional 1D–ML–JCE exhibits the poorest performance, which is also verified by the run of the relative square error $\varepsilon^{(1)}_{n_\mathrm{F},\,n_\mathrm{B}}$ of (7.8) shown in Fig. 7.7.

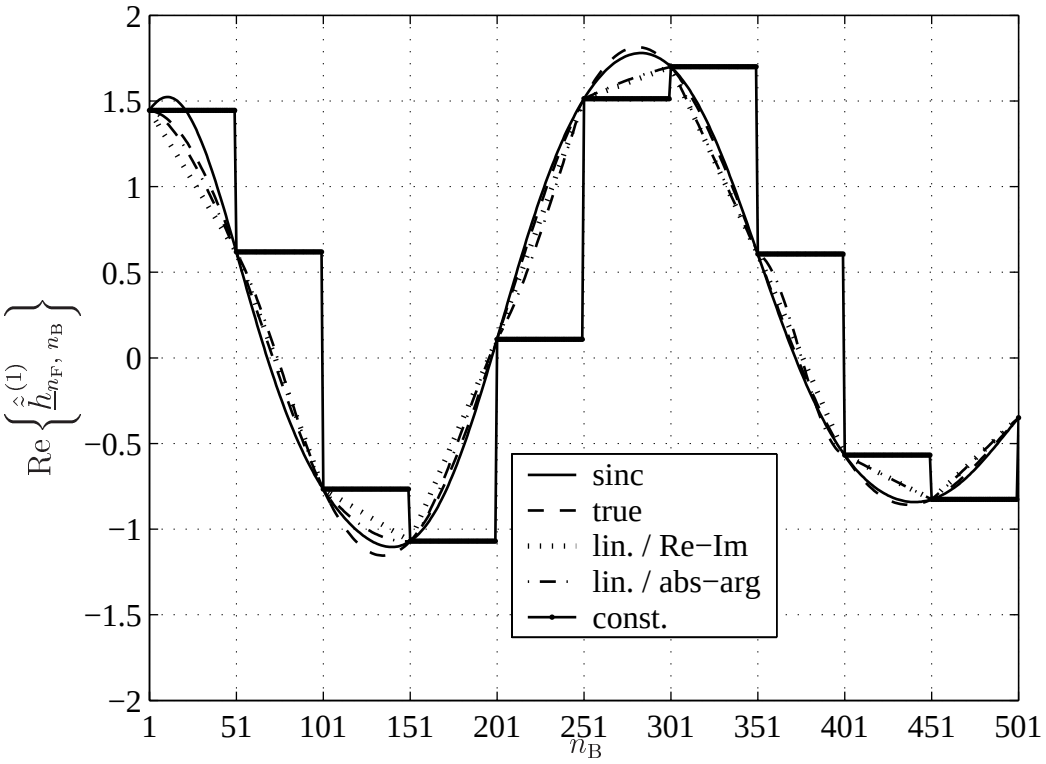

Fig. 7.2. Real part of the interpolated CTF $\hat{\underline{\hat{h}}}^{(1)}_{n_\mathrm{F},\,n_\mathrm{B}}$ in each OFDM symbol slot n_B; $v = 25$ km/h

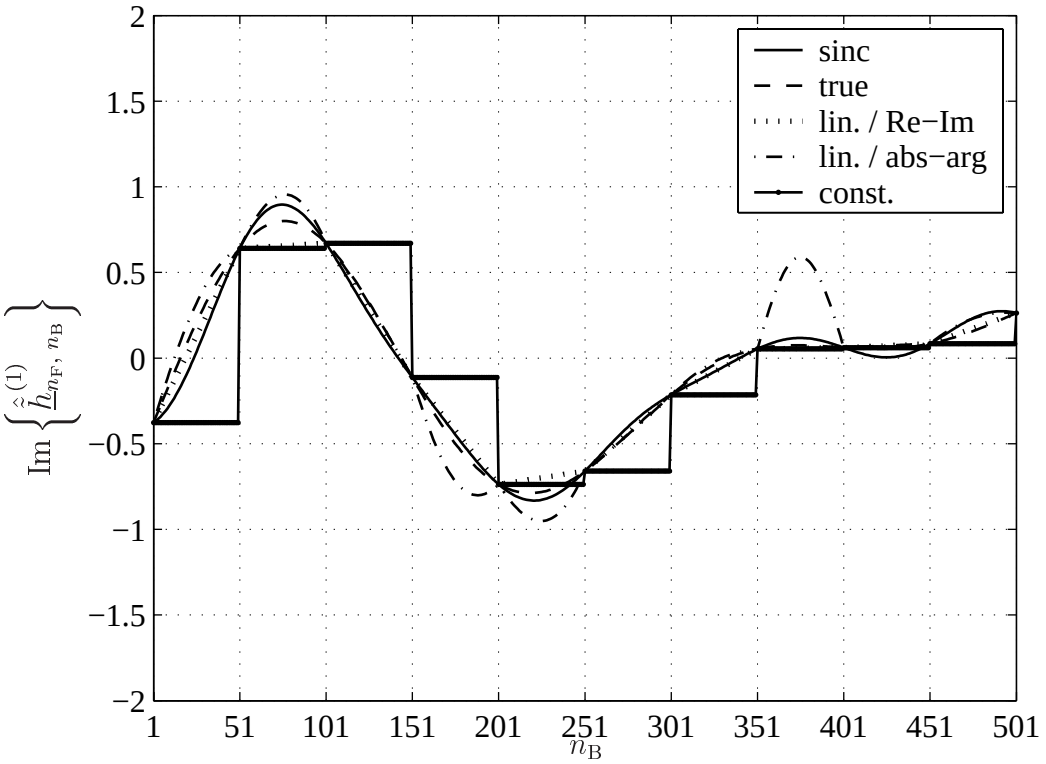

Fig. 7.3. Imaginary part of the interpolated CTF $\hat{\underline{\hat{h}}}^{(1)}_{n_\mathrm{F},\,n_\mathrm{B}}$ in each OFDM symbol slot n_B; $v = 25$ km/h

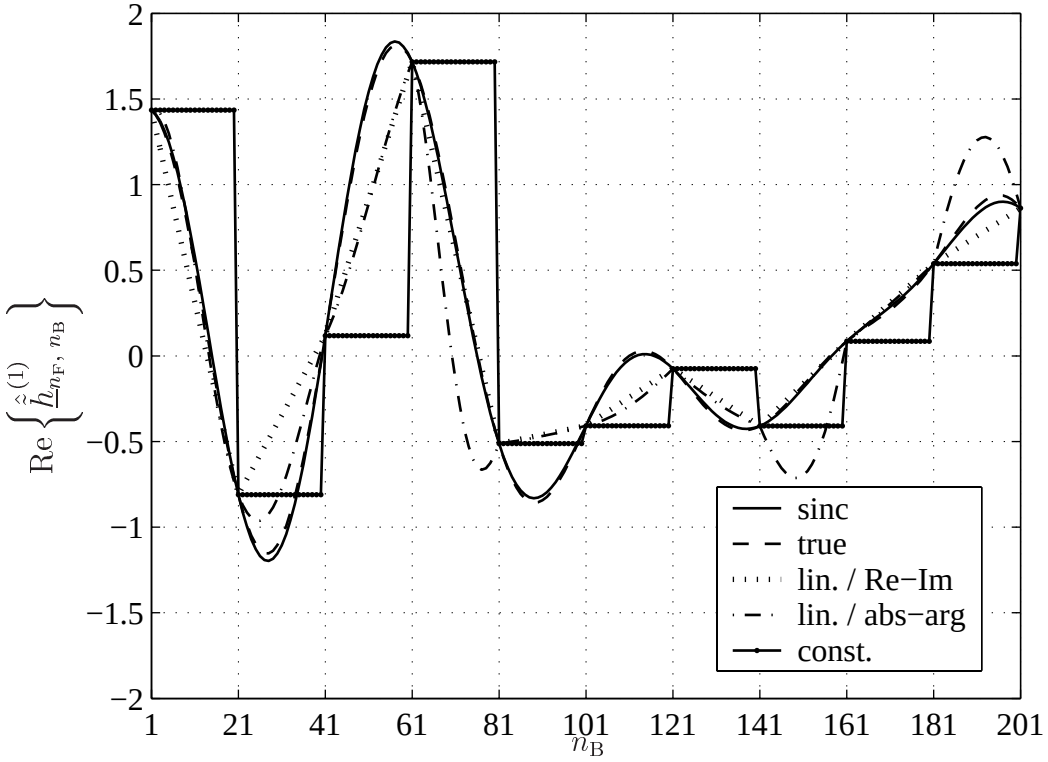

Fig. 7.4. Real part of the interpolated CTF $\hat{\underline{\hat{h}}}^{(1)}_{n_\mathrm{F},\,n_\mathrm{B}}$ in each OFDM symbol slot n_B; $v = 120$ km/h

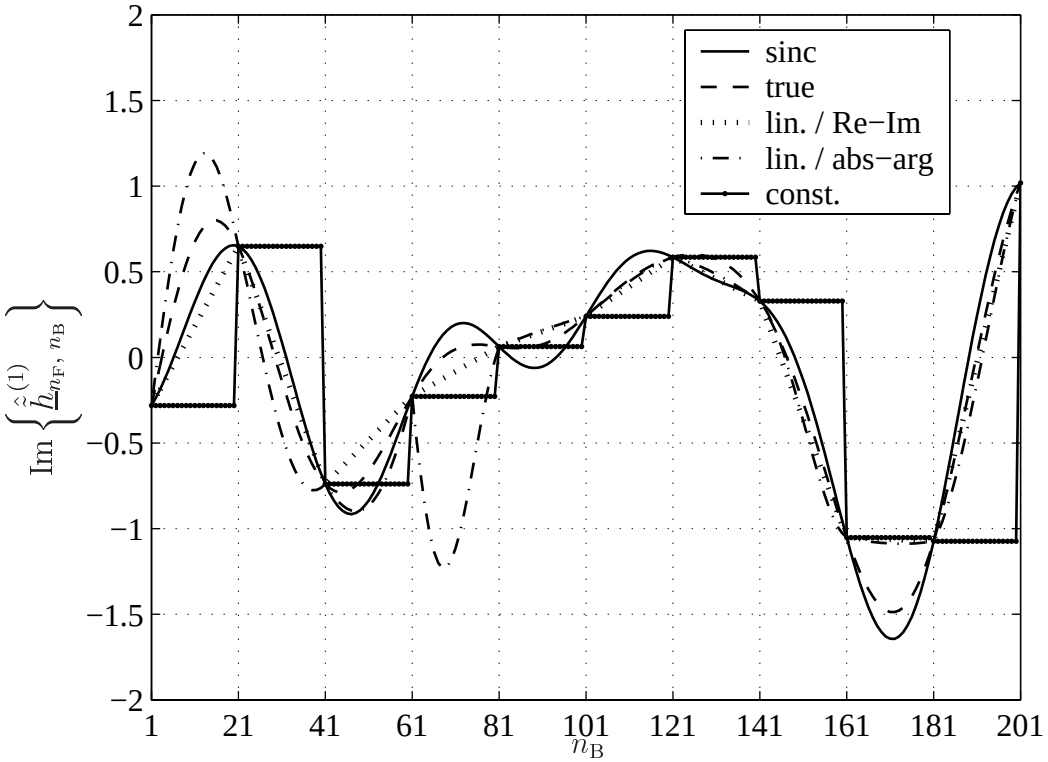

Fig. 7.5. Imaginary part of the interpolated CTF $\hat{\underline{\hat{h}}}^{(1)}_{n_\mathrm{F},\,n_\mathrm{B}}$ in each OFDM symbol slot n_B; $v = 120$ km/h

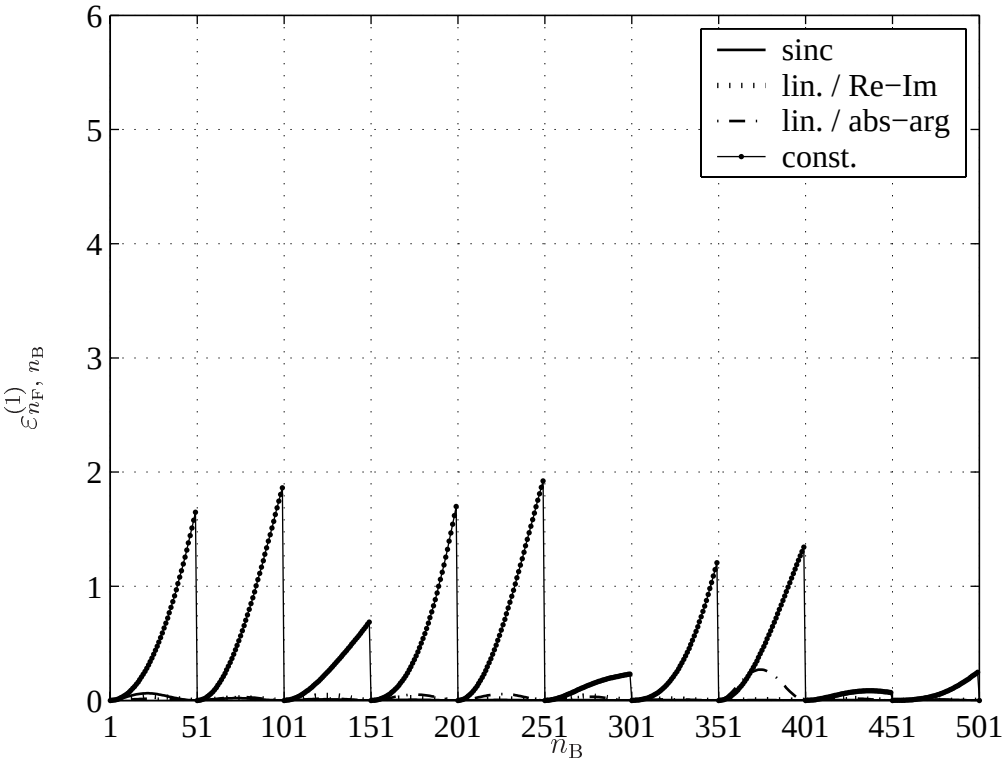

Fig. 7.6. Normalized square error $\varepsilon^{(1)}_{n_\mathrm{F},\,n_\mathrm{B}}$ for subcarrier n_F in each OFDM symbol slot n_B; $v = 25$ km/h

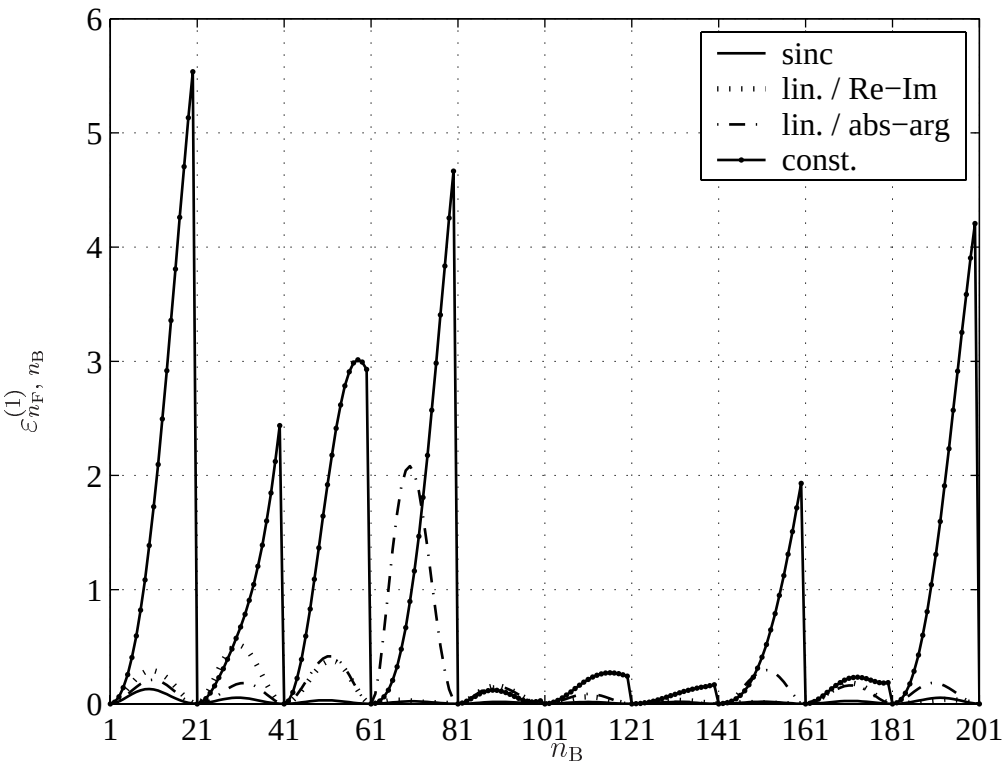

Fig. 7.7. Normalized square error $\varepsilon^{(1)}_{n_\mathrm{F},\,n_\mathrm{B}}$ for subcarrier n_F in each OFDM symbol slot n_B; $v = 120$ km/h

Chapter 8

Impact of non-perfect channel knowledge on JD and JT in JOINT

8.1 JCE error

As mentioned in Section 1.1, in each SA of JOINT the transmission schemes JD and JT [Skl04] are applied in UL and DL, respectively. Both techniques rely on channel knowledge gained in the UL of JOINT by JCE to deliver estimates of the data transmitted from the MTs/APs to the APs/MTs. The investigations conducted and presented in [Skl04] concerning JD and JT in JOINT presuppose perfect channel knowledge available at the CU of the considered SA. However, it is seen in Section 4.4 that, although the applied ML estimator delivers unbiased CTF estimates, these estimates are also corrupted by the presence of noise at the considered AP, see (4.33).

This chapter discusses the impact of non-perfect channel knowledge on the performance of JD and JT in a SA of JOINT. We shall assume that for the short time period elapsing between the application of JCE and JD or JT, respectively, the mobile radio channel is time invariant. For the considerations given in the following the subscripts h and d shall be introduced once more, see Sections 3.3 and 3.4, in order to distinguish between the cases of pilot transmission and data transmission. Let us consider the UL scenario depicted in Fig. 8.1 for the single-element receive antenna case. K MTs are active in the considered SA, each MT radiating the MT-specific pilot vector $\underline{\tilde{\mathbf{p}}}^{(k)}$ of (3.3). The radiated signals reach the considered AP over the respective mobile radio channels characterized by the MT-specific CTFs $\underline{\tilde{\mathbf{h}}}^{(k)}$ of (4.2). At the AP, the noise $\underline{\tilde{\mathbf{n}}}_{\mathrm{h}}$ corrupts the undisturbed receive signal $\underline{\tilde{\mathbf{e}}}_{\mathrm{h}}$ and the noise corrupted receive signal

$$\underline{\tilde{\mathbf{r}}}_{\mathrm{h}} = \underline{\tilde{\mathbf{e}}}_{\mathrm{h}} + \underline{\tilde{\mathbf{n}}}_{\mathrm{h}} = \underline{\tilde{\mathbf{P}}}\,\underline{\tilde{\mathbf{h}}} + \underline{\tilde{\mathbf{n}}}_{\mathrm{h}} \tag{8.1}$$

can be obtained, see also (4.11). $\underline{\tilde{\mathbf{r}}}_{\mathrm{h}}$ of (8.1) is forwarded to the CU. Assuming the components $\underline{\tilde{n}}_{\mathrm{h},n_{\mathrm{F}}}$ of the noise $\underline{\tilde{\mathbf{n}}}_{\mathrm{h}}$ to be uncorrelated, Gaussian with zero mean, variance σ^2 of the real and imaginary parts and the respective covariance matrix $\underline{\mathbf{R}}_{\tilde{\mathbf{n}}_{\mathrm{h}}}$ given by (4.30), and applying ML-JCE as described in Section 4.4, the ML estimate

$$\underline{\hat{\tilde{\mathbf{h}}}} = \underline{\tilde{\mathbf{h}}} + \underline{\tilde{\mathbf{Z}}}_{\mathrm{JCE}}\,\underline{\tilde{\mathbf{n}}}_{\mathrm{h}} = \underline{\tilde{\mathbf{h}}} + \underline{\tilde{\boldsymbol{\mathcal{F}}}}_{\mathrm{W}} \left(\underline{\tilde{\boldsymbol{\mathcal{G}}}}^{\mathsf{H}}\,\underline{\tilde{\boldsymbol{\mathcal{G}}}}\right)^{-1} \underline{\tilde{\boldsymbol{\mathcal{G}}}}^{\mathsf{H}}\,\underline{\tilde{\mathbf{n}}}_{\mathrm{h}} \tag{8.2}$$

of the total CTF $\underline{\tilde{\mathbf{h}}}$ of (4.9) is obtained, see also (4.33). The CTF estimate $\underline{\hat{\tilde{\mathbf{h}}}}$ of (8.2) is unbiased and it is corrupted by the noise term $\underline{\tilde{\mathbf{Z}}}_{\mathrm{JCE}}\,\underline{\tilde{\mathbf{n}}}_{\mathrm{h}}$ termed effective noise. Although AWGN is assumed, this effective noise is in general non-white. From (8.2) the JCE error

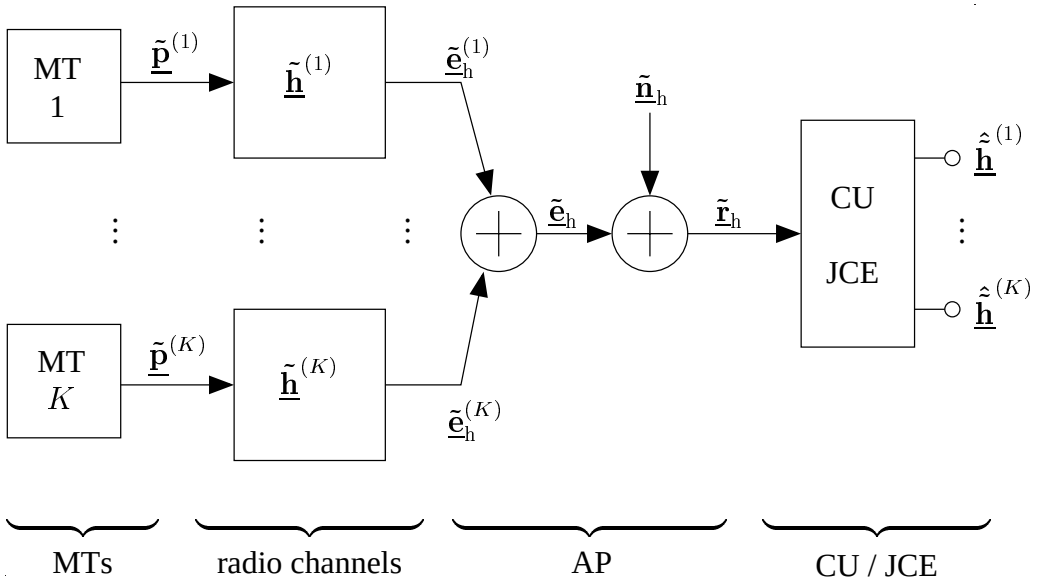

Fig. 8.1. UL channel estimation scenario in the considered SA of JOINT

$$\underline{\tilde{\varepsilon}}_{\mathrm{JCE}} = \left(\underline{\tilde{\varepsilon}}_{\mathrm{JCE}}^{(1)^{\mathrm{T}}} \ \cdots \ \underline{\tilde{\varepsilon}}_{\mathrm{JCE}}^{(K)^{\mathrm{T}}}\right)^{\mathrm{T}} = \underline{\hat{\tilde{\mathrm{h}}}} - \underline{\tilde{\mathrm{h}}} = \underline{\tilde{\boldsymbol{\mathcal{F}}}}_{\mathrm{W}} \left(\underline{\tilde{\boldsymbol{\mathcal{G}}}}^{\mathsf{H}} \underline{\tilde{\boldsymbol{\mathcal{G}}}}\right)^{-1} \underline{\tilde{\boldsymbol{\mathcal{G}}}}^{\mathsf{H}} \, \underline{\tilde{\mathrm{n}}}_{\mathrm{h}} \tag{8.3}$$

can be obtained. For the $(KN_{\mathrm{F}}) \times (KN_{\mathrm{F}})$ covariance matrix $\underline{\mathbf{R}}_{\underline{\tilde{\varepsilon}}_{\mathrm{JCE}}}$ of the JCE error $\underline{\tilde{\varepsilon}}_{\mathrm{JCE}}$ of (8.3)

$$\underline{\mathbf{R}}_{\underline{\tilde{\varepsilon}}_{\mathrm{JCE}}} = \mathrm{E}\left\{\underline{\tilde{\varepsilon}}_{\mathrm{JCE}} \, \underline{\tilde{\varepsilon}}_{\mathrm{JCE}}^{\mathsf{H}}\right\} = 2\sigma^2 \cdot \underline{\tilde{\boldsymbol{\mathcal{F}}}}_{\mathrm{W}} \left(\underline{\tilde{\boldsymbol{\mathcal{G}}}}^{\mathsf{H}} \underline{\tilde{\boldsymbol{\mathcal{G}}}}\right)^{-1} \underline{\tilde{\boldsymbol{\mathcal{F}}}}_{\mathrm{W}}^{\mathsf{H}} \tag{8.4}$$

holds. Applying the ideal pilot vectors based on Walsh codes, see Section 5.5, and assuming (5.1) leads to

$$\underline{\tilde{\boldsymbol{\mathcal{G}}}}^{\mathsf{H}} \underline{\tilde{\boldsymbol{\mathcal{G}}}} = 2E_{\mathrm{p}} \cdot \mathbf{I}^{(KW \times KW)}, \tag{8.5}$$

and with (8.5), (8.4) can be rewritten as

$$\underline{\mathbf{R}}_{\underline{\tilde{\varepsilon}}_{\mathrm{JCE}}} = \frac{\sigma^2}{E_{\mathrm{p}}} \cdot \underline{\tilde{\boldsymbol{\mathcal{F}}}}_{\mathrm{W}} \underline{\tilde{\boldsymbol{\mathcal{F}}}}_{\mathrm{W}}^{\mathsf{H}}. \tag{8.6}$$

$\underline{\mathbf{R}}_{\underline{\tilde{\varepsilon}}_{\mathrm{JCE}}}$ of (8.6) is a blockdiagonal matrix due to the blockdiagonal structure of $\underline{\tilde{\boldsymbol{\mathcal{F}}}}_{\mathrm{W}}$ of (4.21). With (8.6) and (4.39), the variance $\sigma^{(k)^2}_{\underline{\tilde{\varepsilon}}_{\mathrm{JCE}},\, n_{\mathrm{F}}}$ of the JCE error $\underline{\tilde{\varepsilon}}_{\mathrm{JCE}}$ of (8.3) is obtained as

$$\begin{aligned} 2\sigma^{(k)^2}_{\underline{\tilde{\varepsilon}}_{\mathrm{JCE}}, n_{\mathrm{F}}} \quad &= \quad 2\sigma^2_{\underline{\tilde{\varepsilon}}_{\mathrm{JCE}}} = \left[\underline{\mathbf{R}}_{\underline{\tilde{\varepsilon}}_{\mathrm{JCE}}}\right]_{(k-1)N_{\mathrm{F}}+n_{\mathrm{F}},\,(k-1)N_{\mathrm{F}}+n_{\mathrm{F}}} = \frac{\sigma^2 W}{E_{\mathrm{p}}}, \\ &\forall\, k = 1 \ \ldots \ K, \ \forall\, n_{\mathrm{F}} = 1 \ldots N_{\mathrm{F}}. \end{aligned} \tag{8.7}$$

From (8.6) and (8.7) we can conclude that the variance $\sigma^2_{\underline{\tilde{\varepsilon}}_{\mathrm{JCE}}}$ of the JCE error $\underline{\tilde{\varepsilon}}_{\mathrm{JCE}}$ of (8.3) depends on the variance σ^2 of the noise $\underline{\tilde{\mathrm{n}}}_{\mathrm{h}}$ present at the AP, and that the JCE error $\underline{\tilde{\varepsilon}}_{\mathrm{JCE}}$ is zero mean and Gaussian. Further, due to the blockdiagonal structure of the covariance

matrix $\underline{\mathbf{R}}_{\underline{\tilde{\varepsilon}}_{\mathrm{JCE}}}$ of (8.6), which results due to the application of the ideal pilot vectors based on Walsh codes, we can conclude that the JCE errors $\underline{\tilde{\varepsilon}}_{\mathrm{JCE}}^{(k)}$ and $\underline{\tilde{\varepsilon}}_{\mathrm{JCE}}^{(k')}$, $k \neq k'$, are uncorrelated with each other. The application of the ideal pilot vectors based on the approach of disjoint subcarriers and of the ideal pilot vectors based on CAZAC codes, see Chapter 5, also leads to uncorrelatedness between the JCE errors $\underline{\tilde{\varepsilon}}_{\mathrm{JCE}}^{(k)}$ and $\underline{\tilde{\varepsilon}}_{\mathrm{JCE}}^{(k')}$ of two different MTs k and k'.

For each AP k_{B}, $k_{\mathrm{B}} = 1 \ \ldots \ K_{\mathrm{B}}$, in the considered SA of JOINT one vector $\underline{\tilde{\varepsilon}}_{\mathrm{JCE}}$ of the JCE error can be obtained according to (8.3). In the following considerations of the impact of non-perfect channel knowledge on the performance of JD and JT, small JCE errors $\underline{\tilde{\varepsilon}}_{\mathrm{JCE}}$ of (8.3) are assumed, i. e.

$$\left| \underline{\tilde{\varepsilon}}_{\mathrm{JCE},n_{\mathrm{F}}}^{(k,k_{\mathrm{B}})} \right|^2 \approx 0 \tag{8.8}$$

holds for the absolute square value of the component $\underline{\tilde{\varepsilon}}_{\mathrm{JCE},n_{\mathrm{F}}}^{(k,k_{\mathrm{B}})}$ of the JCE error of MT k at AP k_{B} and subcarrier n_{F}.

8.2 Impact of the JCE error on the performance of JD

8.2.1 JD error

For the investigations presented in this subsection, the case of UL data transmission in the considered SA of JOINT illustrated in Fig. 3.2 shall be considered. Each MT k, $k = 1 \ \ldots \ K$, radiates the MT-specific data vector $\underline{\tilde{\mathbf{d}}}^{(k)}$ of (3.10). The K radiated signals reach the K_{B} APs of the SA over the respective radio channels represented by the CTFs $\underline{\tilde{\mathbf{h}}}^{(k,\,k_{\mathrm{B}})}$ of (3.2). Along with the noise $\underline{\tilde{\mathbf{n}}}_{\mathrm{d}}^{(k_{\mathrm{B}})}$ of (3.13) present at AP k_{B}, the radiated signals introduce the AP-specific noise corrupted received signal $\underline{\tilde{\mathbf{r}}}_{\mathrm{d}}^{(k_{\mathrm{B}})}$ of (3.14) at AP k_{B}. All K_{B} signals $\underline{\tilde{\mathbf{r}}}_{\mathrm{d}}^{(k_{\mathrm{B}})}$ are forwarded to the CU, which now has the task to determine estimates $\underline{\hat{\tilde{\mathbf{d}}}}^{(k)}$ of the MT-specific data vectors $\underline{\tilde{\mathbf{d}}}^{(k)}$ of (3.10). To this end, the CU applies JD exploiting the knowledge of the modulation alphabet, the estimated CTFs $\underline{\hat{\tilde{\mathbf{h}}}}^{(k,\,k_{\mathrm{B}})}$ of (3.9) and the AP-specific noise corrupted receive signals $\underline{\tilde{\mathbf{r}}}_{\mathrm{d}}^{(k_{\mathrm{B}})}$ of (3.14) [Skl04].

Stacking all KK_{B} CTFs $\underline{\tilde{\mathbf{h}}}^{(k,\,k_{\mathrm{B}})}$ to form the total channel matrix

$$\underline{\tilde{\mathbf{H}}} = \begin{pmatrix} \mathrm{diag}\left(\underline{\tilde{\mathbf{h}}}^{(1,1)}\right) & \cdots & \mathrm{diag}\left(\underline{\tilde{\mathbf{h}}}^{(K,1)}\right) \\ \vdots & & \vdots \\ \mathrm{diag}\left(\underline{\tilde{\mathbf{h}}}^{(1,K_{\mathrm{B}})}\right) & \cdots & \mathrm{diag}\left(\underline{\tilde{\mathbf{h}}}^{(K,K_{\mathrm{B}})}\right) \end{pmatrix} \tag{8.9}$$

of dimension $(K_{\mathrm{B}}N_{\mathrm{F}}) \times (KN_{\mathrm{F}})$ together with the total data vector

$$\underline{\tilde{\mathbf{d}}} = \left(\underline{\tilde{\mathbf{d}}}^{(1)^{\mathrm{T}}} \ \ldots \ \underline{\tilde{\mathbf{d}}}^{(K)^{\mathrm{T}}} \right)^{\mathrm{T}} \tag{8.10}$$

of dimension KN_{F} and the total noise vector

$$\underline{\tilde{\mathbf{n}}}_{\mathrm{d}} = \left(\underline{\tilde{\mathbf{n}}}_{\mathrm{d}}^{(1)^{\mathrm{T}}} \ \ldots \ \underline{\tilde{\mathbf{n}}}_{\mathrm{d}}^{(K_{\mathrm{B}})^{\mathrm{T}}} \right)^{\mathrm{T}} \tag{8.11}$$

of dimension$K_{\mathrm{B}}N_{\mathrm{F}}$, the total noise corrupted receive signal

$$\underline{\tilde{\mathbf{r}}}_{\mathrm{d}} = \underline{\tilde{\mathbf{H}}}\, \underline{\tilde{\mathbf{d}}} + \ \underline{\tilde{\mathbf{n}}}_{\mathrm{d}} \tag{8.12}$$

of dimension$K_{\mathrm{B}}N_{\mathrm{F}}$ can be obtained. With the JD matrix $\underline{\tilde{\mathbf{Z}}}_{\mathrm{JD}}$ of dimension $(KN_{\mathrm{F}}) \times (K_{\mathrm{B}}N_{\mathrm{F}})$ the estimate

$$\underline{\hat{\tilde{\mathbf{d}}}} = \underline{\tilde{\mathbf{Z}}}_{\mathrm{JD}}\ \underline{\tilde{\mathbf{r}}}_{\mathrm{d}} \tag{8.13}$$

of the total data $\underline{\tilde{\mathbf{d}}}$ of (8.10) results at the JD output.

As explained in [Skl04], due to the application of OFDM, JD can be performed subcarrier-wise, thus relaxing the computational complexity behind the calculation of the JD matrix $\underline{\tilde{\mathbf{Z}}}_{\mathrm{JD}}$. Introducing the subcarrier specific channel matrix

$$\underline{\tilde{\mathbf{H}}}_{n_{\mathrm{F}}} = \begin{pmatrix} \underline{\tilde{h}}_{n_{\mathrm{F}}}^{(1,1)} & \cdots & \underline{\tilde{h}}_{n_{\mathrm{F}}}^{(K,1)} \\ \vdots & & \vdots \\ \underline{\tilde{h}}_{n_{\mathrm{F}}}^{(1,K_{\mathrm{B}})} & \cdots & \underline{\tilde{h}}_{n_{\mathrm{F}}}^{(K,K_{\mathrm{B}})} \end{pmatrix} \tag{8.14}$$

of dimension $K_{\mathrm{B}} \times K$ containing the respective CTF components $\underline{\tilde{h}}_{n_{\mathrm{F}}}^{(k,k_{\mathrm{B}})}$ on subcarrier n_{F} together with the subcarrier specific data vector

$$\underline{\tilde{\mathbf{d}}}_{n_{\mathrm{F}}} = \left(\underline{\tilde{d}}_{n_{\mathrm{F}}}^{(1)} \ \ldots \ \underline{\tilde{d}}_{n_{\mathrm{F}}}^{(K)} \right)^{\mathrm{T}} \tag{8.15}$$

of dimension K and the subcarrier specific noise vector

$$\underline{\tilde{\mathbf{n}}}_{\mathrm{d},n_{\mathrm{F}}} = \left(\underline{\tilde{n}}_{\mathrm{d},n_{\mathrm{F}}}^{(1)} \ \ldots \ \underline{\tilde{n}}_{\mathrm{d},n_{\mathrm{F}}}^{(K_{\mathrm{B}})} \right)^{\mathrm{T}} \tag{8.16}$$

of dimensionK_{B}, the subcarrier-wise representation of the noise corrupted receive signal yields

$$\underline{\tilde{\mathbf{r}}}_{\mathrm{d},n_{\mathrm{F}}} = \underline{\tilde{\mathbf{H}}}_{n_{\mathrm{F}}} \underline{\tilde{\mathbf{d}}}_{n_{\mathrm{F}}} + \ \underline{\tilde{\mathbf{n}}}_{\mathrm{d},n_{\mathrm{F}}}. \tag{8.17}$$

Assuming AWGN, see Section 8.1, and introducing the subcarrier specific JD matrix [Skl04]

$$\underline{\tilde{\mathbf{Z}}}_{\mathrm{JD},n_{\mathrm{F}}} = \left(\underline{\hat{\tilde{\mathbf{H}}}}_{n_{\mathrm{F}}}^{\mathsf{H}} \underline{\hat{\tilde{\mathbf{H}}}}_{n_{\mathrm{F}}} \right)^{-1} \underline{\hat{\tilde{\mathbf{H}}}}_{n_{\mathrm{F}}}^{\mathsf{H}} \tag{8.18}$$

of dimension $K \times K_{\mathrm{B}}$ containing the estimated subcarrier specific channel matrix $\underline{\hat{\tilde{\mathbf{H}}}}_{n_{\mathrm{F}}}$, the ML estimate [Skl04]

$$\underline{\hat{\tilde{\mathbf{d}}}}_{n_{\mathrm{F}}} = \underline{\tilde{\mathbf{Z}}}_{\mathrm{JD},n_{\mathrm{F}}}\, \underline{\tilde{\mathbf{r}}}_{\mathrm{d},n_{\mathrm{F}}} = \left(\underline{\hat{\tilde{\mathbf{H}}}}_{n_{\mathrm{F}}}^{\mathsf{H}} \underline{\hat{\tilde{\mathbf{H}}}}_{n_{\mathrm{F}}}\right)^{-1} \underline{\hat{\tilde{\mathbf{H}}}}_{n_{\mathrm{F}}}^{\mathsf{H}} \left(\underline{\tilde{\mathbf{H}}}_{n_{\mathrm{F}}} \underline{\tilde{\mathbf{d}}}_{n_{\mathrm{F}}} + \underline{\tilde{\mathbf{n}}}_{\mathrm{d},n_{\mathrm{F}}}\right) \tag{8.19}$$

of the subcarrier specific data vector $\underline{\tilde{\mathbf{d}}}_{n_{\mathrm{F}}}$ of (8.15) is obtained.

In the case of perfect channel knowledge and analogously to ML-JCE, see (4.33), the unbiased estimate $\underline{\hat{\tilde{\mathbf{d}}}}_{n_{\mathrm{F}}}$ of (8.19) is corrupted by the effective noise $\underline{\tilde{\mathbf{Z}}}_{\mathrm{JD},n_{\mathrm{F}}}\, \underline{\tilde{\mathbf{n}}}_{\mathrm{d},n_{\mathrm{F}}}$. Due to the presence of JCE errors, see Section 8.1, the estimate of the subcarrier specific channel matrix $\underline{\hat{\tilde{\mathbf{H}}}}_{n_{\mathrm{F}}}$ of (8.18) consists of the true subcarrier specific channel matrix $\underline{\tilde{\mathbf{H}}}_{n_{\mathrm{F}}}$ of (8.14) plus the matrix

$$\underline{\tilde{\mathbf{E}}}_{n_{\mathrm{F}}} = \begin{pmatrix} \underline{\tilde{\varepsilon}}_{\mathrm{JCE},n_{\mathrm{F}}}^{(1,1)} & \cdots & \underline{\tilde{\varepsilon}}_{\mathrm{JCE},n_{\mathrm{F}}}^{(K,1)} \\ \vdots & & \vdots \\ \underline{\tilde{\varepsilon}}_{\mathrm{JCE},n_{\mathrm{F}}}^{(1,K_{\mathrm{B}})} & \cdots & \underline{\tilde{\varepsilon}}_{\mathrm{JCE},n_{\mathrm{F}}}^{(K,K_{\mathrm{B}})} \end{pmatrix} \tag{8.20}$$

containing the respective components $\underline{\tilde{\varepsilon}}_{\mathrm{JCE},n_{\mathrm{F}}}^{(k,k_{\mathrm{B}})}$ of the JCE error $\underline{\tilde{\boldsymbol{\varepsilon}}}_{\mathrm{JCE}}$ of (8.3) on subcarrier n_{F}, i. e.

$$\underline{\hat{\tilde{\mathbf{H}}}}_{n_{\mathrm{F}}} = \underline{\tilde{\mathbf{H}}}_{n_{\mathrm{F}}} + \underline{\tilde{\mathbf{E}}}_{n_{\mathrm{F}}} \tag{8.21}$$

holds. With (8.21), (8.19) now reads

$$\underline{\hat{\tilde{\mathbf{d}}}}_{n_{\mathrm{F}}} = \left[\left(\underline{\tilde{\mathbf{H}}}_{n_{\mathrm{F}}} + \underline{\tilde{\mathbf{E}}}_{n_{\mathrm{F}}}\right)^{\mathsf{H}} \left(\underline{\tilde{\mathbf{H}}}_{n_{\mathrm{F}}} + \underline{\tilde{\mathbf{E}}}_{n_{\mathrm{F}}}\right)\right]^{-1} \left(\underline{\tilde{\mathbf{H}}}_{n_{\mathrm{F}}} + \underline{\tilde{\mathbf{E}}}_{n_{\mathrm{F}}}\right)^{\mathsf{H}} \cdot \left(\underline{\tilde{\mathbf{H}}}_{n_{\mathrm{F}}} \underline{\tilde{\mathbf{d}}}_{n_{\mathrm{F}}} + \underline{\tilde{\mathbf{n}}}_{\mathrm{d},n_{\mathrm{F}}}\right), \tag{8.22}$$

and from (8.22) we can obtain the subcarrier specific JD error

$$\begin{aligned}
\underline{\tilde{\boldsymbol{\varepsilon}}}_{\mathrm{JD},n_{\mathrm{F}}} &= \left(\underline{\tilde{\varepsilon}}_{\mathrm{JD},n_{\mathrm{F}}}^{(1)} \ \cdots \ \underline{\tilde{\varepsilon}}_{\mathrm{JD},n_{\mathrm{F}}}^{(K)}\right)^{\mathrm{T}} = \underline{\hat{\tilde{\mathbf{d}}}}_{n_{\mathrm{F}}} - \underline{\tilde{\mathbf{d}}}_{n_{\mathrm{F}}} \qquad (8.23)\\
&= \left[\left(\underline{\tilde{\mathbf{H}}}_{n_{\mathrm{F}}}^{\mathsf{H}} + \underline{\tilde{\mathbf{E}}}_{n_{\mathrm{F}}}^{\mathsf{H}}\right)\left(\underline{\tilde{\mathbf{H}}}_{n_{\mathrm{F}}} + \underline{\tilde{\mathbf{E}}}_{n_{\mathrm{F}}}\right)\right]^{-1} \left(\underline{\tilde{\mathbf{H}}}_{n_{\mathrm{F}}}^{\mathsf{H}} + \underline{\tilde{\mathbf{E}}}_{n_{\mathrm{F}}}^{\mathsf{H}}\right) \cdot \left(\underline{\tilde{\mathbf{H}}}_{n_{\mathrm{F}}} \underline{\tilde{\mathbf{d}}}_{n_{\mathrm{F}}} + \underline{\tilde{\mathbf{n}}}_{\mathrm{d},n_{\mathrm{F}}}\right) - \underline{\tilde{\mathbf{d}}}_{n_{\mathrm{F}}}\\
&= \left[\left(\underline{\tilde{\mathbf{H}}}_{n_{\mathrm{F}}}^{\mathsf{H}} + \underline{\tilde{\mathbf{E}}}_{n_{\mathrm{F}}}^{\mathsf{H}}\right)\left(\underline{\tilde{\mathbf{H}}}_{n_{\mathrm{F}}} + \underline{\tilde{\mathbf{E}}}_{n_{\mathrm{F}}}\right)\right]^{-1} \left(\underline{\tilde{\mathbf{H}}}_{n_{\mathrm{F}}}^{\mathsf{H}} + \underline{\tilde{\mathbf{E}}}_{n_{\mathrm{F}}}^{\mathsf{H}}\right) \cdot \left(\underline{\tilde{\mathbf{H}}}_{n_{\mathrm{F}}} \underline{\tilde{\mathbf{d}}}_{n_{\mathrm{F}}} + \underline{\tilde{\mathbf{n}}}_{\mathrm{d},n_{\mathrm{F}}}\right) -\\
&\quad \underbrace{\left[\left(\underline{\tilde{\mathbf{H}}}_{n_{\mathrm{F}}}^{\mathsf{H}} + \underline{\tilde{\mathbf{E}}}_{n_{\mathrm{F}}}^{\mathsf{H}}\right)\left(\underline{\tilde{\mathbf{H}}}_{n_{\mathrm{F}}} + \underline{\tilde{\mathbf{E}}}_{n_{\mathrm{F}}}\right)\right]^{-1} \left(\underline{\tilde{\mathbf{H}}}_{n_{\mathrm{F}}}^{\mathsf{H}} + \underline{\tilde{\mathbf{E}}}_{n_{\mathrm{F}}}^{\mathsf{H}}\right)\left(\underline{\tilde{\mathbf{H}}}_{n_{\mathrm{F}}} + \underline{\tilde{\mathbf{E}}}_{n_{\mathrm{F}}}\right)}_{\mathbf{I}^{(K\times K)}} \underline{\tilde{\mathbf{d}}}_{n_{\mathrm{F}}}\\
&= \left[\left(\underline{\tilde{\mathbf{H}}}_{n_{\mathrm{F}}}^{\mathsf{H}} + \underline{\tilde{\mathbf{E}}}_{n_{\mathrm{F}}}^{\mathsf{H}}\right)\left(\underline{\tilde{\mathbf{H}}}_{n_{\mathrm{F}}} + \underline{\tilde{\mathbf{E}}}_{n_{\mathrm{F}}}\right)\right]^{-1} \left(\underline{\tilde{\mathbf{H}}}_{n_{\mathrm{F}}}^{\mathsf{H}} + \underline{\tilde{\mathbf{E}}}_{n_{\mathrm{F}}}^{\mathsf{H}}\right) \left(-\underline{\tilde{\mathbf{E}}}_{n_{\mathrm{F}}} \underline{\tilde{\mathbf{d}}}_{n_{\mathrm{F}}} + \underline{\tilde{\mathbf{n}}}_{\mathrm{d},n_{\mathrm{F}}}\right)\\
&= -\underline{\tilde{\mathbf{Z}}}_{\mathrm{JD},n_{\mathrm{F}}} \underline{\tilde{\mathbf{E}}}_{n_{\mathrm{F}}} \underline{\tilde{\mathbf{d}}}_{n_{\mathrm{F}}} + \underline{\tilde{\mathbf{Z}}}_{\mathrm{JD},n_{\mathrm{F}}}\, \underline{\tilde{\mathbf{n}}}_{\mathrm{d},n_{\mathrm{F}}}.
\end{aligned}$$

We can see from (8.23) that $\underline{\tilde{\boldsymbol{\varepsilon}}}_{\mathrm{JD},n_{\mathrm{F}}}$ depends on the noise $\underline{\tilde{\mathbf{n}}}_{\mathrm{d},n_{\mathrm{F}}}$ present in the considered SA, and that it is a non linear function of the components $\underline{\tilde{\varepsilon}}_{\mathrm{JCE},n_{\mathrm{F}}}^{(k,k_{\mathrm{B}})}$ of the subcarrier specific JCE error matrix $\underline{\tilde{\mathbf{E}}}_{n_{\mathrm{F}}}$ of (8.20).

For the considered case of small JCE errors, see (8.8), the non linear terms of the subcarrier specific JD error $\underline{\tilde{\varepsilon}}_{\mathrm{JD},n_\mathrm{F}}$ of (8.23) can be approximated by a linear Taylor expansion [MW03, MW04]. The development point of the Taylor series will be chosen as

$$\underline{\tilde{\mathbf{E}}}_{n_\mathrm{F}} = \mathbf{0}, \tag{8.24}$$

and the Taylor series shall be truncated after the linear terms. This truncation will not have a significant impact on the quality of the approximation, since small channel estimation errors are considered, see (8.8). With (8.24) and said truncation, the matrix product $\underline{\tilde{\mathbf{Z}}}_{\mathrm{JD},n_\mathrm{F}}\underline{\tilde{\mathbf{E}}}_{n_\mathrm{F}}$ of (8.23) can be approximated by

$$\underline{\tilde{\mathbf{Z}}}_{\mathrm{JD},n_\mathrm{F}}\underline{\tilde{\mathbf{E}}}_{n_\mathrm{F}} \approx \underbrace{\underline{\tilde{\mathbf{Z}}}_{\mathrm{JD},n_\mathrm{F}}\underline{\tilde{\mathbf{E}}}_{n_\mathrm{F}}\Big|_{\underline{\tilde{\mathbf{E}}}_{n_\mathrm{F}}=\mathbf{0}}}_{=\mathbf{0}} + \tag{8.25}$$

$$\sum_{\forall\, i}\sum_{\forall\, j}\left[\frac{\partial\left(\underline{\tilde{\mathbf{Z}}}_{\mathrm{JD},n_\mathrm{F}}\underline{\tilde{\mathbf{E}}}_{n_\mathrm{F}}\right)}{\partial\mathrm{Re}\left\{\left[\underline{\tilde{\mathbf{E}}}_{n_\mathrm{F}}\right]_{i,j}\right\}}\Bigg|_{\underline{\tilde{\mathbf{E}}}_{n_\mathrm{F}}=\mathbf{0}}\mathrm{Re}\left\{\left[\underline{\tilde{\mathbf{E}}}_{n_\mathrm{F}}\right]_{i,j}\right\} + \mathrm{j}\frac{\partial\left(\underline{\tilde{\mathbf{Z}}}_{\mathrm{JD},n_\mathrm{F}}\underline{\tilde{\mathbf{E}}}_{n_\mathrm{F}}\right)}{\partial\mathrm{Im}\left\{\left[\underline{\tilde{\mathbf{E}}}_{n_\mathrm{F}}\right]_{i,j}\right\}}\Bigg|_{\underline{\tilde{\mathbf{E}}}_{n_\mathrm{F}}=\mathbf{0}}\mathrm{Im}\left\{\left[\underline{\tilde{\mathbf{E}}}_{n_\mathrm{F}}\right]_{i,j}\right\}\right],$$

$$i = 1\ \ldots\ K_\mathrm{B},\ j = 1\ \ldots\ K.$$

With the notation

$$\mathbf{1}_{i,j} = (\alpha_{\mu,\nu}) = \begin{cases} 1 & \text{for } \mu = i \wedge \nu = j, \\ 0 & \text{else}, \end{cases} \tag{8.26}$$

the derivatives in (8.25) yield

$$\frac{\partial\left(\underline{\tilde{\mathbf{Z}}}_{\mathrm{JD},n_\mathrm{F}}\underline{\tilde{\mathbf{E}}}_{n_\mathrm{F}}\right)}{\partial\mathrm{Re}\left\{\left[\underline{\tilde{\mathbf{E}}}_{n_\mathrm{F}}\right]_{i,j}\right\}}\Bigg|_{\underline{\tilde{\mathbf{E}}}_{n_\mathrm{F}}=\mathbf{0}} + \mathrm{j}\,\frac{\partial\left(\underline{\tilde{\mathbf{Z}}}_{\mathrm{JD},n_\mathrm{F}}\underline{\tilde{\mathbf{E}}}_{n_\mathrm{F}}\right)}{\partial\mathrm{Im}\left\{\left[\underline{\tilde{\mathbf{E}}}_{n_\mathrm{F}}\right]_{i,j}\right\}}\Bigg|_{\underline{\tilde{\mathbf{E}}}_{n_\mathrm{F}}=\mathbf{0}} = \tag{8.27}$$

$$\frac{\partial\left[\left(\underline{\tilde{\mathbf{H}}}^{\mathsf{H}}_{n_\mathrm{F}} + \underline{\tilde{\mathbf{E}}}^{\mathsf{H}}_{n_\mathrm{F}}\right)\left(\underline{\tilde{\mathbf{H}}}_{n_\mathrm{F}} + \underline{\tilde{\mathbf{E}}}_{n_\mathrm{F}}\right)\right]^{-1}}{\partial\mathrm{Re}\left\{\left[\underline{\tilde{\mathbf{E}}}_{n_\mathrm{F}}\right]_{i,j}\right\}}\cdot\left(\underline{\tilde{\mathbf{H}}}^{\mathsf{H}}_{n_\mathrm{F}} + \underline{\tilde{\mathbf{E}}}^{\mathsf{H}}_{n_\mathrm{F}}\right)\underline{\tilde{\mathbf{E}}}_{n_\mathrm{F}}\Bigg|_{\underline{\tilde{\mathbf{E}}}_{n_\mathrm{F}}=\mathbf{0}} +$$

$$\left[\left(\underline{\tilde{\mathbf{H}}}^{\mathsf{H}}_{n_\mathrm{F}} + \underline{\tilde{\mathbf{E}}}^{\mathsf{H}}_{n_\mathrm{F}}\right)\left(\underline{\tilde{\mathbf{H}}}_{n_\mathrm{F}} + \underline{\tilde{\mathbf{E}}}_{n_\mathrm{F}}\right)\right]^{-1}\cdot\frac{\partial\left(\underline{\tilde{\mathbf{H}}}^{\mathsf{H}}_{n_\mathrm{F}} + \underline{\tilde{\mathbf{E}}}^{\mathsf{H}}_{n_\mathrm{F}}\right)\cdot\underline{\tilde{\mathbf{E}}}_{n_\mathrm{F}}}{\partial\mathrm{Re}\left\{\left[\underline{\tilde{\mathbf{E}}}_{n_\mathrm{F}}\right]_{i,j}\right\}}\Bigg|_{\underline{\tilde{\mathbf{E}}}_{n_\mathrm{F}}=\mathbf{0}} +$$

$$\mathrm{j}\,\frac{\partial\left[\left(\underline{\tilde{\mathbf{H}}}_{n_\mathrm{F}}^{\mathsf{H}}+\underline{\tilde{\mathbf{E}}}_{n_\mathrm{F}}^{\mathsf{H}}\right)\left(\underline{\tilde{\mathbf{H}}}_{n_\mathrm{F}}+\underline{\tilde{\mathbf{E}}}_{n_\mathrm{F}}\right)\right]^{-1}}{\partial\mathrm{Im}\left\{\left[\underline{\tilde{\mathbf{E}}}_{n_\mathrm{F}}\right]_{i,j}\right\}}\cdot\left(\underline{\tilde{\mathbf{H}}}_{n_\mathrm{F}}^{\mathsf{H}}+\underline{\tilde{\mathbf{E}}}_{n_\mathrm{F}}^{\mathsf{H}}\right)\underline{\tilde{\mathbf{E}}}_{n_\mathrm{F}}\Bigg|_{\underline{\tilde{\mathbf{E}}}_{n_\mathrm{F}}=\mathbf{0}}+$$

$$\mathrm{j}\left[\left(\underline{\tilde{\mathbf{H}}}_{n_\mathrm{F}}^{\mathsf{H}}+\underline{\tilde{\mathbf{E}}}_{n_\mathrm{F}}^{\mathsf{H}}\right)\left(\underline{\tilde{\mathbf{H}}}_{n_\mathrm{F}}+\underline{\tilde{\mathbf{E}}}_{n_\mathrm{F}}\right)\right]^{-1}\cdot\frac{\partial\left(\underline{\tilde{\mathbf{H}}}_{n_\mathrm{F}}^{\mathsf{H}}+\underline{\tilde{\mathbf{E}}}_{n_\mathrm{F}}^{\mathsf{H}}\right)\cdot\underline{\tilde{\mathbf{E}}}_{n_\mathrm{F}}}{\partial\mathrm{Im}\left\{\left[\underline{\tilde{\mathbf{E}}}_{n_\mathrm{F}}\right]_{i,j}\right\}}\Bigg|_{\underline{\tilde{\mathbf{E}}}_{n_\mathrm{F}}=\mathbf{0}}=$$

$$\mathbf{0}+\left(\underline{\tilde{\mathbf{H}}}_{n_\mathrm{F}}^{\mathsf{H}}\underline{\tilde{\mathbf{H}}}_{n_\mathrm{F}}\right)^{-1}\cdot\left[\frac{\partial\left(\underline{\tilde{\mathbf{H}}}_{n_\mathrm{F}}^{\mathsf{H}}+\underline{\tilde{\mathbf{E}}}_{n_\mathrm{F}}^{\mathsf{H}}\right)}{\partial\mathrm{Re}\left\{\left[\underline{\tilde{\mathbf{E}}}_{n_\mathrm{F}}\right]_{i,j}\right\}}\cdot\underline{\tilde{\mathbf{E}}}_{n_\mathrm{F}}+\left(\underline{\tilde{\mathbf{H}}}_{n_\mathrm{F}}^{\mathsf{H}}+\underline{\tilde{\mathbf{E}}}_{n_\mathrm{F}}^{\mathsf{H}}\right)\cdot\frac{\partial\underline{\tilde{\mathbf{E}}}_{n_\mathrm{F}}}{\partial\mathrm{Re}\left\{\left[\underline{\tilde{\mathbf{E}}}_{n_\mathrm{F}}\right]_{i,j}\right\}}\right]\Bigg|_{\underline{\tilde{\mathbf{E}}}_{n_\mathrm{F}}=\mathbf{0}}+$$

$$\mathrm{j}\mathbf{0}+\mathrm{j}\left(\underline{\tilde{\mathbf{H}}}_{n_\mathrm{F}}^{\mathsf{H}}\underline{\tilde{\mathbf{H}}}_{n_\mathrm{F}}\right)^{-1}\cdot\left[\frac{\partial\left(\underline{\tilde{\mathbf{H}}}_{n_\mathrm{F}}^{\mathsf{H}}+\underline{\tilde{\mathbf{E}}}_{n_\mathrm{F}}^{\mathsf{H}}\right)}{\partial\mathrm{Im}\left\{\left[\underline{\tilde{\mathbf{E}}}_{n_\mathrm{F}}\right]_{i,j}\right\}}\cdot\underline{\tilde{\mathbf{E}}}_{n_\mathrm{F}}+\left(\underline{\tilde{\mathbf{H}}}_{n_\mathrm{F}}^{\mathsf{H}}+\underline{\tilde{\mathbf{E}}}_{n_\mathrm{F}}^{\mathsf{H}}\right)\cdot\frac{\partial\underline{\tilde{\mathbf{E}}}_{n_\mathrm{F}}}{\partial\mathrm{Im}\left\{\left[\underline{\tilde{\mathbf{E}}}_{n_\mathrm{F}}\right]_{i,j}\right\}}\right]\Bigg|_{\underline{\tilde{\mathbf{E}}}_{n_\mathrm{F}}=\mathbf{0}}=$$

$$\left(\underline{\tilde{\mathbf{H}}}_{n_\mathrm{F}}^{\mathsf{H}}\underline{\tilde{\mathbf{H}}}_{n_\mathrm{F}}\right)^{-1}\cdot\left[\mathbf{0}+\underline{\tilde{\mathbf{H}}}_{n_\mathrm{F}}^{\mathsf{H}}\mathrm{Re}\left\{\mathbf{1}_{i,j}\right\}\right]+\mathrm{j}\left(\underline{\tilde{\mathbf{H}}}_{n_\mathrm{F}}^{\mathsf{H}}\underline{\tilde{\mathbf{H}}}_{n_\mathrm{F}}\right)^{-1}\cdot\left[\mathbf{0}+\underline{\tilde{\mathbf{H}}}_{n_\mathrm{F}}^{\mathsf{H}}\mathrm{Im}\left\{\mathbf{1}_{i,j}\right\}\right]=$$

$$\left(\underline{\tilde{\mathbf{H}}}_{n_\mathrm{F}}^{\mathsf{H}}\underline{\tilde{\mathbf{H}}}_{n_\mathrm{F}}\right)^{-1}\underline{\tilde{\mathbf{H}}}_{n_\mathrm{F}}^{\mathsf{H}}\cdot\mathbf{1}_{i,j}.$$

With (8.27) the matrix product $\underline{\tilde{\mathbf{Z}}}_{\mathrm{JD},n_\mathrm{F}}\underline{\tilde{\mathbf{E}}}_{n_\mathrm{F}}$ of (8.25) can be approximated by

$$\underline{\tilde{\mathbf{Z}}}_{\mathrm{JD},n_\mathrm{F}}\underline{\tilde{\mathbf{E}}}_{n_\mathrm{F}}\approx\left(\underline{\tilde{\mathbf{H}}}_{n_\mathrm{F}}^{\mathsf{H}}\underline{\tilde{\mathbf{H}}}_{n_\mathrm{F}}\right)^{-1}\underline{\tilde{\mathbf{H}}}_{n_\mathrm{F}}^{\mathsf{H}}\cdot\underline{\tilde{\mathbf{E}}}_{n_\mathrm{F}}. \tag{8.28}$$

The subcarrier specific JD matrix $\underline{\tilde{\mathbf{Z}}}_{\mathrm{JD},n_\mathrm{F}}$ can be approximated analogously:

$$\underline{\tilde{\mathbf{Z}}}_{\mathrm{JD},n_\mathrm{F}}\approx\underline{\tilde{\mathbf{Z}}}_{\mathrm{JD},n_\mathrm{F}}\Big|_{\underline{\tilde{\mathbf{E}}}_{n_\mathrm{F}}=\mathbf{0}}+ \tag{8.29}$$

$$\sum_{\forall\,i}\sum_{\forall\,j}\left[\frac{\partial\left(\underline{\tilde{\mathbf{Z}}}_{\mathrm{JD},n_\mathrm{F}}\right)}{\partial\mathrm{Re}\left\{\left[\underline{\tilde{\mathbf{E}}}_{n_\mathrm{F}}\right]_{i,j}\right\}}\Bigg|_{\underline{\tilde{\mathbf{E}}}_{n_\mathrm{F}}=\mathbf{0}}\mathrm{Re}\left\{\left[\underline{\tilde{\mathbf{E}}}_{n_\mathrm{F}}\right]_{i,j}\right\}+\mathrm{j}\frac{\partial\left(\underline{\tilde{\mathbf{Z}}}_{\mathrm{JD},n_\mathrm{F}}\right)}{\partial\mathrm{Im}\left\{\left[\underline{\tilde{\mathbf{E}}}_{n_\mathrm{F}}\right]_{i,j}\right\}}\Bigg|_{\underline{\tilde{\mathbf{E}}}_{n_\mathrm{F}}=\mathbf{0}}\mathrm{Im}\left\{\left[\underline{\tilde{\mathbf{E}}}_{n_\mathrm{F}}\right]_{i,j}\right\}\right],$$

where the derivatives in (8.29) read

$$\frac{\partial\left(\underline{\tilde{\mathbf{Z}}}_{\mathrm{JD},n_\mathrm{F}}\right)}{\partial\mathrm{Re}\left\{\left[\underline{\tilde{\mathbf{E}}}_{n_\mathrm{F}}\right]_{i,j}\right\}}\Bigg|_{\underline{\tilde{\mathbf{E}}}_{n_\mathrm{F}}=\mathbf{0}}+\mathrm{j}\frac{\partial\left(\underline{\tilde{\mathbf{Z}}}_{\mathrm{JD},n_\mathrm{F}}\right)}{\partial\mathrm{Im}\left\{\left[\underline{\tilde{\mathbf{E}}}_{n_\mathrm{F}}\right]_{i,j}\right\}}\Bigg|_{\underline{\tilde{\mathbf{E}}}_{n_\mathrm{F}}=\mathbf{0}}= \tag{8.30}$$

$$\left.\frac{\partial\left[\left(\underline{\tilde{\mathbf{H}}}_{n_\mathrm{F}}^{\mathsf{H}}+\underline{\tilde{\mathbf{E}}}_{n_\mathrm{F}}^{\mathsf{H}}\right)\left(\underline{\tilde{\mathbf{H}}}_{n_\mathrm{F}}+\underline{\tilde{\mathbf{E}}}_{n_\mathrm{F}}\right)\right]^{-1}}{\partial\mathrm{Re}\left\{\left[\underline{\tilde{\mathbf{E}}}_{n_\mathrm{F}}\right]_{i,j}\right\}}\cdot\left(\underline{\tilde{\mathbf{H}}}_{n_\mathrm{F}}^{\mathsf{H}}+\underline{\tilde{\mathbf{E}}}_{n_\mathrm{F}}^{\mathsf{H}}\right)\right|_{\underline{\tilde{\mathbf{E}}}_{n_\mathrm{F}}=\mathbf{0}}+$$

$$\left[\left(\underline{\tilde{\mathbf{H}}}_{n_\mathrm{F}}^{\mathsf{H}}+\underline{\tilde{\mathbf{E}}}_{n_\mathrm{F}}^{\mathsf{H}}\right)\left(\underline{\tilde{\mathbf{H}}}_{n_\mathrm{F}}+\underline{\tilde{\mathbf{E}}}_{n_\mathrm{F}}\right)\right]^{-1}\cdot\left.\frac{\partial\left(\underline{\tilde{\mathbf{H}}}_{n_\mathrm{F}}^{\mathsf{H}}+\underline{\tilde{\mathbf{E}}}_{n_\mathrm{F}}^{\mathsf{H}}\right)}{\partial\mathrm{Re}\left\{\left[\underline{\tilde{\mathbf{E}}}_{n_\mathrm{F}}\right]_{i,j}\right\}}\right|_{\underline{\tilde{\mathbf{E}}}_{n_\mathrm{F}}=\mathbf{0}}+$$

$$\mathrm{j}\left.\frac{\partial\left[\left(\underline{\tilde{\mathbf{H}}}_{n_\mathrm{F}}^{\mathsf{H}}+\underline{\tilde{\mathbf{E}}}_{n_\mathrm{F}}^{\mathsf{H}}\right)\left(\underline{\tilde{\mathbf{H}}}_{n_\mathrm{F}}+\underline{\tilde{\mathbf{E}}}_{n_\mathrm{F}}\right)\right]^{-1}}{\partial\mathrm{Re}\left\{\left[\underline{\tilde{\mathbf{E}}}_{n_\mathrm{F}}\right]_{i,j}\right\}}\cdot\left(\underline{\tilde{\mathbf{H}}}_{n_\mathrm{F}}^{\mathsf{H}}+\underline{\tilde{\mathbf{E}}}_{n_\mathrm{F}}^{\mathsf{H}}\right)\right|_{\underline{\tilde{\mathbf{E}}}_{n_\mathrm{F}}=\mathbf{0}}+$$

$$\mathrm{j}\left[\left(\underline{\tilde{\mathbf{H}}}_{n_\mathrm{F}}^{\mathsf{H}}+\underline{\tilde{\mathbf{E}}}_{n_\mathrm{F}}^{\mathsf{H}}\right)\left(\underline{\tilde{\mathbf{H}}}_{n_\mathrm{F}}+\underline{\tilde{\mathbf{E}}}_{n_\mathrm{F}}\right)\right]^{-1}\cdot\left.\frac{\partial\left(\underline{\tilde{\mathbf{H}}}_{n_\mathrm{F}}^{\mathsf{H}}+\underline{\tilde{\mathbf{E}}}_{n_\mathrm{F}}^{\mathsf{H}}\right)}{\partial\mathrm{Re}\left\{\left[\underline{\tilde{\mathbf{E}}}_{n_\mathrm{F}}\right]_{i,j}\right\}}\right|_{\underline{\tilde{\mathbf{E}}}_{n_\mathrm{F}}=\mathbf{0}}.$$

With (8.30), with the relation [Lut96]

$$\frac{\partial\underline{\mathbf{A}}^{-1}}{\partial z}=-\underline{\mathbf{A}}^{-1}\cdot\frac{\partial\underline{\mathbf{A}}}{\partial z}\cdot\underline{\mathbf{A}}^{-1},\tag{8.31}$$

where $\underline{\mathbf{A}}$ is a full rank square matrix and z a real-valued scalar, and with

$$\underline{\tilde{\mathbf{Z}}}_{\mathrm{JD},n_\mathrm{F}}\Big|_{\underline{\tilde{\mathbf{E}}}_{n_\mathrm{F}}=\mathbf{0}}=\left(\underline{\tilde{\mathbf{H}}}_{n_\mathrm{F}}^{\mathsf{H}}\underline{\tilde{\mathbf{H}}}_{n_\mathrm{F}}\right)^{-1}\underline{\tilde{\mathbf{H}}}_{n_\mathrm{F}}^{\mathsf{H}}\tag{8.32}$$

the approximation of the subcarrier specific JD matrix $\underline{\tilde{\mathbf{Z}}}_{\mathrm{JD},n_\mathrm{F}}$ yields

$$\begin{aligned}\underline{\tilde{\mathbf{Z}}}_{\mathrm{JD},n_\mathrm{F}}\;\approx\;&\left(\underline{\tilde{\mathbf{H}}}_{n_\mathrm{F}}^{\mathsf{H}}\underline{\tilde{\mathbf{H}}}_{n_\mathrm{F}}\right)^{-1}\underline{\tilde{\mathbf{H}}}_{n_\mathrm{F}}^{\mathsf{H}}+\left(\underline{\tilde{\mathbf{H}}}_{n_\mathrm{F}}^{\mathsf{H}}\underline{\tilde{\mathbf{H}}}_{n_\mathrm{F}}\right)^{-1}\underline{\tilde{\mathbf{E}}}_{n_\mathrm{F}}^{\mathsf{H}}-\\&\left(\underline{\tilde{\mathbf{H}}}_{n_\mathrm{F}}^{\mathsf{H}}\underline{\tilde{\mathbf{H}}}_{n_\mathrm{F}}\right)^{-1}\left(\underline{\tilde{\mathbf{H}}}_{n_\mathrm{F}}^{\mathsf{H}}\underline{\tilde{\mathbf{E}}}_{n_\mathrm{F}}+\underline{\tilde{\mathbf{E}}}_{n_\mathrm{F}}^{\mathsf{H}}\underline{\tilde{\mathbf{H}}}_{n_\mathrm{F}}\right)\left(\underline{\tilde{\mathbf{H}}}_{n_\mathrm{F}}^{\mathsf{H}}\underline{\tilde{\mathbf{H}}}_{n_\mathrm{F}}\right)^{-1}\underline{\tilde{\mathbf{H}}}_{n_\mathrm{F}}^{\mathsf{H}}.\end{aligned}\tag{8.33}$$

Finally, applying (8.28) and (8.33) the subcarrier specific JD error $\underline{\tilde{\boldsymbol{\varepsilon}}}_{\mathrm{JD},n_\mathrm{F}}$ of (8.23) can be approximated by

$$\begin{aligned}\underline{\tilde{\boldsymbol{\varepsilon}}}_{\mathrm{JD},n_\mathrm{F}}\;\approx\;&-\left(\underline{\tilde{\mathbf{H}}}_{n_\mathrm{F}}^{\mathsf{H}}\underline{\tilde{\mathbf{H}}}_{n_\mathrm{F}}\right)^{-1}\underline{\tilde{\mathbf{H}}}_{n_\mathrm{F}}^{\mathsf{H}}\underline{\tilde{\mathbf{E}}}_{n_\mathrm{F}}\underline{\tilde{\mathbf{d}}}_{n_\mathrm{F}}+\\&\left(\underline{\tilde{\mathbf{H}}}_{n_\mathrm{F}}^{\mathsf{H}}\underline{\tilde{\mathbf{H}}}_{n_\mathrm{F}}\right)^{-1}\underline{\tilde{\mathbf{H}}}_{n_\mathrm{F}}^{\mathsf{H}}\,\underline{\tilde{\mathbf{n}}}_{\mathrm{d},n_\mathrm{F}}+\left(\underline{\tilde{\mathbf{H}}}_{n_\mathrm{F}}^{\mathsf{H}}\underline{\tilde{\mathbf{H}}}_{n_\mathrm{F}}\right)^{-1}\underline{\tilde{\mathbf{E}}}_{n_\mathrm{F}}^{\mathsf{H}}\,\underline{\tilde{\mathbf{n}}}_{\mathrm{d},n_\mathrm{F}}-\\&\left(\underline{\tilde{\mathbf{H}}}_{n_\mathrm{F}}^{\mathsf{H}}\underline{\tilde{\mathbf{H}}}_{n_\mathrm{F}}\right)^{-1}\left(\underline{\tilde{\mathbf{H}}}_{n_\mathrm{F}}^{\mathsf{H}}\underline{\tilde{\mathbf{E}}}_{n_\mathrm{F}}+\underline{\tilde{\mathbf{E}}}_{n_\mathrm{F}}^{\mathsf{H}}\underline{\tilde{\mathbf{H}}}_{n_\mathrm{F}}\right)\left(\underline{\tilde{\mathbf{H}}}_{n_\mathrm{F}}^{\mathsf{H}}\underline{\tilde{\mathbf{H}}}_{n_\mathrm{F}}\right)^{-1}\underline{\tilde{\mathbf{H}}}_{n_\mathrm{F}}^{\mathsf{H}}\,\underline{\tilde{\mathbf{n}}}_{\mathrm{d},n_\mathrm{F}}.\end{aligned}\tag{8.34}$$

Introducing the energy

$$E_{\mathrm{d},n_\mathrm{F}}^{(k)} = \frac{1}{2}\left|\underline{\tilde{d}}_{n_\mathrm{F}}^{(k)}\right|^2 = E_\mathrm{d} \tag{8.35}$$

of the data symbol $\underline{\tilde{d}}_{n_\mathrm{F}}^{(k)}$ and assuming the transmitted data and the noise at the APs to be uncorrelated with each other, together with the relations

$$\begin{aligned}
\mathrm{E}\left\{\underline{\tilde{\mathbf{d}}}_{n_\mathrm{F}}\underline{\tilde{\mathbf{d}}}_{n_\mathrm{F}}^{\mathsf{H}}\right\} &= 2E_\mathrm{d}\cdot\mathbf{I}^{(K\times K)},\\
\mathrm{E}\left\{\,\underline{\tilde{\mathbf{n}}}_{\mathrm{d},n_\mathrm{F}}\,\underline{\tilde{\mathbf{n}}}_{\mathrm{d},n_\mathrm{F}}^{\mathsf{H}}\right\} &= 2\sigma^2\cdot\mathbf{I}^{(K_\mathrm{B}\times K_\mathrm{B})},\\
\mathrm{E}\left\{\underline{\tilde{\mathbf{E}}}_{n_\mathrm{F}}\underline{\tilde{\mathbf{E}}}_{n_\mathrm{F}}^{\mathsf{H}}\right\} &= 2\sigma_\mathrm{JCE}^2K\cdot\mathbf{I}^{(K_\mathrm{B}\times K_\mathrm{B})},\\
\mathrm{E}\left\{\underline{\tilde{\mathbf{E}}}_{n_\mathrm{F}}^{\mathsf{H}}\underline{\tilde{\mathbf{E}}}_{n_\mathrm{F}}\right\} &= 2\sigma_\mathrm{JCE}^2K_\mathrm{B}\cdot\mathbf{I}^{(K\times K)}
\end{aligned} \tag{8.36}$$

the covariance matrix

$$\underline{\mathbf{R}}_{\underline{\tilde{\boldsymbol{\varepsilon}}}_{\mathrm{JD},n_\mathrm{F}}} = \mathrm{E}\left\{\underline{\tilde{\boldsymbol{\varepsilon}}}_{\mathrm{JD},n_\mathrm{F}}\underline{\tilde{\boldsymbol{\varepsilon}}}_{\mathrm{JD},n_\mathrm{F}}^{\mathsf{H}}\right\} \approx \tag{8.37}$$

$$2\sigma_\mathrm{JCE}^2K\cdot 2E_\mathrm{d}\left(\underline{\tilde{\mathbf{H}}}_{n_\mathrm{F}}^{\mathsf{H}}\underline{\tilde{\mathbf{H}}}_{n_\mathrm{F}}\right)^{-1} + 2\sigma^2\left(\underline{\tilde{\mathbf{H}}}_{n_\mathrm{F}}^{\mathsf{H}}\underline{\tilde{\mathbf{H}}}_{n_\mathrm{F}}\right)^{-1} + 2\sigma_\mathrm{JCE}^2K_\mathrm{B}\cdot 2\sigma^2\left(\underline{\tilde{\mathbf{H}}}_{n_\mathrm{F}}^{\mathsf{H}}\underline{\tilde{\mathbf{H}}}_{n_\mathrm{F}}\right)^{-2} +$$

$$2\sigma^2\left(\underline{\tilde{\mathbf{H}}}_{n_\mathrm{F}}^{\mathsf{H}}\underline{\tilde{\mathbf{H}}}_{n_\mathrm{F}}\right)^{-1}\left[\mathrm{E}\left\{\left(\underline{\tilde{\mathbf{H}}}_{n_\mathrm{F}}^{\mathsf{H}}\underline{\tilde{\mathbf{E}}}_{n_\mathrm{F}} + \underline{\tilde{\mathbf{E}}}_{n_\mathrm{F}}^{\mathsf{H}}\underline{\tilde{\mathbf{H}}}_{n_\mathrm{F}}\right)\left(\underline{\tilde{\mathbf{H}}}_{n_\mathrm{F}}^{\mathsf{H}}\underline{\tilde{\mathbf{H}}}_{n_\mathrm{F}}\right)^{-1}\left(\underline{\tilde{\mathbf{E}}}_{n_\mathrm{F}}^{\mathsf{H}}\underline{\tilde{\mathbf{H}}}_{n_\mathrm{F}} + \underline{\tilde{\mathbf{H}}}_{n_\mathrm{F}}^{\mathsf{H}}\underline{\tilde{\mathbf{E}}}_{n_\mathrm{F}}\right)\right\}\right]$$
$$\left(\underline{\tilde{\mathbf{H}}}_{n_\mathrm{F}}^{\mathsf{H}}\underline{\tilde{\mathbf{H}}}_{n_\mathrm{F}}\right)^{-1} -$$

$$2\sigma^2\left(\underline{\tilde{\mathbf{H}}}_{n_\mathrm{F}}^{\mathsf{H}}\underline{\tilde{\mathbf{H}}}_{n_\mathrm{F}}\right)^{-1}\left[\mathrm{E}\left\{\underline{\tilde{\mathbf{E}}}_{n_\mathrm{F}}^{\mathsf{H}}\underline{\tilde{\mathbf{H}}}_{n_\mathrm{F}}\left(\underline{\tilde{\mathbf{H}}}_{n_\mathrm{F}}^{\mathsf{H}}\underline{\tilde{\mathbf{H}}}_{n_\mathrm{F}}\right)^{-1}\left(\underline{\tilde{\mathbf{E}}}_{n_\mathrm{F}}^{\mathsf{H}}\underline{\tilde{\mathbf{H}}}_{n_\mathrm{F}} + \underline{\tilde{\mathbf{H}}}_{n_\mathrm{F}}^{\mathsf{H}}\underline{\tilde{\mathbf{E}}}_{n_\mathrm{F}}\right)\right\}\right]\left(\underline{\tilde{\mathbf{H}}}_{n_\mathrm{F}}^{\mathsf{H}}\underline{\tilde{\mathbf{H}}}_{n_\mathrm{F}}\right)^{-1} -$$

$$2\sigma^2\left(\underline{\tilde{\mathbf{H}}}_{n_\mathrm{F}}^{\mathsf{H}}\underline{\tilde{\mathbf{H}}}_{n_\mathrm{F}}\right)^{-1}\left[\mathrm{E}\left\{\left(\underline{\tilde{\mathbf{E}}}_{n_\mathrm{F}}^{\mathsf{H}}\underline{\tilde{\mathbf{H}}}_{n_\mathrm{F}} + \underline{\tilde{\mathbf{H}}}_{n_\mathrm{F}}^{\mathsf{H}}\underline{\tilde{\mathbf{E}}}_{n_\mathrm{F}}\right)\left(\underline{\tilde{\mathbf{H}}}_{n_\mathrm{F}}^{\mathsf{H}}\underline{\tilde{\mathbf{H}}}_{n_\mathrm{F}}\right)^{-1}\underline{\tilde{\mathbf{H}}}_{n_\mathrm{F}}^{\mathsf{H}}\underline{\tilde{\mathbf{E}}}_{n_\mathrm{F}}\right\}\right]\left(\underline{\tilde{\mathbf{H}}}_{n_\mathrm{F}}^{\mathsf{H}}\underline{\tilde{\mathbf{H}}}_{n_\mathrm{F}}\right)^{-1}$$

of the subcarrier specific JD error $\underline{\tilde{\boldsymbol{\varepsilon}}}_{\mathrm{JD},n_\mathrm{F}}$ is obtained. After some manipulation of (8.37) and application of the relation [Wha71]

$$\mathrm{E}\left\{\underline{\tilde{\mathbf{E}}}_{n_\mathrm{F}}^{\mathsf{H}}\left(\underline{\tilde{\mathbf{H}}}_{n_\mathrm{F}}^{\mathsf{H}}\underline{\tilde{\mathbf{H}}}_{n_\mathrm{F}}\right)^{-1}\underline{\tilde{\mathbf{E}}}_{n_\mathrm{F}}\right\} = 2\sigma_\mathrm{JCE}^2\cdot\mathrm{trace}\left\{\left(\underline{\tilde{\mathbf{H}}}_{n_\mathrm{F}}^{\mathsf{H}}\underline{\tilde{\mathbf{H}}}_{n_\mathrm{F}}\right)^{-1}\right\}\cdot\mathbf{I}^{(K\times K)}, \tag{8.38}$$

(8.37) reads

$$\underline{\mathbf{R}}_{\underline{\tilde{\boldsymbol{\varepsilon}}}_{\mathrm{JD},n_\mathrm{F}}} = \left(\underline{\tilde{\mathbf{H}}}_{n_\mathrm{F}}^{\mathsf{H}}\underline{\tilde{\mathbf{H}}}_{n_\mathrm{F}}\right)^{-2}\cdot 2\sigma_\mathrm{JCE}^2\cdot 2\sigma^2\cdot(K_\mathrm{B}-K) + \tag{8.39}$$

$$\left(\underline{\tilde{\mathbf{H}}}_{n_\mathrm{F}}^{\mathsf{H}}\underline{\tilde{\mathbf{H}}}_{n_\mathrm{F}}\right)^{-1}\left(2\sigma_\mathrm{JCE}^2K\cdot 2E_\mathrm{d} + 2\sigma^2 + 2\sigma^2\cdot 2\sigma_\mathrm{JCE}^2\cdot\mathrm{trace}\left\{\left(\underline{\tilde{\mathbf{H}}}_{n_\mathrm{F}}^{\mathsf{H}}\underline{\tilde{\mathbf{H}}}_{n_\mathrm{F}}\right)^{-1}\right\}\right).$$

The variance $\sigma^{(k)^2}_{\underline{\tilde{\varepsilon}}_{\mathrm{JD},n_\mathrm{F}}}$ of the subcarrier specific JD error $\underline{\tilde{\varepsilon}}_{\mathrm{JD},n_\mathrm{F}}$ is obtained as

$$2\sigma^{(k)^2}_{\underline{\tilde{\varepsilon}}_{\mathrm{JD},n_\mathrm{F}}} = \left[\underline{\mathbf{R}}_{\underline{\tilde{\varepsilon}}_{\mathrm{JD},n_\mathrm{F}}}\right]_{k,k} \approx \left[\left(\underline{\tilde{\mathbf{H}}}^{\mathsf{H}}_{n_\mathrm{F}}\underline{\tilde{\mathbf{H}}}_{n_\mathrm{F}}\right)^{-2}\right]_{k,k} \cdot 2\sigma^2_{\mathrm{JCE}} \cdot 2\sigma^2 \cdot (K_\mathrm{B} - K) + \tag{8.40}$$

$$\left[\left(\underline{\tilde{\mathbf{H}}}^{\mathsf{H}}_{n_\mathrm{F}}\underline{\tilde{\mathbf{H}}}_{n_\mathrm{F}}\right)^{-1}\right]_{k,k} \left(2\sigma^2_{\mathrm{JCE}}K \cdot 2E_\mathrm{d} + 2\sigma^2 + 2\sigma^2 \cdot 2\sigma^2_{\mathrm{JCE}} \cdot \mathrm{trace}\left\{\left(\underline{\tilde{\mathbf{H}}}^{\mathsf{H}}_{n_\mathrm{F}}\underline{\tilde{\mathbf{H}}}_{n_\mathrm{F}}\right)^{-1}\right\}\right).$$

Finally, we can obtain the SNRs [WLM+03, Skl04]

$$\gamma^{(k)}_{\mathrm{JD},n_\mathrm{F}} = \frac{2E_\mathrm{d}}{\left[\underline{\mathbf{R}}_{\underline{\tilde{\varepsilon}}_{\mathrm{JD},n_\mathrm{F}}}\right]_{k,k}} = \frac{E_\mathrm{d}}{\sigma^{(k)^2}_{\underline{\tilde{\varepsilon}}_{\mathrm{JD},n_\mathrm{F}}}} \tag{8.41}$$

of the estimated data symbols $\underline{\tilde{d}}^{(k)}_{n_\mathrm{F}}$ at the output of the joint detector, to be used in the JD performance evaluation presented in the following subsection.

8.2.2 Investigation results

As shown in Section 8.1 the presence of noise at the APs of the considered SA results in JCE errors. Applying this non-perfect channel knowledge at the CU for JD causes the subcarrier specific JD error $\underline{\tilde{\varepsilon}}_{\mathrm{JD},n_\mathrm{F}}$ approximated by (8.34). The impact of $\underline{\tilde{\varepsilon}}_{\mathrm{JD},n_\mathrm{F}}$ on the performance of JD shall be illustrated by means of the bit error probability $P^{(k)}_{\mathrm{b},n_\mathrm{F}}$. Along with QPSK modulation, we shall assume that one data symbol $\underline{\tilde{d}}^{(k)}_{n_\mathrm{F}}$ is transmitted per subcarrier n_F and MT k. With the SNR degradations [WLM+03, Skl04]

$$\delta^{(k)}_{\mathrm{JD},n_\mathrm{F}} = \frac{\gamma^{(k)}_{\mathrm{ref},n_\mathrm{F}}}{\gamma^{(k)}_{\mathrm{JD},n_\mathrm{F}}} \tag{8.42}$$

and the receive energy $E^{(k)}_\mathrm{b}$ per bit, the bit error probability

$$P^{(k)}_{\mathrm{b},n_\mathrm{F}} = \frac{1}{2}\mathrm{erfc}\left(\sqrt{\frac{E^{(k)}_\mathrm{b}}{\sigma^2\delta^{(k)}_{\mathrm{JD},n_\mathrm{F}}}}\right) \tag{8.43}$$

is obtained [Lük92, WLM+03]. The MIMO parametric channel model described in [Skl04] is applied, for which the subcarrier specific channel matrix $\underline{\tilde{\mathbf{H}}}_{n_\mathrm{F}}$ of (8.14) is given by

$$\underline{\tilde{\mathbf{H}}}_{n_\mathrm{F}} = \begin{pmatrix} 1 & \rho & \cdots & \rho \\ \rho & 1 & \cdots & \rho \\ \vdots & \vdots & \ddots & \vdots \\ \rho & \rho & \cdots & 1 \end{pmatrix}, \tag{8.44}$$

where ρ is set equal to 0.5. In this case the receive energy per bit $E_{\mathrm{b}}^{(k)}$ is the same for all K MTs and it will be denoted by E_{b}. Further, we shall consider the case where the number K_{B} of APs and the number K of MTs in the SA under investigation are equal. In this case and for the MIMO parametric channel model described by (8.44), the SNRs $\gamma_{\mathrm{JD},n_{\mathrm{F}}}^{(k)}$ of (8.41) become

$$\gamma_{\mathrm{JD},n_{\mathrm{F}}}^{(k)} = \frac{E_{\mathrm{d}}}{\left[\left(\underline{\tilde{\mathbf{H}}}_{n_{\mathrm{F}}}^{\mathsf{H}}\underline{\tilde{\mathbf{H}}}_{n_{\mathrm{F}}}\right)^{-1}\right]_{k,k}\left(\sigma_{\mathrm{JCE}}^2 K\cdot 2E_{\mathrm{d}} + \sigma^2 + \sigma^2\cdot 2\sigma_{\mathrm{JCE}}^2\cdot\mathrm{trace}\left\{\left(\underline{\tilde{\mathbf{H}}}_{n_{\mathrm{F}}}^{\mathsf{H}}\underline{\tilde{\mathbf{H}}}_{n_{\mathrm{F}}}\right)^{-1}\right\}\right)}. \tag{8.45}$$

With the reference SNRs

$$\gamma_{\mathrm{ref},n_{\mathrm{F}}}^{(k)} = \frac{E_{\mathrm{d}}}{\sigma^2}\cdot\left[\underline{\tilde{\mathbf{H}}}_{n_{\mathrm{F}}}^{\mathsf{H}}\underline{\tilde{\mathbf{H}}}_{n_{\mathrm{F}}}\right]_{k,k} = \gamma_{\mathrm{MF},n_{\mathrm{F}}}^{(k)} \tag{8.46}$$

valid for the reference case of matched filter (MF) estimation of a single transmitted data symbol $\underline{\tilde{d}}_{n_{\mathrm{F}}}^{(k)}$ [Skl04], the SNR degradations $\delta_{\mathrm{JD},n_{\mathrm{F}}}^{(k)}$ of (8.42) are given by

$$\begin{aligned}\delta_{\mathrm{JD},n_{\mathrm{F}}}^{(k)} &= \delta_{\mathrm{JD},n_{\mathrm{F}}} = \underbrace{\left[\left(\underline{\tilde{\mathbf{H}}}_{n_{\mathrm{F}}}^{\mathsf{H}}\underline{\tilde{\mathbf{H}}}_{n_{\mathrm{F}}}\right)^{-1}\right]_{k,k}\left[\underline{\tilde{\mathbf{H}}}_{n_{\mathrm{F}}}^{\mathsf{H}}\underline{\tilde{\mathbf{H}}}_{n_{\mathrm{F}}}\right]_{k,k}}_{\left(\delta_{\mathrm{JD},n_{\mathrm{F}}}^{(k)}\right)_{\mathrm{perf}}}\cdot \\ &\quad\left(1+\frac{\sigma_{\mathrm{JCE}}^2 K\cdot 2E_{\mathrm{d}}}{\sigma^2} + 2\sigma_{\mathrm{JCE}}^2\cdot\mathrm{trace}\left\{\left(\underline{\tilde{\mathbf{H}}}_{n_{\mathrm{F}}}^{\mathsf{H}}\underline{\tilde{\mathbf{H}}}_{n_{\mathrm{F}}}\right)^{-1}\right\}\right) \\ &= \left(\delta_{\mathrm{JD},n_{\mathrm{F}}}\right)_{\mathrm{perf}}\cdot\left(1+\frac{\sigma_{\mathrm{JCE}}^2 K\cdot 2E_{\mathrm{d}}}{\sigma^2} + 2\sigma_{\mathrm{JCE}}^2\cdot\mathrm{trace}\left\{\left(\underline{\tilde{\mathbf{H}}}_{n_{\mathrm{F}}}^{\mathsf{H}}\underline{\tilde{\mathbf{H}}}_{n_{\mathrm{F}}}\right)^{-1}\right\}\right).\end{aligned} \tag{8.47}$$

The underbraced term in (8.47) denotes the SNR degradations $\left(\delta_{\mathrm{JD},n_{\mathrm{F}}}^{(k)}\right)_{\mathrm{perf}}$ for the case of perfect channel knowledge [Skl04]. From (8.47) we can obtain the ratios

$$\frac{\delta_{\mathrm{JD},n_{\mathrm{F}}}^{(k)}}{\left(\delta_{\mathrm{JD},n_{\mathrm{F}}}\right)_{\mathrm{perf}}} = 1+\frac{\sigma_{\mathrm{JCE}}^2 K\cdot 2E_{\mathrm{d}}}{\sigma^2} + 2\sigma_{\mathrm{JCE}}^2\cdot\mathrm{trace}\left\{\left(\underline{\tilde{\mathbf{H}}}_{n_{\mathrm{F}}}^{\mathsf{H}}\underline{\tilde{\mathbf{H}}}_{n_{\mathrm{F}}}\right)^{-1}\right\}, \tag{8.48}$$

which describe the extent to which the SNR degradations $\delta_{\mathrm{JD},n_{\mathrm{F}}}^{(k)}$ are influenced by the presence of JCE errors. The ratios of (8.48) are always larger than one, which means that the presence of non-perfect channel knowledge leads to an increase of the SNR degradations $\delta_{\mathrm{JD},n_{\mathrm{F}}}^{(k)}$ and, consequently, to a decrease of the SNRs $\gamma_{\mathrm{JD},n_{\mathrm{F}}}^{(k)}$ at the JD output. This loss in SNR or, equivalently, this SNR degradation is the price to be paid for working with non-perfect channel knowledge.

(8.47) shows that for the considered MIMO parametric channel model with the channel matrix $\underline{\tilde{\mathbf{H}}}_{n_{\mathrm{F}}}$ of (8.44) the SNR degradations $\left(\delta_{\mathrm{JD},n_{\mathrm{F}}}^{(k)}\right)_{\mathrm{perf}}$ and $\delta_{\mathrm{JD},n_{\mathrm{F}}}^{(k)}$ are the same for all K MTs.

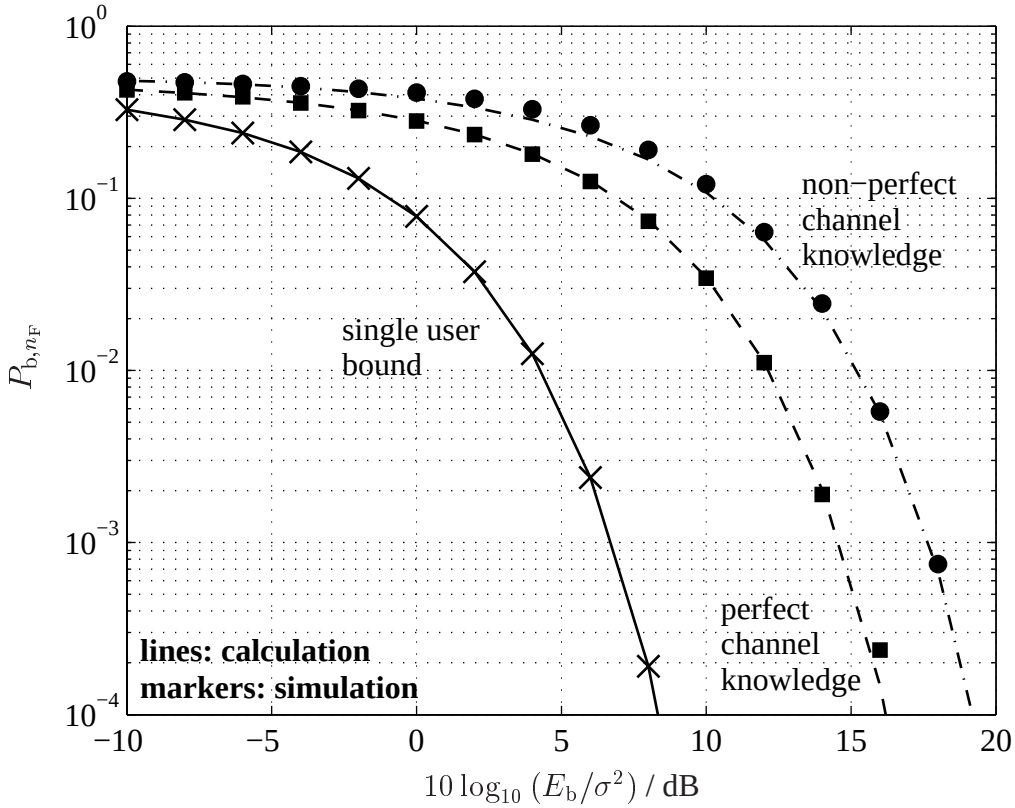

Fig. 8.2. Bit error probability $P_{\mathrm{b},n_\mathrm{F}}$ versus the ratio E_b/σ^2; MIMO parametric channel model, $\rho = 0.5$, $K = 4 = K_\mathrm{B}$

With (8.47), (8.43) reads

$$P_{\mathrm{b},n_\mathrm{F}}^{(k)} = P_{\mathrm{b},n_\mathrm{F}} \tag{8.49}$$

$$= \frac{1}{2}\mathrm{erfc}\left(\sqrt{\frac{E_\mathrm{b}}{(\delta_{\mathrm{JD},n_\mathrm{F}})_{\mathrm{perf}}\left(\sigma^2 + \sigma_{\mathrm{JCE}}^2 K \cdot 2E_\mathrm{d} + 2\sigma_{\mathrm{JCE}}^2\sigma^2 \cdot \mathrm{trace}\left\{\left(\underline{\tilde{\mathbf{H}}}_{n_\mathrm{F}}^{\mathsf{H}}\underline{\tilde{\mathbf{H}}}_{n_\mathrm{F}}\right)^{-1}\right\}\right)}}\right).$$

For the considered channel model described by the subcarrier specific channel matrix $\underline{\tilde{\mathbf{H}}}_{n_\mathrm{F}}$ of (8.44), $P_{\mathrm{b},n_\mathrm{F}}^{(k)}$ is the same for all K MTs and shall be denoted by $P_{\mathrm{b},n_\mathrm{F}}$. For the considered channel model $P_{\mathrm{b},n_\mathrm{F}}$ is equal to the average bit error probability averaged over many channel snapshots as depicted in [Skl04] for the respective investigations under the assumption of perfect channel knowledge. In addition, (8.43) and (8.47) show that $P_{\mathrm{b},n_\mathrm{F}}$ depends on the variance $\sigma_{\underline{\tilde{\varepsilon}}_{\mathrm{JCE}}}^2$ of the JCE error $\underline{\tilde{\varepsilon}}_{\mathrm{JCE}}$ and on the variance σ^2 of the noise at the APs. For the investigations concerning the performance of JD two different cases are considered:

1. $\sigma_{\underline{\tilde{\varepsilon}}_{\mathrm{JCE}}}^2$ depends on the noise variance σ^2 as shown in (8.7), and
2. $\sigma_{\underline{\tilde{\varepsilon}}_{\mathrm{JCE}}}^2$ is fixed and does not depend on σ^2.

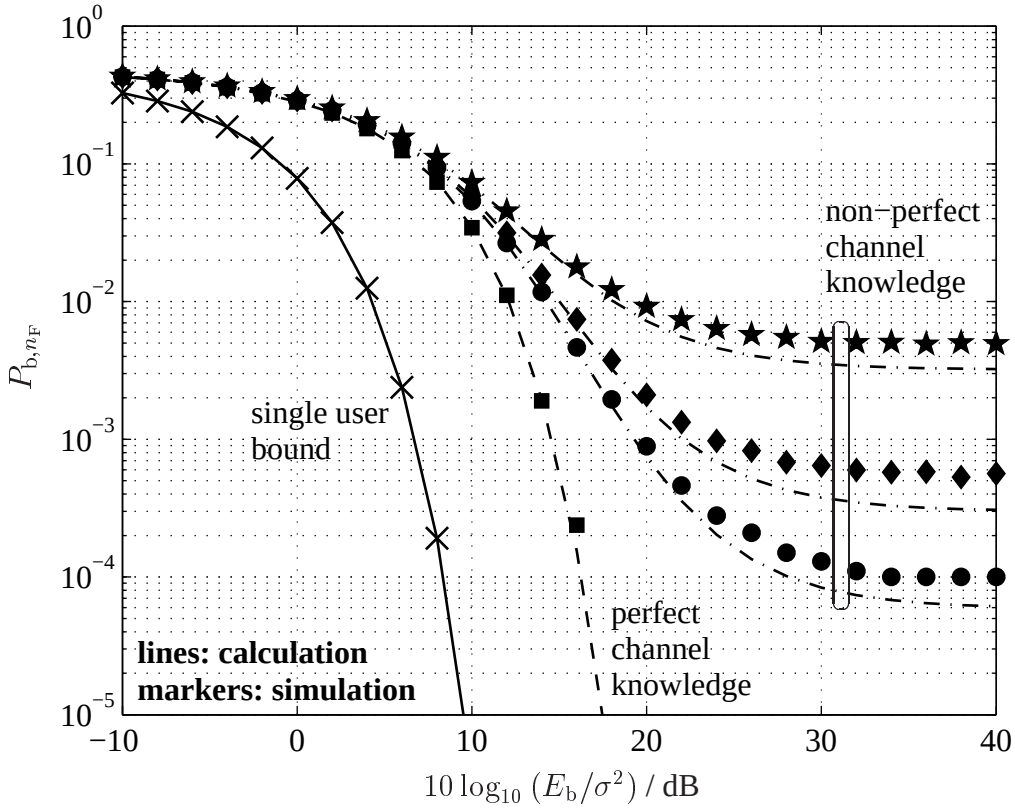

Fig. 8.3. Bit error probability $P_{\mathrm{b},n_\mathrm{F}}$ versus the ratio E_b/σ^2; MIMO parametric channel model, $\rho = 0.5$, $K = 4 = K_\mathrm{B}$; fixed variance σ^2_{JCE} of the JCE error

Fig. 8.2 shows the obtained results for the first case. Here, we have assumed that the noise $\underline{\tilde{\mathbf{n}}}_{\mathrm{h},n_\mathrm{F}}$ in the case of JCE and the noise $\underline{\tilde{\mathbf{n}}}_{\mathrm{d},n_\mathrm{F}}$ in the case of JD have the same variance σ^2. The bit error probability $P_{\mathrm{b},n_\mathrm{F}}$ of (8.43) is plotted versus the ratio of the receive energy per bit E_b over the noise power σ^2. Four APs and four MTs are assumed in the considered SA. The plotted lines correspond to $P_{\mathrm{b},n_\mathrm{F}}$ calculated by (8.43), and the plotted markers correspond to $P_{\mathrm{b},n_\mathrm{F}}$ obtained by computer simulations. For comparison, the curves valid for the single user bound and the case of perfect channel knowledge [Skl04] are also plotted. For the case of perfect channel knowledge and in the region of low values for $P_{\mathrm{b},n_\mathrm{F}}$ the resulting curve is a shifted version of the single user bound curve shifted by the value $10\log_{10}\left((\delta_{\mathrm{JD},n_\mathrm{F}})_{\mathrm{perf}}\right)$. Due to the fact that $\sigma^2_{\underline{\tilde{\boldsymbol{\varepsilon}}}_{\mathrm{JCE}}}$ depends on σ^2 according to (8.7), the resulting curves for the case of non-perfect channel knowledge are also shifted versions of the single user bound curve shifted by the value $10\log_{10}(\delta_{\mathrm{JD},n_\mathrm{F}})$ of the SNR degradations of (8.47).

For the second case, where $\sigma^2_{\underline{\tilde{\boldsymbol{\varepsilon}}}_{\mathrm{JCE}}}$ is fixed and independent of σ^2, the respective curves are plotted in Fig. 8.3 for the same parameters as in Fig. 8.2. For non-perfect channel knowledge

three different pairs of curves are plotted in Fig. 8.3 corresponding to the SNR value

$$10\log_{10}\left(\gamma_{\underline{\tilde{\varepsilon}}_{\mathrm{JCE}}}\right) \ / \ \mathrm{dB} = 10\log_{10}\left(\frac{\mathrm{E}\left\{\left[\underline{\tilde{\mathbf{H}}}_{n_{\mathrm{F}}}^{\mathsf{H}}\underline{\tilde{\mathbf{H}}}_{n_{\mathrm{F}}}\right]_{k,k}\right\}}{2\sigma^2_{\underline{\tilde{\varepsilon}}_{\mathrm{JCE}}}}\right) \overset{(8.44)}{=}$$

$$10\log_{10}\left(\frac{\left[\underline{\tilde{\mathbf{H}}}_{n_{\mathrm{F}}}^{\mathsf{H}}\underline{\tilde{\mathbf{H}}}_{n_{\mathrm{F}}}\right]_{k,k}}{2\sigma^2_{\underline{\tilde{\varepsilon}}_{\mathrm{JCE}}}}\right) \overset{(8.44)}{=} 10\log_{10}\left(\frac{1+(K_{\mathrm{B}}-1)\rho^2}{2\sigma^2_{\underline{\tilde{\varepsilon}}_{\mathrm{JCE}}}}\right) \tag{8.50}$$

at the output of the joint channel estimator depending on the fixed value of $\sigma^2_{\underline{\tilde{\varepsilon}}_{\mathrm{JCE}}}$. The three pairs of curves correspond to the values 25 dB, 27 dB and 29 dB of $10\log_{10}\left(\gamma_{\underline{\tilde{\varepsilon}}_{\mathrm{JCE}}}\right)$ of (8.50), respectively, starting from the top pair. When $10\log_{10}\left(E_{\mathrm{b}}/\sigma^2\right)$ takes large values, i. e., when σ^2 goes to zero, it can be seen from (8.49) that $P_{\mathrm{b},n_{\mathrm{F}}}$ is lower bounded by the minimum bit error probability

$$\lim_{\sigma^2\to 0} P_{\mathrm{b},n_{\mathrm{F}}} = \left(P_{\mathrm{b},n_{\mathrm{F}}}\right)_{\min} = \frac{1}{2}\mathrm{erfc}\left(\sqrt{\left(\delta_{\mathrm{JD},n_{\mathrm{F}}}\right)_{\mathrm{perf}}\cdot\sigma^2_{\underline{\tilde{\varepsilon}}_{\mathrm{JCE}}}K\cdot 2E_{\mathrm{d}}}\right) > 0 \tag{8.51}$$

and runs into an error floor. The larger $10\log_{10}\left(\gamma_{\underline{\tilde{\varepsilon}}_{\mathrm{JCE}}}\right)$ of (8.50) is, i. e., the smaller $\sigma^2_{\underline{\tilde{\varepsilon}}_{\mathrm{JCE}}}$ is, the lower $P_{\mathrm{b},n_{\mathrm{F}}}$ will be when it runs into said error floor.

Finally, for both considered cases with respect to $\sigma^2_{\underline{\tilde{\varepsilon}}_{\mathrm{JCE}}}$ it can be seen from Figs. 8.2 and 8.3 that the approximations given in Subsection 8.2.1 are of good quality, since the markers and the corresponding curves match very well.

8.3 Impact of the JCE error on the performance of JT

8.3.1 JT error

After having discussed the impact of the JCE error $\underline{\tilde{\varepsilon}}_{\mathrm{JCE}}$ on the performance of JD in Section 8.2, this section deals with the investigation of the DL performance in JOINT in the presence of non-perfect channel knowledge at the CU. The considered DL data transmission scenario is illustrated in Fig. 8.4. As in the case of JD, see Fig. 3.2, K MTs and K_{B} APs are considered. The CU has the knowledge of the estimated CTFs $\underline{\hat{\tilde{\mathbf{h}}}}^{(k,k_{\mathrm{B}})}$ of (3.9) and of the MT-specific data vectors $\underline{\tilde{\mathbf{d}}}^{(k)}$ of (3.10) at its disposition. With this knowledge the CU performs JT as described in [Skl04] and generates the total transmit signal

$$\underline{\tilde{\mathbf{s}}} = \left(\underline{\tilde{s}}_1^{(1)} \ \ldots \ \underline{\tilde{s}}_{N_{\mathrm{F}}}^{(1)} \ \ldots \ \underline{\tilde{s}}_1^{(K_{\mathrm{B}})} \ \ldots \ \underline{\tilde{s}}_{N_{\mathrm{F}}}^{(K_{\mathrm{B}})}\right)^{\mathrm{T}} \tag{8.52}$$

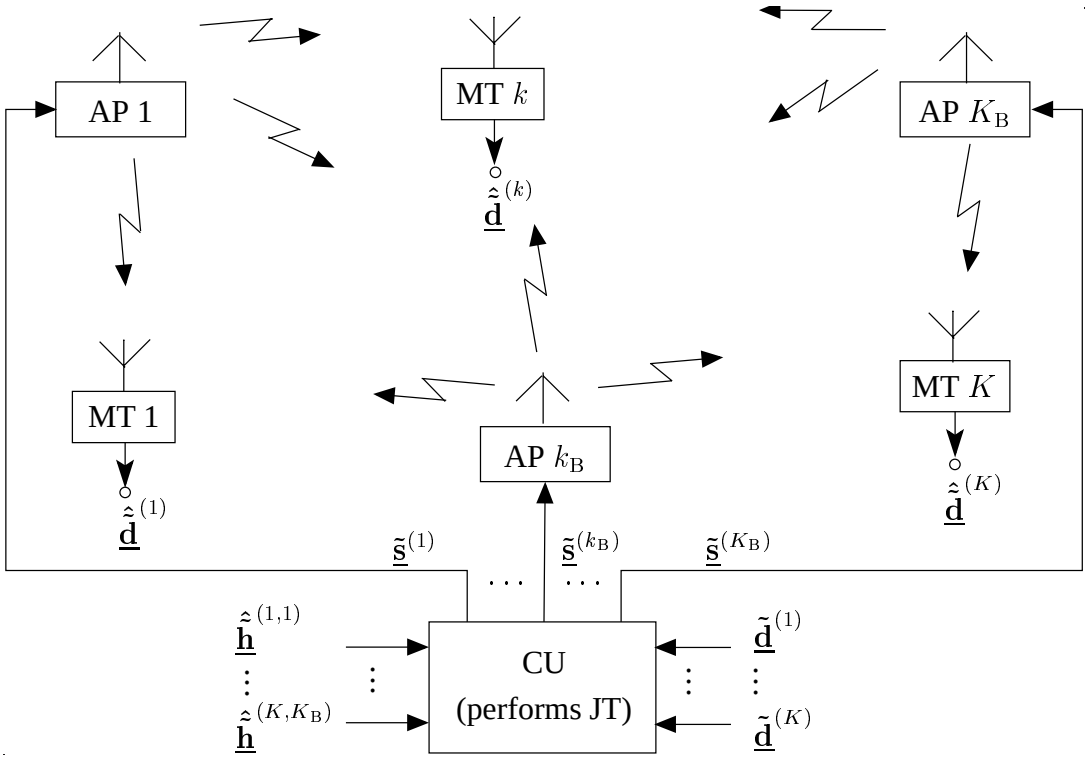

Fig. 8.4. DL data transmission scenario in the considered SA of JOINT

of dimension $K_{\mathrm{B}}N_{\mathrm{F}}$. $\underline{\tilde{\mathbf{s}}}$ contains the AP-specific transmit signal components $\underline{\tilde{s}}_{n_{\mathrm{F}}}^{(k_{\mathrm{B}})}$, which are forwarded to the respective APs of the considered SA and are then radiated over the radio channel.

Since TDD is applied as the duplexing scheme, see Section 1.2, and under the assumption that the time elapsing between the UL and the DL transmission is sufficiently smaller than the coherence time of the radio channel, the reciprocity between the UL and the DL radio channel can be exploited. Therefore, as the $K_{\mathrm{B}}N_{\mathrm{F}} \times KN_{\mathrm{F}}$ channel matrix $\underline{\tilde{\mathbf{H}}}$ of (8.9) is used for the description of the UL radio channel, its transpose $\underline{\tilde{\mathbf{H}}}^{\mathrm{T}}$ of dimension $KN_{\mathrm{F}} \times K_{\mathrm{B}}N_{\mathrm{F}}$ will be used for the description of the respective DL radio channel. Then, in the scenario of Fig. 8.4 the noise corrupted receive signal

$$\underline{\tilde{\mathbf{r}}}_{\mathrm{d}} = \left(\underline{\tilde{r}}_{\mathrm{d},1}^{(1)} \ \cdots \ \underline{\tilde{r}}_{\mathrm{d},N_{\mathrm{F}}}^{(1)} \ \cdots \ \underline{\tilde{r}}_{\mathrm{d},1}^{(K)} \ \cdots \ \underline{\tilde{r}}_{\mathrm{d},N_{\mathrm{F}}}^{(K)}\right)^{\mathrm{T}} = \underline{\tilde{\mathbf{H}}}^{\mathrm{T}}\,\underline{\tilde{\mathbf{s}}} + \underline{\tilde{\mathbf{n}}}_{\mathrm{d}} \tag{8.53}$$

of dimension KN_{F} can be obtained. Similar to the case of JD, we can apply the subcarrier-wise representation of vectors and matrices also for the case of JT [Skl04]. To this end, we

consider the transposed subcarrier specific channel matrix

$$\underline{\tilde{\mathbf{H}}}_{n_\mathrm{F}}^{\mathrm{T}} = \begin{pmatrix} \underline{\tilde{h}}_{n_\mathrm{F}}^{(1,1)} & \cdots & \underline{\tilde{h}}_{n_\mathrm{F}}^{(1,K_\mathrm{B})} \\ \vdots & & \vdots \\ \underline{\tilde{h}}_{n_\mathrm{F}}^{(K,1)} & \cdots & \underline{\tilde{h}}_{n_\mathrm{F}}^{(K,K_\mathrm{B})} \end{pmatrix} \tag{8.54}$$

of dimension $K \times K_\mathrm{B}$ of (8.14) and the subcarrier specific transmit signal

$$\underline{\tilde{\mathbf{s}}}_{n_\mathrm{F}} = \left(\underline{\tilde{s}}_{n_\mathrm{F}}^{(1)} \ \cdots \ \underline{\tilde{s}}_{n_\mathrm{F}}^{(K_\mathrm{B})}\right)^{\mathrm{T}} \tag{8.55}$$

of dimension K_B. With (8.54) and (8.55) we can obtain the subcarrier specific noise corrupted receive signal

$$\underline{\tilde{\mathbf{r}}}_{\mathrm{d},n_\mathrm{F}} = \left(\underline{\tilde{r}}_{\mathrm{d},n_\mathrm{F}}^{(1)} \ \cdots \ \underline{\tilde{r}}_{\mathrm{d},n_\mathrm{F}}^{(K)}\right)^{\mathrm{T}} = \underline{\tilde{\mathbf{H}}}_{n_\mathrm{F}}^{\mathrm{T}} \, \underline{\tilde{\mathbf{s}}}_{n_\mathrm{F}} + \underline{\tilde{\mathbf{n}}}_{\mathrm{d},n_\mathrm{F}} \tag{8.56}$$

of dimension K. Each MT k, $k = 1 \ \ldots \ K$, contains a simple OFDM receiver applying very simple signal processing, taking the receive component $\underline{\tilde{r}}_{\mathrm{d},n_\mathrm{F}}^{(k)}$ on subcarrier n_F as the respective estimated data symbol $\underline{\hat{\tilde{d}}}_{n_\mathrm{F}}^{(k)}$, i. e., we can extend (8.56) to [Skl04]

$$\underline{\tilde{\mathbf{r}}}_{\mathrm{d},n_\mathrm{F}} = \underline{\tilde{\mathbf{H}}}_{n_\mathrm{F}}^{\mathrm{T}} \, \underline{\tilde{\mathbf{s}}}_{n_\mathrm{F}} + \underline{\tilde{\mathbf{n}}}_{\mathrm{d},n_\mathrm{F}} \stackrel{!}{=} \underline{\hat{\tilde{\mathbf{d}}}}_{n_\mathrm{F}}. \tag{8.57}$$

Considering the linear JT scheme TxZF JT as described in [Skl04], the subcarrier specific transmit signal $\underline{\tilde{\mathbf{s}}}_{n_\mathrm{F}}$ of (8.55) is linearly related to the subcarrier specific data vector $\underline{\tilde{\mathbf{d}}}_{n_\mathrm{F}}$ by the $K_\mathrm{B} \times K$ matrix $\underline{\tilde{\mathbf{M}}}_{n_\mathrm{F}}$ as

$$\underline{\tilde{\mathbf{s}}}_{n_\mathrm{F}} = \underline{\tilde{\mathbf{M}}}_{n_\mathrm{F}} \, \underline{\tilde{\mathbf{d}}}_{n_\mathrm{F}}. \tag{8.58}$$

$\underline{\tilde{\mathbf{M}}}_{n_\mathrm{F}}$ is termed subcarrier specific modulator matrix. In the case of linear TxZF JT $\underline{\tilde{\mathbf{s}}}_{n_\mathrm{F}}$ is generated by (8.58) based on two criteria. According to the first criterion, in the absence of noise the subcarrier specific data estimates $\underline{\hat{\tilde{\mathbf{d}}}}_{n_\mathrm{F}}^{(k)}$ at the MTs shall be free from interference, i. e.

$$\underline{\tilde{\mathbf{r}}}_{\mathrm{d},n_\mathrm{F}} = \underline{\tilde{\mathbf{H}}}_{n_\mathrm{F}}^{\mathrm{T}} \, \underline{\tilde{\mathbf{s}}}_{n_\mathrm{F}} = \underline{\hat{\tilde{\mathbf{d}}}}_{n_\mathrm{F}} = \underline{\tilde{\mathbf{d}}}_{n_\mathrm{F}} \tag{8.59}$$

should hold. As explained in [Skl04], there exists an infinite large number of subcarrier specific transmit signals $\underline{\tilde{\mathbf{s}}}_{n_\mathrm{F}}$, for which (8.59) is fulfilled. Therefore, a second criterion is imposed concerning the total transmit energy

$$T_{\mathrm{tot},n_\mathrm{F}} = \frac{1}{2} \, \underline{\tilde{\mathbf{s}}}_{n_\mathrm{F}}^{\mathsf{H}} \, \underline{\tilde{\mathbf{s}}}_{n_\mathrm{F}} \tag{8.60}$$

radiated in the considered SA. With respect to the inter-SA interference it is desirable to obtain such subcarrier specific transmit signals $\underline{\tilde{\mathbf{s}}}_{n_\mathrm{F}}$, which, in addition to fulfilling (8.59), also minimize $T_{\mathrm{tot},n_\mathrm{F}}$ of (8.60). Following these two criteria, (8.58) reads [Skl04]

$$\underline{\tilde{\mathbf{s}}}_{n_\mathrm{F}} = \underbrace{\underline{\hat{\tilde{\mathbf{H}}}}_{n_\mathrm{F}}^{*} \left(\underline{\hat{\tilde{\mathbf{H}}}}_{n_\mathrm{F}}^{\mathrm{T}} \underline{\hat{\tilde{\mathbf{H}}}}_{n_\mathrm{F}}^{*}\right)^{-1}}_{\underline{\tilde{\mathbf{M}}}_{n_\mathrm{F}}} \underline{\tilde{\mathbf{d}}}_{n_\mathrm{F}} \tag{8.61}$$

for the considered case of linear TxZF JT, where the estimated CTF components $\hat{\underline{h}}_{n_\mathrm{F}}^{(k,k_\mathrm{B})}$ are contained in the subcarrier specific modulator matrix $\underline{\tilde{\mathbf{M}}}_{n_\mathrm{F}}$. With (8.61) we can rewrite (8.57) as

$$\underline{\tilde{\mathbf{r}}}_{\mathrm{d},n_\mathrm{F}} = \underline{\hat{\tilde{\mathbf{d}}}}_{n_\mathrm{F}} = \underline{\tilde{\mathbf{H}}}_{n_\mathrm{F}}^{\mathrm{T}} \underline{\hat{\tilde{\mathbf{H}}}}_{n_\mathrm{F}}^{*} \left(\underline{\hat{\tilde{\mathbf{H}}}}_{n_\mathrm{F}}^{\mathrm{T}} \underline{\hat{\tilde{\mathbf{H}}}}_{n_\mathrm{F}}^{*} \right)^{-1} \underline{\tilde{\mathbf{d}}}_{n_\mathrm{F}} + \underline{\tilde{\mathbf{n}}}_{\mathrm{d},n_\mathrm{F}}. \tag{8.62}$$

With (8.21) and (8.62) we can obtain the subcarrier specific JT error

$$\begin{aligned}
\underline{\tilde{\boldsymbol{\varepsilon}}}_{\mathrm{JT},n_\mathrm{F}} &= \underline{\hat{\tilde{\mathbf{d}}}}_{n_\mathrm{F}} - \underline{\tilde{\mathbf{d}}}_{n_\mathrm{F}} \qquad (8.63)\\
&= \underline{\tilde{\mathbf{H}}}_{n_\mathrm{F}}^{\mathrm{T}} \underline{\hat{\tilde{\mathbf{H}}}}_{n_\mathrm{F}}^{*} \left(\underline{\hat{\tilde{\mathbf{H}}}}_{n_\mathrm{F}}^{\mathrm{T}} \underline{\hat{\tilde{\mathbf{H}}}}_{n_\mathrm{F}}^{*} \right)^{-1} \underline{\tilde{\mathbf{d}}}_{n_\mathrm{F}} + \underline{\tilde{\mathbf{n}}}_{\mathrm{d},n_\mathrm{F}} - \underbrace{\underline{\hat{\tilde{\mathbf{H}}}}_{n_\mathrm{F}}^{\mathrm{T}} \underline{\hat{\tilde{\mathbf{H}}}}_{n_\mathrm{F}}^{*} \left(\underline{\hat{\tilde{\mathbf{H}}}}_{n_\mathrm{F}}^{\mathrm{T}} \underline{\hat{\tilde{\mathbf{H}}}}_{n_\mathrm{F}}^{*} \right)^{-1}}_{\mathbf{I}^{(K\times K)}} \underline{\tilde{\mathbf{d}}}_{n_\mathrm{F}}\\
&= -\underline{\tilde{\mathbf{E}}}_{n_\mathrm{F}}^{\mathrm{T}} \left(\underline{\tilde{\mathbf{H}}}_{n_\mathrm{F}}^{*} + \underline{\tilde{\mathbf{E}}}_{n_\mathrm{F}}^{*} \right) \left[\left(\underline{\tilde{\mathbf{H}}}_{n_\mathrm{F}}^{\mathrm{T}} + \underline{\tilde{\mathbf{E}}}_{n_\mathrm{F}}^{\mathrm{T}} \right) \left(\underline{\tilde{\mathbf{H}}}_{n_\mathrm{F}}^{*} + \underline{\tilde{\mathbf{E}}}_{n_\mathrm{F}}^{*} \right) \right]^{-1} \underline{\tilde{\mathbf{d}}}_{n_\mathrm{F}} + \underline{\tilde{\mathbf{n}}}_{\mathrm{d},n_\mathrm{F}}.
\end{aligned}$$

It can be seen from (8.62) and (8.63) that in the case of perfect channel knowledge only the noise $\underline{\tilde{\mathbf{n}}}_{\mathrm{d},n_\mathrm{F}}$ at the MT input influences the quality of the data estimate $\underline{\hat{\tilde{\mathbf{d}}}}_{n_\mathrm{F}}$. $\underline{\tilde{\boldsymbol{\varepsilon}}}_{\mathrm{JT},n_\mathrm{F}}$ of (8.63) depends on the noise $\underline{\tilde{\mathbf{n}}}_{\mathrm{d},n_\mathrm{F}}$ in the SA and it is a non linear function of the components $\tilde{\varepsilon}_{\mathrm{JCE},n_\mathrm{F}}^{(k,k_\mathrm{B})}$ of the subcarrier specific JCE error matrix $\underline{\tilde{\mathbf{E}}}_{n_\mathrm{F}}$. Similar to the case of the JD error presented in Subsection 8.2.1, we shall approximate the subcarrier specific JT error $\underline{\tilde{\boldsymbol{\varepsilon}}}_{\mathrm{JT},n_\mathrm{F}}$ of (8.63) by the linear Taylor expansion. Applying (8.8), (8.24), (8.26) and truncating the Taylor series after the linear terms leads to

$$\underline{\tilde{\boldsymbol{\varepsilon}}}_{\mathrm{JT},n_\mathrm{F}} \approx -\underline{\tilde{\mathbf{E}}}_{n_\mathrm{F}}^{\mathrm{T}} \underline{\tilde{\mathbf{H}}}_{n_\mathrm{F}}^{*} \left(\underline{\tilde{\mathbf{H}}}_{n_\mathrm{F}}^{\mathrm{T}} \underline{\tilde{\mathbf{H}}}_{n_\mathrm{F}}^{*} \right)^{-1} \underline{\tilde{\mathbf{d}}}_{n_\mathrm{F}} + \underline{\tilde{\mathbf{n}}}_{\mathrm{d},n_\mathrm{F}}. \tag{8.64}$$

Assuming the data and the noise to be uncorrelated with each other together with (8.36) we obtain the $K \times K$ covariance matrix

$$\begin{aligned}
\mathbf{R}_{\underline{\tilde{\boldsymbol{\varepsilon}}}_{\mathrm{JT},n_\mathrm{F}}} &= \mathrm{E}\left\{ \underline{\tilde{\boldsymbol{\varepsilon}}}_{\mathrm{JT},n_\mathrm{F}} \underline{\tilde{\boldsymbol{\varepsilon}}}_{\mathrm{JT},n_\mathrm{F}}^{\mathsf{H}} \right\} \qquad (8.65)\\
&\approx 2\sigma^2 \cdot \mathbf{I}^{(K\times K)} + 2E_\mathrm{d} \cdot \mathrm{E}\left\{ \underline{\tilde{\mathbf{E}}}_{n_\mathrm{F}}^{\mathrm{T}} \underline{\tilde{\mathbf{H}}}_{n_\mathrm{F}}^{*} \left(\underline{\tilde{\mathbf{H}}}_{n_\mathrm{F}}^{\mathrm{T}} \underline{\tilde{\mathbf{H}}}_{n_\mathrm{F}}^{*} \right)^{-2} \underline{\tilde{\mathbf{H}}}_{n_\mathrm{F}}^{\mathrm{T}} \underline{\tilde{\mathbf{E}}}_{n_\mathrm{F}}^{*} \right\}
\end{aligned}$$

of the subcarrier specific JT error. The matrix product inside the expectation in the second row of (8.65) can be reformed as

$$\begin{aligned}
\underbrace{\underline{\tilde{\mathbf{E}}}_{n_\mathrm{F}}^{\mathrm{T}} \underline{\tilde{\mathbf{H}}}_{n_\mathrm{F}}^{*}}_{\underline{\tilde{\mathbf{X}}}_{n_\mathrm{F}}^{\mathsf{H}}} \left(\underline{\tilde{\mathbf{H}}}_{n_\mathrm{F}}^{\mathrm{T}} \underline{\tilde{\mathbf{H}}}_{n_\mathrm{F}}^{*} \right)^{-2} \underbrace{\underline{\tilde{\mathbf{H}}}_{n_\mathrm{F}}^{\mathrm{T}} \underline{\tilde{\mathbf{E}}}_{n_\mathrm{F}}^{*}}_{\underline{\tilde{\mathbf{Y}}}_{n_\mathrm{F}}} &= \underline{\tilde{\mathbf{X}}}_{n_\mathrm{F}}^{\mathsf{H}} \left(\underline{\tilde{\mathbf{H}}}_{n_\mathrm{F}}^{\mathrm{T}} \underline{\tilde{\mathbf{H}}}_{n_\mathrm{F}}^{*} \right)^{-2} \underline{\tilde{\mathbf{Y}}}_{n_\mathrm{F}} \qquad (8.66)\\
&= \begin{pmatrix} \underline{\tilde{\mathbf{x}}}_{n_\mathrm{F}}^{(1)\mathsf{H}} \\ \vdots \\ \underline{\tilde{\mathbf{x}}}_{n_\mathrm{F}}^{(K)\mathsf{H}} \end{pmatrix} \left(\underline{\tilde{\mathbf{H}}}_{n_\mathrm{F}}^{\mathrm{T}} \underline{\tilde{\mathbf{H}}}_{n_\mathrm{F}}^{*} \right)^{-2} \begin{pmatrix} \underline{\tilde{\mathbf{y}}}_{n_\mathrm{F}}^{(1)} & \cdots & \underline{\tilde{\mathbf{y}}}_{n_\mathrm{F}}^{(K)} \end{pmatrix}.
\end{aligned}$$

With (8.36), (8.66) and the property [Wha71]

$$\mathrm{E}\left\{ \underline{\mathbf{x}}^{\mathsf{H}} \, \underline{\mathbf{A}} \, \underline{\mathbf{y}} \right\} = \mathrm{trace}\left\{ \underline{\mathbf{A}} \, \underline{\mathbf{R}}_{\mathbf{yx}} \right\}, \tag{8.67}$$

where $\underline{\mathbf{R}}_{\mathbf{yx}}$ is the covariance matrix between the vectors $\underline{\mathbf{x}}$ and $\underline{\mathbf{y}}$,

$$\left[\mathrm{E}\left\{ \begin{pmatrix} \tilde{\underline{\mathbf{x}}}_{n_\mathrm{F}}^{(1)\mathsf{H}} \\ \vdots \\ \tilde{\underline{\mathbf{x}}}_{n_\mathrm{F}}^{(K)\mathsf{H}} \end{pmatrix} \left(\tilde{\underline{\mathbf{H}}}_{n_\mathrm{F}}^{\mathrm{T}} \tilde{\underline{\mathbf{H}}}_{n_\mathrm{F}}^{*} \right)^{-2} \begin{pmatrix} \tilde{\underline{\mathbf{y}}}_{n_\mathrm{F}}^{(1)} & \cdots & \tilde{\underline{\mathbf{y}}}_{n_\mathrm{F}}^{(K)} \end{pmatrix} \right\} \right]_{k,k'} = \tag{8.68}$$

$$\begin{cases} 2\sigma_{\tilde{\underline{\boldsymbol{\varepsilon}}}_\mathrm{JCE}}^2 \cdot \mathrm{trace}\left\{ \left(\tilde{\underline{\mathbf{H}}}_{n_\mathrm{F}}^{\mathrm{T}} \tilde{\underline{\mathbf{H}}}_{n_\mathrm{F}}^{*} \right)^{-1} \right\} & \text{for } k = k', \\ 0 & \text{else}, \end{cases}$$

holds for the elements of the expectation of the matrix product of (8.65). With (8.68) we obtain the approximations

$$\underline{\mathbf{R}}_{\tilde{\underline{\boldsymbol{\varepsilon}}}_{\mathrm{JT},n_\mathrm{F}}} \approx \left(2\sigma^2 + 2E_\mathrm{d} \cdot 2\sigma_{\tilde{\underline{\boldsymbol{\varepsilon}}}_\mathrm{JCE}}^2 \cdot \mathrm{trace}\left\{ \left(\tilde{\underline{\mathbf{H}}}_{n_\mathrm{F}}^{\mathrm{T}} \tilde{\underline{\mathbf{H}}}_{n_\mathrm{F}}^{*} \right)^{-1} \right\} \right) \cdot \mathbf{I}^{(K \times K)} \tag{8.69}$$

and

$$2\sigma_{\tilde{\underline{\boldsymbol{\varepsilon}}}_{\mathrm{JT},n_\mathrm{F}}}^{(k)^2} = \left[\underline{\mathbf{R}}_{\tilde{\underline{\boldsymbol{\varepsilon}}}_{\mathrm{JT},n_\mathrm{F}}} \right]_{k,k} \approx 2\sigma^2 + 2E_\mathrm{d} \cdot 2\sigma_{\tilde{\underline{\boldsymbol{\varepsilon}}}_\mathrm{JCE}}^2 \cdot \mathrm{trace}\left\{ \left(\tilde{\underline{\mathbf{H}}}_{n_\mathrm{F}}^{\mathrm{T}} \tilde{\underline{\mathbf{H}}}_{n_\mathrm{F}}^{*} \right)^{-1} \right\} \tag{8.70}$$

for the covariance matrix $\underline{\mathbf{R}}_{\tilde{\underline{\boldsymbol{\varepsilon}}}_{\mathrm{JT},n_\mathrm{F}}}$ and the variance $\sigma_{\tilde{\underline{\boldsymbol{\varepsilon}}}_{\mathrm{JT},n_\mathrm{F}}}^{(k)^2}$, respectively, of the subcarrier specific JT error $\tilde{\underline{\boldsymbol{\varepsilon}}}_{\mathrm{JT},n_\mathrm{F}}$. Similar to the case of JD, the SNRs [MW04]

$$\gamma_{\mathrm{JT},n_\mathrm{F}}^{(k)} = \frac{\left| \tilde{\underline{d}}_{n_\mathrm{F}}^{(k)} \right|^2}{2\sigma_{\tilde{\underline{\boldsymbol{\varepsilon}}}_{\mathrm{JT},n_\mathrm{F}}}^{(k)^2}} \approx \frac{E_\mathrm{d}}{\sigma^2 + E_\mathrm{d} \cdot 2\sigma_{\tilde{\underline{\boldsymbol{\varepsilon}}}_\mathrm{JCE}}^2 \cdot \mathrm{trace}\left\{ \left(\tilde{\underline{\mathbf{H}}}_{n_\mathrm{F}}^{\mathrm{T}} \tilde{\underline{\mathbf{H}}}_{n_\mathrm{F}}^{*} \right)^{-1} \right\}} \tag{8.71}$$

of the estimated data symbols $\tilde{\underline{d}}_{n_\mathrm{F}}^{(k)}$ can be obtained.

8.3.2 Investigation results

Given the assumptions and calculations presented in Subsection 8.3.1, this subsection discusses the impact of non-perfect channel knowledge on the performance of JT. To this end, the run of the bit error probability $P_{\mathrm{b},n_\mathrm{F}}^{(k)}$ calculated by [MW04]

$$P_{\mathrm{b},n_\mathrm{F}}^{(k)} = \frac{1}{2}\mathrm{erfc}\left(\sqrt{\frac{\gamma_{\mathrm{JT},n_\mathrm{F}}^{(k)}}{2}} \right) \tag{8.72}$$

for the considered case of QPSK modulation versus the ratio of the mean transmit energy $\overline{T}_{n_\mathrm{F}}$ per data symbol over the noise power σ^2 is studied [Skl04]. Along with QPSK modulation, we shall assume that one data symbol $\underline{\tilde{d}}_{n_\mathrm{F}}^{(k)}$ is transmitted per subcarrier n_F and MT k. The case of small-valued JCE errors $\underline{\tilde{\varepsilon}}_{\mathrm{JCE}}$ characterized by (8.8) and the MIMO parametric channel model described by the subcarrier specific channel matrix $\underline{\tilde{\mathbf{H}}}_{n_\mathrm{F}}$ of (8.44) are considered. Again, ρ is set equal to 0.5. The two cases described in Subsection 8.2.2 concerning the variance $\sigma^2_{\underline{\tilde{\varepsilon}}_{\mathrm{JCE}}}$ of the JCE error are also considered.

The transmit energy $T_{n_\mathrm{F}}^{(k)}$ spent for the radiation of data symbol $\underline{\tilde{d}}_{n_\mathrm{F}}^{(k)}$ is given as [Skl04]

$$T_{n_\mathrm{F}}^{(k)} = E_\mathrm{d} \cdot \left[\underline{\tilde{\mathbf{M}}}_{n_\mathrm{F}}^{\mathsf{H}} \, \underline{\tilde{\mathbf{M}}}_{n_\mathrm{F}}\right]_{k,k}. \tag{8.73}$$

In the case of non-perfect channel knowledge the subcarrier specific modulator matrix $\underline{\tilde{\mathbf{M}}}_{n_\mathrm{F}}$ is a function of the subcarrier specific JCE error matrix $\underline{\tilde{\mathbf{E}}}_{n_\mathrm{F}}$ and, consequently, so is $T_{n_\mathrm{F}}^{(k)}$ of (8.73). Since the components $\underline{\tilde{\varepsilon}}_{\mathrm{JCE},n_\mathrm{F}}^{(k,k_\mathrm{B})}$ of the subcarrier specific JCE error matrix $\underline{\tilde{\mathbf{E}}}_{n_\mathrm{F}}$ are unknown to the CU, they are treated as random variables with a certain distribution, see Section 8.1. Therefore, $T_{n_\mathrm{F}}^{(k)}$ of (8.73) should also be treated as a random variable with a certain distribution. In what follows, we shall consider the expectation

$$\overline{T}_{n_\mathrm{F}} = \mathrm{E}\left\{T_{n_\mathrm{F}}^{(k)}\right\} = E_\mathrm{d} \cdot \mathrm{E}\left\{\left[\underline{\tilde{\mathbf{M}}}_{n_\mathrm{F}}^{\mathsf{H}} \, \underline{\tilde{\mathbf{M}}}_{n_\mathrm{F}}\right]_{k,k}\right\} \tag{8.74}$$

of this random variable over said components $\underline{\tilde{\varepsilon}}_{\mathrm{JCE},n_\mathrm{F}}^{(k,k_\mathrm{B})}$. $\overline{T}_{n_\mathrm{F}}$ of (8.74) is termed mean symbol transmit energy [MW04]. The subcarrier specific modulator matrix $\underline{\tilde{\mathbf{M}}}_{n_\mathrm{F}}$ and, thus, also $\overline{T}_{n_\mathrm{F}}$ of (8.74), is a non linear function of the components $\underline{\tilde{\varepsilon}}_{\mathrm{JCE},n_\mathrm{F}}^{(k,k_\mathrm{B})}$ of the JCE error $\underline{\tilde{\varepsilon}}_{\mathrm{JCE}}$. Again, by means of the linear Taylor expansion the subcarrier specific modulator matrix $\underline{\tilde{\mathbf{M}}}_{n_\mathrm{F}}$ can be approximated. Following the procedure and the assumptions given in Subsections 8.2.1 and 8.3.1, $\underline{\tilde{\mathbf{M}}}_{n_\mathrm{F}}$ of (8.61) can be approximately calculated as [MW04]

$$\begin{aligned}\underline{\tilde{\mathbf{M}}}_{n_\mathrm{F}} \;\approx\; & \underline{\tilde{\mathbf{H}}}_{n_\mathrm{F}}^{*}\left(\underline{\tilde{\mathbf{H}}}_{n_\mathrm{F}}^{\mathrm{T}}\underline{\tilde{\mathbf{H}}}_{n_\mathrm{F}}^{*}\right)^{-1} + \underline{\tilde{\mathbf{E}}}_{n_\mathrm{F}}^{*}\left(\underline{\tilde{\mathbf{H}}}_{n_\mathrm{F}}^{\mathrm{T}}\underline{\tilde{\mathbf{H}}}_{n_\mathrm{F}}^{*}\right)^{-1} - \\ & \underline{\tilde{\mathbf{H}}}_{n_\mathrm{F}}^{*}\left(\underline{\tilde{\mathbf{H}}}_{n_\mathrm{F}}^{\mathrm{T}}\underline{\tilde{\mathbf{H}}}_{n_\mathrm{F}}^{*}\right)^{-1}\left(\underline{\tilde{\mathbf{E}}}_{n_\mathrm{F}}^{\mathrm{T}}\underline{\tilde{\mathbf{H}}}_{n_\mathrm{F}}^{*} + \underline{\tilde{\mathbf{H}}}_{n_\mathrm{F}}^{\mathrm{T}}\underline{\tilde{\mathbf{E}}}_{n_\mathrm{F}}^{*}\right)\left(\underline{\tilde{\mathbf{H}}}_{n_\mathrm{F}}^{\mathrm{T}}\underline{\tilde{\mathbf{H}}}_{n_\mathrm{F}}^{*}\right)^{-1}.\end{aligned} \tag{8.75}$$

With (8.36), (8.38), (8.67) and (8.75), $\overline{T}_{n_\mathrm{F}}$ of (8.74) is approximately calculated by

$$\begin{aligned}\overline{T}_{n_\mathrm{F}} \;\approx\; & E_\mathrm{d} \cdot \left(1 + 2\sigma^2_{\underline{\tilde{\varepsilon}}_{\mathrm{JCE}}} \cdot \mathrm{trace}\left\{\left(\underline{\tilde{\mathbf{H}}}_{n_\mathrm{F}}^{\mathrm{T}}\underline{\tilde{\mathbf{H}}}_{n_\mathrm{F}}^{*}\right)^{-1}\right\}\right) \cdot \left[\left(\underline{\tilde{\mathbf{H}}}_{n_\mathrm{F}}^{\mathrm{T}}\underline{\tilde{\mathbf{H}}}_{n_\mathrm{F}}^{*}\right)^{-1}\right]_{k,k} + \\ & E_\mathrm{d} \cdot 2\sigma^2_{\underline{\tilde{\varepsilon}}_{\mathrm{JCE}}}(K_\mathrm{B} - K) \cdot \left[\left(\underline{\tilde{\mathbf{H}}}_{n_\mathrm{F}}^{\mathrm{T}}\underline{\tilde{\mathbf{H}}}_{n_\mathrm{F}}^{*}\right)^{-2}\right]_{k,k}\end{aligned} \tag{8.76}$$

The case of perfect channel knowledge is also included in (8.76), where [Skl04]

$$\left(\overline{T}_{n_\mathrm{F}}\right)_{\mathrm{perf}} = E_\mathrm{d} \cdot \left[\left(\underline{\tilde{\mathbf{H}}}_{n_\mathrm{F}}^{\mathrm{T}}\underline{\tilde{\mathbf{H}}}_{n_\mathrm{F}}^{*}\right)^{-1}\right]_{k,k} \tag{8.77}$$

holds for the mean transmit energy per data symbol. Comparing (8.76) and (8.77) we can obtain the ratios [MW04]

$$\frac{\overline{T}_{n_\mathrm{F}}}{\left(\overline{T}_{n_\mathrm{F}}\right)_{\mathrm{perf}}} = 1 + 2\sigma^2_{\underline{\tilde{\varepsilon}}_{\mathrm{JCE}}} \cdot \mathrm{trace}\left\{\left(\underline{\tilde{\mathbf{H}}}^{\mathrm{T}}_{n_\mathrm{F}}\underline{\tilde{\mathbf{H}}}^{*}_{n_\mathrm{F}}\right)^{-1}\right\} + 2\sigma^2_{\underline{\tilde{\varepsilon}}_{\mathrm{JCE}}}(K_\mathrm{B}-K)\cdot\frac{\left[\left(\underline{\tilde{\mathbf{H}}}^{\mathrm{T}}_{n_\mathrm{F}}\underline{\tilde{\mathbf{H}}}^{*}_{n_\mathrm{F}}\right)^{-2}\right]_{k,k}}{\left[\left(\underline{\tilde{\mathbf{H}}}^{\mathrm{T}}_{n_\mathrm{F}}\underline{\tilde{\mathbf{H}}}^{*}_{n_\mathrm{F}}\right)^{-1}\right]_{k,k}}, \tag{8.78}$$

which describe the extend to which the mean symbol energy $\overline{T}_{n_\mathrm{F}}$ is influenced by the presence of JCE errors as compared to the case of perfect channel knowledge. The ratios in (8.78) are always larger than one, which means that non-perfect channel knowledge results in an increase of the mean transmit energy $\overline{T}_{n_\mathrm{F}}$. Also, the relative increase $\overline{T}_{n_\mathrm{F}}/\left(\overline{T}_{n_\mathrm{F}}\right)_{\mathrm{perf}}$ - 1 is proportional to the variance $\sigma^2_{\underline{\tilde{\varepsilon}}_{\mathrm{JCE}}}$ of the JCE error $\underline{\tilde{\varepsilon}}_{\mathrm{JCE}}$ and it is influenced by the subcarrier specific channel matrix $\underline{\tilde{\mathbf{H}}}_{n_\mathrm{F}}$. The SNRs $\gamma^{(k)}_{\mathrm{JT},n_\mathrm{F}}$ of (8.71) can be related to the mean transmit energy $\overline{T}_{n_\mathrm{F}}$ of (8.76) by

$$\gamma^{(k)}_{\mathrm{JT},n_\mathrm{F}} \approx 2\overline{T}_{n_\mathrm{F}} \Bigg/ \Bigg(\left(2\sigma^2 + 2\sigma^2\cdot 2\sigma^2_{\underline{\tilde{\varepsilon}}_{\mathrm{JCE}}}\mathrm{trace}\left\{\left(\underline{\tilde{\mathbf{H}}}^{\mathrm{T}}_{n_\mathrm{F}}\underline{\tilde{\mathbf{H}}}^{*}_{n_\mathrm{F}}\right)^{-1}\right\}\right)\cdot \left[\left(\underline{\tilde{\mathbf{H}}}^{\mathrm{T}}_{n_\mathrm{F}}\underline{\tilde{\mathbf{H}}}^{*}_{n_\mathrm{F}}\right)^{-1}\right]_{k,k} + 2\sigma^2\cdot 2\sigma^2_{\underline{\tilde{\varepsilon}}_{\mathrm{JCE}}}\cdot(K_\mathrm{B}-K)\cdot\left[\left(\underline{\tilde{\mathbf{H}}}^{\mathrm{T}}_{n_\mathrm{F}}\underline{\tilde{\mathbf{H}}}^{*}_{n_\mathrm{F}}\right)^{-2}\right]_{k,k} + 2\overline{T}_{n_\mathrm{F}}\cdot 2\sigma^2_{\underline{\tilde{\varepsilon}}_{\mathrm{JCE}}}\mathrm{trace}\left\{\left(\underline{\tilde{\mathbf{H}}}^{\mathrm{T}}_{n_\mathrm{F}}\underline{\tilde{\mathbf{H}}}^{*}_{n_\mathrm{F}}\right)^{-1}\right\}\Bigg). \tag{8.79}$$

With (8.79) we can approximately calculate the bit error probability $P^{(k)}_{\mathrm{b},n_\mathrm{F}}$ of (8.72) in addition to obtaining it by computer simulations. Figs. 8.5 and 8.6 show the obtained results for the two considered cases of the variance $\sigma^2_{\underline{\tilde{\varepsilon}}_{\mathrm{JCE}}}$ of the JCE error. The simulation and calculation results for the first case, where $\sigma^2_{\underline{\tilde{\varepsilon}}_{\mathrm{JCE}}}$ depends on the noise variance σ^2, are displayed in Fig. 8.5. Here, the assumption is made that the noise variance σ^2 is the same at the receivers in both the UL and the DL. The number K_B of APs and the number K of MTs are both set equal to four. In this case and together with the considered MIMO parametric channel model, see (8.44)

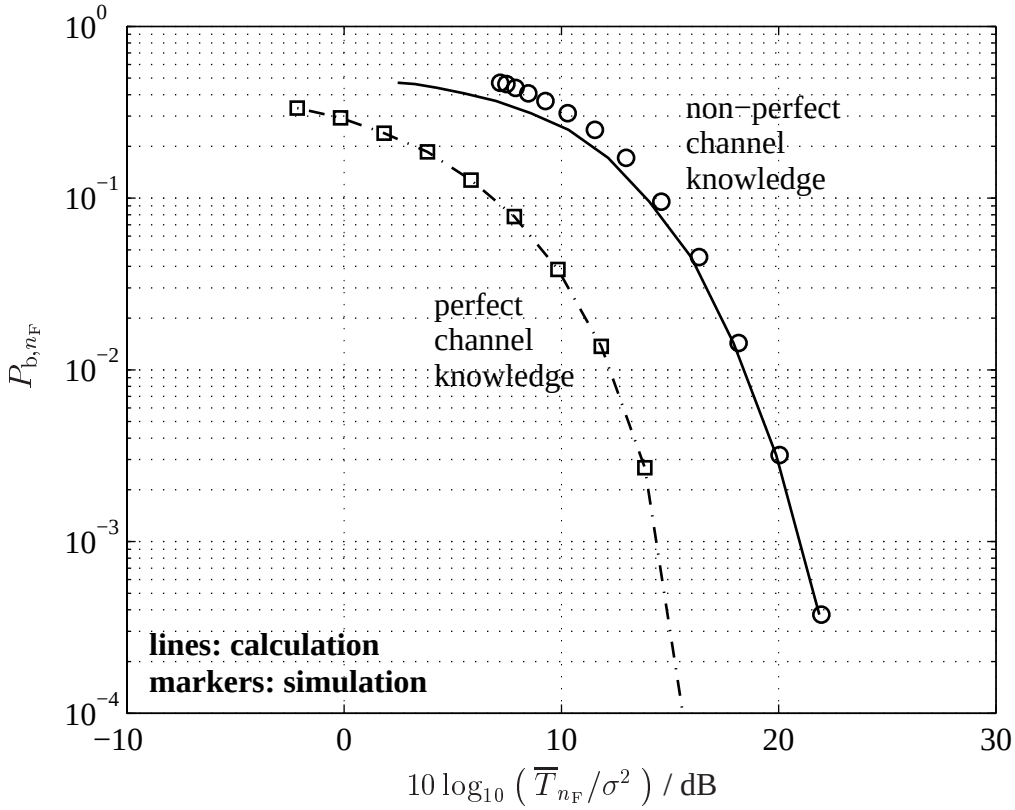

Fig. 8.5. Bit error probability $P_{\mathrm{b},n_\mathrm{F}}$ versus the ratio $\overline{T}_{n_\mathrm{F}}/\sigma^2$; MIMO parametric channel model, $\rho = 0.5$, $K_\mathrm{B} = K = 4$;

$$
\begin{aligned}
P_{\mathrm{b}n_\mathrm{F}}^{(k)} &= P_{\mathrm{b},n_\mathrm{F}} \qquad (8.80)\\
&\approx \frac{1}{2}\mathrm{erfc}\left(\left[\overline{T}_{n_\mathrm{F}}\Big/\left(2\sigma^2 + 2\sigma^2\cdot 2\sigma^2_{\underline{\tilde{\varepsilon}}_{\mathrm{JCE}}}\,\mathrm{trace}\left\{\left(\underline{\tilde{\mathbf{H}}}^{\mathrm{T}}_{n_\mathrm{F}}\underline{\tilde{\mathbf{H}}}^{*}_{n_\mathrm{F}}\right)^{-1}\right\}\right)\cdot\right.\\
&\qquad\left.\left[\left(\underline{\tilde{\mathbf{H}}}^{\mathrm{T}}_{n_\mathrm{F}}\underline{\tilde{\mathbf{H}}}^{*}_{n_\mathrm{F}}\right)^{-1}\right]_{k,k} + 2\overline{T}_{n_\mathrm{F}}\cdot 2\sigma^2_{\underline{\tilde{\varepsilon}}_{\mathrm{JCE}}}\,\mathrm{trace}\left\{\left(\underline{\tilde{\mathbf{H}}}^{\mathrm{T}}_{n_\mathrm{F}}\underline{\tilde{\mathbf{H}}}^{*}_{n_\mathrm{F}}\right)^{-1}\right\}\right]^{1/2}\Bigg)
\end{aligned}
$$

holds for the bit error probability of (8.72). Similarly to the respective graphs for JD, see Subsection 8.2.2, the lines mark the calculation results, and the markers stand for the simulation results. The impact of the JCE error on the performance of JT is expressed in Fig. 8.5 by the shift of the resulting curves to the right as compared to the case of perfect channel knowledge. This shift can be interpreted in two ways, namely that in the presence of JCE errors

1. for the same value of the ratio $\overline{T}_{n_\mathrm{F}}/\sigma^2$ the bit error probability increases dramatically, and

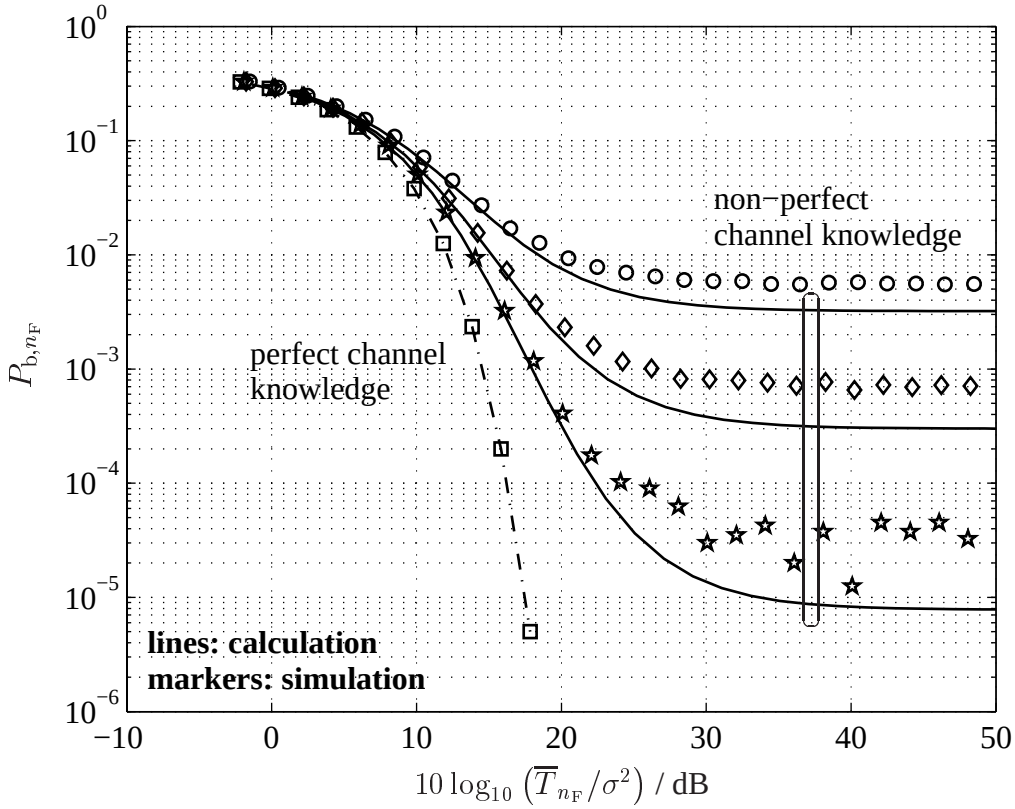

Fig. 8.6. Bit error probability $P_{\mathrm{b},n_\mathrm{F}}$ versus the ratio $\overline{T}_{n_\mathrm{F}}/\sigma^2$; MIMO parametric channel model, $\rho = 0.5$, $K_\mathrm{B} = K = 4$; fixed variance σ^2_{JCE} of the JCE error

2. in order to reach a predefined value of $P_{\mathrm{b},n_\mathrm{F}}$ a higher mean transmit energy $\overline{T}_{n_\mathrm{F}}$ is required, see also (8.78).

Fig. 8.6 shows the results for the second case concerning the variance $\sigma^2_{\underline{\tilde{\varepsilon}}_{\mathrm{JCE}}}$ of the JCE error, which is now independent of the noise variance σ^2 at the MTs and it has a fixed value. Similar to the case of JD, for the SNR $\gamma_{\underline{\tilde{\varepsilon}}_{\mathrm{JCE}}}$ defined in (8.50) the values of 25 dB, 27 dB and 29 dB are considered. We can see from (8.80) that for increasing $\overline{T}_{n_\mathrm{F}}/\sigma^2$ values, i. e., σ^2 goes to zero, $P_{\mathrm{b},n_\mathrm{F}}$ is lower bounded by the minimum bit error probability

$$\lim_{\sigma^2\to 0} P_{\mathrm{b},n_\mathrm{F}} = (P_{\mathrm{b},n_\mathrm{F}})_{\min} = \frac{1}{2}\mathrm{erfc}\left(\frac{1}{2\sqrt{\sigma^2_{\underline{\tilde{\varepsilon}}_{\mathrm{JCE}}}\,\mathrm{trace}\left\{\left(\underline{\tilde{\mathbf{H}}}^{\mathrm{T}}_{n_\mathrm{F}}\underline{\tilde{\mathbf{H}}}^{*}_{n_\mathrm{F}}\right)^{-1}\right\}}}\right) \tag{8.81}$$

resulting into an error floor, as it is also verified by the results displayed in Fig. 8.6 for the three different values of $\gamma_{\underline{\tilde{\varepsilon}}_{\mathrm{JCE}}}$.

Finally, as in the case of JD, the quality of the approximations given in this and in the previous subsections is justified by the good match between the simulated and the calculated results.

Chapter 9
Summary

9.1 English

In the thesis the task of channel estimation in beyond 3G service area based mobile radio air interfaces is considered. A system concept named Joint Transmission and Detection Integrated Network (JOINT) forms the target platform for the investigations. A single service area of JOINT is considered, in which a number of mobile terminals is supported by a number of radio access points, which are connected to a central unit responsible for the signal processing. The modulation scheme of JOINT is OFDM.

Pilot-aided channel estimation is considered, which has to be performed only in the uplink of JOINT, because the duplexing scheme TDD is applied. In this way, the complexity of the mobile terminals is reduced, because they do not need a channel estimator. Based on the signals received by the access points, the central unit estimates the channel transfer functions jointly for all mobile terminals. This is done by resorting to the a priori knowledge of the radiated pilot signals and by applying the technique of joint channel estimation, which is developed in the thesis. The quality of the gained estimates is judged by the degradation of their signal-to-noise ratio as compared to the signal-to-noise ratio of the respective estimates gained in the case of a single mobile terminal radiating its pilots. In the case of single-element receive antennas at the access points, said degradation depends solely on the structure of the applied pilots. In the thesis it is shown how by a proper design of the pilots the SNR degradation can be minimized.

Besides using appropriate pilots, the performance of joint channel estimation can be further improved by the inclusion of additional a-priori information in the estimation process. An example of such additional information would be the knowledge of the directional properties of the radio channels. This knowledge can be gained if multi-element antennas are applied at the access points. Further, a-priori channel state information in the form of the power delay profiles of the radio channels can be included in the estimation process by the application of the minimum mean square error estimation principle for joint channel estimation.

After having intensively studied the problem of joint channel estimation in JOINT, the thesis rounds itself by considering the impact of the unavoidable channel estimation errors on the performance of data estimation in JOINT. For the case of small channel estimation errors occurring due to the presence of noise at the access points, the performance of joint detection in the uplink and of joint transmission in the downlink of JOINT are investigated based on simulations. For the uplink, which utilizes joint detection, it is shown to which degree the bit error probability increases due to channel estimation errors. For the downlink, which utilizes joint transmission, channel estimation errors lead to an increase of the required transmit power, which can be quantified by the simulation results.

9.2 Deutsch

Die vorliegende Dissertation betrachtet die Aufgabe der Kanalschätzung in Mobilfunksystemen jenseits der 3. Generation auf der Basis von Service-Gebieten. Das Mobilfunksystem mit der Bezeichnung Joint Transmission and Detection Integrated Network (JOINT) dient als die erforderliche Plattform für die entsprechenden Untersuchungen. Es wird ein einziges Service-Gebiet von JOINT betrachtet, innerhalb dessen eine Anzahl mobiler Endgeräte über eine Anzahl von Zugangspunkten versorgt wird, die ihrerseits mit einer zentralen Einheit verbunden sind. Die zentrale Einheit trägt die Aufgabe der Signalverarbeitung. Das Modulationsverfahren von JOINT ist OFDM.

Es wird die pilot-basierte Kanalschätzung betrachtet, die aufgrund des Einsatzes von Zeitduplex nur in der Aufwärtsstrecke von JOINT durchgeführt werden muß. Dadurch wird die Komplexität der mobilen Endgeräte reduziert, da diese keinen Kanalschätzer benötigen. Basierend auf an den Zugangspunkten empfangenen Signalen schätzt die zentrale Einheit die Kanalübertragungsfunktionen gemeinsam für alle Teilnehmer. Dies geschieht durch das Anwenden der a-priori Kenntnis der abgestrahlten Pilotsignale und der Technik der gemeinsamen Kanalschätzung, welche in der Arbeit vorgestellt wird. Die Qualität der Schätzung wird mittels der Degradation ihres Signal-Stör-Verhältnisses im Vergleich zum Signal-Stör-Verhältnis der Kanalschätzung bei einem Einteilnehmersystem beurteilt. Im Falle des Einsatzes nur eines Antennenelements an den Zugangspunkten hängt diese SNR-Degradation einzig und allein von der Struktur der benutzten Piloten ab. In der Arbeit wird gezeigt, wie durch einen geeigneten Entwurf der Pilotsignale die SNR-Degradation minimiert werden kann.

Neben dem Einsatz vorteilhaft gewählter Piloten kann man die Performanz der gemeinsamen Kanalschätzung durch das Einbringen zusätzlicher a-priori Information in den Schätzprozeß weiter verbessern. Ein Beispiel solcher zusätzlicher Information ist die Kenntnis der direktionellen Eigenschaften der Mobilfunkkanäle. Diese Kenntnis kann gewonnen werden, wenn mehrere Antennenelemente an den Zugangspunkten eingesetzt werden. Des weiteren kann a-priori Information über die Verzögerungsleistungsdichtespektren der Mobilfunkkanäle in den Schätzprozeß eingebracht werden, indem man das Minimum Mean Square Error Schätzprinzip einsetzt.

Nachdem das Problem der gemeinsamen Kanalschätzung in JOINT ausführlich diskutiert wurde, wird die Arbeit abgerundet durch die Untersuchung des Einflußes unvermeidbarer Kanalschätzfehler auf die Performanz der Datenschätzung in JOINT. Im Falle kleiner Kanalschätzfehler, die durch die Präsenz von Rauschen an den Zugangspunkten zustandekommen, werden die Performanz von Joint Detection in der Aufwärtsstrecke und die Performanz von Joint Transmission in der Abwärtsstrecke von JOINT simulativ untersucht. Im Falle der Aufwärtsstrecke, wo Joint Detection zum Einsatz kommt, wird der Grad der Erhöhung der Bitfehlerwahrscheinlichkeit aufgrund der vorhandenen Kanalschätzfehlern gezeigt. Im Falle der Abwärts- strecke, wo Joint Transmission zum Einsatz kommt, führen Kanalschätzfehler zu einem Anstieg der erforderlichen Sendeenergie, welcher durch die Simulationsergebnisse quantifiziert werden kann.

Appendix A
Ideal set of pilot vectors based on the Walsh codes

A.1 Illustrative example

The statement made at the end of Subsection 5.5.2 about the off-diagonal elements of Type III of $\underline{\tilde{\mathcal{G}}}^{\mathsf{H}}\underline{\tilde{\mathcal{G}}}$ being equal to zero due to the respective choice of the pilot vectors based on Walsh codes shall be mathematically proven by means of induction. To begin with, basic properties of the pilot vectors based on Walsh codes are demonstrated by three simple examples. Let us consider a scenario characterized by the parameter triplet of (5.10). The Walsh codes of dimension four are the columns of the 4×4 Hadamard matrix [Pro95]

$$\tilde{\mathbf{W}} = \left(\tilde{\mathbf{w}}^{(1)} \;\; \tilde{\mathbf{w}}^{(2)} \;\; \tilde{\mathbf{w}}^{(3)} \;\; \tilde{\mathbf{w}}^{(4)} \right) = \begin{pmatrix} 1 & 1 & 1 & 1 \\ 1 & -1 & 1 & -1 \\ 1 & 1 & -1 & -1 \\ 1 & -1 & -1 & 1 \end{pmatrix}. \tag{A.1}$$

For the parameter triplet of (5.10) the reduced Fourier matrix of (4.21) is given in (5.15). According to (5.33), we may chose the first two column vectors $\tilde{\mathbf{w}}^{(1)}$ and $\tilde{\mathbf{w}}^{(2)}$ of the Hadamard matrix $\tilde{\mathbf{W}}$ of (A.1) and form the MT-specific pilot vectors $\underline{\tilde{\mathbf{p}}}^{(1)}$ and $\underline{\tilde{\mathbf{p}}}^{(2)}$, respectively. This results in the total pilot matrix

$$\underline{\tilde{\mathbf{P}}} = \sqrt{\frac{2E_{\mathrm{p}}}{N_{\mathrm{F}}}} \cdot \begin{pmatrix} 1 & 0 & 0 & 0 & 1 & 0 & 0 & 0 \\ 0 & 1 & 0 & 0 & 0 & -1 & 0 & 0 \\ 0 & 0 & 1 & 0 & 0 & 0 & 1 & 0 \\ 0 & 0 & 0 & 1 & 0 & 0 & 0 & -1 \end{pmatrix}. \tag{A.2}$$

With the blockdiagonal reduced Fourier matrix of (5.15) valid for the considered parameter triplet, the system matrix $\underline{\tilde{\mathcal{G}}}$ of (4.25) reads

$$\underline{\tilde{\mathcal{G}}} = \sqrt{\frac{2E_{\mathrm{p}}}{N_{\mathrm{F}}}} \cdot \begin{pmatrix} 1 & 1 & 1 & 1 \\ 1 & -\mathrm{j} & -1 & \mathrm{j} \\ 1 & -1 & 1 & -1 \\ 1 & \mathrm{j} & -1 & -\mathrm{j} \end{pmatrix} \tag{A.3}$$

and the Gram matrix $\underline{\tilde{\mathcal{G}}}^{\mathsf{H}}\underline{\tilde{\mathcal{G}}}$ becomes

$$\begin{aligned} \underline{\tilde{\mathcal{G}}}^{\mathsf{H}}\underline{\tilde{\mathcal{G}}} &= \sqrt{\frac{2E_{\mathrm{p}}}{N_{\mathrm{F}}}} \cdot \begin{pmatrix} 1 & 1 & 1 & 1 \\ 1 & \mathrm{j} & -1 & -\mathrm{j} \\ 1 & -1 & 1 & -1 \\ 1 & -\mathrm{j} & -1 & \mathrm{j} \end{pmatrix} \begin{pmatrix} 1 & 1 & 1 & 1 \\ 1 & -\mathrm{j} & -1 & \mathrm{j} \\ 1 & -1 & 1 & -1 \\ 1 & \mathrm{j} & -1 & -\mathrm{j} \end{pmatrix} \\ &= \frac{2E_{\mathrm{p}}}{4} \cdot \begin{pmatrix} 4 & 0 & 0 & 0 \\ 0 & 4 & 0 & 0 \\ 0 & 0 & 4 & 0 \\ 0 & 0 & 0 & 4 \end{pmatrix} = 2E_{\mathrm{p}} \cdot \mathbf{I}^{(4\times 4)}. \end{aligned} \tag{A.4}$$

With (A.4) one can verify that the off-diagonal elements of Type III of $\underline{\tilde{\mathcal{G}}}^{\mathsf{H}}\underline{\tilde{\mathcal{G}}}$ are zero and along with the considerations given in Section 5.2 that all SNR degradations $\delta_{n_\mathrm{F}}^{(k)}$, $n_\mathrm{F} = 1 \ldots N_\mathrm{F}$, $k = 1 \ \ldots \ K$, are equal to one.

As a second example, we may chose the third and fourth column vectors $\tilde{\mathbf{w}}^{(3)}$ and $\tilde{\mathbf{w}}^{(4)}$ of the Hadamard matrix $\tilde{\mathbf{W}}$ of (A.1) and form the MT-specific pilot vectors $\underline{\tilde{\mathbf{p}}}^{(1)}$ and $\underline{\tilde{\mathbf{p}}}^{(2)}$, respectively. This choice results in the total pilot matrix

$$\underline{\tilde{\mathbf{P}}} = \sqrt{\frac{2E_\mathrm{p}}{N_\mathrm{F}}} \cdot \begin{pmatrix} 1 & 0 & 0 & 0 & 1 & 0 & 0 & 0 \\ 0 & 1 & 0 & 0 & 0 & -1 & 0 & 0 \\ 0 & 0 & -1 & 0 & 0 & 0 & -1 & 0 \\ 0 & 0 & 0 & -1 & 0 & 0 & 0 & 1 \end{pmatrix}. \tag{A.5}$$

In this case, the system matrix $\underline{\tilde{\mathcal{G}}}$ of (4.25) reads

$$\underline{\tilde{\mathcal{G}}} = \sqrt{\frac{2E_\mathrm{p}}{N_\mathrm{F}}} \cdot \begin{pmatrix} 1 & 1 & 1 & 1 \\ 1 & -\mathrm{j} & -1 & \mathrm{j} \\ -1 & 1 & -1 & 1 \\ -1 & -\mathrm{j} & 1 & \mathrm{j} \end{pmatrix} \tag{A.6}$$

and the respective Gram matrix $\underline{\tilde{\mathcal{G}}}^{\mathsf{H}}\underline{\tilde{\mathcal{G}}}$ becomes

$$\begin{aligned} \underline{\tilde{\mathcal{G}}}^{\mathsf{H}}\underline{\tilde{\mathcal{G}}} &= \sqrt{\frac{2E_\mathrm{p}}{N_\mathrm{F}}} \cdot \begin{pmatrix} 1 & 1 & -1 & -1 \\ 1 & \mathrm{j} & 1 & \mathrm{j} \\ 1 & -1 & -1 & 1 \\ 1 & \mathrm{j} & 1 & -\mathrm{j} \end{pmatrix} \begin{pmatrix} 1 & 1 & 1 & 1 \\ 1 & -\mathrm{j} & -1 & \mathrm{j} \\ -1 & 1 & -1 & 1 \\ -1 & -\mathrm{j} & 1 & \mathrm{j} \end{pmatrix} \\ &= \frac{2E_\mathrm{p}}{4} \cdot \begin{pmatrix} 4 & 0 & 0 & 0 \\ 0 & 4 & 0 & 0 \\ 0 & 0 & 4 & 0 \\ 0 & 0 & 0 & 4 \end{pmatrix} = 2E_\mathrm{p} \cdot \mathbf{I}^{(4\times 4)}. \end{aligned} \tag{A.7}$$

Again, the off-diagonal elements of Type III of $\underline{\tilde{\mathcal{G}}}^{\mathsf{H}}\underline{\tilde{\mathcal{G}}}$ are zero and along with the considerations given in Section 5.2 it can be verified that all SNR degradations $\delta_{n_\mathrm{F}}^{(k)}$, $n_\mathrm{F} = 1 \ldots N_\mathrm{F}$, $k = 1 \ \ldots \ K$, are equal to one.

However, if we chose the two pilot vectors $\underline{\tilde{\mathbf{p}}}^{(1)}$ and $\underline{\tilde{\mathbf{p}}}^{(2)}$ to be equal to the first and the third column vector $\tilde{\mathbf{w}}^{(1)}$ and $\tilde{\mathbf{w}}^{(3)}$, respectively, of the Hadamard matrix $\tilde{\mathbf{W}}$ of (A.1) the system matrix $\underline{\tilde{\mathcal{G}}}$ of (4.25) becomes

$$\underline{\tilde{\mathcal{G}}} = \sqrt{\frac{2E_\mathrm{p}}{N_\mathrm{F}}} \cdot \begin{pmatrix} 1 & 1 & 1 & 1 \\ 1 & -\mathrm{j} & 1 & -\mathrm{j} \\ 1 & -1 & -1 & 1 \\ 1 & \mathrm{j} & -1 & -\mathrm{j} \end{pmatrix} \tag{A.8}$$

and the respective Gram matrix $\underline{\tilde{\mathcal{G}}}^{\mathsf{H}}\underline{\tilde{\mathcal{G}}}$ reads

$$\begin{aligned}\underline{\tilde{\mathcal{G}}}^{\mathsf{H}}\underline{\tilde{\mathcal{G}}} &= \sqrt{\frac{2E_{\mathrm{p}}}{N_{\mathrm{F}}}}\cdot\begin{pmatrix}1 & 1 & 1 & 1\\ 1 & \mathrm{j} & -1 & -\mathrm{j}\\ 1 & 1 & -1 & -1\\ 1 & \mathrm{j} & 1 & \mathrm{j}\end{pmatrix}\begin{pmatrix}1 & 1 & 1 & 1\\ 1 & -\mathrm{j} & 1 & -\mathrm{j}\\ 1 & -1 & -1 & 1\\ 1 & \mathrm{j} & -1 & -\mathrm{j}\end{pmatrix}\\ &= \frac{2E_{\mathrm{p}}}{4}\cdot\begin{pmatrix}4 & 0 & 0 & 2-2\mathrm{j}\\ 0 & 4 & 2-2\mathrm{j} & 0\\ 0 & 2-2\mathrm{j} & 4 & 0\\ 2+2\mathrm{j} & 0 & 0 & 4\end{pmatrix}.\end{aligned} \tag{A.9}$$

Since the off-diagonal elements of Type III of $\underline{\tilde{\mathcal{G}}}^{\mathsf{H}}\underline{\tilde{\mathcal{G}}}$ of (A.9) are non-zero, the resulting SNR degradations $\delta_{n_{\mathrm{F}}}^{(k)}$, $n_{\mathrm{F}} = 1 \ldots N_{\mathrm{F}}$, $k = 1 \ \ldots \ K$, will not be equal to one. For this specific example the SNR degradations $\delta_{n_{\mathrm{F}}}^{(k)}$ are equal to two. Out of these simple examples it can be concluded that

- there exist pilot vectors based on Walsh codes which result in the optimum SNR degradation values of one,
- it is even possible to find more than one set of such pilot vectors for a fixed parameter triplet $\{N_{\mathrm{F}},\ K,\ W\}$, as it is seen by the first two examples, and
- orthogonality between the pilot vectors does not necessarily lead to SNR degradations equal to one.

A.2 Proposition

According to (5.33), it is proposed that the M sets

$$\mathbb{P}^{(m)} = \left\{\ \underline{\tilde{\mathbf{p}}}^{(1,m)},\ \ldots,\ \underline{\tilde{\mathbf{p}}}^{(K,m)}\right\},\ m = 1\ \ldots\ M, \tag{A.10}$$

of pilot vectors

$$\underline{\tilde{\mathbf{p}}}^{(k,m)} = \sqrt{\frac{2E_{\mathrm{p}}}{N_{\mathrm{F}}}}\cdot\left[\ \tilde{\mathbf{W}}^{(N_{\mathrm{F}}\times N_{\mathrm{F}})}\right]_{N_{\mathrm{F}},\ (m-1)K+k}^{1,\ (m-1)K+k},\ k = 1\ \ldots\ K, \tag{A.11}$$

for JCE in a scenario with maximum CIR dimension

$$W = M \tag{A.12}$$

lead to SNR degradation values $\delta_{n_{\mathrm{F}}}^{(k)}$, $n_{\mathrm{F}} = 1 \ldots N_{\mathrm{F}}$, $k = 1 \ \ldots \ K$, equal to one. In what follows, this proposal will be proven by means of induction. For the total pilot matrix of (4.10)

$$\underline{\tilde{\mathbf{P}}} = \left(\mathrm{diag}\left(\ \underline{\tilde{\mathbf{p}}}^{(1,m)}\right)\ \ldots\ \mathrm{diag}\left(\ \underline{\tilde{\mathbf{p}}}^{(K,m)}\right)\right) \tag{A.13}$$

holds.

A.3 Proof by induction

The base case for the induction proof is characterized by $N_\mathrm{F} = 1$. Consequently, due to (4.15), $K = 1$ and $W = 1$ follow. For the base case, the total pilot matrix $\underline{\tilde{\mathbf{P}}}$ of (4.10) is the 1×1 matrix

$$\underline{\tilde{\mathbf{P}}} = \sqrt{2E_\mathrm{p}} \cdot (1) \tag{A.14}$$

and the reduced Fourier matrix of (4.21) becomes

$$\underline{\tilde{\boldsymbol{\mathcal{F}}}}_\mathrm{W} = (1)\,. \tag{A.15}$$

With (A.14), (A.15) and the resulting system matrix

$$\underline{\tilde{\boldsymbol{\mathcal{G}}}} = \underline{\tilde{\mathbf{P}}}\,\underline{\tilde{\boldsymbol{\mathcal{F}}}}_\mathrm{W} = \sqrt{2E_\mathrm{p}} \cdot (1) \tag{A.16}$$

it is easily verified that the SNR degradations $\delta_{n_\mathrm{F}}^{(k)}$ of (4.42) are equal to one.

A.4 Induction hypothesis

In the induction hypothesis it is assumed that

$$\underline{\tilde{\boldsymbol{\mathcal{G}}}}^\mathsf{H}\,\underline{\tilde{\boldsymbol{\mathcal{G}}}} = 2E_\mathrm{p} \cdot \mathbf{I}^{(KW \times KW)} \tag{A.17}$$

holds for the value N_F and all possible values of

$$\begin{aligned} K &= 1,\ 2,\ 4,\ \ldots,\ N_\mathrm{F}, \\ M &= W = \frac{N_\mathrm{F}}{K}, \\ m &= 1\ \ldots\ M. \end{aligned} \tag{A.18}$$

In particular, with the complex exponential

$$\underline{\varepsilon} = \mathrm{e}^{-\mathrm{j}\frac{\pi}{N_\mathrm{F}}} \tag{A.19}$$

the system matrix $\underline{\tilde{\mathcal{G}}}$ reads

$$\underline{\tilde{\mathcal{G}}} = \sqrt{\frac{2E_\mathrm{p}}{N_\mathrm{F}}} \cdot \begin{pmatrix} 1 \cdot \left[\tilde{\mathbf{W}}^{(N_\mathrm{F} \times N_\mathrm{F})} \right]_{1,\ (m-1)K+1} & 1 \cdot \left[\tilde{\mathbf{W}}^{(N_\mathrm{F} \times N_\mathrm{F})} \right]_{1,\ (m-1)K+1} & \cdots \\ 1 \cdot \left[\tilde{\mathbf{W}}^{(N_\mathrm{F} \times N_\mathrm{F})} \right]_{2,\ (m-1)K+1} & \underline{\varepsilon}^2 \cdot \left[\tilde{\mathbf{W}}^{(N_\mathrm{F} \times N_\mathrm{F})} \right]_{2,\ (m-1)K+1} & \cdots \\ \vdots & \vdots & \vdots \\ 1 \cdot \left[\tilde{\mathbf{W}}^{(N_\mathrm{F} \times N_\mathrm{F})} \right]_{N_\mathrm{F},\ (m-1)K+1} & \underline{\varepsilon}^{2(N_\mathrm{F}-1)} \cdot \left[\tilde{\mathbf{W}}^{(N_\mathrm{F} \times N_\mathrm{F})} \right]_{N_\mathrm{F},\ (m-1)K+1} & \cdots \end{pmatrix}$$

$$\begin{pmatrix} \cdots & \cdots & 1 \cdot \left[\tilde{\mathbf{W}}^{(N_\mathrm{F} \times N_\mathrm{F})} \right]_{1,\ (m-1)K+K} \\ \cdots & \cdots & \underline{\varepsilon}^{2(W-1)} \cdot \left[\tilde{\mathbf{W}}^{(N_\mathrm{F} \times N_\mathrm{F})} \right]_{2,\ (m-1)K+K} \\ \vdots & \vdots & \vdots \\ \cdots & \cdots & \underline{\varepsilon}^{2(W-1)(N_\mathrm{F}-1)} \cdot \left[\tilde{\mathbf{W}}^{(N_\mathrm{F} \times N_\mathrm{F})} \right]_{N_\mathrm{F},\ (m-1)K+K} \end{pmatrix} . \tag{A.20}$$

The element in the i-th row and j-th column of the system matrix $\underline{\tilde{\mathcal{G}}}$ of (A.20) is

$$\left[\underline{\tilde{\mathcal{G}}} \right]_{i,\ j} = \sqrt{\frac{2E_\mathrm{p}}{N_\mathrm{F}}} \cdot \underline{\varepsilon}^{2(i-1)((j-1)_{\mathrm{mod}\ W})} \cdot \left[\tilde{\mathbf{W}}^{(N_\mathrm{F} \times N_\mathrm{F})} \right]_{i,\ (m-1)K+(j-1)_{\mathrm{div}\ W}+1} \tag{A.21}$$

and with (A.21) the element of the p-th row and q-th column of the matrix product $\underline{\tilde{\mathcal{G}}}^\mathsf{H} \underline{\tilde{\mathcal{G}}}$ of (4.42) is calculated by

$$\begin{aligned} \left[\underline{\tilde{\mathcal{G}}}^\mathsf{H} \underline{\tilde{\mathcal{G}}} \right]_{p,\ q} &= \sum_{i=1}^{N_\mathrm{F}} \left[\underline{\tilde{\mathcal{G}}} \right]^*_{i,\ p} \left[\underline{\tilde{\mathcal{G}}} \right]_{i,\ q} \\ &= \frac{2E_\mathrm{p}}{N_\mathrm{F}} \cdot \sum_{i=1}^{N_\mathrm{F}} \underline{\varepsilon}^{2(i-1)((q-1)_{\mathrm{mod}\ W}-(p-1)_{\mathrm{mod}\ W})} \cdot \\ &\quad \left[\tilde{\mathbf{W}}^{(N_\mathrm{F} \times N_\mathrm{F})} \right]_{i,\ (m-1)K+(p-1)_{\mathrm{div}\ W}+1} \cdot \\ &\quad \left[\tilde{\mathbf{W}}^{(N_\mathrm{F} \times N_\mathrm{F})} \right]_{i,\ (m-1)K+(q-1)_{\mathrm{div}\ W}+1} \\ &= \begin{cases} 2E_\mathrm{p}, & p = q, \\ 0, & \text{else.} \end{cases} \end{aligned} \tag{A.22}$$

A.5 Induction step

Following the basic case for $N_\mathrm{F} = 1$ and the induction hypothesis for the value N_F, now, we have to prove that

$$\underline{\tilde{\mathcal{G}}}^{\mathsf{H}}\,\underline{\tilde{\mathcal{G}}} = 2E_\mathrm{p} \cdot \mathbf{I}^{(KW \times KW)} \tag{A.23}$$

holds for the value $2N_\mathrm{F}$ and for all values

$$\begin{aligned} K &= 1,\ 2,\ 4\ \ldots\ 2N_\mathrm{F}, \\ M &= W = \frac{2N_\mathrm{F}}{K}, \\ m &= 1\ \ldots\ M, \end{aligned} \tag{A.24}$$

by using the induction hypothesis of (A.17). First of all, the special case $K = 2N_\mathrm{F}$ and $M = W = 1$ is considered. In this case,

$$\underline{\tilde{\boldsymbol{\mathcal{F}}}}_\mathrm{W} = \begin{pmatrix} 1 & & \\ 1 & & \\ \vdots & & \\ 1 & & \\ & \ddots & \\ & & 1 \\ & & 1 \\ & & \vdots \\ & & 1 \end{pmatrix} \tag{A.25}$$

holds for the reduced Fourier matrix of (4.21) of dimension $(2KN_\mathrm{F}) \times K$. With (A.25), (A.20) is rewritten as

$$\underline{\tilde{\mathcal{G}}} = \sqrt{\frac{2E_\mathrm{p}}{2N_\mathrm{F}}} \cdot\ \tilde{\mathbf{W}}^{(2N_\mathrm{F} \times 2N_\mathrm{F})} \tag{A.26}$$

and, consequently, due to the orthogonality property of the Walsh codes [Pro95, Kam96], (A.23) holds. Now, we consider the remaining cases $K = 1,\ 2,\ 4,\ \ldots,\ N_\mathrm{F}$. With (A.19), the $(2N_\mathrm{F}) \times (2N_\mathrm{F})$ Fourier matrix

$$\underline{\tilde{\boldsymbol{\mathcal{F}}}} = \begin{pmatrix} 1 & 1 & 1 & 1 & 1 & 1 \\ 1 & \underline{\varepsilon}^{1} & \underline{\varepsilon}^{2} & \underline{\varepsilon}^{3} & \ldots & \underline{\varepsilon}^{(2N_\mathrm{F}-1)} \\ 1 & \underline{\varepsilon}^{2} & \underline{\varepsilon}^{4} & \underline{\varepsilon}^{6} & \ldots & \underline{\varepsilon}^{2(2N_\mathrm{F}-1)} \\ 1 & \underline{\varepsilon}^{3} & \underline{\varepsilon}^{6} & \underline{\varepsilon}^{9} & \ldots & \underline{\varepsilon}^{3(2N_\mathrm{F}-1)} \\ \vdots & \vdots & \vdots & \vdots & \vdots & \vdots \\ 1 & \underline{\varepsilon}^{(2N_\mathrm{F}-1)} & \underline{\varepsilon}^{2(2N_\mathrm{F}-1)} & \underline{\varepsilon}^{3(2N_\mathrm{F}-1)} & \ldots & \underline{\varepsilon}^{(2N_\mathrm{F}-1)^2} \end{pmatrix}, \tag{A.27}$$

(A.11) and (A.13), the $(2N_{\mathrm{F}}) \times (KW)$ system matrix $\underline{\tilde{\boldsymbol{\mathcal{G}}}}$ reads

$$\underline{\tilde{\boldsymbol{\mathcal{G}}}} = \sqrt{\frac{E_{\mathrm{p}}}{N_{\mathrm{F}}}} \cdot \begin{pmatrix} 1 \cdot \left[\tilde{\mathbf{W}}^{(2N_{\mathrm{F}} \times 2N_{\mathrm{F}})} \right]_{1,\,(m-1)K+1} & 1 \cdot \left[\tilde{\mathbf{W}}^{(2N_{\mathrm{F}} \times 2N_{\mathrm{F}})} \right]_{1,\,(m-1)K+1} & \cdots \\ 1 \cdot \left[\tilde{\mathbf{W}}^{(2N_{\mathrm{F}} \times 2N_{\mathrm{F}})} \right]_{2,\,(m-1)K+1} & \underline{\varepsilon}^{1} \cdot \left[\tilde{\mathbf{W}}^{(2N_{\mathrm{F}} \times 2N_{\mathrm{F}})} \right]_{2,\,(m-1)K+1} & \cdots \\ \vdots & \vdots & \vdots \\ 1 \cdot \left[\tilde{\mathbf{W}}^{(2N_{\mathrm{F}} \times 2N_{\mathrm{F}})} \right]_{2N_{\mathrm{F}},\,(m-1)K+1} & \underline{\varepsilon}^{(2N_{\mathrm{F}}-1)} \cdot \left[\tilde{\mathbf{W}}^{(2N_{\mathrm{F}} \times 2N_{\mathrm{F}})} \right]_{2N_{\mathrm{F}},\,(m-1)K+1} & \cdots \end{pmatrix}$$

$$\begin{pmatrix} \cdots & \cdots & 1 \cdot \left[\tilde{\mathbf{W}}^{(2N_{\mathrm{F}} \times 2N_{\mathrm{F}})} \right]_{1,\,(m-1)K+K} \\ \cdots & \cdots & \underline{\varepsilon}^{(W-1)} \cdot \left[\tilde{\mathbf{W}}^{(2N_{\mathrm{F}} \times 2N_{\mathrm{F}})} \right]_{2,\,(m-1)K+K} \\ \vdots & \vdots & \vdots \\ \cdots & \cdots & \underline{\varepsilon}^{(W-1)(2N_{\mathrm{F}}-1)} \cdot \left[\tilde{\mathbf{W}}^{(2N_{\mathrm{F}} \times 2N_{\mathrm{F}})} \right]_{2N_{\mathrm{F}},\,(m-1)K+K} \end{pmatrix} . \tag{A.28}$$

In particular, the element in the i-th row and j-th column of the system matrix $\underline{\tilde{\boldsymbol{\mathcal{G}}}}$ of (A.28) is

$$\left[\underline{\tilde{\boldsymbol{\mathcal{G}}}} \right]_{i,\,j} = \sqrt{\frac{E_{\mathrm{p}}}{N_{\mathrm{F}}}} \cdot \underline{\varepsilon}^{(i-1)((j-1)_{\mathrm{mod}\ W})} \cdot \left[\tilde{\mathbf{W}}^{(2N_{\mathrm{F}} \times 2N_{\mathrm{F}})} \right]_{i,\,(m-1)K+(j-1)_{\mathrm{div}\ W}+1} , \tag{A.29}$$

and with (A.29) the element of the p-th row and q-th column of the matrix product $\underline{\tilde{\boldsymbol{\mathcal{G}}}}^{\mathsf{H}} \underline{\tilde{\boldsymbol{\mathcal{G}}}}$ is calculated by

$$\begin{aligned} \left[\underline{\tilde{\boldsymbol{\mathcal{G}}}}^{\mathsf{H}} \underline{\tilde{\boldsymbol{\mathcal{G}}}} \right]_{p,\,q} &= \sum_{i=1}^{2N_{\mathrm{F}}} \left[\underline{\tilde{\boldsymbol{\mathcal{G}}}} \right]^{*}_{i,\,p} \left[\underline{\tilde{\boldsymbol{\mathcal{G}}}} \right]_{i,\,q} \\ &= \frac{E_{\mathrm{p}}}{N_{\mathrm{F}}} \cdot \sum_{i=1}^{2N_{\mathrm{F}}} \underline{\varepsilon}^{(i-1)((q-1)_{\mathrm{mod}\ W}-(p-1)_{\mathrm{mod}\ W})} \cdot \\ &\quad \left[\tilde{\mathbf{W}}^{(2N_{\mathrm{F}} \times 2N_{\mathrm{F}})} \right]_{i,\,(m-1)K+(p-1)_{\mathrm{div}\ W}+1} \cdot \\ &\quad \left[\tilde{\mathbf{W}}^{(2N_{\mathrm{F}} \times 2N_{\mathrm{F}})} \right]_{i,\,(m-1)K+(q-1)_{\mathrm{div}\ W}+1} \end{aligned} \tag{A.30}$$

$$
\begin{aligned}
= \quad & \frac{E_\mathrm{p}}{N_\mathrm{F}} \cdot \left(\sum_{i=1}^{N_\mathrm{F}} \underline{\varepsilon}^{(i-1)((q-1)_{\mathrm{mod}\ W}-(p-1)_{\mathrm{mod}\ W})} \cdot \right. \\
& \left[\tilde{\mathbf{W}}^{(2N_\mathrm{F}\times 2N_\mathrm{F})} \right]_{i,\ (m-1)K+(p-1)_{\mathrm{div}\ W}+1} \cdot \\
& \left[\tilde{\mathbf{W}}^{(2N_\mathrm{F}\times 2N_\mathrm{F})} \right]_{i,\ (m-1)K+(q-1)_{\mathrm{div}\ W}+1} \\
& + \underline{\varepsilon}^{N_\mathrm{F}((q-1)_{\mathrm{mod}\ W}-(p-1)_{\mathrm{mod}\ W})} \cdot \\
& \sum_{i=1}^{N_\mathrm{F}} \underline{\varepsilon}^{(i-1)((q-1)_{\mathrm{mod}\ W}-(p-1)_{\mathrm{mod}\ W})} \cdot \\
& \left[\tilde{\mathbf{W}}^{(2N_\mathrm{F}\times 2N_\mathrm{F})} \right]_{i+N_\mathrm{F},\ (m-1)K+(p-1)_{\mathrm{div}\ W}+1} \cdot \\
& \left. \left[\tilde{\mathbf{W}}^{(2N_\mathrm{F}\times 2N_\mathrm{F})} \right]_{i+N_\mathrm{F},\ (m-1)K+(q-1)_{\mathrm{div}\ W}+1} \right) .
\end{aligned}
$$

Using the construction principle of the Walsh codes [Pro95], the elements of the matrix product $\underline{\tilde{\boldsymbol{\mathcal{G}}}}^{\mathsf{H}} \underline{\tilde{\boldsymbol{\mathcal{G}}}}$ for $2N_\mathrm{F}$ can be expressed as functions of the Walsh codes of length N_F:

$$
\begin{aligned}
\left[\underline{\tilde{\boldsymbol{\mathcal{G}}}}^{\mathsf{H}} \underline{\tilde{\boldsymbol{\mathcal{G}}}} \right]_{p,\ q} \quad = \quad & \frac{E_\mathrm{p}}{N_\mathrm{F}} \cdot \left(\sum_{i=1}^{N_\mathrm{F}} \underline{\varepsilon}^{(i-1)((q-1)_{\mathrm{mod}\ W}-(p-1)_{\mathrm{mod}\ W})} \cdot \right. \\
& \left[\tilde{\mathbf{W}}^{(N_\mathrm{F}\times N_\mathrm{F})} \right]_{i,\ (m-1)K+(p-1)_{\mathrm{div}\ W}+1} \cdot \\
& \left[\tilde{\mathbf{W}}^{(N_\mathrm{F}\times N_\mathrm{F})} \right]_{i,\ (m-1)K+(q-1)_{\mathrm{div}\ W}+1} \\
& + \underline{\varepsilon}^{N_\mathrm{F}((q-1)_{\mathrm{mod}\ W}-(p-1)_{\mathrm{mod}\ W})} \cdot \\
& \sum_{i=1}^{N_\mathrm{F}} \underline{\varepsilon}^{(i-1)((q-1)_{\mathrm{mod}\ W}-(p-1)_{\mathrm{mod}\ W})} \cdot \\
& \left[\tilde{\mathbf{W}}^{(N_\mathrm{F}\times N_\mathrm{F})} \right]_{i,\ (m-1)K+(p-1)_{\mathrm{div}\ W}+1} \cdot \\
& \left. \left[\tilde{\mathbf{W}}^{(N_\mathrm{F}\times N_\mathrm{F})} \right]_{i,\ (m-1)K+(q-1)_{\mathrm{div}\ W}+1} \right) . \qquad \text{(A.31)}
\end{aligned}
$$

Now, we have to distinguish the two cases

$$
\underline{\varepsilon}^{N_\mathrm{F}((q-1)_{\mathrm{mod}\ W}-(p-1)_{\mathrm{mod}\ W})} = \begin{cases} -1, & ((q-1)_{\mathrm{mod}\ W}-(p-1)_{\mathrm{mod}\ W}) \text{ is odd}, \\ +1, & ((q-1)_{\mathrm{mod}\ W}-(p-1)_{\mathrm{mod}\ W}) \text{ is even}, \end{cases} \qquad \text{(A.32)}
$$

see (A.19). Substituting (A.32) to (A.31) leads to

$$\left[\underline{\tilde{\mathcal{G}}}^{\mathsf{H}}\,\underline{\tilde{\mathcal{G}}}\right]_{p,\,q}$$

$$= \begin{cases} 0, & ((q-1)_{\mathrm{mod}\ W} - (p-1)_{\mathrm{mod}\ W}) \text{ is odd}, \\ \dfrac{2E_{\mathrm{p}}}{N_{\mathrm{F}}} \cdot \sum\limits_{i=1}^{N_{\mathrm{F}}} \underline{\varepsilon}^{(i-1)((q-1)_{\mathrm{mod}\ W} - (p-1)_{\mathrm{mod}\ W})} \cdot & \\ \quad \left[\tilde{\mathbf{W}}^{(N_{\mathrm{F}} \times N_{\mathrm{F}})}\right]_{i,\,(m-1)K+(p-1)_{\mathrm{div}\ W}+1} \cdot & \\ \quad \left[\tilde{\mathbf{W}}^{(N_{\mathrm{F}} \times N_{\mathrm{F}})}\right]_{i,\,(m-1)K+(q-1)_{\mathrm{div}\ W}+1}, & \\ & ((q-1)_{\mathrm{mod}\ W} - (p-1)_{\mathrm{mod}\ W}) \text{ is even}, \end{cases} \tag{A.33}$$

Using the induction hypothesis of (A.17) we finally obtain for (A.33)

$$\left[\underline{\tilde{\mathcal{G}}}^{\mathsf{H}}\,\underline{\tilde{\mathcal{G}}}\right]_{p,\,q} = \begin{cases} 2E_{\mathrm{p}}, & p = q, \\ 0, & \text{else}. \end{cases} \tag{A.34}$$

Appendix B

Derivation of the Wiener estimator of (6.50)

In what follows the derivation of the matrix $\underline{\mathbf{W}}_0$ of (6.50) is given. To do so, we resort to the fact that

$$\underline{\mathbf{W}}_0 \left(\tilde{\underline{\boldsymbol{\mathcal{G}}}}_{\mathrm{d}}^{\mathsf{H}} \underline{\mathbf{R}}_{\tilde{\mathbf{n}}_{\mathrm{tot}}}^{-1} \tilde{\underline{\boldsymbol{\mathcal{G}}}}_{\mathrm{d}}\right)^{-1} \tilde{\underline{\boldsymbol{\mathcal{G}}}}_{\mathrm{d}}^{\mathsf{H}} \underline{\mathbf{R}}_{\tilde{\mathbf{n}}_{\mathrm{tot}}}^{-1} = \underline{\mathbf{R}}_{\mathbf{h}_{\mathrm{d}}} \tilde{\underline{\boldsymbol{\mathcal{G}}}}_{\mathrm{d}}^{\mathsf{H}} \left(\underline{\mathbf{R}}_{\tilde{\mathbf{n}}_{\mathrm{tot}}} + \tilde{\underline{\boldsymbol{\mathcal{G}}}}_{\mathrm{d}} \underline{\mathbf{R}}_{\mathbf{h}_{\mathrm{d}}} \tilde{\underline{\boldsymbol{\mathcal{G}}}}_{\mathrm{d}}^{\mathsf{H}}\right)^{-1} \tag{B.1}$$

holds [Kle96]. The lemma

$$(\underline{\mathbf{A}} + \underline{\mathbf{B}}\,\underline{\mathbf{C}}\,\underline{\mathbf{D}})^{-1} = \underline{\mathbf{A}}^{-1} - \underline{\mathbf{A}}^{-1}\underline{\mathbf{B}} \left(\underline{\mathbf{D}}\,\underline{\mathbf{A}}^{-1}\underline{\mathbf{B}} + \underline{\mathbf{C}}^{-1}\right)^{-1} \underline{\mathbf{D}}\,\underline{\mathbf{A}}^{-1} \tag{B.2}$$

of matrix inversion [Wha71, ZF97] is applied on the matrix to be inverted on the right side of (B.1) and leads to

$$\left(\underline{\mathbf{R}}_{\tilde{\mathbf{n}}_{\mathrm{tot}}} + \tilde{\underline{\boldsymbol{\mathcal{G}}}}_{\mathrm{d}} \underline{\mathbf{R}}_{\mathbf{h}_{\mathrm{d}}} \tilde{\underline{\boldsymbol{\mathcal{G}}}}_{\mathrm{d}}^{\mathsf{H}}\right)^{-1} = \underline{\mathbf{R}}_{\tilde{\mathbf{n}}_{\mathrm{tot}}}^{-1} - \underline{\mathbf{R}}_{\tilde{\mathbf{n}}_{\mathrm{tot}}}^{-1} \tilde{\underline{\boldsymbol{\mathcal{G}}}}_{\mathrm{d}} \left(\tilde{\underline{\boldsymbol{\mathcal{G}}}}_{\mathrm{d}}^{\mathsf{H}} \underline{\mathbf{R}}_{\tilde{\mathbf{n}}_{\mathrm{tot}}}^{-1} \tilde{\underline{\boldsymbol{\mathcal{G}}}}_{\mathrm{d}} + \underline{\mathbf{R}}_{\mathbf{h}_{\mathrm{d}}}^{-1}\right)^{-1} \tilde{\underline{\boldsymbol{\mathcal{G}}}}_{\mathrm{d}}^{\mathsf{H}} \underline{\mathbf{R}}_{\tilde{\mathbf{n}}_{\mathrm{tot}}}^{-1}. \tag{B.3}$$

Multiplying (B.3) from the left side with the matrix $\underline{\mathbf{R}}_{\mathbf{h}_{\mathrm{d}}} \tilde{\underline{\boldsymbol{\mathcal{G}}}}_{\mathrm{d}}^{\mathsf{H}}$ yields

$$\begin{aligned} \underline{\mathbf{R}}_{\mathbf{h}_{\mathrm{d}}} \tilde{\underline{\boldsymbol{\mathcal{G}}}}_{\mathrm{d}}^{\mathsf{H}} \left(\underline{\mathbf{R}}_{\tilde{\mathbf{n}}_{\mathrm{tot}}} + \tilde{\underline{\boldsymbol{\mathcal{G}}}}_{\mathrm{d}} \underline{\mathbf{R}}_{\mathbf{h}_{\mathrm{d}}} \tilde{\underline{\boldsymbol{\mathcal{G}}}}_{\mathrm{d}}^{\mathsf{H}}\right)^{-1} &= \underline{\mathbf{R}}_{\mathbf{h}_{\mathrm{d}}} \tilde{\underline{\boldsymbol{\mathcal{G}}}}_{\mathrm{d}}^{\mathsf{H}} \underline{\mathbf{R}}_{\tilde{\mathbf{n}}_{\mathrm{tot}}}^{-1} - \\ &\quad \underline{\mathbf{R}}_{\mathbf{h}_{\mathrm{d}}} \tilde{\underline{\boldsymbol{\mathcal{G}}}}_{\mathrm{d}}^{\mathsf{H}} \underline{\mathbf{R}}_{\tilde{\mathbf{n}}_{\mathrm{tot}}}^{-1} \tilde{\underline{\boldsymbol{\mathcal{G}}}}_{\mathrm{d}} \left(\tilde{\underline{\boldsymbol{\mathcal{G}}}}_{\mathrm{d}}^{\mathsf{H}} \underline{\mathbf{R}}_{\tilde{\mathbf{n}}_{\mathrm{tot}}}^{-1} \tilde{\underline{\boldsymbol{\mathcal{G}}}}_{\mathrm{d}} + \underline{\mathbf{R}}_{\mathbf{h}_{\mathrm{d}}}^{-1}\right)^{-1} \tilde{\underline{\boldsymbol{\mathcal{G}}}}_{\mathrm{d}}^{\mathsf{H}} \underline{\mathbf{R}}_{\tilde{\mathbf{n}}_{\mathrm{tot}}}^{-1} \\ &= \left[\underline{\mathbf{R}}_{\mathbf{h}_{\mathrm{d}}} - \underline{\mathbf{R}}_{\mathbf{h}_{\mathrm{d}}} \tilde{\underline{\boldsymbol{\mathcal{G}}}}_{\mathrm{d}}^{\mathsf{H}} \underline{\mathbf{R}}_{\tilde{\mathbf{n}}_{\mathrm{tot}}}^{-1} \tilde{\underline{\boldsymbol{\mathcal{G}}}}_{\mathrm{d}} \left(\tilde{\underline{\boldsymbol{\mathcal{G}}}}_{\mathrm{d}}^{\mathsf{H}} \underline{\mathbf{R}}_{\tilde{\mathbf{n}}_{\mathrm{tot}}}^{-1} \tilde{\underline{\boldsymbol{\mathcal{G}}}}_{\mathrm{d}} + \underline{\mathbf{R}}_{\mathbf{h}_{\mathrm{d}}}^{-1}\right)^{-1}\right] \\ &\quad \tilde{\underline{\boldsymbol{\mathcal{G}}}}_{\mathrm{d}}^{\mathsf{H}} \underline{\mathbf{R}}_{\tilde{\mathbf{n}}_{\mathrm{tot}}}^{-1}. \end{aligned} \tag{B.4}$$

Comparing (B.4) with (B.1) leads to

$$\underline{\mathbf{W}}_0 \left(\tilde{\underline{\boldsymbol{\mathcal{G}}}}_{\mathrm{d}}^{\mathsf{H}} \underline{\mathbf{R}}_{\tilde{\mathbf{n}}_{\mathrm{tot}}}^{-1} \tilde{\underline{\boldsymbol{\mathcal{G}}}}_{\mathrm{d}}\right)^{-1} = \underline{\mathbf{R}}_{\mathbf{h}_{\mathrm{d}}} - \underline{\mathbf{R}}_{\mathbf{h}_{\mathrm{d}}} \tilde{\underline{\boldsymbol{\mathcal{G}}}}_{\mathrm{d}}^{\mathsf{H}} \underline{\mathbf{R}}_{\tilde{\mathbf{n}}_{\mathrm{tot}}}^{-1} \tilde{\underline{\boldsymbol{\mathcal{G}}}}_{\mathrm{d}} \left(\tilde{\underline{\boldsymbol{\mathcal{G}}}}_{\mathrm{d}}^{\mathsf{H}} \underline{\mathbf{R}}_{\tilde{\mathbf{n}}_{\mathrm{tot}}}^{-1} \tilde{\underline{\boldsymbol{\mathcal{G}}}}_{\mathrm{d}} + \underline{\mathbf{R}}_{\mathbf{h}_{\mathrm{d}}}^{-1}\right)^{-1}. \tag{B.5}$$

Right-sided multiplication of (B.5) with the matrix $\left(\tilde{\underline{\boldsymbol{\mathcal{G}}}}_{\mathrm{d}}^{\mathsf{H}} \underline{\mathbf{R}}_{\tilde{\mathbf{n}}_{\mathrm{tot}}}^{-1} \tilde{\underline{\boldsymbol{\mathcal{G}}}}_{\mathrm{d}} + \underline{\mathbf{R}}_{\mathbf{h}_{\mathrm{d}}}^{-1}\right)$ results in

$$\begin{aligned} &\underline{\mathbf{W}}_0 \left(\tilde{\underline{\boldsymbol{\mathcal{G}}}}_{\mathrm{d}}^{\mathsf{H}} \underline{\mathbf{R}}_{\tilde{\mathbf{n}}_{\mathrm{tot}}}^{-1} \tilde{\underline{\boldsymbol{\mathcal{G}}}}_{\mathrm{d}}\right)^{-1} \underline{\mathbf{R}}_{\mathbf{h}_{\mathrm{d}}}^{-1} + \underline{\mathbf{W}}_0 \left(\tilde{\underline{\boldsymbol{\mathcal{G}}}}_{\mathrm{d}}^{\mathsf{H}} \underline{\mathbf{R}}_{\tilde{\mathbf{n}}_{\mathrm{tot}}}^{-1} \tilde{\underline{\boldsymbol{\mathcal{G}}}}_{\mathrm{d}}\right)^{-1} \tilde{\underline{\boldsymbol{\mathcal{G}}}}_{\mathrm{d}}^{\mathsf{H}} \underline{\mathbf{R}}_{\tilde{\mathbf{n}}_{\mathrm{tot}}}^{-1} \tilde{\underline{\boldsymbol{\mathcal{G}}}}_{\mathrm{d}} = \\ &\underline{\mathbf{R}}_{\mathbf{h}_{\mathrm{d}}} \underline{\mathbf{R}}_{\mathbf{h}_{\mathrm{d}}}^{-1} + \underline{\mathbf{R}}_{\mathbf{h}_{\mathrm{d}}} \tilde{\underline{\boldsymbol{\mathcal{G}}}}_{\mathrm{d}}^{\mathsf{H}} \underline{\mathbf{R}}_{\tilde{\mathbf{n}}_{\mathrm{tot}}}^{-1} \tilde{\underline{\boldsymbol{\mathcal{G}}}}_{\mathrm{d}} - \underline{\mathbf{R}}_{\mathbf{h}_{\mathrm{d}}} \tilde{\underline{\boldsymbol{\mathcal{G}}}}_{\mathrm{d}}^{\mathsf{H}} \underline{\mathbf{R}}_{\tilde{\mathbf{n}}_{\mathrm{tot}}}^{-1} \tilde{\underline{\boldsymbol{\mathcal{G}}}}_{\mathrm{d}}, \end{aligned} \tag{B.6}$$

which can be rewritten as

$$\underline{\mathbf{W}}_0 \left(\mathbf{I}^{(KW \times KW)} + \left(\tilde{\underline{\boldsymbol{\mathcal{G}}}}_{\mathrm{d}}^{\mathsf{H}} \underline{\mathbf{R}}_{\tilde{\mathbf{n}}_{\mathrm{tot}}}^{-1} \tilde{\underline{\boldsymbol{\mathcal{G}}}}_{\mathrm{d}}\right)^{-1} \underline{\mathbf{R}}_{\mathbf{h}_{\mathrm{d}}}^{-1}\right) = \mathbf{I}^{(KW \times KW)}. \tag{B.7}$$

From (B.7)

$$\underline{\mathbf{W}}_{\mathbf{0}} = \left(\mathbf{I}^{(KW \times KW)} + \left(\underline{\tilde{\mathcal{G}}}_{\mathrm{d}}^{\mathsf{H}} \underline{\mathbf{R}}_{\tilde{\mathbf{n}}_{\mathrm{tot}}}^{-1} \underline{\tilde{\mathcal{G}}}_{\mathrm{d}} \right)^{-1} \underline{\mathbf{R}}_{\mathbf{h}_{\mathrm{d}}}^{-1} \right)^{-1} \tag{B.8}$$

follows, and with the property [ZF97]

$$(\mathbf{A}\,\mathbf{B})^{-1} = \mathbf{B}^{-1}\mathbf{A}^{-1} \tag{B.9}$$

of matrix inversion, $\underline{\mathbf{W}}_{\mathbf{0}}$ is obtained as

$$\underline{\mathbf{W}}_{\mathbf{0}} = \left(\mathbf{I}^{(KW \times KW)} + \left(\underline{\mathbf{R}}_{\mathbf{h}_{\mathrm{d}}} \underline{\tilde{\mathcal{G}}}_{\mathrm{d}}^{\mathsf{H}} \underline{\mathbf{R}}_{\tilde{\mathbf{n}}_{\mathrm{tot}}}^{-1} \underline{\tilde{\mathcal{G}}}_{\mathrm{d}} \right)^{-1} \right)^{-1} . \tag{B.10}$$

Acronyms

2G	Second generation
3G	Third generation
AP	Access point
BS	Base station
B3G	Beyond 3G
CAZAC	Constant amplitude zero autocorrelation
CDMA	Code division multiple access
CIR	Channel impulse response
CTF	Channel transfer function
CU	Central unit
DL	Downlink
FDD	Frequency division duplex
FDMA	Frequency division multiple access
GSM	Global System for Mobile Communications
ICI	Intercarrier interference
ISI	Intersymbol interference
JCE	Joint channel estimation
JD	Joint detection
JT	Joint transmission
JOINT	Joint Transmission and Detection Integrated Network
MAI	Multiple access interference
MIMO	Multiple input multiple output
MISO	Multiple input single output
ML	Maximum likelihood
MMSE	Minimum mean square error
OFDM	Orthogonal frequency division multiplexing
RF	Radio frequency
SA	Service area
$\mathrm{SA}_{\mathrm{ref}}$	Reference service area
SA_{I}	Dominant interfering service area adjacent to $\mathrm{SA}_{\mathrm{ref}}$
SIMO	Single input multiple output
SISO	Single input single output
SNR	Signal-to-noise ratio
TDD	Time division duplex
TDMA	Time division multiple access
UMTS	Universal Mobile Telecommunication System
UL	Uplink

Mathematical symbols

$\underline{\tilde{\mathbf{a}}}^{(k)}$	MT-specific steering vector
$\underline{\tilde{\mathbf{A}}}^{(k)}$	MT-specific steering matrix
$\underline{\tilde{\mathbf{A}}}$	Total steering matrix containing all MT-specific steering matrices
$\underline{\tilde{d}}_{n_\mathrm{F}}^{(k)}$	Complex amplitude of the MT-specific data symbol on subcarrier n_F
$\underline{\tilde{\mathbf{d}}}^{(k)}$	MT-specific data vector containing the complex amplitudes of the MT-specific data symbols on all subcarriers
$\underline{\tilde{\mathbf{d}}}_{n_\mathrm{F}}$	Subcarrier specific data vector containing the K complex amplitudes of the MT-specific data symbols
$\underline{\tilde{\mathbf{d}}}$	Total data vector containing all MT-specific data vectors $\underline{\tilde{\mathbf{d}}}^{(k)}$
$\underline{\tilde{e}}_{\mathrm{h},n_\mathrm{F}}^{(k_\mathrm{B})}$	Complex amplitude of the undisturbed AP-specific receive signal on subcarrier n_F in the case of channel estimation
$\underline{\tilde{\mathbf{e}}}_\mathrm{h}^{(k_\mathrm{B})}$	Undisturbed AP-specific receive vector containing the complex amplitudes $\underline{\tilde{e}}_{\mathrm{h},n_\mathrm{F}}^{(k_\mathrm{B})}$ of the undisturbed AP-specific receive signal on all subcarriers in the case of channel estimation
$\underline{\tilde{\mathbf{e}}}_\mathrm{h}$	Total vector of the undisturbed receive signal containing all undisturbed AP-specific receive vectors $\underline{\tilde{\mathbf{e}}}_\mathrm{h}^{(k_\mathrm{B})}$ in the case of channel estimation
$\underline{\tilde{e}}_{\mathrm{d},n_\mathrm{F}}^{(k_\mathrm{B})}$	Complex amplitude of the undisturbed AP-specific receive signal on subcarrier n_F in the case of data estimation
$\underline{\tilde{\mathbf{e}}}_\mathrm{d}^{(k_\mathrm{B})}$	Undisturbed AP-specific receive vector containing the complex amplitudes $\underline{\tilde{e}}_{\mathrm{d},n_\mathrm{F}}^{(k_\mathrm{B})}$ of the undisturbed AP-specific receive signal on all subcarriers in the case of data estimation
$\underline{\tilde{\mathbf{e}}}_\mathrm{d}$	Total vector of the undisturbed receive signal containing all undisturbed AP-specific receive vectors $\underline{\tilde{\mathbf{e}}}_\mathrm{d}^{(k_\mathrm{B})}$ in the case of data estimation
$E_\mathrm{p}^{(k)}$	Energy of the MT-specific pilot vector $\underline{\tilde{\mathbf{p}}}^{(k)}$
E_p	Energy of the MT-specific pilot vector $\underline{\tilde{\mathbf{p}}}^{(k)}$ equal for all MTs
$E_{\mathrm{d},n_\mathrm{F}}^{(k)}$	Energy of the MT-specific data symbol $\underline{\tilde{d}}_{n_\mathrm{F}}^{(k)}$
E_d	Energy of the MT-specific data symbol $\underline{\tilde{d}}_{n_\mathrm{F}}^{(k)}$ equal for all subcarriers and all MTs
$E_\mathrm{b}^{(k)}$	Receive energy per bit referring to MT k
E_b	Receive energy per bit equal for all MTs
$\underline{\tilde{\mathbf{E}}}_{n_\mathrm{F}}$	Subcarrier specific error matrix containing the JCE error amplitudes $\underline{\tilde{\varepsilon}}_{\mathrm{JCE},n_\mathrm{F}}^{(k,k_\mathrm{B})}$
f_c	Carrier frequency
$f_{\mathrm{D,\,max}}$	Maximum Doppler frequency
$\underline{\tilde{\boldsymbol{\mathcal{F}}}}$	Fourier matrix
$\underline{\tilde{\boldsymbol{\mathcal{F}}}}_\mathrm{W}$	Reduced blockdiagonal Fourier matrix
$\underline{\tilde{\boldsymbol{\mathcal{G}}}}$	System matrix of SA_ref for the single-element receive antenna case of JCE
$\underline{\tilde{\boldsymbol{\mathcal{G}}}}_\mathrm{I}^{(k_\mathrm{I})}$	Interferer specific system matrix of SA_I for the single-element receive antenna case of JCE

$\underline{\tilde{\boldsymbol{\mathcal{G}}}}_{\mathrm{I}}$	System matrix of $\mathrm{SA_I}$ for the single-element receive antenna case of JCE
$\underline{\tilde{\boldsymbol{\mathcal{G}}}}_{\mathrm{d}}$	System matrix of $\mathrm{SA_{ref}}$ for the multi-element receive antenna case of JCE
$\underline{h}_{w}^{(k,\,k_{\mathrm{B}})}$	Complex amplitude of the CIR characterizing the radio channel between MT k and AP k_{B}
$\underline{\mathbf{h}}^{(k,\,k_{\mathrm{B}})}$	CIR vector containing all W complex amplitudes $\underline{h}_{w}^{(k,\,k_{\mathrm{B}})}$ of the radio channel between MT k and AP k_{B}
$\underline{\mathbf{h}}^{(k)}$	MT-specific CIR vector describing the K_{B} radio channels between MT k and all K_{B} APs in a SA
$\underline{\mathbf{h}}$	Total CIR vector containing all K MT-specific CIR vectors $\underline{\mathbf{h}}^{(k)}$
$\underline{\tilde{h}}_{n_{\mathrm{F}}}^{(k,\,k_{\mathrm{B}})}$	Complex amplitude of the CTF characterizing the radio channel between MT k and AP k_{B} on subcarrier n_{F}
$\underline{\tilde{\mathbf{h}}}^{(k,\,k_{\mathrm{B}})}$	CTF vector containing the complex amplitudes $\underline{\tilde{h}}_{n_{\mathrm{F}}}^{(k,\,k_{\mathrm{B}})}$ of the radio channel between MT k and AP k_{B}
$\underline{\tilde{h}}_{n_{\mathrm{F}}}^{(k,\,k_{\mathrm{A}})}$	Complex amplitude of the CTF characterizing the radio channel between MT k and AP antenna element k_{A} on subcarrier n_{F}
$\underline{\tilde{\mathbf{h}}}^{(k,\,k_{\mathrm{A}})}$	CTF vector containing the complex amplitudes $\underline{\tilde{h}}_{n_{\mathrm{F}}}^{(k,\,k_{\mathrm{A}})}$ of the radio channel between MT k and AP antenna element k_{A}
$\underline{\tilde{\mathbf{h}}}^{(k)}$	MT-specific CTF vector
$\underline{\tilde{\mathbf{h}}}$	Total CTF vector containing all K MT-specific CTF vectors $\underline{\tilde{\mathbf{h}}}^{(k)}$
$\underline{\tilde{\mathbf{H}}}_{n_{\mathrm{F}}}$	Subcarrier specific channel matrix containing the CTF components $\underline{\tilde{h}}_{n_{\mathrm{F}}}^{(k,k_{\mathrm{B}})}$ on subcarrier n_{F}
$\underline{\boldsymbol{\mathcal{I}}}$	Inter-SA interference matrix
$\overline{\mathcal{I}}^{(k_{\mathrm{I}})}$	Interferer specific mean value of the inter-SA interference
K	Number of MTs inside the considered SA, which use the entire available bandwidth simultaneously
k	Indicator of a specific MT in $\mathrm{SA_{ref}}$
k_{I}	Indicator of a specific MT in $\mathrm{SA_I}$
K_{A}	Number of antenna elements utilized at the AP array antenna
k_{A}	Indicator of a specific antenna element of the AP array antenna
K_{B}	Number of APs in the considered SA of JOINT
k_{B}	Indicator of a specific AP in the SA
l	Distance between adjacent antenna elements of the AP array
$\underline{\tilde{\mathbf{M}}}_{n_{\mathrm{F}}}$	Subcarrier specific modulator matrix for JT
$\underline{\tilde{n}}_{n_{\mathrm{F}}}^{(k_{\mathrm{B}})}$	Complex amplitude of the AP-specific noise on subcarrier n_{F}
$\underline{\tilde{\mathbf{n}}}^{(k_{\mathrm{B}})}$	AP-specific noise vector containing all N_{F} complex amplitudes $\underline{\tilde{n}}_{n_{\mathrm{F}}}^{(k_{\mathrm{B}})}$
$\underline{\tilde{\mathbf{n}}}$	Total noise vector containing all K_{B} AP-specific noise vectors $\underline{\tilde{\mathbf{n}}}^{(k_{\mathrm{B}})}$
$\underline{\tilde{p}}_{n_{\mathrm{F}}}^{(k)}$	Complex amplitude of the pilot symbol radiated by MT k on subcarrier n_{F}
$\underline{\tilde{\mathbf{p}}}^{(k)}$	MT-specific pilot vector applied by MT k in $\mathrm{SA_{ref}}$ containing all N_{F} complex amplitudes $\underline{\tilde{p}}_{n_{\mathrm{F}}}^{(k)}$
$\underline{\tilde{\mathbf{p}}}^{(k_{\mathrm{I}})}$	MT-specific pilot vector applied by MT k_{I} in $\mathrm{SA_I}$ containing all N_{F} complex amplitudes $\underline{\tilde{p}}_{n_{\mathrm{F}}}^{(k_{\mathrm{I}})}$

$\underline{\tilde{\mathbf{P}}}^{(k)}$	MT-specific pilot matrix of $\mathrm{SA}_{\mathrm{ref}}$
$\underline{\tilde{\mathbf{P}}}^{(k_{\mathrm{I}})}$	MT-specific pilot matrix of SA_{I}
$\underline{\tilde{\mathbf{P}}}$	Total pilot matrix of $\mathrm{SA}_{\mathrm{ref}}$ containing all K MT-specific pilot matrices $\underline{\tilde{\mathbf{P}}}^{(k)}$ in the single-element receive antenna case of JCE
$\underline{\tilde{\mathbf{P}}}_{\mathrm{I}}$	Total pilot matrix of SA_{I} containing all K_{I} MT-specific pilot matrices $\underline{\tilde{\mathbf{P}}}^{(k_{\mathrm{I}})}$ in the single-element receive antenna case of JCE
$\underline{\tilde{\mathbf{P}}}_{\mathrm{tot}}$	Total pilot matrix of $\mathrm{SA}_{\mathrm{ref}}$ containing all K MT-specific pilot matrices $\underline{\tilde{\mathbf{P}}}^{(k)}$ in the multi-element receive antenna case of JCE
$\underline{\tilde{r}}_{\mathrm{h},n_{\mathrm{F}}}^{(k_{\mathrm{A}})}$	Complex amplitude of the noise corrupted receive signal at antenna element k_{A} in the multi-element receive antenna case of JCE
$\underline{\tilde{\mathbf{r}}}_{\mathrm{h}}^{(k_{\mathrm{A}})}$	Noise corrupted receive signal at antenna element k_{A} in the multi-element receive antenna case of JCE
$\underline{\tilde{\mathbf{r}}}_{\mathrm{h}}^{(k_{\mathrm{B}})}$	Noise corrupted AP-specific receive signal in the single-element receive antenna case of JCE
$\underline{\tilde{\mathbf{r}}}_{\mathrm{d}}^{(k_{\mathrm{B}})}$	Noise corrupted AP-specific receive signal in the single-element receive antenna case of data estimation
$\underline{\tilde{\mathbf{r}}}_{\mathrm{d},n_{\mathrm{F}}}$	Subcarrier specific noise corrupted receive signal containing all K_{B} complex amplitudes received on subcarrier n_{F}
$\underline{\tilde{\mathbf{r}}}$	Total noise corrupted receive signal
$\underline{\mathbf{R}}_{\tilde{\mathbf{h}}}$	Total channel covariance matrix of the multipoint–to–multipoint CTF in the frequency domain
$\underline{\mathbf{R}}_{\mathbf{h}_{\mathrm{d}}}$	Total channel covariance matrix representing the point–to–point directional CIR
$\underline{\mathbf{R}}_{\tilde{\mathbf{n}}}$	Total noise covariance matrix
$\underline{\mathbf{R}}_{\mathrm{s}}$	Spatial noise covariance matrix
$\underline{\mathbf{R}}_{\mathrm{s,omni}}$	Spatial noise covariance matrix of the omnidirectional noise component
$\underline{\mathbf{R}}_{\mathrm{s,dir}}$	Spatial noise covariance matrix of the directional noise component
$\underline{\mathbf{R}}_{\mathrm{t}}$	Temporal noise covariance matrix
$\underline{\tilde{s}}_{n_{\mathrm{F}}}^{(k_{\mathrm{B}})}$	Transmit signal component on subcarrier n_{F} generated for AP k_{B}
$\underline{\tilde{\mathbf{s}}}_{n_{\mathrm{F}}}$	Subcarrier specific transmit signal containing K_{B} components $\underline{\tilde{s}}_{n_{\mathrm{F}}}^{(k_{\mathrm{B}})}$ on subcarrier n_{F}
$T_{\mathrm{tot},n_{\mathrm{F}}}$	Total transmit energy radiated in a considered SA
$\gamma_{n_{\mathrm{F}}}^{(k)}$	SNR of MT k at subcarrier n_{F}
$\gamma_{\mathrm{max},n_{\mathrm{F}}}^{(k)}$	Maximum possible SNR of MT k at subcarrier n_{F}
$\delta_{n_{\mathrm{F}}}^{(k)}$	SNR degradation of MT k at subcarrier n_{F}
$\underline{\tilde{\boldsymbol{\varepsilon}}}_{\mathrm{JCE}}$	Total vector of the JCE error
$\underline{\tilde{\varepsilon}}_{\mathrm{JCE},n_{\mathrm{F}}}^{(k,k_{\mathrm{B}})}$	Complex value of the JCE error of MT k at AP k_{B} and subcarrier n_{F}
$\underline{\tilde{\boldsymbol{\varepsilon}}}_{\mathrm{JD},n_{\mathrm{F}}}$	Vector of the JD error for subcarrier n_{F}
$\underline{\tilde{\varepsilon}}_{\mathrm{JD},n_{\mathrm{F}}}^{(k,k_{\mathrm{B}})}$	Complex value of the JD error of MT k at AP k_{B} and subcarrier n_{F}
$\underline{\tilde{\boldsymbol{\varepsilon}}}_{\mathrm{JT},n_{\mathrm{F}}}$	Vector of the JT error for subcarrier n_{F}
$\underline{\tilde{\varepsilon}}_{\mathrm{JT},n_{\mathrm{F}}}^{(k)}$	Complex value of the JD error of MT k at subcarrier n_{F}
σ^2	Noise variance
$\sigma^{(k_{\mathrm{I}})^2}$	Interferer specific variance of the inter-SA interference

$\sigma^2_{\underline{\tilde{\varepsilon}}_{\mathrm{JCE}}}$	Variance of the JCE error $\underline{\tilde{\varepsilon}}_{\mathrm{JCE}}$
$\sigma^{(k)^2}_{\underline{\tilde{\varepsilon}}_{\mathrm{JD},n_{\mathrm{F}}}}$	Variance of the JD error $\underline{\tilde{\varepsilon}}_{\mathrm{JD},n_{\mathrm{F}}}$
$\sigma^{(k)^2}_{\underline{\tilde{\varepsilon}}_{\mathrm{JT},n_{\mathrm{F}}}}$	Variance of the JT error $\underline{\tilde{\varepsilon}}_{\mathrm{JT},n_{\mathrm{F}}}$

References

[Bin90] Bingham, J.: Multicarrier Modualtion for Data Transmission: An Idea whos Time has come. *IEEE Communications Magazine*, vol. 28, 1990, pp. 5–14.

[Bla98] Blanz, J. J.: *Empfangsantennendiversität in CDMA-Mobilfunksystemen mit gemeinsamer Detektion der Teilnehmersignale*. Fortschrittberichte VDI, Reihe 10, no. 535. Düsseldorf: VDI-Verlag, 1998.

[BS79] Bronstein, I. N.; Semendjajew, K. A.: *Taschenbuch der Mathematik*. Leipzig: B. G. Teubner, 1979.

[BXX+03] Bing, H.; Xiqi, G.; Xiaohu, Y.; Jianming, W.; Costa, E.: An iterative joint channel estimation and symbol detection algorithm applied in OFDM system with high data to pilot power ratio. *Proc. IEEE International Conference on Communications (ICC'03)*, vol. 3, Nanjing, 2003, pp. 2076–2080.

[Chu72] Chu, D.: Polyphase codes with good periodic correlation properties. vol. 18, 1972, pp. 531–532.

[COS89] *COST 207: Digital land mobile radio communications*. Final Report, Office for Official Publications of the European Communities, Luxemburg, 1989.

[DB96] David, K.; Benkner, T.: *Digitale Mobilfunksysteme*. Stuttgart: B. G. Teubner, 1996.

[Doe57] Doelz, M.: Binary Data Transmission Technique for Linear Systems. *Proc. IRE*, 1957, pp. 656–661.

[EF86] Effelsberg, W.; Fleischmann, A.: Das ISO-Referenzmodell für offene Systeme und seine sieben Schichten. *Informatik-Spektrum*, vol. 9, 1986, pp. 280–299.

[EKLG+03] El-Khazen, K.; Lefevre, F.; Garrec, D.; Guiraudou, M.; Benali, O.: Beyond 3G demonstrator for enhanced service signaling, discovery and management. *Proc. 8th IEEE International Symposium on Computers and Communication ISCC'03*, vol. 2, 2003, pp. 1367–1372.

[ESvdB+96] Edfors, O.; Sandell, M.; van de Beek, J.; Wilson, S.; Börjesson, P.: OFDM channel estimation by singular value decomposition. *Proc. IEEE 46th Vehicular Technology Conference (VTC'96)*, vol. 2, 1996, pp. 923–927.

[ETS97] *Universal Mobile Telecommunications System (UMTS); Selection procedures for the choice of radio transmission technologies of the UMTS (UMTS 30.03 version 3.1.0)*. Technical Report TR 101 112, ETSI, 1997.

[EV97] Eberspächer, J.; Vögel, H. J.: *GSM Global System for Mobile Communication*. Stuttgart: B. G. Teubner, 1997.

[Fel94] Felhauer, T.: *Optimale erwartungstreue Algorithmen zur hochauflösenden Kanalschätzung mit Bandspreizsignalen*. Fortschrittberichte VDI, Reihe 10, no. 278. Düsseldorf: VDI-Verlag, 1994.

[Fis76] Fisz, M.: *Wahrscheinlichkeitsrechnung und mathematische Statistik*. Berlin: Deutscher Verlag der Wissenschaften, 1976.

[FK03] Fazel, K.; Kaiser, S.: *Multi-Carrier and Spread Spectrum Systems*. Chichester: John Wiley & Sons, 2003.

[FN94] Farsakh, C.; Nossek, J.: Application of SDMA to mobile radio. *Proc. IEEE 5th International Symposium on Personal, Indoor and Mobile Radio Communications (PIMRC'94)*, The Hague, 1994, pp. 736–739.

[FTH+99] Fleury, B.; Tschudin, M.; Heddergott, R.; Dahlhaus, D.; Pedersen, K.: Channel parameter estimation in mobile radio environments using the SAGE algorithm. *IEEE Journal on Selected Areas in Communications*, vol. 17, 1999, pp. 434–450.

[FZ62] Frank, R.; Zadoff, S.: Phase shift pulse codes with good periodic correlation properties. vol. 8, 1962, pp. 381–382.

[Gib99] Gibson, J. D. (Ed.): *The Mobile Communications Handbook*. 2. edition. Heidelberg: Springer-Verlag, 1999.

[God97] Godara, L. C.: Applications of antenna arrays to mobile communications, part I: Performance improvement, feasibility, and system considerations. *Proceedings of the IEEE*, vol. 85, 1997, pp. 1031–1060.

[Gra81] Graham, A.: *Kronecker Products and Matrix Calculus with Appliations*. Chichester: Ellis Horwood Limited, 1981.

[Haa97] Haardt, M.: *Efficient one- two- and multidimensional array signal processing*. Berichte aus dem Lehrstuhl für Netzwerktheorie und Schaltungstechnik der Technischen Universität München. Aachen: Shaker-Verlag, 1997.

[Hal67] Hald, A.: *Statistical Theory with Engineering Applications*. 7. edition. New York: John Wiley & Sons, 1967.

[Hay01] Haykin, S. (Ed.): *Communication Systems*. Chichester: John Wiley & Sons, 2001.

[Hei61] Heimiller, R.: Phase shift pulse codes with good periodic correlation properties. *IEEE Transactions on Information Theory*, vol. 7, 1961, pp. 254–257.

[HKR97a] Hoeher, P.; Kaiser, S.; Robertson, P.: Pilot-symbol-aided channel estimation in time and frequency. *Proc. IEEE Global Telecommunications Conference (GLOBECOM'97)*, Phoenix, 1997, pp. 90–96.

[HKR97b] Hoeher, P.; Kaiser, S.; Robertson, P.: Two-dimensional pilot-symbol-aided channel estimation by Wiener filtering. *Proc. of the IEEE International Conference on Acoustics, Speech and Signal Processing (ICASSP'97)*, Munich, 1997, pp. 1845–1848.

[HN95] Haardt, M.; Nossek, J. A.: Unitary ESPRIT: How to obtain increased estimation accuracy with a reduced computational burden. *IEEE Transactions on Signal Processing*, vol. 43, 1995, pp. 1232–1242.

[Kam96] Kammeyer, K. D.: *Nachrichtenübertragung*. Stuttgart: B. G. Teubner, 1996.

[Kan05] Kang, G.: *Time and frequency domain joint channel estimation in multi-carrier multi-branch systems*. Dissertation, Lehrstuhl für hochfrequente Signalübertragung und -verarbeitung, Universität Kaiserslautern, 2005.

[KCWS03] Kang, G.; Costa, E.; Weckerle, M.; Schulz, E.: Optimum channel estimation over frequency-selective fading channel in multiple antenna systems. *Proc. International Conference on Communication Technology (ICCT'03)*, vol. 2, Beijing, 2003, pp. 17999–1803.

[KJ02] Kyeong, J. K.; Jiang, Y.: Joint channel estimation and data detection algorithms for MIMO-OFDM systems. *Conference record of the thirty-sixth Asilomar conference on signals, systems and computers*, vol. 2, Irving, 2002, pp. 1857–1861.

[Kle96] Klein, A.: *Multi-user detection of CDMA signals – algorithms and their application to cellular mobile radio*. Fortschrittberichte VDI, Reihe 10, no. 423. Düsseldorf: VDI-Verlag, 1996.

[KMH98] Kapoor, S.; Marchok, D.; Huang, Y.-F.: Pilot assisted synchronization for wireless OFDM systems over fast time varying fading channels. *Proc. IEEE 48th Vehicular Technology Conference (VTC'98)*, vol. 3, Ottawa, Ont. Canada, 1998, pp. 2077–2080.

[KS01] Kammeyer, K.-D.; Schmidt, H.: OFDM: An old idea solves new problems. *Proc. International Symposium on Theoretical Electrical Engineering (ISTET01)*, Linz, 2001, pp. K1–K9.

[LCS98] Li, Y.; Cimini, L.; Sollenberger, N.: Robust Channel Estimation for OFDM Systems with Rapid Dispersive Fading Channels. *IEEE Transactions on Communications*, vol. 46, 1998, pp. 1320–1324.

[Li99] Li, Y.: Pilot-Symbol-Aided Channel Estimation for OFDM in Wireless Systems. *Proc. IEEE 59th Vehicular Technology Conference (VTC'99-Spring)*, vol. 2, 1999, pp. 1131–1135.

[Li02] Li, Y.: Simplified Channel Estimation for OFDM with Multiple Transmit Antennas. *IEEE Transactions on Wireless Communications*, vol. 1, 2002, pp. 67–75.

[Liu05] Liu, Y.: *Modelling and simulation of service area based OFDM air interfaces for beyond 3G mobile radio systems*. Dissertation, Lehrstuhl für hochfrequente Signalübertragung und -verarbeitung, Universität Kaiserslautern, 2005.

[LSA99] Li, Y.; Seshadri, N.; Ariyavisitakul, S.: Channel Estimation for OFDM Systems with Transmitter Diversity in Mobile Wireless Channels. *IEEE Journal on Selected Areas in Communications*, vol. 17, 1999, pp. 461–471.

[Lük92] Lüke, H. D.: *Signalübertragung*. Berlin: Springer-Verlag, 1992.

[Lut96] Lutkepohl, H.: *Handbook of Matrices*. New York: John Wiley & Sons, 1996.

[LWS02] Li, Y.; Winters, J.; Sollenberger, N.: MIMO-OFDM for Wireless Communications: Signal Detection with Enhanced Channel Estimation. *IEEE Transactions on Communications*, vol. 50, 2002, pp. 1471–1477.

[MBW+00] Meurer, M.; Baier, P. W.; Weber, T.; Lu, Y.; Papathanassiou, A.: Joint transmission: advantageous downlink concept for CDMA mobile radio systems using time division duplexing. *IEE Electronics Letters*, vol. 36, 2000, pp. 900–901.

[MD79] Mac Donald, V. H.: The cellular concept. *The Bell System Technical Journal*, vol. 58, 1979, pp. 15–41.

[Mil83] Milewski, A.: Periodic sequences with optimal properties for channel estimation and fast start-up equalization. *IBM Journal on Research and Development*, vol. 27, 1983, pp. 426–431.

[MM80] Monzingo, R. A.; Miller, T. W.: *Introduction to Adaptive Arrays*. New York: John Wiley & Sons, 1980.

[MW03] Maniatis, I.; Weber, T.: Joint Channel Estimation with Array Antennas in OFDM based Mobile Radio Systems. *COST 273 TD(04)009*, Athens, 2003.

[MW04] Meurer, M.; Weber, T.: Imperfect channel knowledge: An insurmountable barrier in Rx oriented multi-user MIMO transmission? *Proc. 5th International ITG Conference on Source and Channel Coding 2004 (SCC'04)*, Erlangen, 2004, pp. 371–380.

[MWSL02] Maniatis, I.; Weber, T.; Sklavos, A.; Liu, Y.: Pilots for joint channel estimation in multi-user OFDM mobile radio systems. *Proc. IEEE 7th International Symposium on Spread Spectrum Techniques & Applications (ISSSTA'02)*, vol. 1, Prague, 2002, pp. 44–48.

[MWW03] Maniatis, I.; Weber, T.; Weckerle, M.: Eploiting a-priori information for channel estimation in multiuser OFDM mobile radio systems. Fazel, K.; Kaiser, S. (Eds.): *Multi-Carrier Spread-Spectrum & Related Topics*. pp. 235–242. Boston: Kluwer Academic Publishers, 2003. Proc. 3rd International Workshop on Multi-Carrier Spread Spectrum (MC-SS 2003).

[Nat03] Natarajan, N.: On systems beyond 3G: requirements and approaches. *Proc. International Conference on Communication Technology (ICCT'03)*, vol. 2, 2003, pp. 1305–1309.

[Pap00] Papathanassiou, A.: *Adaptive antennas for mobile radio systems using Time Division CDMA and joint detection*. Dissertation, Lehrstuhl für hochfrequente Signalübertragung und -verarbeitung, Universität Kaiserslautern, 2000.

[PK02] Pei, C.; Kobayashi, H.: Maximum likelihood channel estimation and signal detection for OFDM systems. *Proc. IEEE International Conference on Communications (ICC'02)*, vol. 3, New Jersey, 2002, pp. 1640–1645.

[PR80] Peled, A.; Ruiz, A.: Frequency Domain Data Transmission Using Reduced Computational Complexity Algorithms. *Proc. of the IEEE International Conference on Acoustics, Speech and Signal Processing (ICASSP'80)*, vol. 5, Denver, 1980, pp. 964–967.

[Pra72] Pratt, W. K.: Generalized Wiener filtering computation techniques. *IEEE Transactions on Computers*, vol. C-21, 1972, pp. 636–641.

[Pra98] Prasad, R.: *Universal Wireless Personal Communications*. Boston: Artech House, 1998.

[Pro95] Proakis, J. G.: *Digital Communications*. 3. edition. New York: McGraw-Hill, 1995.

[Rap98] Rappaport, T. S. (Ed.): *Smart Antennas*. Hoes Lane: Institute of Electrical and Electronics Engineers, 1998.

[RGG01] Rohling, H.; Grünheid, R.; Galda, D.: OFDM transmission technique for the 4th generation of mobile communication systems. *Proc. 6th International OFDM-Workshop (InOWo'01)*, Hamburg, 2001, pp. 0–1–0–28.

[RK89] Roy, R.; Kailath, T.: ESPRIT – estimation of signal parameters via rotational invariance techniques. *IEEE Transactions on Acoustics, Speech, and Signal Processing*, vol. 37, 1989, pp. 984–995.

[Rup82] Rupprecht, W.: *Nachrichtentechnik: Nachrichtenübertragung*. vol. 2. 3. edition. Berlin: Springer-Verlag, 1982.

[Rup93] Rupprecht, W.: *Signale und Übertragungssysteme*. Berlin: Springer-Verlag, 1993.

[RW95] Redl, S.; Weber, M.: *GSM-Technik und Meßpraxis, Netzeigenschaften, Übertragungsverfahren, praktische Meßtechnik*. 2. edition. München: Franzis-Verlag, 1995.

[Sch79] Schneider, K. S.: Optimum detection for code division multiplexed signals. *IEEE Transactions on Aerospace and Electronic Systems*, vol. 15, 1979, pp. 181–185.

[Sch86] Schmidt, R. O.: Multiple emitter location and signal parameter estimation. *IEEE Transactions on Antennas and Propagation*, vol. 34, 1986, pp. 276–280.

[Sch90] Schrüfer, E.: *Elektrische Meßtechnik*. 4. edition. München: Carl Hanser Verlag, 1990.

[Sch92] Schrüfer, E.: *Signalverarbeitung*. 2. edition. München: Carl Hanser Verlag, 1992.

[Skl04] Sklavos, A.: *Service area based OFDM air interfaces for beyond 3G mobile radio systems*. Dissertation, Lehrstuhl für hochfrequente Signalübertragung und -verarbeitung, Universität Kaiserslautern, 2004.

[SMWB01] Sklavos, A.; Maniatis, I.; Weber, T.; Baier, P. W.: Joint channel estimation in multi-user OFDM systems. *Proc. 6th International OFDM-Workshop (InOWo'01)*, Hamburg, 2001, pp. 3–1–3–4.

[Ste95] Steiner, B.: *Ein Beitrag zur Mobilfunk-Kanalschätzung unter besonderer Berücksichtigung synchroner CDMA-Mobilfunksysteme mit Joint Detection*. Fortschrittberichte VDI, Reihe 10, no. 337. Düsseldorf: VDI-Verlag, 1995.

[Ste96] Steil, A.: *Spektrale Effizienz digitaler CDMA–Mobilfunksysteme mit gemeinsamer Detektion*. Fortschrittberichte VDI, Reihe 10, no. 437. Düsseldorf: VDI-Verlag, 1996.

[SWBC02] Sklavos, A.; Weber, T.; Baier, P. W.; Costa, E.: Beyond 3G radio interface JOINT: Optimum uplink data detection when applying OFDM. *Proc. 7th International OFDM-Workshop (InOWo'02)*, Hamburg, 2002, pp. 11–15.

[THT98] Tschudin, M.; Heddergott, R.; Truffer, P.: Validation of a high resolution measurement technique for estimating the parameters of impinging waves in indoor environments. *Proc. IEEE 9th International Symposium on Personal, Indoor and Mobile Radio Communications (PIMRC'98)*, vol. 3, Boston, 1998, pp. 1411–1416.

[TNA+01] Tjelta, T.; Nordbotten, A.; Annoni, M.; Scarrone, E.; Bizzarri, S.; Tokarchuk, L.; Adams, C.; Craig, K.; Dinis, M.: Future broadband radio access systems for integrated services and flexible resource management. *IEEE Communications Magazine*, vol. 39, 2001, pp. 56–63.

[TWMB01] Tröger, H.; Weber, T.; Meurer, M.; Baier, P. W.: Performance assessment of joint transmission (JT) multi-user downlinks with multi-element transmit antennas. *European Transactions on Telecommunications*, vol. 12, 2001, pp. 407–415.

[vdBBB+99] van de Beek, J.-J.; Borjesson, P.; Boucheret, M.-L.; Landstrom, D.; Arenas, J.; Odling, P.; Ostberg, C.; Wahlqvist, M.; Wilson, S.: A time and frequency synchronization scheme for multiuser OFDM. *IEEE Journal on Selected Areas in Communications*, vol. 17, 1999, pp. 1900–1914.

[vdBES+95] van de Beek, J.; Edfors, O.; Sandell, M.; Wilson, S.; Börjesson, P.: On channel estimation in OFDM systems. *Proc. IEEE 45th Vehicular Technology Conference (VTC'95)*, vol. 2, 1995, pp. 815–819.

[vdVTP97] van der Veen, A.-J.; Talwar, S.; Paulraj, A.: A subspace approach to blind space-time signal processing for wireless communication systems. *IEEE Transactions on Signal Processing*, vol. 45, 1997, pp. 173–190.

[Ver98] Verdú, S.: *Multiuser Detection*. Cambridge: Cambridge University Press, 1998.

[vNP00] van Nee, R. D. J.; Prasad, R.: *OFDM for Wireless Multimedia Communications*. Boston: Artech House, 2000.

[Wal98] Walke, B.: *Mobilfunknetze und ihre Protokolle: Grundlagen, GSM, UMTS und andere zellulare Mobilfunknetze*. vol. 1. Stuttgart: B. G. Teubner, 1998.

[WE71] Weinstein, S.; Ebert, P.: Data Transmission by Frequency Division Multiplexing Using the Discrete Fourier Transform. *IEEE Transactions on Communications*, vol. 19, 1971, pp. 628–634.

[Wec02] Weckerle, M.: *Utilization of Correlation Matrices in Adaptive Array Processors for Time Slotted CDMA Uplinks*. Dissertation, Lehrstuhl für hochfrequente Signalübertragung und -verarbeitung, Universität Kaiserslautern, 2002.

[Wes02] Wesołowski, K.: *Mobile Communication Systems*. New York: John Wiley & Sons, 2002.

[Wha71] Whalen, A. D.: *Detection of Signals in Noise*. New York: Academic Press, 1971.

[WLM+03] Weber, T.; Liu, Y.; Maniatis, I.; Meurer, M.; Costa, E.: Performance of a Multiuser OFDM Mobile Radio System with Joint Detection. *Proc. 8th International OFDM Workshop (InOWo '03)*, Hamburg, 2003, pp. 191–195.

[WM02] Wisely, D.; Mitjana, E.: Paving the road to systems beyond 3G - the IST MIND project. *Proc. IEEE 13th International Symposium on Personal, Indoor and Mobile Radio Communications (PIMRC'02)*, vol. 3, 2002, pp. 1042–1046.

[WMSL02] Weber, T.; Maniatis, I.; Sklavos, A.; Liu, Y.: Joint transmission and detection integrated network (JOINT), a generic proposal for beyond 3G systems. *Proc. 9th International Conference on Telecommunications (ICT'02)*, vol. 3, Beijing, 2002, pp. 479–483.

[WPE98] Weckerle, M.; Papathanassiou, A.; Emmer, D.: The benefits of intelligent antenna arrays in TD-CDMA – a study based on measured channel impulse responses. *Proc. IEEE 9th International Symposium on Personal, Indoor and Mobile Radio Communications (PIMRC'98)*, vol. 2, Boston, 1998, pp. 965–966.

[WPS99] Weckerle, M.; Papathanassiou, A.; Schmalenberger, R.: Spatial interference covariance matrix estimation in multiantenna TD-CDMA systems. *COST 259 TD(99)*, Thessaloniki, 1999.

[ZF97] Zurmühl, R.; Falk, S.: *Matrizen und ihre Anwendungen*. vol. 1. 7. edition. Berlin: Springer-Verlag, 1997.

Tabellarischer Lebenslauf

Name:	Ioannis Maniatis
Adresse:	Mozartstrasse 25 67655 Kaiserslautern
Geburtsdatum:	12. August 1971
Familienstand:	ledig
Staatsangehörigkeit:	griechisch / deutsch
Schulausbildung:	1976 – 1983 Deutschsprachiger Kindergarten und Grundschule in Athen 1983 – 1989 Deutsche Schule Athen
Schulabschluß:	griechisches Abitur
Studium:	1991 – 1995 Studium im FB Maschinenwesen der Universität Kaiserslautern 1995 – 2001 Wechsel zum Studium der Elektrotechnik an der Universität Kaiserslautern
Studienabschluß:	Diplom
Berufstätigkeit:	seit April 2001 wissenschaftlicher Mitarbeiter am Lehrstuhl für hochfrequente Signalübertragung und -verarbeitung der Universität Kaiserslautern